The Development of a Slagging and Fouling Predictive Methodology for Large Scale Pulverised Boilers Fired with Coal/Biomass Blends

By

Piotr Patryk PŁAZA

M.Sc., Power and Mechanical Engineering
M.Sc., Environmental Engineering

A Thesis submitted to Cardiff University
for the Degree of Doctor of Philosophy
in Mechanical Engineering

Institute of Energy
Cardiff School of Engineering
Cardiff University
Cardiff, UK
2013

Supervisors:
Prof. Nicholas Syred
Prof. Anthony J. Griffiths

Declaration

This work has not been submitted in substance for any other degree or award at this or any other university or place of learning, nor is being submitted concurrently in candidature for any degree or other award.

Signed …… (Piotr Patryk Płaza) Date ……

Statement 1

This thesis is being submitted in partial fulfilment of the requirements for the degree of PhD

Signed …… (Piotr Patryk Płaza) Date ……

Statement 2

This thesis is the result of my own independent work/investigation, except where otherwise stated. Other sources are acknowledged by explicit references. The views expressed are my own.

Signed …… (Piotr Patryk Płaza) Date ……

Statement 3

I hereby give consent for my thesis, if accepted, to be available for photocopying and for inter-library loan, and for the title and summary to be made available to outside organisations.

Signed …… (Piotr Patryk Płaza) Date ……

To the women of my life:
my wife Adrianna
my two daughters Antonina and Amelia
my mother and sister
and mother-in-law

for their love, encouragement
and excellent cuisine

ABSTRACT

This dissertation deals with the development of a co-firing advisory tool capable of predicting the effects of biomass co-firing with coal on the ash deposition and thermal performance of pulverised fired (pf) boilers. The developed predictive methodology integrates a one-dimensional zone model of a pf boiler to determine the heat transfer conditions and midsection temperature profile throughout the boiler, with the phase equilibrium–based ash deposition mechanistic model that utilises FactSage^{TM} thermo-chemical data. The designed model enables advanced thermal analysis of a boiler for investigating the impact of fuel switching on boiler performance including the ash deposition effects.

With respect to the ash deposition predictive model, the improved phase equilibrium approach, adjusted to the pf boiler conditions was proposed that allows the assessment of the slagging and high temperature fouling severity caused by the deposition of the sticky ash as well as low-temperature fouling due to salts condensation. An additional ash interaction phase equilibrium module was designed in order to estimate the interactions occurring in the furnace between alumino-silicate fly ash and alkali metals originating from biomass. Based on the developed model, the new slagging/fouling indices were defined which take into account the ash burden, slag ratio in the fly ash approaching the tube banks as well as the slag viscosity corresponded to the conditions within the pf boiler.

The developed model was validated against field observations data derived from semi-industrial pf coal-fired furnace as well as a large scale 518 MW_e pf boiler fired with a blend of imported bituminous coals and biomass mix composed of the various quality biomass/residues, such as meat and bone meal, wood pellets and biomass mix pellets produced on-site: the power plant typically fired up to 20wt% coal substitution. Good agreement has been found for the comparison between predictions and slagging/fouling observations. Based on the validated model the fuel blend optimisation was performed up to 30wt% co-firing shares revealing highly non-additive ash behaviour of the investigated fuel blends.

Acknowledgements

First and foremost, I would like to express my deepest gratitude to Prof. Nick Syred and Prof. Tony Griffiths for their supervision, inspiration and continuous guidance throughout my PhD course. Thank you for giving me the opportunity to be a Marie Curie Fellow at Cardiff University.

Special thanks to Dr. ir. Wiebren de Jong from TU Delft, The Netherlands for giving me a possibility to continue my doctoral research within the post-doctoral research project at TU Delft. Thank you for your valuable scientific discussions, patience and trust in me. Without your help and encouragement I would never have finished this thesis.

To Prof. Mikko Hupa and Dr. Maria Zevenhoven, my Marie Curie supervisors in Åbo Akademi University, Turku, Finland. Thank you for your invaluable guidance during my few months stay in Turku and continuous inspiration during my research.

To E.ON Benelux Partners: Hans de Vries, Mark Mulder, Cees Gast (DNV KEMA) and Yash Joshi (TU Delft) from the "Energy from Biomass" project. Thank you for your professional and successful cooperation. Your help in gathering the ash deposition data used for the model validation within this thesis is gratefully appreciated.

To Prof. Wiesław Rybak from Wrocław University of Technology, Poland. Thank you for your supervision and encouragement at the beginning of my research path at WUT.

Finally, I would like to deeply thank my mother Christina, my bellowed Adrianna, family and friends for their endless support and understanding. Thank you Adrianna for our two beautiful little princesses who fill my life with absolute joy and happiness.

Delft-Warsaw, July 2013 Piotr P.

The support of the European Union for the Marie Curie training programme - "INECSE" is gratefully acknowledged via contract No. MEST-CT-2005-021018.

Contents

List of Figures

List of Tables

Nomenclature

Mathematical Symbols

a_i	activity of pure species i	-
A	surface area	m^2
R	(thermal) resistance	m^2K/kW
C	deposition rate by the condensation per unit surface area	$kg/(m^2s)$
C_{ash}	ash concentration per volume of the flue gas stream	kg/m^3
C^*_{ash}	ash concentration per mass of the flue gas stream	g/kg
d	diameter	m
D_i	diffusion coefficient	m^2/s
G	Gibbs energy	J
m	mass	kg
$\dot{M}$	mass flow rate	kg/s
T	absolute temperature	K
t	time or temperature	s or ^oC
p	pressure	Pa
P	probability	-
u	velocity	m/s
n_B	mass fraction of the fuel burnt	-
n_i	mole fraction of ith species	-
h	enthalpy	kJ/kg
$\overline{H}$	relative height	-
V	volume	m^3
I	deposition rate by impaction per unit surface area	$kg/(m^2s)$
k_{eff}	effective thermal conductivity	W/(mK)
$k_{c,i}$	mass transfer coefficient of ith component	m/s
K_e	erosion coefficient	-
q_{UBC}	heat loss due to unburned carbon in the ash	%
$\dot{q}$	heat flux density	W/m^2
$\dot{q}_{Air}$	heat of air delivered into zone	J/kg
$\dot{Q}$	heat flux	W
$\dot{Q}_B$	heat flux from burning fuel	W
$\dot{Q}_{Air}$	heat flux from preheated air	W
$\dot{Q}_{FG}$	heat flux from flue gas	W
$\dot{Q}_{EM}$	heat flux emitted	W
$\dot{Q}_{Con}$	heat flux transferred by convection	W
$\dot{Q}_{Ad}$	theoretical combustion heat	W
$\dot{Q}_{Evap}$	overall heat flux transferred to the furnace walls	W
REA	mass of reactive Al-SI based ash	%
Stk	Stokes number	-
S	system entropy	J/K

SD	shedding rate of deposits per unit surface area	kg/(m^{2}s)
Sh	Sherwood's number	-
Th	thermophoresis rate	kg/(m^{2}s)
u_g	velocity of the flue gas	m/s
$Vc_{p,t}$	average specific heat of the flue gas	kJ/(kg^{o}C)

Subscripts

abs	absorbed	-
ad	adiabatic	-
con	convection	-
d	deposit	-
e	electrical	-
eff	effective	-
fl	flame	-
furn	furnace	-
g	gas	-
HTF	high temperature fouling	-
inc	incident	-
p	particle	-
s	water/steam	-
rad	radiation	-
ref	reference	-
refl	reflected	-
th	thermal	-
SL	slagging	-
tot	total	-
w	wall	-

Greek Letters

α	convective heat transfer coefficient	W/m^{2}K
β	the current fuel burn-out fraction	-
δ	thickness	m
ε	emissivity	-
η	efficiency	-
λ	air excess ratio	-
μ	viscosity	Pa*s
μ_i	chemical potential of component	J/mole
ν	kinematic viscosity	m^2/s
ρ	density	kg/m^3
σ_0	Stefan-Boltzmann constant	W/m^{2}K^4
ϕ	ratio of molten slag in the ash	-
$\overline{\phi}$	average slag ratio	-
Ψ	thermal efficiency factor	-

Abbreviations

AC	Availability coefficient
AFT	Ash fusion test
AS	Australian standards
ASTM	American Society for Testing and Materials
BMP	Biomass mix pellets
CCSEM	Computer-controlled scanning electron microscopy
CFD	Computational fluid dynamics
DEA	Direct exchange areas
DFA	Direct flux areas
DIN	Deutsches Institut für Normung
DSC	Differential scanning calorimetry
FBC	Fluidised bed combustion
FC	Fixed carbon
FEGT	Furnace exit gas temperature
FT	Fluid temperature
HT	Hemispherical temperature
ICP-AES	Inductively coupled plasma atomic emission spectroscopy
IDT	Initial deformation temperature
IFRF	International Flame Research Foundation
ISO	International Organisation for Standardisation
LHV	Lower heating value
MBM	Meat and bone meal
NNT	Neural Network
PF	Pulverised fuel fired boiler
Ppm	Parts per million
SA	South African
ST	Softening temperature
STA	Simultaneous thermal analysis
TGA	Thermal gravimetric analysis
WSGGM	Weighted-sum-of-gray-gases model
VM	Volatile matter
UBC	Unburnt carbon
1D, 2D, 3D	One-, two-, three- dimensional

1

INTRODUCTION

1.1 Background Information

Nowadays, more than 85% of primary energy consumption originates from fossil fuels whilst the coal is still the largest energy source accounting to around 40% of world's generated electricity [1, 2]. Pressure on the dwindling traditional economic fossil fuel reserves along with stringent environmental legislation, especially those associated with greenhouse gas production, has led to sectors such as that of power generation to reanalyse the way in which they produce electricity. The EU target is to increase share of renewable energy sources by generating 20% of its energy from renewable energy by 2020 (15% in case of the UK) [3]. One such promising route to achieve in short-time scale the set targets is to co-fire using a mixture of coal and biomass in existing large scale pulverised fuel fired boilers.

Currently, coal substitution rates have been conservative, typically operating at about 10wt% when co-firing less quality agricultural biomass. However, within the European Union there is a drive to substantially increase the biomass co-firing ratios to around 30wt% or even to higher percentages when utilising good quality wood pellets or torrefied biomass. This is especially encountered in European countries where biomass (co-)firing is subsidised by governments, namely in Belgium, The Netherlands, the UK, Spain, Italy and Poland. Amongst these countries the UK and Poland have the largest estimated technical potential, in terms of available pulverised coal-fired boilers capacity for biomass co-firing [4]. In the view of the most extensive, and long experience in biomass combustion, the Nordic countries, such as Denmark, Sweden, and Finland, have been found to be the leaders in this field due to good biomass supply, contributing to favourable conditions for biomass (co-) firing.

According to carried out estimations [5], in 2011 around 230 power plants placed globally, with a range of power capacities varied between 50-700 MW_e, use, have used or announced the intention to co-fire biomass with coal. Assuming switching of the 10% of the global coal-fired capacity to biomass co-firing, it would result in approximately of 150 GW

biomass capacity [5]. This is around 10 times higher than today's co-firing capacity estimations and about 2.5 times higher compared to the globally installed biomass power capacity (in 2010).

The technology of biomass co-firing in large pulverised coal-fired boilers is the most cost-effective way of biomass utilisation due to the need for only relatively minor, low cost, system modifications, and the higher boiler efficiency in comparison with 100% firing biomass in smaller boilers. Limitations develop due to supply chain problems for the physical quantities of biomass needed. The by-product of raising biomass thresholds can be operational problems associated with the generation of slagging and fouling and/or corrosion within pulverised fuel boilers.

The ash deposition process, inevitably associated with the combustion of solid fuels, can lead to substantial financial losses to an operator as a result of reduced boiler efficiency, reduced availability (unplanned shut-downs), and high maintenance costs due to blockage, erosion, and corrosion. These operational boiler problems are often, but not exclusively, caused by utilisation of high alkali content biomass fuels, whose fly ash behaviour significantly differs from that of conventional fuels. The pioneering straw co-firing campaign undertaken in the 1990s in Denmark revealed serious problems with slagging, fouling, and corrosion encountered in conventional boilers such as stoker-fired (up to 100% straw firing), fluidised bed boilers (with up to 50% biomass on an energy basis) and also increased ash deposition in pulverised boilers (up to 20th% straw shares) [6-8]. It has been established that the main reason for such operational problems lay in the high concentrations of potassium and chlorine present in straw.

With respect to coal impacts, the results obtained from the UK collaborative programme (in 1990s) on slagging in pulverised coal-fired furnaces revealed that iron and calcium (both abundant in the inorganic matter of the UK native coals) originated from pyrite and calcium carbonate, respectively, are the major fluxing agents of alumina-silicates which led to decrease ash viscosity, thus enhancing slagging [9].

Nowadays most of the hard coals fired in European Power Plants originate from various worldwide sources (e.g. Russia, Colombia, South Africa, US), except in Poland which is the largest hard-coal producer in EU27. In all of these plants, co-firing of different quality coal blends with biomass is very common. To date, the requirements with respect to the use of diverse biomass fuels co-fired at higher levels in existing large pulverised fuel boilers has rapidly increased. Therefore, there is a need to assess the safe, economical operating limits on

the level of co-firing fuels that can be used in existing boilers while maintaining efficient boiler performance without severe slagging and fouling.

Although many ash behaviour indices and prediction techniques are available, most of them have been developed for addressing slagging and fouling during coal combustion and are also limited to certain coal types. These indices do not include the non-additive ash interactions between coal and biomass which may occur when the fuels are fired together, leading to inaccurate predictions if available coal indices were used. Other predictive indices and methods, postulated to be more accurate, require more detailed fuel information regarding the mineralogical composition, particle size distribution and solubility of inorganic elements to assess slagging/fouling propensity. These non-standard additional fuel data are not easily available on a daily basis, and even so, when it comes to more complex fuel blends of different origin and ash chemistry, the interactions between inorganics need to be assessed which is still a big challenge.

In recent years, a number of CFD-based models/simulators including ash deposition phenomena have been developed. Nowadays, multipurpose CFD codes combine the modelling of turbulent flow in combustion systems with other combustion phenomena. These include advanced models of ash deposition with complex stages of ash behaviour from ash formation, transport to the heat surfaces, deposition, and growth. The integration of CFD combustion modelling with advanced mineral matter chemistry, multicomponent, multiphase thermo-chemical equilibrium calculation, and advanced fuel analyses are the goal for the development of reliable complex simulation tools for accurate predictions of slagging and fouling processes.

Despite the apparent advantages associated with CFD tools, these comprehensive models are too bulky for use in case studies with strongly variable fuel properties or those considering various possible design changes to the boiler and furnace. In addition to the expertise required and time taken to prepare the simulation, CFD models can at best take several hours or days to run and at worst several weeks. This makes it very difficult and time-consuming to evaluate the effect of even small changes to fuel specification. Indeed, most operators test new fuels in model 0.5-1 MW boiler simulators with residence time similar to large boilers, looking at slagging, fouling, corrosion effects, as well as a range of other parameters. This allows appropriate fuel blends to be developed, but it is expensive. When a co-firing approach or retrofitting an existing unit is considered, design engineers as well as the boiler’s management have to take into account a large number of potential problems and case studies related to the efficiency and reliable operation of the boiler furnace.

In such cases, the models should be simple, capable of incorporating experimental data, since a rapid response is required so that numerous runs can be conducted. With sufficient accuracy, the required thermal characteristics of the furnace can be obtained within a relatively short period of time, with the aid of zone-based engineering computational models. These simplified models are capable of delivering sufficient information regarding the thermal conditions within the boiler that can be further used or employed for more complex thermo-chemical investigations on slagging and fouling when co-firing various fuel blends.

1.2 Objectives and Main Research Questions

The aim of the research was to develop a generic slagging/fouling prediction tool for large scale utility boilers when co-firing biomass/coal blends. This should be capable of giving relatively quick responses of the predictions when simulating the effects of different fuel types and operating conditions while being easily implemented for various furnace types. The objectives of the research are as follows:

- to perform an overview of the variety of the solid fuel ash chemistries, as well as to identify the major factors affecting slagging and fouling,
- to carry out the critical review of the slagging and fouling predictive methods and boiler thermal performance simulation tools to highlight their capabilities and limitations,
- to develop an integrated package of methodologies capable of predicting the slagging and fouling tendencies of solid fuels blends as well as assessing the impact of fuel quality change on thermal boiler performance,
- to validate the developed predictive modelling approach on slagging/fouling data derived from a large scale pulverised fuel boiler,
- to investigate the optimal fuel flexibility windows to avoid severe slagging and fouling of coal/biomass blends containing residual biomass with increased proportion of low quality ash.

Based on the performed studies and obtained research findings the following research questions will be answered:

- Is it possible to assess successfully the slagging/fouling tendencies of complex coal/biomass fuel blends with the aid of models based on the phase equilibrium analysis? How much detailed fuel data are required for such analysis?
- How the quality of coal ash would affect the slagging and fouling when co-firing of coal with biomass?

The set of investigated fuels includes various ash quality trade hard-coals and their blends with biomass containing poor quality ash, such as straw and mixtures composed of the meat and bone meal, paper/sewage sludge and wood residues. The optimal co-firing rates for certain fuel blends aimed to be identified.

1.3 Thesis Outline

Following by the introduction part, the Chapter 2 starts off by outlining the major factors affecting slagging and fouling in boilers. The differences in the inorganic species origin, composition and behaviour between various coals and biomass fuels are outlined and the ash deposition mechanisms described. In Chapter 3, a critical review of existing slagging and fouling predictive methods and boiler simulation tools is carried out, which resulted in defining the conceptual approach of the model to be developed. Chapter 4 presents the development of a slagging and fouling predictive methodology, firstly by outlining the improved zone-based thermal model, and then by performing the sensitivity analysis of the model applied to the large scale pulverised fuel boiler supported with discussion of the results obtained. It is then followed by the development of the thermo-chemical module that is employed to predict and investigate slagging/fouling tendencies, which is defined in Chapter 5. In this Chapter the results obtained from the fuel blend optimisation analysis as well as the effects of biomass co-firing are discussed in more details. The Chapter 6 presents the results from the validation of the slagging/fouling model with the slagging/fouling observations gathered from a semi-industrial coal-fired furnace and a large scale coal/biomass fired pf boiler. Additionally, the methodology used to optimise more complex coal/biomass blends to minimise their slagging/fouling propensity is presented and the obtained findings discussed. Finally, in Chapter 7, the conclusions drawn from the research are given, followed by the recommendations for continuation of the work.

2

UNDERSTANDING SLAGGING AND FOULING

This Chapter aims at providing a brief overview of the mechanisms involved in the ash deposition process when co-firing of solid fuels, including coal/biomass mixtures, in large utility pulverised fuel boilers. Apart from outlining the basics of mineral matter influence on boiler design, here a particular focus is on the ash behaviour, including the release of ash forming matter from the fuels, ash formation process, and finally the formation of ash deposits on heat exchanger surfaces. Understanding these phenomena, but also the knowledge on how the inorganics are associated with fuel is seen to be crucial in a development of reliable slagging and fouling predictive tools. Throughout the Chapter, a number of relevant references are mentioned to highlight the state of the art knowledge in this field.

2.1 Introduction

The accumulation of fireside deposits on the heat transfer surfaces decreases boiler efficiency and availability due to unplanned shut-downs contributing to substantial losses to an operator. Ash deposition is inevitably associated with combustion of solid fuels. This most common and serious boiler's operational problem cannot be avoided but may be reduced by the appropriate boiler design, firing less ash-problematic fuel blends as well as proper boiler operation. In all of these factors, understanding the nature of inorganic constituents present in solid fuels but also their behaviour under combustion conditions in boilers are the most crucial elements to minimise effectively inorganic material impact, also by the use of other design and boiler operation methods.

2.2 Influence of Fuel Impurities on Boiler Design

Since the industrial revolution, the encountered problems with the ash deposition during coal combustion have been dominant influences on the design and operation of boiler furnaces [10]. The industrial scale precursors to modern pf fired boilers were stoker-fired boilers, first introduced for coal combustion in the second decade of the 20th century. In its basic design, coal is fired on a moving grate in the bottom furnace, cooled by underfire air. The thermal capacity of these boilers ranges from 15 kW_{th} up to about 150 MW_{th}. The major issue encountered in stoked-fired furnaces was slag formation on the grate which hinders the fuel material transport and disturbs the air distribution through the grate. These problems were heightened when firing a high-alkali content biomass (such as straw) and the low ash-melting waste fuels. To minimise slagging/fouling in the entrance to the convective pass of the boiler, in some designs the increased water-wall areas are used to lower furnace exit gas temperatures to approximately 760^{o}C [11]. Other design changes included staged combustion, where one-third of the combustion air is supplied through the grate so that fuel is initially burned at low temperatures (see Figure 2-1). Furthermore, slagging screens are placed at the furnace outlet to capture molten ash particles and to minimise development of deposits downstream of the furnace.

In 1920 the concept of combustion of pulverised coal in clouds and with a hot oxidising atmosphere was introduced instead of burning in a thick bed on grate. This was a major step towards improving the fuel conversion process, raising the steam temperature and pressure parameters and scale-up the units (now even above 1000 MW_e) to produce electricity more efficiently. The short residence time of pulverised coal particles in the hot flame zones (up to

a few seconds) was believed to substantially reduce the melting of inorganic species while ensuring a high fuel burn-out. Although the pulverised fuel fired boilers can be designed for a relatively wide range of coals (i.e. by designing the wall-furnace surfaces to achieve required flue exit gas temperature which corresponds to the coal ash melting characteristic), switching to other different or lower ash quality solid fuels may cause increased ash-deposition problems.

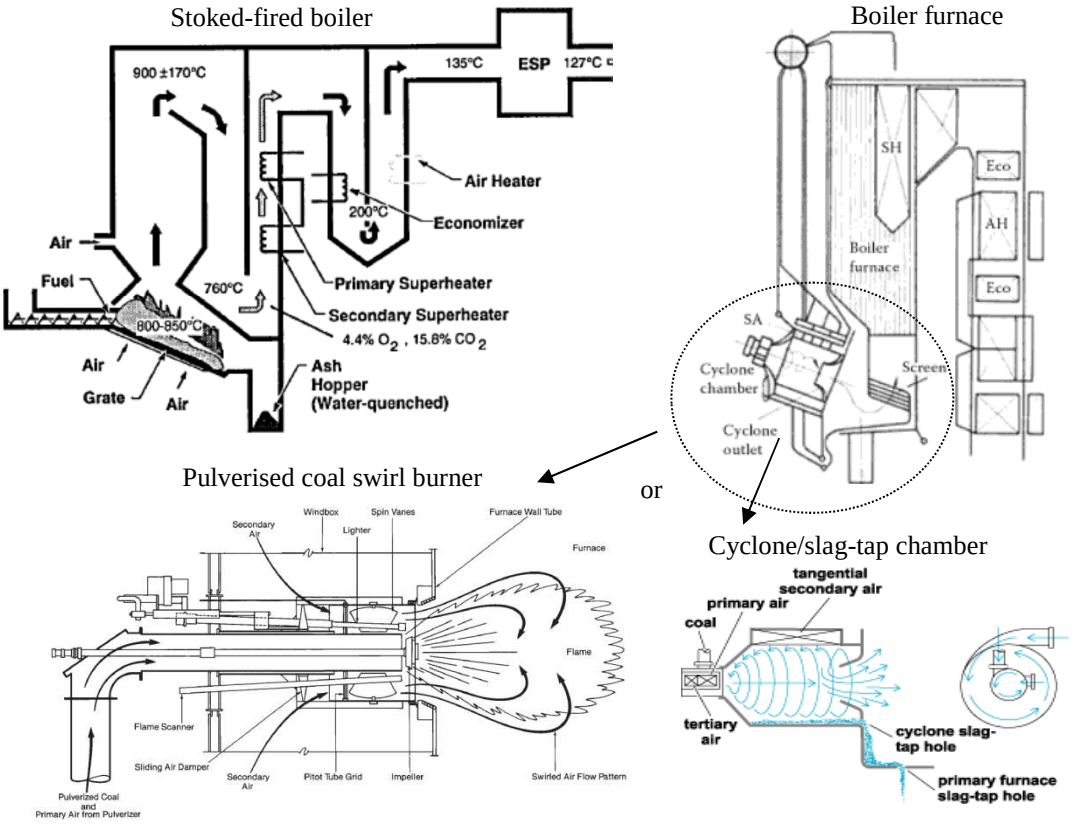

Figure 2-1. Scheme of stoked-fired [11], cyclone [12] and pulverised fuel fired technologies [13].

Other boiler types, designed specifically to utilise high slagging coals are equipped with the cyclone or slag-tap (wet-bottom) chambers for firing coals within the furnace instead of pulverised coal-fired burners (see Figure 2-1). The larger coal particles are trapped in the molten and sticky layer covering the surface of the cyclone chamber, being fired in the temperature range between 1650°C to 2000°C [12]. Most of the ash (80-90%) leaves the bottom of the boiler as a molten slag, thus decreasing the fly ash burden passing through the superheater/reheater sections. Although, a number of slag discharge boilers were designed and operated for utilising US and German coals, in the UK only a few were built, and after 1950s no more were erected at large, industrial scale. This was due to the strict criteria of slag viscosities of coals which should be specifically low to obtain efficient ash removal and boiler

operation [10] and UK coals were not particularly suitable. Hence, the slag-tap boiler types do not have the fuel flexibility of dry-bottom pulverised fuel boilers.

When switching the existing pf coal-fired boilers to co-fire coal/biomass blends, various options can be considered. The simplest and cost-effective way is a direct biomass co-firing with coal using the current or modified burner and appropriate fuel feeding/milling installations. However, this may lead to serious limitations with respect to milling system capacity as well as slagging/fouling issues. Biomass can be also co-fired in-directly in a more complex and thus expensive ways, which also reduce ash impact, e.g. through a gasification of biomass in a separate gasification unit, and then burning the generated gas with coal in pf boilers.

Combustion of biomass in dedicated-biomass fluidised bed boilers (FBC) appears to be an attractive way of utilising of low ash quality solid fuels. This is due to the relatively low temperature (850^{o}C) of the combustion process, giving high thermal efficiency compared to grate-fired boilers. However, according to the reported operational experience, the risk of bed agglomeration may occur when co-firing high alkali content biomass, also the increased erosion of the heat transfer surface may be an issue [10, 14] whilst capital and running costs are elevated compared to comparable sized pf boilers.

In all cases, whatever the combustion system is, the ash-related problems will be always associated with burning of solid fuels. In this work, the focus is on reducing the ash impact on pulverised fuel-fired boilers performance. Such boilers are widespread, and are recently more intensively exploited to co-fire biomass with coal to achieve targeted CO_2 emission reduction.

2.3 Slagging and Fouling in PF Boilers

In this subsection the types of deposits found in pulverised fuel fired boilers are described as well as the major factors affecting slagging and fouling are discussed.

Slagging deposits occur on the furnace walls and other surfaces in the radiant section of the boiler, including burner areas. These deposits often consist of an inner powdery layer, covered by a molten or partly molten ash layer [15]. Furnace wall deposits are dominated by silicate, iron and alkali species whereas deposits developed around the burners are composed, in particular, of not completely oxidised fused iron-based minerals. Slagging reduces the heat absorption in the furnace, therefore leads to increased furnace exit gas temperature. As a result, the overheating of the platen superheater placed at the furnace outlet occurs, followed by the formation of highly sintered deposits on heat transfer sections.

Fouling deposits form on the heat exchange surfaces, such as superheaters and reheaters, placed in the furnace outlet and convective pass of a boiler. High temperature fouling is defined by the formation of semi-fused, sintered ash deposits found typically in the flue gas temperature range of 1300-900^{o}C whereas the low temperature fouling is associated with formation of the loose or slightly sintered deposits built-up in flue gas temperature between 900^{o}C-300^{o}C. The primary mechanism involves the condensation of previously volatilised in flame species which occurs in different temperature ranges depending upon the composition and concentrations of the gaseous inorganic compounds present in the flue gas. As a result, the inner deposit layer on the tubes is often composed of condensed alkali salts, which provides a sticky surface for trapping other non-sticky particles [10, 15]. The trapped calcium oxide particles once sulphated can significantly contribute to the mass of these deposits, binding particles and increasing the deposits strength.

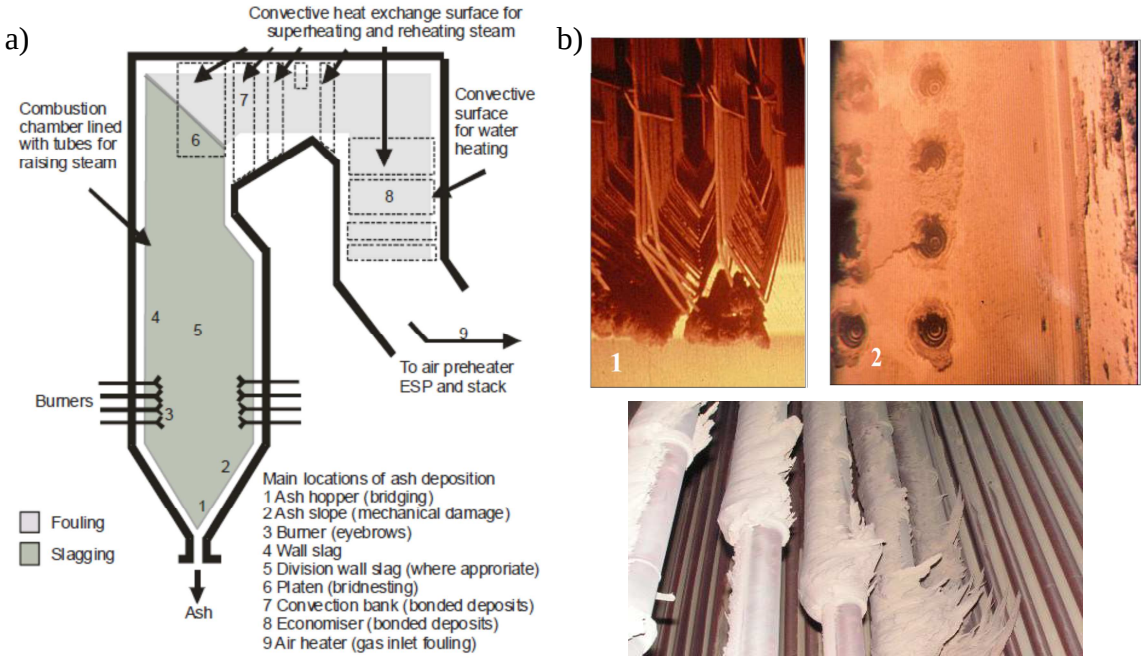

Figure 2-2. a) Scheme of heat-exchange surfaces arrangement in pf boiler [16], b) Images of ash deposits found in coal-fired boilers: 1-platen superheater, 2-furnace wall, 3-at the entrance to convective pass of boiler [17].

Fireside Corrosion is commonly associated with the ash deposition problems, and usually results from the combustion of fuels enriched in chlorine or sulphur. Corrosion can be accelerated during reducing conditions existing due to air-staging and operation of low NOx burners (high temperature corrosion). Formation of low melting alkali iron sulphate or alkali chloride deposits can significantly increase corrosion rates. In comparison with slagging, corrosion is usually a long-term process [10].

The wide variation in deposit types and locations in which deposits may be formed indicates that besides the fuel nature, the slagging and fouling are very much dependent on the boiler design and operating conditions [18]. The major factors affecting slagging and fouling are summarised schematically in Figure 2-4. In pulverised boilers, slagging is a major determinant in fixing the furnace size whereas fouling dictates the spacing and location of convective tube banks for superheating and reheating steam for a given fuel [10, 19]. All these factors determine the relative costs of the heat transfer surfaces needed for a given steam output.

The pf boiler furnace should be designed to achieve the furnace exit temperature (FEGT) at least 50°C lower than the softening temperature of the ash. Typical design values of FEGT for pulverised boilers fired with hard coals are in the range 1150-1200°C whereas for lignite burning plants, the FEGT is 150-200°C lower than this [18-20]. The impact of coal quality on the furnace design concept is illustrated in Figure 2-3.

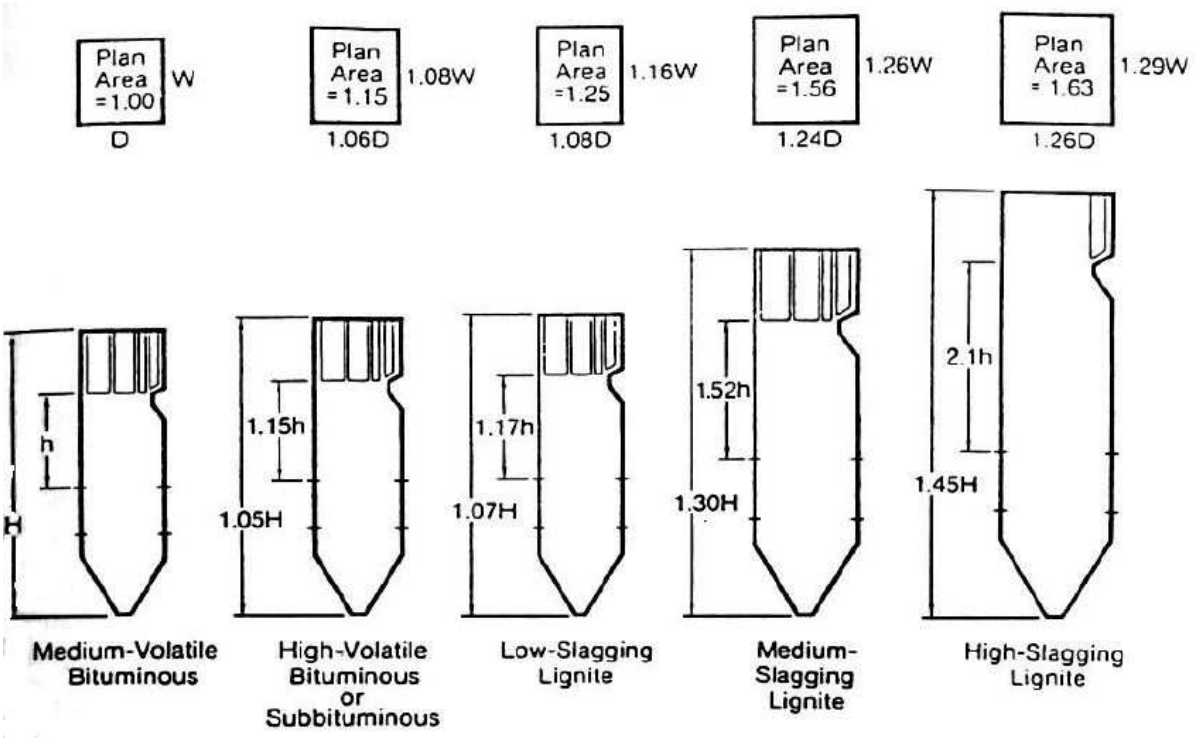

Figure 2-3**.** Impact of coal quality on furnace design concepts [21].

In general, the lignite-fired boilers have to be taller with a much greater cross section areas than boilers designed for hard coals, which results in significantly higher capital cost. This is due to a larger amount of flue gas produced when firing lignite coals but also their increased slagging propensities which affect the design furnace volumes. Furthermore, the increased soot-blowing activity is also required for lignite-fired boilers to minimise the ash deposition built-up.

Other boiler-design factors which may affect increased furnace slagging are related with the use of in furnace low-NOx emission reduction methods (i.e. air/fuel staging, low NOx-burners), which lead to reducing conditions occurring in the burner zones. Therefore, the firing system as well as the furnace flow aerodynamics should be designed properly to increase the residence time of particles in the oxidising atmosphere and to avoid flame impingement onto walls. The particle size distribution of fuel also matters, as it determines the aerodynamics as well as the temperature of burning particles and transformations in the flame minerals.

In order to keep the heat-exchange surface relatively clean for long periods during the boiler operation, the soot-blowing system need to be periodically activated which is often not sufficient when medium/high slagging fuels are unexpectedly fired. As a consequence the "snow-ball" effect of accelerated ash deposition may occur. To avoid such operational situations, there is still on-going research efforts towards developing highly efficient and economic intelligent soot-blowing systems for more challenging fuels including the co-firing of biomass [22].

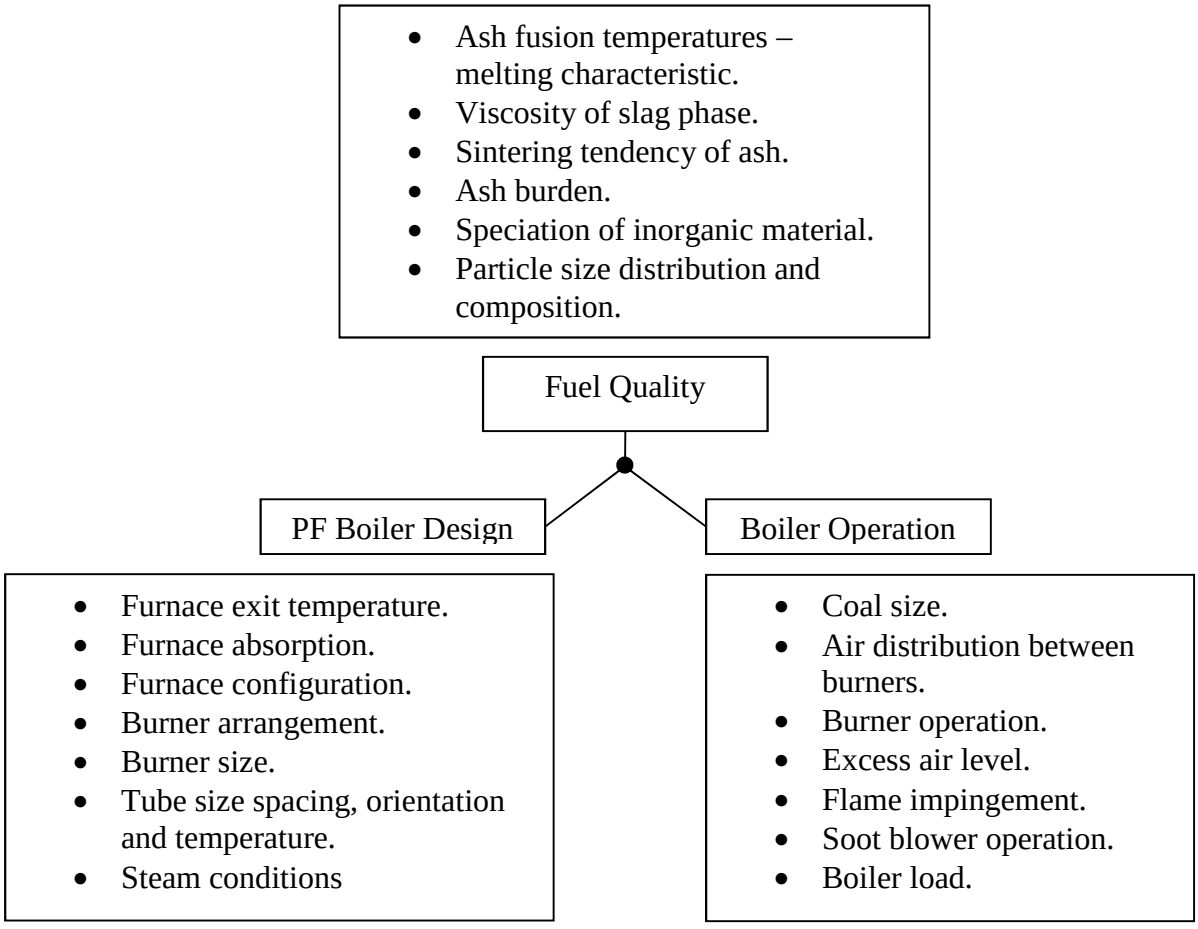

Figure 2-4**.** Factors affecting slagging/fouling in pf boilers (Modified after Bryers [18]).

Due to the current environmental regulatory requirements for the power utility sector as well as increased competition in the solid fuel market, the utilisation of other fuels than those for which boilers were originally designed is recently very common. Therefore, more attention is needed to optimise composition of fuel blends fired as well as in improving the efficiency of soot-blowing system in order to avoid severe slagging and fouling.

2.4 Inorganic Constituents in Solid Fuels

Understanding the nature of inorganic species (incombustibles) present in solid fuels is crucial to analyse and describe their behaviour during the fuel combustion process. In this subsection, the fundamental information are outlined with respect to the origin and forms of inorganic constituents found in solid fuels, including different quality coals and biomass fuels.

2.4.1 Origin of Inorganic Constituents in Coal and Biomass

The inorganic constituents, their origin, abundance and forms differ significantly between coal ranks as well as various biomass fuels. There are several factors which influence the variety and abundance of inorganics present in solid fuels, from which for coals the most important are the coal rank and related geological and environmental history of the coal deposit. For biomass fuels the crucial factor is the growing phases of the plants, the origin of agricultural/municipal wastes, as well as other processing steps, such as fuel collection, handling and storage.

2.4.1.1 Coal

Coal is a fossil fuel and can be defined as a combustible sedimentary rock formed primarily from the accumulated plant matter, contaminated with inorganic impurities which have been deposited during its formation.

During coal formation, the organic and inorganic matter have been accumulated and undergone transformation leading to subsequent increase in coal rank by a slow coalification process lasting million years to present, in which the geological conditions, pressure, temperature and climate were the important influencing factors.

With respect to origin of inorganic constituent in coal, they can be classified as [18, 23]: i) inorganic elements originated from plants, that were incorporated during peat formation, ii) wind or water-borne detritus that settled in the peat-forming environment, and iii) epigenetic minerals that formed during or after burial of the peat. The most common mineral found in coals are summarised in Table 2-1.

Detrital deposited minerals include mostly clays, silicates and quartz minerals. Along with undergoing coalification process, an enrichment of silicates and clays occurred due to increasing coal density. Subsequently, the chemical bonds in the coal matrix are slowly destroyed resulting in a transformation of the released organo-metalic elements (e.g. alkali metals) to dissolved salts and eventually silicates [18]. Other mineral such as carbonates, sulphides, chlorides are formed through a precipitation of soluble ions (mainly of Fe, Mg, Ca, Cl) derived from rock weathering or marine waters or else, were released from the organic coal matrix [24]. In time, calcium carbonate or sulphate were transformed to calcite or reacted with silicates. With increasing coal rank, iron was transformed to sulphide rather than carbonate. Apart from the precipitated primary phases in the basin, secondary phases occurred such as calcite, pyrite, quartz, clay, which filled the cavities and cracks of the coal deposit [18].

In general, the change in coal rank from lignite via sub-bituminous to bituminous coals and anthracite has led to a gradual coal densification and increase of carbon in organic matter. Simultaneously, this has resulted in decreasing the inorganic constituents' due to formation of clay mineral dispersions in fuel deposits. The variation in the ash oxide compositions for various quality coals is discussed more extensively in section 3.5.2.

Table 2-1. Major minerals found in coals [10, 18, 25].

Clay minerals - up to 50%		**Chemical formula**	
Kaolinite		$Al_2O_3 \cdot 2SiO_2 \cdot 2H_2O$	
Illite, Muscovite		$K_2O \cdot 3Al_2O_3 \cdot 6SiO_2 \cdot 2H_2O$	
Montmorillonite		$(1-x)Al_2O_3 \cdot x(MgO,Na_2O) \cdot 4SiO_2 \cdot nH_2O$	
Oxides	**Chemical formula**	**Carbonates** Up to 20%	**Chemical formula**
Quartz- 1-15%	SiO_2	Calcite/Aragonite	$CaCO_3$
Rutile	TiO_2	Dolomite	$CaCO_3 \cdot MgCO_3$
Magnetite	Fe_3O_4	Siderite	$FeCO_3$
Hematite	Fe_2O_3	Ankerite	$CaCO_3 \cdot FeCO_3$
Sulphides		**Sulphates**	
Pyrite	FeS_2	Gypsum	$CaSO_4 \cdot 2H_2O$
Pyrrhotite	FeS_x	Barytes	$BaSO_4$
Phosphates		**Chlorides**	
Fluorapatite	$Ca_5F(PO_4)_3$	Halite	$NaCl$
		Sylvite	KCl

2.4.1.2 Biomass Solid Fuels

Biomass solid fuels are defined here, as the bio-gradable fraction of energy derived from plant or animal matter or substances originated directly or indirectly from them. The biomass fuels group includes various woody/forestry biomass, agricultural wastes or other animal/domestic residues, including sewage sludge but also energy crops (of herbaceous or woody nature) which are grown for the purpose of being used as a fuel [26, 27]. Such a diverse origin of biomass solid fuels give rise to a variety of inorganic species.

In general, as far as solid biomass derived from plants is concerned, the inorganics have been accumulated during the growing phase of the plants and further biomass processing steps, such as harvesting, handling or storage, which may additionally increase biomass fuel contamination by foreign inorganic matter. The inorganics present in plants are important nutrients or other key inorganics adsorbed by plants from soil, and have various functional roles in plant metabolism and physiology which enables proper plant growing through the photosynthesis process. The primary macronutrients in biomass, such as e.g. straw consist of Nitrogen (N), Phosphorous (P), Potassium (K), Calcium (Ca), Magnesium (Mg) and Sulphur (S) whose concentration are higher than 0.1wt% (dry matter) in plant tissue [15, 26]. Other nutrients, such as Fe, Mo, Cl and Ni are present in quantities less than 0.1% dry weight. Often, fertilisers are added to artificially modify soil in order to provide plants with sufficient quantities of nutrients needed for a vigorous growth and increased yield. The use of fertilisers (such as KCl, K_2SO_4 or KNO_3), amongst which KCl is the cheapest and the most widely used in general agriculture, can significantly increase concentrations of potassium, chlorine and nitrogen in biomass [26].

Overall with respect to inorganics occurrence in biomass fuels, there are large variations observed in the key inorganic elements, not only between biomass groups (e.g. woody or herbaceous/grass biomass), but also within the group itself (e.g. between wood and bark) as seen in Figure 2-5. In general in **herbaceous biomass**, such as straw there is a higher content of potassium, chlorine and silica as compared with **woody biomass** where calcium is more abundant, especially as far as bark is concerned. Another important factor which influences the inorganics quantities and moisture content in plants is harvesting time. Delayed harvesting (winter or following spring harvest, instead of a traditional harvest in autumn) of energy crops has been observed to have a positive effect on reducing moisture content as well as undesirable components in biomass such as Cl, K, Ca, P, S and N [28, 29]. Leaching of the cut straw after harvesting on fields by rainfall is another common way to decrease the

chlorine content in straw. However, the drawbacks of this are the increased moisture in biomass and a related higher risk of straw degradation.

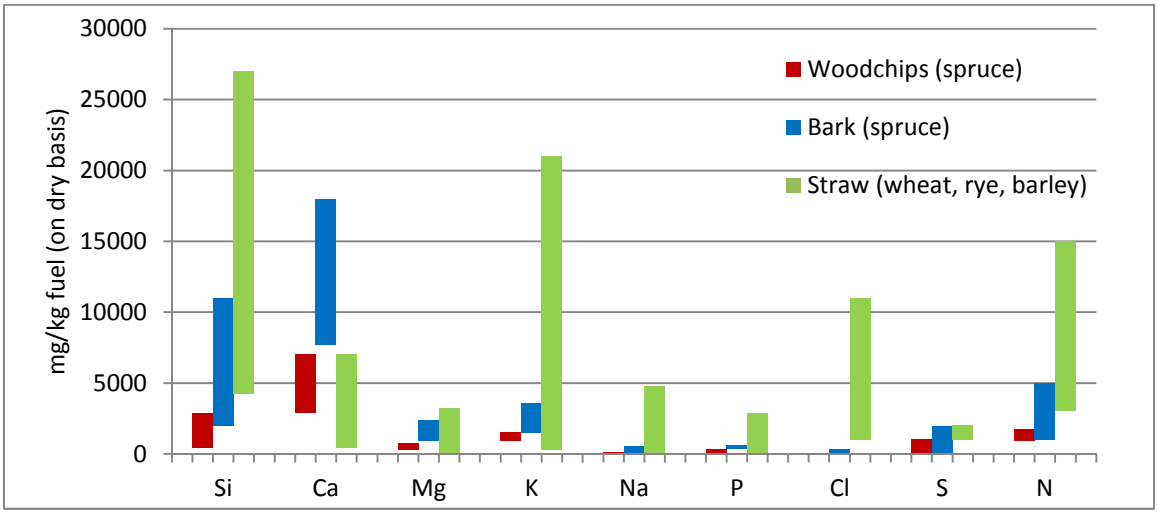

Figure 2-5**.** Variations of key inorganic elements in woody and herbaceous (straw) types of biomass [15, 26].

Animal and domestic/industrial residues, such as poultry litter, meat and bone meal or sewage sludge in comparison with biomass originated from plants, include significantly higher quantities of inorganic material of different origin. **Poultry litter** is a by-product of poultry industry which consists of the poultry excrement of chickens, turkeys and the bedding material, wasted feed and feathers [26]. The bedding material may be wood shavings, sawdust, straw, peanut hulls or other fibrous materials. Poultry litter is rich in nutrients like P, K and N and therefore is usually used as fertiliser. The phosphorus can be in organic and inorganic forms. Another by-product of the poultry industry is eggshell waste which can contribute to increased calcium carbonate ($CaCO_3$) in poultry litter. **Meat and bone meal** (MBM) as a by-product of the rendering industry, includes parts of animal bones, and meat residues in form of approximately 50% protein, 10% fat and incombustible mineral matter. A dominant mineral in MBM is hydroxyapatite – derived from bones and rich in phosphorous and calcium [30]. Other abundant inorganics present in MBM are nitrogen rich originating from proteins and alkali metals. **Sewage sludge** is a by-product of waste-water (contaminated by human and other waste from households and industries) treatment processes. Besides the organic matter, which is mostly of biological origin (with approximately 60% content on a dry basis) and other organic, pathogens and microbiological pollutants, sewage sludge consist of very high quantities of inorganic material (on dry basis %). Inorganic constituents include: i) silicates, aluminates, and calcium- and magnesium containing species, ii) organically originated Nitrogen (N)- and Phosphorous (P)-containing components, iii) precipitated P in form of Al-, Ca- or Fe- phosphates in quantities depending upon the type of precipitated agent

used, iv) heavy toxic metals (Zn, Pb, Cu, Cr, Ni, Cd, Hg, and As (with concentrations varied from more than 1000 ppm to less than 1 ppm) [30, 31].

More detailed discussion regarding the differences in inorganics content between various biomass types with relation to their impact on the melting tendencies of the ashes is carried out in section 3.5.3.

2.4.2 Association of Inorganic Constituents with Organic Matter

Apart from the organic matter and moisture, the solid fuels contain inorganic constituents which can be divided into four groups depending upon their association with fuels, namely: organically associated inorganic elements, simple salts dissolved in pore water of fuel, and more common for coals - mineral inclusions which can be classified either as included or excluded minerals, as seen in Figure 2-6.

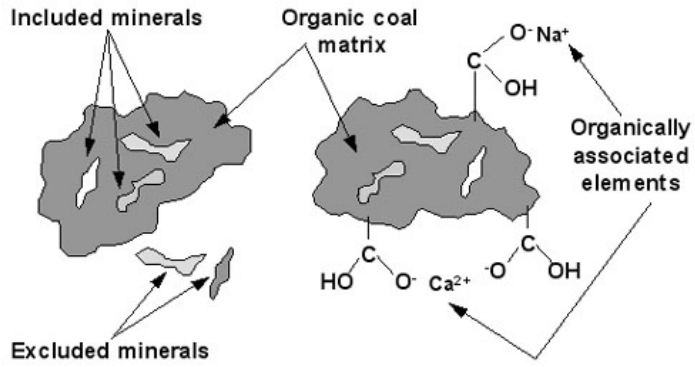

Figure 2-6**.** Types of ash-forming elements association in solid fuels [25].

Organically bound inorganics are a part of organic structure of the fuel and can be either ionically (metals) or covalently (non-metals) bound with fuel matrix. In case of metal ions they are mostly associated with oxygen containing anionic, organic functional groups such as e.g. carboxylic acids (-COOH), which can act as bonding sites for metal cations such as e.g. Na^+, K^+, Ca^{2+} [10, 25, 32]. The metal cations can be also bound with more complex structures of organic oxygen functional groups known as chelates. Organically bound non-metals, such as Sulphur, Phosphorous and Chlorine are covalently associated with organic phase of the fuel. The abundance of organically associated metals decreases with increasing coal rank, due to lower presence of oxygen containing functional groups in higher rank coals. Correspondingly, the inorganic constituents which belong to this group are rather dominant in biomass fuels. Typically the organically associated metal ions bound to anionic organic groups of biomass consist of K, Na, Ca, Mg and present in a minor fraction Mn, Fe and Al,

whereas covalently bound non-metals include mostly P, Cl and less common in biomass S [33].

Dissolved salts include generally simple dissolved salts (e.g. NaCl, KCl) in pore water of the solid fuels including coals and biomass, but also salts dissolved in biomass plant fluids. Amongst the most common metals cations present are: K, Na and Ca whereas anions may include Cl-, HPO_4^{2-}, $H_2PO_4^-$, SO_4^{2-}, $Si(OH)_4$ [33].

Mineral inclusion present in solid fuels, can be either closely bound with the organic fuel matrix (included minerals) or not, being individual mineral grains (excluded minerals). This group of inorganics is dominant for coals and includes mostly clay minerals (often contaminated with K, Na, Ca etc.), silicates and other Ca-,Fe -based minerals [10, 32]. As already mentioned the minerals have contaminated coals through geological processes or have been precipitated during the growing phase of the biomass, or else during harvesting, handling and processing of the fuels. Included minerals commonly found in biomass are quartz (SiO_2), calcium oxalate (CaC_2O_4), iron oxide or hydroxides ($Fe(OH)_3$) [33]. The foreign minerals derived from the processing of biomass or waste can include for instance iron and alumina phosphates present in sewage sludge resulting from the phosphorus precipitation in wastewater treatment plant. Other waste derived foreign impurities in waste fuels (e.g. such as PVC) can be metallic aluminum, Pb, Zn and Cu depending on the source of solid fuel.

The organically associated inorganics and dissolved salts can be analytically determined by the use of chemical fractionation methods which are based on a leaching procedure of the fuel elements in aqueous solutions that is gradually made stronger [33, 34]. The inorganics speciation in woody biomass determined by leaching is illustratively shown in Figure 2-7.

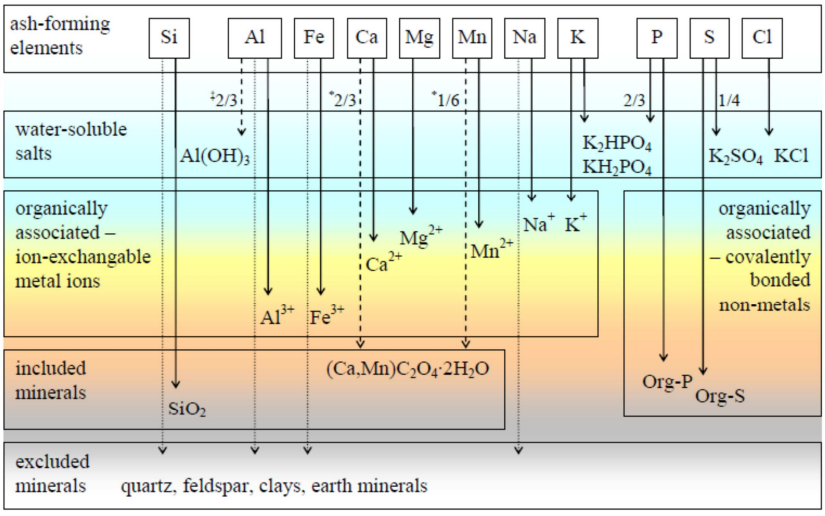

Figure 2-7. Types of ash-forming elements association in wood biomass fuels (Werkelin [34]).

To obtain the quantitative information on minerals found in coals, in terms of the mineral types, they mode of occurrence and size distributions, the Computer Controlled Scanning Electron Microscopy (CCSEM) method is commonly used [32, 35].

2.5 Ash Content and Composition

Ash-forming species (or inorganic constituents) present in solid fuels are transformed during fuel combustion into fly and bottom ash. Since a determination of the ash content is a quite simple process under laboratory conditions, it became one of the basic standard properties to characterise the fuel quality.

Ash content amongst the volatile and moisture content in fuel as well as calorific value belongs to the standard proximate analysis of solid fuels. Besides the proximate analysis, the ultimate analysis is usually performed, which includes the assessment of C, H, N, S, O (as difference) elements content in fuel. Major classes of components characterising fuel quality recalculated for different reference fuel states are shown in Figure 2-8.

Regarding the ash content measurement standards, the representative amount of fuel is slowly heated in laboratory furnace in air until it attains a constant mass representative of the remaining incombustible matter. It is then weighted. The ashing temperature for coals is 815^{o}C whereas for biomass is lower (550^{o}C) in order to minimise volatilisation of inorganic material [26]. The drawback of this process is that all inorganic constituents associations with the fuel are destroyed.

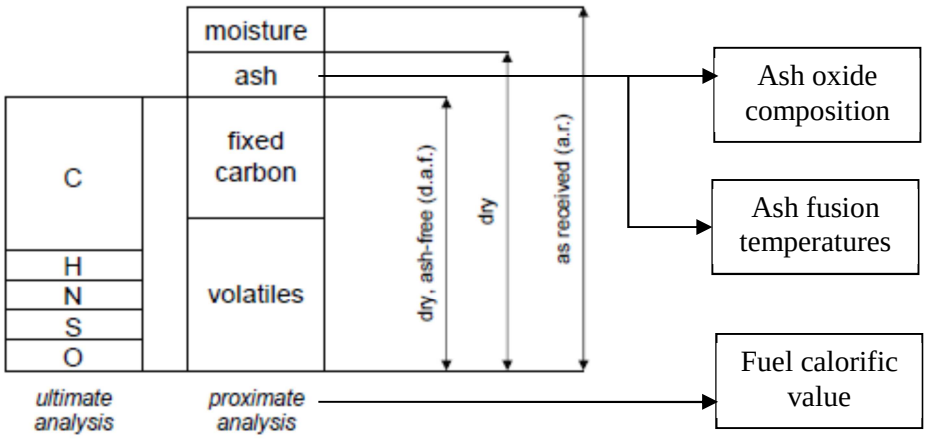

Figure 2-8**.** Standard characterisation of quality of solid fuels.

The elemental composition of ashes is then determined, using inductively coupled plasma-atomic emission spectrometry (ICP-AES). Then, as typical for coals, elements are recalculated to obtain oxide composition in their highest oxidation state, including commonly 10 oxides: $SiO_2+Al_2O_3+TiO_2+Fe_2O_3+CaO+MgO+Na_2O+K_2O+P_2O_5+SO_3 = 100$.

In case of determining elemental composition for biomass fuels, it is suggested to carry out a wet digestion of raw biomass prior to using the ICP-AES technique instead of biomass ashing. It is due to concerns of potential loss of inorganic material during the ashing process [15, 26].

The oxide ash composition is a basic measure of ash quality which allows the assessment of the composition of mineral matter as well as roughly assesses the slagging/fouling propensity of fuels with the use of empirical correlations. Another standard predictive method to assess the ash behaviour is based on the measurements of the ash fusion temperatures. These methods are described in more detail and critically evaluated in Chapter 3.

2.5.1 Ash Content Variations in Solid Fuels

The ash content in the solid fuels can very significantly and depends upon the conditions of fuel formation/coal rank and other processes such as mining, harvesting or handling of fuels. The relation between the ash content (on dry basis) and volatile amount (dry ash free basis) throughout a wide range of coal ranks originating from Poland, from brown coal to anthracite, as well as various biomass types (wood, bark, various straw types) and sewage sludge feedstocks is shown in Figure 2-9 [36]. The performed analysis revealed a trend in increasing ash amount (on dry basis) and its variation with lowering coal rank for higher volatile content coals, with the exception of biomass fuels. Amongst the analysed fuels, the lowest ash content was observed for high-volatile biomass (woody biomass, bark, straw) and very low-volatile anthracite coal.

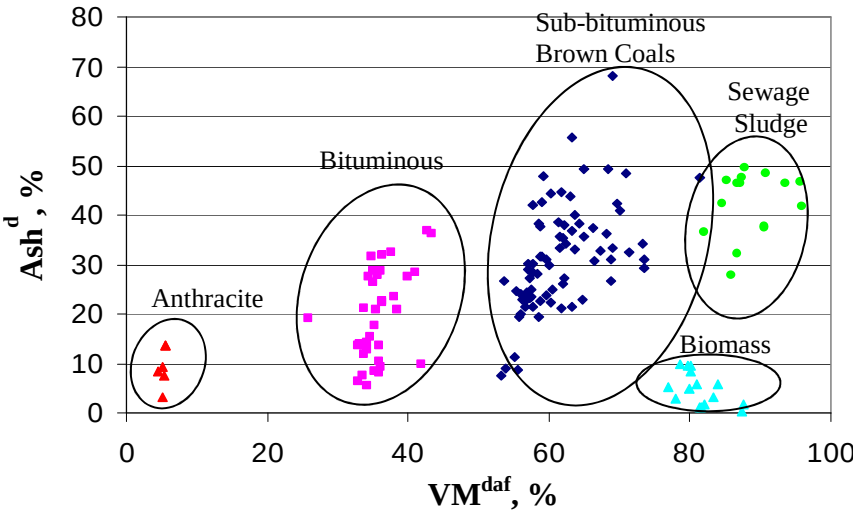

Figure 2-9. Relation between ash content (dry) and volatile content (daf) for various quality coals, biomass and sewage sludge fuels (Modified after Ferens [36]).

For biomass fuels the ash content (on dry basis) varied between less than 1 % (some woody biomass) to 10% (straw) whereas for anthracite coal up to 20%. In case of sewage sludge the dry ash content ranges between 30-50%. The ash content for bituminous coals was in a range of a few percentages to almost 40%. The highest variations in the ash amount were observed for the samples of brown coal, ranging from a few percentages to approximately 50%, in some extreme cases approaching 68% of dry ash content. In the high energy density anthracite and bituminous coals, most of the detected carbon was found to be in a carbon fixed form (C=70-95% in coal on "daf" basis). In case of a highly volatile biomass and sewage sludge the carbon concentrations varied between 45-55% (on "daf" basis) indicating the presence of carbon in a volatile form.

2.5.2 Ash Composition of Trade vs. Native EU Coals

The composition of coal ashes can vary significantly throughout the coal ranks but also can differ widely from mine to mine or seam to seam for a given coal rank. In general, the oxides which dominate in the coal ashes consist of SiO_2, Al_2O_3, SO_3, CaO and Fe_2O_3 whereas the remaining part is below 10% in the ash. A comparison of the ash oxide compositions and ash melting temperatures (defined in Chapter 3 sec. 3.2.1.) of typical imported hard coals used nowadays for power generation in Europe with the indigenous UK and Polish hard coals as well as brown coals originating from Germany, Poland and Greece is shown in Table 2-2.

Low rank coals, such as brown (lignite, sub-bituminous) coals typically have increased amount of alkaline earth metals which may be higher than the iron content ($CaO+MgO>Fe_2O_3$) in the ash (defined here as a lignitic type ash) [19]. However, this observation is not always apparent for other coals within the rank, since e.g. brown coals from the Turów (Poland) mine are characterised by the opposite relation. Furthermore, some bituminous coals, i.e. those originated from South Africa have higher content of alkali-earth metals than iron in their ashes and would have a lignitic nature according to this category. With regards to silica and alumina elements, both of them dominate in the ash composition of coals ($SiO_2+Al_2O3>50\%$) and the increased content of these elements is usually associated with the higher ash content in coals.

Currently, the UK is increasingly dependent on imported coals to fuel their coal-fired power plants with the percentage of indigenous coals share below 40%. The UK bituminous coals are usually enriched in iron and can have additionally low or increased calcium content which lower their melting temperatures as compared with other coals (see Table 2-2).

Table 2-2. Ash oxide compositions and standard ash fusion temperatures of typical trade coals in comparison with the UK indigenous coals and brown EU coals.

	Imported Bituminous Coals						UK Bituminous Coals					Brown Coals		
Fuel Name	RUS	COL	SA	US high S	IND	PL	UK-K Low-Si	UK-D Low-Si	UK-T Low-Si	UK-K High-Si	UK-D High-Si	GR-P	GER-H	PL-T
Ash^{db} %	11.9	9.7	13.9	8.5	3.59	12.6	4.2	4.4	5.2	15.0	11.2	36.11	4.3	29.5
SiO_2, %	55.6	61.8	43.7	43.5	25.6	46.8	31.4	36.8	34.3	47.8	47.0	31.07	1.3	55.0
Al_2O_3, %	24.5	21.1	34.0	22.6	7.50	21.8	17.6	23.9	23.8	26.8	25.5	12.85	1.5	24.1
TiO_2, %	0.8	0.9	1.7	1.06	0.37	0.7	0.6	1.1	0.9	1.1	1.1	0.67	<0.1	1.1
Fe_2O_3, %	**7.15**	6.6	3.0	**21.2**	**11.2**	**9.6**	**23.2**	**11.2**	**26.3**	**16.6**	**14.1**	**7.69**	**18.6**	9.3
CaO, %	3.15	2.2	**7.2**	4.03	**14.3**	**5.8**	**12.5**	**12.0**	**3.3**	**1.3**	**6.4**	**38.92**	**35.8**	3.4
MgO, %	0.88	2.1	2.2	0.84	4.80	3.5	0.6	2.5	0.7	1.1	3.0	4.45	16.3	1.5
K_2O, %	1.40	2.4	<0.5	1.59	**0.88**	**3.1**	1.5	0.5	1.4	3.5	1.6	0.83	<0.5	1.7
Na_2O, %	1.03	1.1	0.4	0.84	**7.10**	0.8	**4.2**	**1.5**	**5.9**	**1.7**	0.8	0.38	0.7	1.1
P_2O_5, %	0.57	0.2	1.0	0.27	0.03	0.3	6.6	<0.3	<0.2	0.2	0.5	0.26	<0.5	-
SO_3, %	3.0	1.6	6.3	3.50	27.5	6.6	2.6	12.9	3.1	-	-	2.83	20.0	2.8
∑	98.08	100.0	99.5	99.43	99.28	99.0	100.0	100.0	99.7	100.0	100.0	99.95	95.3	100.0
IDT, ^oC	1290	1250r	1390r	1070r	1080r	1182r	1040r	1240r	1060r	-	-	1238	1310r	1250r
HT, ^oC	1425	1305r	1480r	1210r	1120r	1210r	1080r	1270r	1090r	-	-	1250	1350r	1350r
FT, ^oC	1460	1410r	>1500	1300r	1140r	1350r	1110r	1320r	1220r	-	-	1280	1350r	1480r

Ref. Imported Bituminous Coals: Russian (RUS) [37], typical Colombian (COL) [38], South African (SA) [39], US-high Sulphur [40], Indonesian (IND) [41], typical Polish (PL) [38]. UK Bituminous Coals: Kellingley -low silica (UK-K, Low-Si) [39] and -high silica (UK-K, High-Si) [42]; Daw Mill -low silica (UK-D, Low-Si) [39] and -high silica (UK-D, High-Si) [42]; Thoresby -low silica (UK-T, Low-Si) [39]. Brown Coals: Greek coal [43], German Rhenish coal [39], Polish Turów coal [38]. Ash Fusion/Melting Temperatures: IDT – initial deformation temperature, HT- hemispherical temperature, FT- flow temperature, "r" denotes reducing atmosphere; for more see Chapter 3, section 3.2.1.

The amount of silicates can vary in the ash, from the low to high silica presence, and is related with the low or high ash content, respectively. Slagging, fouling and corrosion problems were encountered when firing UK indigenous coals [9]. It was established that iron and calcium play important roles as fluxing elements of alumino-silicates in these coals.

Nowadays, the most common trade coals-fired in European power plants are as follows:

- Intermediate alkalis content Russian, Colombian and Polish coals. These coals may have ashes additionally enriched in both the iron and calcium content (Russian and Polish coals) which may lead to increased slagging and fouling issues. In these coals the chlorine content may vary widely up to high levels especially for Polish coals.
- Low alkalis but with increased calcium content South African (SA) coal. This good ash quality coal is commonly utilised to decrease the amount of alkali metals in coal blends, and thus reduce fouling propensity. However, depending on the calcium and iron content combustion of SA coals may also lead to increased slagging issues, producing highly reflective Ca-silicate/clay based deposits [44].
- US-high sulphur coals. This coal has an increased iron content which is associated mostly with pyrites (Fe_2S). It has been reported to have a high slagging propensity; therefore its contribution is relatively low in typical imported coal blends [10, 44].
- Low ash, high iron/calcium/alkalis content Indonesian coals. Combustion of such coal blends have been reported not to lead to increased ash deposits but to increase their sintering tendencies [45].

2.5.3 Melting Tendencies of Biomass Fuel Ashes

As already mentioned, the chemistry of biomass ashes can vary significantly depending on the biomass origin, cultivation, harvesting and handling process. The ash oxide compositions of various biomass and waste fuels used for combustion are compared in Table 2-3. In general, the following groups can be identified as follows [18]:

- **High silica and alkalis rich ashes**, **with low melting temperatures**. These include most of agricultural straw residues, excluding cereal grains and oilseed rape straw which are enriched in phosphorous and calcium, respectively. Potassium is also abundant in energy crops of grass nature such as switch grass, reed canary grass, miscanthus. Due to the increased risk of slagging and fouling, the straw co-firing shares in a blend with coal fired in pf boilers typically do not exceed 20th% according to Danish experience [46].

Table 2-3. Ash oxide compositions and standard ash fusion temperatures of typical biomass fuels.

	High Si / High K			High Calcium			High Phosphorous		
Fuel Name	Straw	Miscan-thus	Olive pulp	Saw-dust	Willow	Rape Straw	Poultry litter	MBM	Sewage sludge
Ash^{db} %	3.30	1.7	8.1	0.8	2.0	3.8	22.4	15.2	32.3
SiO_2, %	42.00	48.7	41.10	21.33	4.82	2.61	16.0	4.22	22.66
Al_2O_3, %	0.40	1.04	5.94	2.35	0.72	0.5	1.70	0.29	12.78
TiO_2, %	0.02	0.07	-	0.17	0.05	0.04	0.20	0.03	0.69
Fe_2O_3, %	0.20	2.24	5.75	2.95	1.32	0.46	2.40	0.61	**16.84**
CaO, %	14.0	14.1	12.80	**44.44**	**37.2**	**36.9**	**24.0**	**48.65**	**13.81**
MgO, %	2.60	3.48	9.53	7.69	5.7	2.42	11.0	1.67	3.11
K_2O, %	**21.00**	**20.3**	**10.70**	**13.76**	**14.0**	**13.9**	**10.0**	0.68	1.78
Na_2O, %	0.30	0.34	**6.46**	0.91	0.26	0.8	3.40	**6.19**	1.71
P_2O_5, %	4.20	3.31	2.81	3.13	11.9	4.02	**25.0**	**34.16**	**25.42**
SO_3, %	5.0	3.47	3.59	3.27	2.39	8.8	5.20	-	1.18
CO_2, %	1.80	1.31	-	-	20.3	27.5	-	-	-
Cl, %	0.65	0.63	-	-	0.61	1.15	-	-	-
∑	92.17	98.99	98.68	100.0	99.27	99.10	98.90	96.50	99.98
IDT, ^{o}C	870	850	1020	1270	>1500	1480	1113	1370	1000
HT, ^{o}C	1050	1080	1120	1410	>1500	1490	1179	1700	1150
FT, ^{o}C	1240	1120	1140	1430	>1500	1500	1368	1700	1180

Ref: Straw [47], Miscanthus [48], Olive pulp [40], Sawdust [49], Willow [48], Rape Straw [48], Poultry litter [40], MBM [40], Sewage Sludge [49].

- **Low silica and high calcium ashes**, **with high melting temperatures.** These originate from various woody biomass fuels which have the lowest ash content amongst all solid fuels e.g. forest residues, sawdust but also high calcium content rape straw and energy crops of the woody nature such as willow. Fuels in this group may additionally include increased contents of phosphorous and alkali metals which decreases their melting temperatures. Currently, due to recognised low ash impact of woody biomass, full biomass conversion projects to run pf boilers on woody biomass have been reported [50].
- **Phosphorous-rich biomass/waste fuels.** Ash melting behaviour of phosphorous-rich solid fuels is very complex and depends on the concentrations of other elements, such as potassium, calcium, magnesium but also iron and alumina. Depending on the fuel ash chemistry the low melting K-rich phosphates and higher melting K-Ca/Mg phosphates can be formed. Cereal grains are relatively high sources of phosphorous, potassium and magnesium. High calcium and phosphorous ashes include most manures, poultry litters and animal wastes. The dominant mineral present in meat and bone meal is hydroxyapatite (melting temp. 1670^{o}C), a constituent of bones: also high contents of easily soluble alkali metals are also present in this animal residue. The phosphorous is also abundantly present in the low melting point ash of sewage sludge, in the form of iron, calcium or alumina phosphates, depending on the type of phosphorus precipitation agents used during the water treatment process. Typically, the shares of sewage sludge or MBM do not exceed 4th% when co-firing with coal in pf boilers based on German experience [30].

2.6 Ash Deposition Process in PF Boiler

Fireside ash deposition on the heat transfer surfaces is a very complex chemical and physical process which involves the four most relevant steps, such as: i) releasing of the ash-forming elements from solid fuels during combustion and mineral matter transformation to form ash particles, ii) transport of the ash particles to the surfaces, iii) adhesion to the surface, and, iv) consolidation of the deposit.

2.6.1 Release of Ash Forming Elements

After injection of the pulverised fuel with entrained air into flame of the boiler, the fuel particles heat up rapidly (at the rate of up to approximately 10^{6} ^{o}C/s) and dry at first. This

rapid heating of the fuel particles is caused by radiation and mixing with hot gases which may approach the temperatures as high as 1600°C. After this, the devolatilisation of organic species from the fuel occurs and the released organic gases will start to burn, followed by char burning. Simultaneously, during the devolatilisation but also char burning stage of fuel, ionically or organically bound inorganic species (such as K, Ca, P, S and Cl) are released forming inorganic vapours [18, 32]. Depending upon how they are released and during which phase of combustion (i.e. devolatilisation or char burning), a part of inorganic vapours may be recaptured by the mineral inclusions [18].

The remaining, not vaporised mineral inclusions will undergo a series of overlapping physical and chemical processes, such as phase transformations, fragmentation, melting and coalescence of the mineral matter [32, 51]. The degree of the mineral transformation and amount of generated molten phase depends on several factors. These include the minerals chemistry and their association with fuel (included/excluded minerals), their residence time in high temperature zones as well as the presence of reducing/oxidising conditions [32].

The overall process of coal particle combustion resulting in the formation of fly ash takes less than 2-3 seconds, usually producing fly ash with the bi-modal particle size distribution as schematically shown in Figure 2-10.

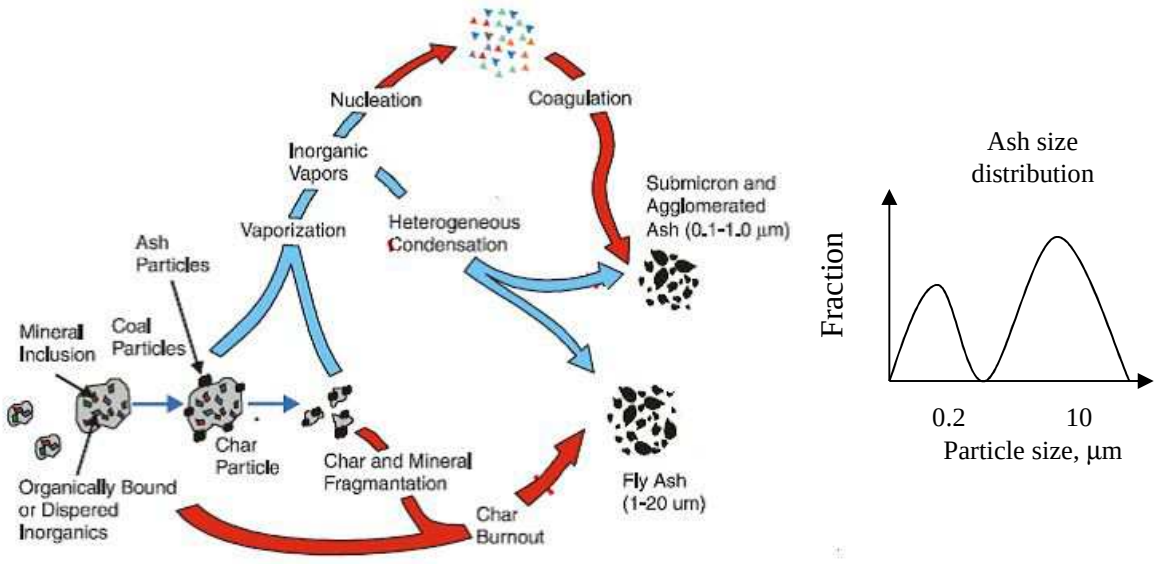

Figure 2-10. Ash formation during combustion of solid fuels [32].

The formation of larger particles (with diameters above 1.0 micron) is associated mainly with the fragmentation and coalescence of the mineral matter whereas the vaporisation, and then heterogeneous condensation and/or homogeneous nucleation of inorganic vapours are responsible for a generation of submicron particles [18, 32, 51]. In case of coal combustion,

the percentage of produced sub-micron ash is relatively low (typically 1.0wt%) in comparison with combustion of biomass fuels rich in a highly volatilised ash-forming elements.

2.6.2 Minerals Transformation and Salts Formation

Amongst the most crucial inorganic species responsible for slagging are: iron-, calcium-, potassium- based minerals, including alumino-silicates whereas the release of alkaline-earth (Ca, Mg) and alkali metals (Na, K) from the fuel may enhance fouling [10].

Iron can exist in many forms in coal minerals (as sulphide, carbonates and oxides); however, the most common form of occurrence is pyrite (FeS_2) either existing in inherent or/and extraneous mineral matter, which has been identified as a key factor determining slagging propensity of coals. On the one hand, during coal combustion conditions the extraneous pyrite decomposes to pyrrohotite (FeS) and rapidly forms an iron sulphide melt (Fe-O-S) before a full oxidation under reducing conditions [10, 52]. Therefore, extraneous pyrite can play a role in slag deposits initiation, especially in fuel rich zones around the burners, prior to complete mixing and fuel burn-out. On another hand, the inherent pyrite is more likely to be captured by alumino-silicate slag lowering its melting temperature and viscosity, therefore extending ash deposition to the furnace outlet heat transfer sections.

Transformation of Ca-based minerals, abundantly present in brown/lignite coals, and their likely interaction with alumino-silicates, can significantly increase slagging, even more when iron is involved forming low melting eutectics. In IFRF studies on slagging and fly ash formation when firing blends of sub-bituminous coals, the likely in-flame interactions between minerals were identified [53]. These included interactions between Ca- (dolomite and calcite) and Fe-rich (pyrite) minerals with clay minerals (kaolinite, aluminosilicate and illite) and quartz, leading to formation of Ca-Al-Fe-silicates. Calcium can be also organically associated with the coal matrix, and then released during combustion forming submicron CaO particles which can be either captured by alumino-silicate slag or be further sulphated to form calcium sulphates ($CaSO_4$). Under reducing conditions the mixtures of $CaSO_4$ and CaS can be formed, which have an eutectic melting temperature of 850^{o}C.

As far as alkali metals are concerned, the potassium is mostly present in coal as a constituent of clay minerals whereas sodium usually exists in form of sodium chloride which can be easily released from the fuel. Several studies confirmed that increased presence of sodium chlorine, or organically bound chlorine in coal can intensify the release of potassium from silicates to the gas phase whereas the highly volatile sodium is partly recaptured by the fused ash particles enhancing the slag generation [10]. The alkali metals present in biomass

are usually in easily soluble forms, thus very reactive. When released into the gas phase, alkali metals in the presence of sulphur oxides will form sodium/potassium sulphates which then accelerate fouling in the convective pass of pf boilers, by generating sticky layers on the tube banks and deposition of other non-sticky ash particles. As far as sulphation of alkali gas species is concerned, theoretically there are two possible routes, which are still debated in the research community. According to the first theory, alkali sulphates (e.g. K_2SO_4) are formed in the gas phase, and then subsequently condense on the heat transfer surfaces or lead to increase formation of aerosol particles. The second route considers deposition of alkali chlorides or hydroxides (KCl, KOH) first, followed by a subsequent sulphation of these alkali species within deposits [15].

Phosphorus based salts or minerals can be additional important players which influence the melting behaviour of ashes by a generation of glassy-amorphous particles under pf conditions [10, 30]. The source of low melting phosphate salts (composed of the $CaO{-}K_2O{-}P_2O_5$ oxides) can be agricultural or food industry residues [14]. Other P-rich ashes can originate from burning sewage sludge whose inorganics composition is likely to fall within the low melting eutectic of the $CaO\text{-}P_2O_5\text{-}Al_2O_3$ oxides system [31], or else can form low melting iron phosphates.

2.6.3 Ash Transport and Deposits Formation

The typical processes involved in the ash particle transport to the surface include inertial impaction, diffusion and thermophoresis [32, 33]. The contribution of each process depends on local chemistry, aerodynamics, and boiler operating conditions. According to Bryers [18] the mode transport of fly ash to the heat-transfer surface is preliminary inertial impaction for particles over 10μm and thermophoresis and diffusion for particles 10μm and smaller. The rate of inertial impaction depends on targeted geometry, particle size distribution and gas flow properties. Diffusion and thermophoresis are the process of particle transport in gas due to local concentration and temperature gradients, respectively. There are three type of diffusion defined which describe the movement of molecules to the surface, namely, Fick diffusion-mass transport due to a concentration gradient, Brownian diffusion-random movement of small particles and Eddy diffusion-movement due to turbulent flow effects [33, 51]. All transport processes are strongly influenced by the tube orientation in the gas flow, point of contact on the tube, wall effects, and location in the bundle.

The development of subsequent layers of deposit on the tube banks being a part of a superheater is illustrated in Figure 2-11. Once the ash particles hit the surface it may adhere to

it or rebound. Adhesion can occur either with van der Waals forces or through the stickiness of the molten particles to the surface. Other gaseous inorganic compounds such as e.g. alkali salts can diffuse to the surface and condensate directly on the colder surface [33]. As already mentioned earlier, this leads to formation of the sticky, inner layer of deposits, which then accelerates the accumulation of other particles impacted the tube banks.

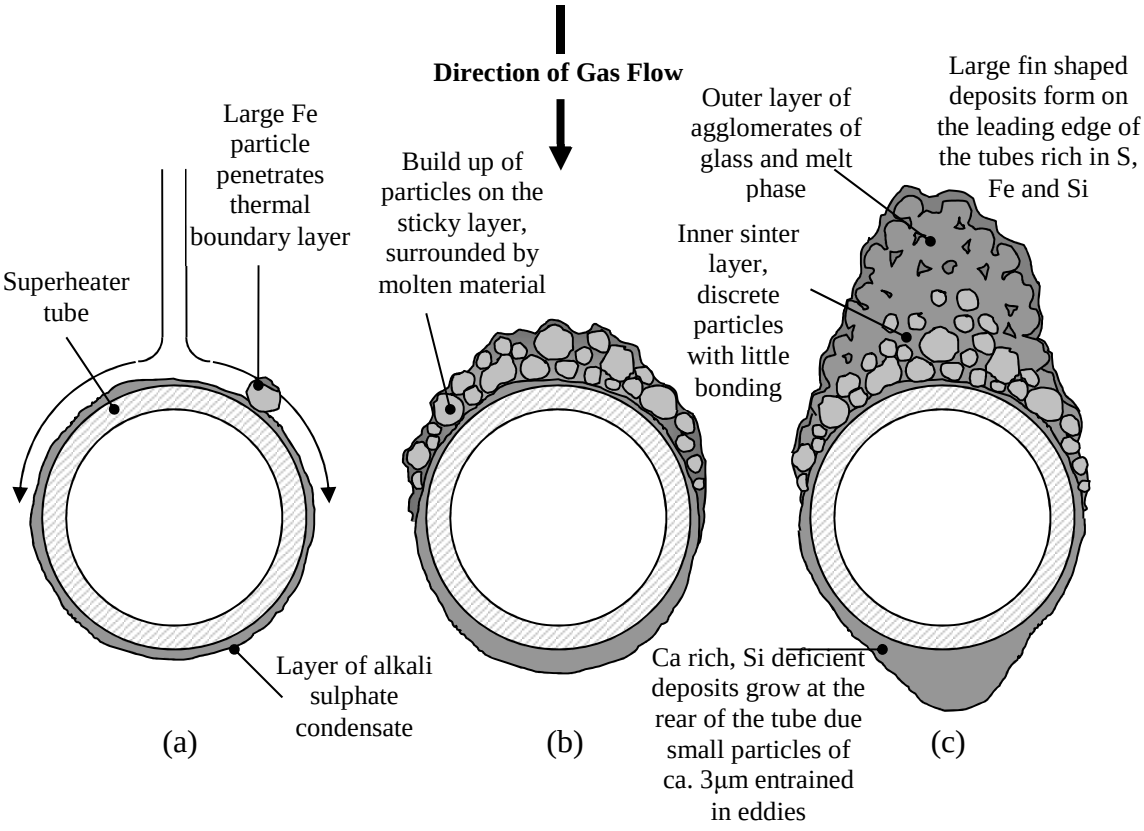

Figure 2-11. Deposit build-up process to the superheater tube [18, 54].

Due to deposit growth the insulation effect of deposit layer occurs creating a temperature gradient throughout the deposit. In time, the outer deposit surface may reach its initial melting temperature. The presence of liquid phase accelerates the sintering and consolidation of deposited material. The deposit is growing until either it reaches the final melting stage at which the viscous slag flows down the surface (typical for furnace wall deposits) or else the heavy deposits will drop down due to the gravitation force acting on them, or soot-blowing system activity.

2.6.4 Corrosive Nature of Ash Deposits

Corrosion of heat-exchange surface in boilers occurs normally at a rate between 8-10 nm/h, of tube wastage but at worst conditions can be as high as 600 nm/h. Corrosion is highly intensified by the presence of reducing conditions (e.g. effect of applied low-NOx emission

firing systems) and by combustion of chlorine, and alkalis rich biomass, coals (Cl > 0.2%) and wastes [18]. In general, corrosion can be induced by sulphur and/or chlorine species.

Sulphur induced corrosion is usually related to formation of corrosive complex sulphates with low-melting temperatures able to interact with tube metal, or else, can be associated with formation, in reducing conditions, of iron sulphide deposits [18]. In the first case, deposited alkali sulphates (such as K_2SO_4, Na_2SO_4) which have generally high melting temperatures (K_2SO_4, 1069^oC) have to be further sulphated with the presence of SO_3. This may lead to formation of low melting alkali pyrosulphates ($Na_2S_2O_7$, 389^oC, and $K_2S_2O_7$, 404^oC) which can then interact with the protective layer of iron oxide and create alkali-iron trisulphates ($Na_3Fe(SO_4)_3$, $K_3Fe(SO_4)_3$). An important factor in this process is availability of SO_3 in the flue gas surrounding corrosive deposits which can be possibly released locally from the molten deposit outer layer or during a catalytic oxidation of SO_2 with the aid of iron oxide. Due to the range of melting temperatures of those complex sulphates, they may occur on the furnace walls as well as on the superheat/reheat steam sections.

Another type of sulphur induced corrosion is related to formation of iron sulphide deposits which may lead to corrosion of the furnace walls. Impingement of the flame into furnace walls, the presence of pyrites (Fe_2S) in coal and reducing conditions are the main factors facilitating this type of corrosion. Pyrite decomposed in reducing conditions and the released H_2S interact with the metallic iron and produce a FeS layer which loses its protective properties thus enabling diffusion of ion metals to occur [18].

Chlorine induced corrosion can be either associated with formation of gaseous chlorine (i.e. HCl, Cl_2) and further interactions with tube metal, or else deposition of alkali chlorides and formation of solid deposits involving tube metal, or at worst case formation of low-temperature melting eutectics [15, 33]. There are several theories explaining the mechanisms of chlorine induced corrosion which are still debatable. In general, it is agreed that gaseous or ionic chlorine penetrates the protective metal oxide layer and then reacts with metallic Fe and Cr forming Fe-, Cr chlorides which are highly volatile. Metal chlorides diffuse back through the material and form again oxides, close to the outer surface of tube where a higher partial pressure of O_2 exist. This cyclic process leads to a high degradation in the structure of tube material by forming cracks and pore inside the protective oxide layer. Formation of molten chlorides enhance contact between deposit and metal surface intensifying interaction between them, and thus increasing corrosion rates [15, 33].

2.6.5 Fuel Additives

In order to minimise ash deposition/corrosion issues various fuel additives potentially can be used. They can be classified into two following groups [15, 33, 55]:

- Additives which influence gas K-S-Cl chemistry and thus aerosols formation. Alkali metals can be captured by various minerals, for instance alumino-silicate based minerals (e.g. kaolinite, betonite, bauxite etc.) including coal ash (eq. 2.3) or else, by mono-calcium phosphate forming more stable and still high melting species (eq. 2.2). On the other side, alkali chlorides can be transformed in the gas phase to alkali sulphates which have higher melting temperatures, and thus are less corrosive (eq. 2.1). Easily decomposable sulphates used for this purpose may include e.g.$(NH_4)_2SO_4$, $Al_2(SO_4)_3$ or $Fe_2(SO_4)_3$) [55]. Sulphur present in coal can reduce chloride formation from biomass co-firing.

- Additives which can change the physical and chemical properties of deposited ash making it easier removable by soot-blowing system. An example of such additive is copper oxychloride, $3CuO{\cdot}CuCl_2{\cdot}4H_2O$, which was reported to reduce slagging when utilising iron rich UK coals, producing a soft friable deposits [10]. The volatilised in flame additive condenses then on the surface of fly ash or in the open pores of sintered slag deposits, affecting the crystallisation of iron phases. This results in generating a more open structure in slag deposits and consequently a lower mechanical strength [10].

$$2KCl(g) + SO_3(g) + H_2O(g) \rightarrow K_2SO_4(g) + 2HCl(g) \quad (2.1)$$

$$2KCl(g) + Ca(H_2PO_4)_2(s) \rightarrow CaK_2P_2O_7(s) + 2HCl(g) \quad (2.2)$$

$$2KCl(g) + Al_2Si_2O_5(OH)_4(s) \rightarrow 2KAlSiO_4(s,l) + H_2O(g) + 2HCl(g) \quad (2.3)$$

Although fuel addtives may help to mitigate ash-related issues, this is usually not the most cost-effective option, therefore a proper optimisation of coal/biomass blend can give more profits for a power generator.

2.7 Summary

Slagging and fouling are very complex phenomena which depend upon many factors related with the fuel nature, boiler design and operation. In case of coal combustion the ash behaviour in boilers is mostly dictated by coal minerals which undergo in flame transformation and melting whereas for the majority of biomass fuels, especially those originating from plants, the ash-forming vapours are responsible for initiating slagging and fouling. It was established that coarser fly ash particles are formed during coal combustion, for which the inertial impaction is a dominant mechanism of ash deposition. When co-firing of biomass, the fraction of sub-micron ash and aerosols increases, and other ash mechanisms such as condensation and diffusion become more important. The released inorganic species from biomass can be recaptured in the furnace by coal minerals or other Al-Si-based additives used for this purpose. Optimum composition of the coal/biomass blend may reduce the risk of ash deposition.

Nowadays, much more focus is on utilising imported hard-coals blends, also in a mixture of various biomass types. In comparison with bituminous coals, the ash composition of low rank coals vary significantly and apart from the alumino-silicates is typically more dominated by calcium, magnesium and iron capable of accelerating slagging whereas coals enriched in sodium may lead to fouling. In case of biomass, their low melting ashes were found to be composed mainly of silicates and potassium (as typical for straw), or else potassium phosphates (animal/agricultural residues). The less ash-troublesome biomass appears to be woody biomass due to its low ash content whilst being enriched in calcium, and thus being a high melting point ash.

Conventionally designed pulverised fuel boilers are not suitable to run 100% on alkali-rich biomass such as straw or other agricultural residues. Special boiler designs are needed which enable the lowering of the furnace exit gas temperatures to avoid slagging and fouling. These should include adequate water-wall surface area or parallel heat exchange surfaces but also efficient soot-blowing system to remove deposited material. Grate-firing or fluidised bed boilers, with emphasis on the latter, appear to be the most adequate for biomass combustion at smaller scale.

Optimisation of coal/biomass blends to minimise slagging and fouling seems to be the most appropriate way forward but is also very difficult to achieve for pf boilers. It is due to non-additive behaviour of such fuel blends. Therefore, proper predictive tools need to be developed and critically evaluated which is the major goal of this research.

3

REVIEW OF SLAGGING/FOULING PREDICTIVE METHODS

The main purpose of this Chapter is to provide an outline of the research methods used for predicting ash behaviour and to justify the procedures employed for the development of a predictive model which is attempted in a further part of the Thesis. Firstly, the evaluation of the empirical, still widely used methods is conducted. This is then continued to highlight the new trends in the development of alternative, more objective and accurate experimental techniques. Secondly, along with the experimental methods, more sophisticated modelling tools are discussed. These include the combinations of the phase equilibrium analysis–based approaches with the ash deposition mechanistic models. Finally, a brief introduction into the zone furnace models is conducted, followed by presenting applications of the more comprehensive CFD models used for simulating ash deposition in boilers. The goal is to review and evaluate various methodologies that can be used to predict ash deposition in pf boilers fired with coal and biomass. As a result, the concept of a generic, universal and reliable slagging/fouling prediction tool is proposed.

3.1 Introduction

There are a number of methods used to evaluate ash behaviour, in terms of predicting slagging and fouling propensities of solid fuels. A large number of the developed methods are associated with the continuous need to find a relatively simple, fuel flexible and reliable approach. In general, the following methodologies are in use:

- Standard laboratory methods used to determine the chemical composition and fusion temperatures of laboratory prepared ash;
- Simple empirical indices that utilise ash composition (or inorganic constituents speciation) data to assess the slagging and fouling propensity of coals;
- Non-standard laboratory methods based on the more objective measurements of the physical properties of ashes which change during the ash sintering or fusion process;
- Mechanistic modelling approaches capable of predicting the ash formation, transport and deposit growth;
- Advanced thermodynamic models which predict the slag/liquid, solid and gas phase distribution of the ash under equilibrium conditions over a wide temperature range;
- Comprehensive computational fluid dynamics tools which combine the complex aerodynamics typical of a boiler with basic mechanisms of ash deposition.

All of these techniques have some advantages and limitations, which will be briefly discussed in the following sections.

3.2 Experimental and Empirical Approaches

3.2.1 Ash Fusion Test vs. Non-standard Alternative Methods

The ash fusion standard test (AFT) is based on the observations of the ash sample that changes its shape (due to i.e. deformation, shrinkage or flow) during the gradual temperature increase in a laboratory furnace [10, 56, 57]. The exact procedure and the initial shape of the ash samples can differ (e.g. pyramidal or cylindrical shape) depending on the world standard used (ISO 540, 1981; DIN 51730, 1984; ASTM D1857, 1987; AS1038.15, 1987) as shown in Figure 3-1a [57]. In spite of its subjective nature, AFT is still the most common method used to estimate the slagging/fouling propensities of solid fuels. Several temperatures are defined which characterise the fusion state of the ash sample during heating. Initial deformation temperature (IDT/DT), in other standards (e.g. DIN 51730) can be called the softening temperature (ST), is regarded as an onset of ash sintering process. In this state the ash sample starts to lose its original shape, which can be associated with the first occurrence of liquid

phases. It is then followed by the further slag formation when the sample reaches the shape of a half of sphere (defined as the hemispherical temperature - HT), or becomes completely molten (fluid temperature - FT). Although the ash fusion test is still the most accepted basic method to assess ash slagging propensity, it is also widely criticised in the literature. Its poor accuracy and repeatability especially in determining the first IDT/DT are documented elsewhere [56, 58]. The measurements performed by three independent laboratories revealed the differences between measured IDT/DT, as large as 400°C between the same coal samples [56].

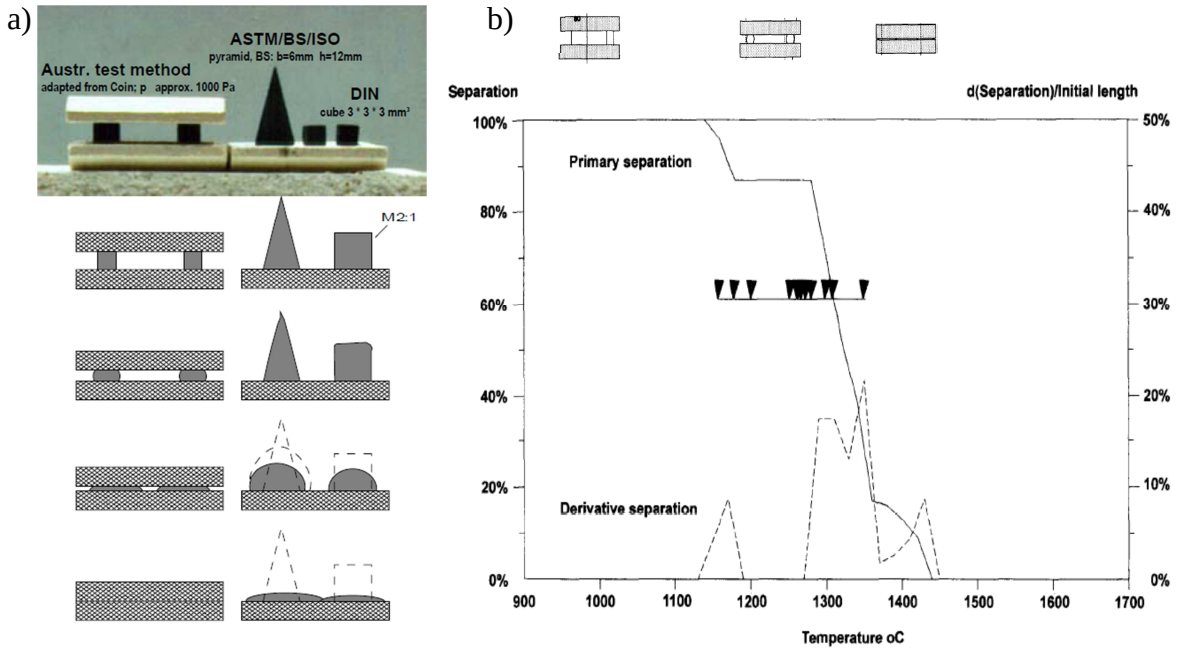

Figure 3-1. Ash fusion standard test vs. non-standard Australian shrinkage-based test: a) Ash fusion characteristic temperatures defined based on the sample geometry change during the heating process [57], b) Comparison of the new method with the IDT temperatures obtained for the same ash analysed in the different laboratories [59].

Due to abovementioned high uncertainties in determining the first-initial deformation temperature of ashes more objective methods have been developed. They are based on the precise measurement of physical properties that change during the sintering and melting process of ash. The most common are different kind of shrinkage, electrical resistance or thermal conductivity measurements and compression strength-based tests [10, 56, 57, 60].

According to the Frenkel sintering theory [10, 61], formation of particle-to-particle bonding leads to the contraction and closure of pores which results in reduction of porosity, decrease in bulk size and strength development of the ash sample. As a consequence the enhanced conductance or decreased resistance can be detected in the sintered ash samples. These changes of the ash physical properties are highly accelerated with the first appearance

of liquid phases. In the thermal conductivity test, the ash sample is placed between two reference materials with known thermal conductivity, and then the heat flux is measured while heating the sample [10, 56]. The sintering temperature is defined, as a temperature at which the thermal conductivity of the ash samples increases markedly.

The results obtained with the aid of the non-standards methods have been reported to improve, in many cases, the predictions of the fuel ash behaviour for both the fluidised bed and pulverised fuel fired combustion systems. Skrifvars [62, 63] used successfully the compression strength-based test to predict fluidised bed agglomeration when burning biomass fuels.

Wall *et al.* [56, 64] developed penetration/shrinkage-based thermo-mechanical method and applied it to evaluate slagging/thermal performance of several coals obtaining reasonable agreement between formulated indices and field observations gathered for the investigated pf boiler of 600 MW capacity.

Hansen and co-workers [15, 58] used the simultaneous thermal analysis (STA), which combines the thermo-gravimetric analysis (TGA) with the differential scanning calorimetry (DSC), to investigate the melting, evaporation or dehydration of transforming inorganic material. Experiments conducted for pure fuels, namely, straw and coal, and its blends revealed the presence of melting phase well below (max. 150°C) the corresponding IDT temperatures.

Although the non-standard methods give more insights into a better understanding of the ash transformation/fusion processes, and in many cases improved indications of slagging/fouling propensities of ashes have been reported, there are still some issues that should be resolved. These are related with the origin of the ash samples tested, which are usually produced in laboratory conditions that are not the same as found in utility boilers. More importantly, during these tests the heating rates and heat fluxes acting on the ash sample are dissimilar to those conditions existing in boiler's furnaces.

3.2.2 Slagging/Fouling Indices

Indices used to assess slagging and fouling tendencies of coals have been developed since the 1960s and are usually constructed based on the analyses of the ash fusion, viscosity and ash chemistry. The most commonly applied indices are defined and summarised in Table 3-1. Reviews on variety of these indices were carried out by Bryers [18] and Couch [16].

Most of the slagging/fouling indices have been developed for coal combustion and are usually limited to the range of coals considered. The most common index utilises the ratio of

base to acid (B/A) oxides identified in the ash to assess its melting behaviour. Based on the ash fusion measurements of several coals studied (i.e. Zelkowski [65]) there is a certain ratio of B/A oxides, between 0.4-0.7, in which a low temperature melting slag occurs due to existence of a low melting eutectic region. This B/A index was then more specifically applied to the high-sulphur US coals to assess their slagging tendencies by taking into account the sulphur content in coal, which may indicate the pyrites presence. As far as fouling is concerned, the sodium content in the coal was recognised as the major fouling influencing fuel-factor, therefore sodium impact is accounted for in most fouling indices developed for coals (e.g. (B/A)xNa_2O).

Table 3-1. Summary of key empirical correlations for slagging and fouling.

Index	Formula	Slagging or Fouling Propensity			
		Low	Medium	High	Severe
Slagging Propensity [38]					
Base-Acid Ratio	$B/A = \frac{Fe_2O_3 + CaO + MgO + K_2O + Na_2O}{SiO_2 + Al_2O3 + TiO_2}$ for lignitic ash*	<0.4 or > 0.7		0.4 to 0.7	
Slagging Factor	$B/A \times Sulphur\ in\ coal\ (dry\%)$ for bituminous ash*	<0.6	0.6 to 2.0	2.0 to 2.6	> 2.6
T_{25}, °C. Temperature at which the viscosity of ash is equal 25 Pa*s.	$T_{25}\ ^oC = \left[\frac{M \times 10^6}{\lg(25) - C}\right]^{0.5} + 150$, where C = 0.0415xSiO_2+0.0192xAl_2O_3+ +0.276xFe_2O_3+0.0160xCaO-3.92 M = 0.00835xSiO_2+0.00601xAl_2O_3-0.109	>1400	1400 to 1245	1245 to 1120	<1120
Iron-Calcium Ratio	$\frac{Fe_2O_3}{CaO}$	<0.3 or > 3.0	0.3 to 3.0		
Iron plus Calcium	$Fe_2O_3 + CaO$	<10%			
Slagging Index, °C	$\frac{4 \cdot (\min IT) + (\max HT)}{5}$	>1340	1340 to 1230	1230 to 1150	<1150
Silica Percentage	$\frac{SiO_2 \times 100}{SiO_2 + Fe_2O_3 + CaO + MgO}$	72-80	65-72		50-65
Fouling Propensity					
Fouling Factor [66]	$B/A \times Na_2O\ in\ the\ ash\ (\%)$ for bituminous ash*	<0.2	0.2 to 0.5	0.5 to 1.0	>1.0
Sodium content [67]	Na_2O % in the ash for bituminous ash*	<0.5	0.5 to 1.0	1.0 to 2.5	>2.5
	Na_2O % in the ash for lignitic ash*	<2.0	2 to 6.0	6 to 8.0	8.0

Note:* Bituminous ash, when Fe_2O_3 > (CaO+MgO); Lignitic ash, when Fe_2O_3 < (CaO+MgO).

Other ash parameter used commonly to evaluate the slagging potential of coals is related with the assessment of slag viscosity, or more precisely with the temperature (T_{25}, see Table 3.1) at which the slag reaches the viscosity of 25 Pa*s (when the ash can be easily removed from the bottom of combustor [18]).

The more advanced indices that utilise more detailed fuel ash data derived from the CCSEM and chemical fractionation analysis were developed by Benson *et al.* (for the US coals [68]) and Gibb (UK coals [9]). Although these indices have been found to be valid for coals of a specific origin, there are also other studies in which the limited applicability of them were reported, especially for the blends composed of different coal ranks [69].

The indices developed for coals are of less value for biomass fuels since the biomass ash chemistry differs significantly. In case of biomass fuels, the most common index is based on the molar ratio of (Na+K)/(2S+Cl) elements present in the fuel. If this ratio is lower than 1.0, it indicates the presence of enough S and Cl to yield low melting alkali sulphates and chlorides [70]. Furthermore, according to the performed experimental studies by Krause *et al*. [71], it is generally agreed, that if the S/Cl molar ratio in the fuel is larger than 4.0, there is far less risk of chlorine induced corrosion. Another useful index utilises the ratio of silica and alumina to alkali metals in the fuel (Si+Al)/(Na+K) allowing the assessment of the potential of the silica/alumina based ashes or additives (e.g. kaolinite) for capturing alkali metals to avoid formation of alkali sulphate/chloride aerosols [72].

Due to the complexity of the ash-forming elements interactions and non-additive ash behaviour, the development of universal indices for various fuel chemistries is virtually impossible without the use of more sophisticated tools based on the phase equilibrium calculations. Furthermore, the boiler related factors, such as a local geometry, aerodynamics and thermal conditions, should be also possibly considered when comparing slagging/fouling propensities of various fuels and their blends.

3.3 Ash Behaviour Mechanistic Models

Most of the ash-related models that aim to describe the complex process of fuel inorganics transformation and behaviour under conditions existing in boilers are of a mechanistic nature. In these models the attempt is made to provide descriptions of some or all of the subsequent processes, starting from the combustion and ash formation process, particle transport phenomena, particle impaction and adhesion, through the deposit growth and the effects on the heat transfer. In this subsection, a brief overview of the above phenomena is presented

highlighting the key factors or parameters that play an important role when simulating the ash deposition process as a whole.

3.3.1 Ash Formation Models

The current ash formations models are capable of predicting fly ash particle size distribution and composition (Beer *et al.* 1992 [73]), Wilemski *et al.* 1992 [74] , Yan *et al.* 2001 [75], 2002 [76]). However, these models require detailed input on the physical and chemical properties of fuel regarding the inorganics speciation and their association with fuel matrix (included/excluded minerals) which are derived by CCSEM and chemical fractionation analyses. In some concepts, e.g. in model developed by Wilemski and Srinivasacher [74] the Monte Carlo techniques is used for redistributing additionally the internal mineral grains in coal particles before simulating the fly ash formation. More comprehensive ash formation models take into account the mineral coalescence and char fragmentation, but also fragmentation of the excluded minerals. The general scheme of this process is illustrated in Figure 3-2. Coalescence of inclusions within the coal matrix minerals is described by char shrinkage and fragmentation sub-models [73-76]. There are various stages of mineral coalescence processes considered with a rate depending upon the char structure, in terms of a relative shell thickness of the char censophere but also related with the coal diameter size and mineral volume fraction or fuel burn-out (Monroe *et al.* [77], Yan *et al.*, 2001 [75]). As far as fragmentation of excluded minerals in concerned, this is simulated by Poisson distribution method, except the identified quartz minerals which are assumed to not undergo fragmentation [73-76].

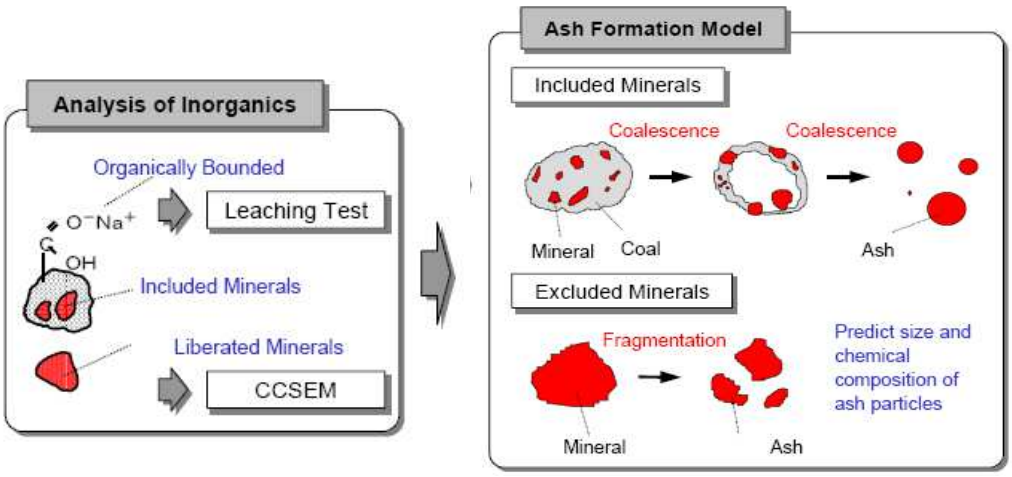

Figure 3-2. Ash formation modelling scheme for included and excluded minerals in coal matrix [78].

Christensen *et al.* (1998 [79], 2000 [80]) investigated gas-to-particle modelling approaches and developed a comprehensive plug-flow model applicable for straw-fired

boilers. The developed Christensen model utilises formulas describing the homogeneous nucleation, growth by multicomponent gas-to-particle conversion, and coagulation of spherical particles. The phase equilibrium calculations including the kinetics rates were used to assess the local gas composition. Although the model predictions, in terms of fine particles (K-Na-Cl-S) and HCl(g) SO_2(g) concentrations in the flue gas, agreed quite well with the experimental results when firing high-K biomass, such as straw, the model was far less accurate for other types of biomass, especially those with high Na content, which affected the gas S/Cl chemistry.

Doshi *et al.* (2009 [81]) investigated the development of a modelling approach to predict ash formation when co-firing of biomass with coal. As input into the model the speciation of inorganics in biomass and coal was required, which was derived from the chemical fractionation or pH leaching method. Based on the phase equilibrium calculations the gas–to-particle formation was determined based on the defined saturation ratio for the homogenous and heterogeneous condensation cases. The predicted results revealed much higher condensation rates obtained for the heterogeneous condensation than is likely to occur on the heat exchange surfaces of boilers as compared with the low homogenous condensation rates predicted for the analysed biomass co-firing cases.

3.3.2 Ash Particle Transport and Deposition

Particle transport and deposition mechanisms responsible for the build-up of the ash deposits depend on the fly ash properties (such as particle size distribution and composition), flow pattern as well as the local physical conditions of the surface. A number of mechanisms influence the fly ash transport to the surface, amongst which the most important are included within the general ash deposition rate formula, as follows [82-84]:

$$\frac{\mathrm{d}m}{\mathrm{d}t} = I(t) + C(t) + TH(t) + BE(t) - SD(t) \qquad (3.1)$$

where, m is the deposit weight, t is the time, $I(t)$ is the inertial impaction which includes upstream side deposition by large sticky particles but also erosion effects, $C(t)$ is the condensation, $TH(t)$ express the thermophoresis forces, $BE(t)$ describes Brownian and eddy diffusion, $SD(t)$ is the shedding rate of deposits [83]. Additionally, the chemical reactions can also contribute to the deposit mass, for instance by the sulphation of the condensed alkali salts on the heat-exchange surfaces [82].

Inertial impaction is regarded as the single most important mechanism for the mass rate of deposition of large particles with a diameter above 10μm [51, 85]. Ash arrival rate onto

heat transfer surfaces (kg/m^{2}s) is proportional to the ash arrival velocity u_g (m/s), the particulate burden in the furnace C_{ash} (kg/m^3 of gas) as well as the impaction and capturing efficiencies [51, 82-84]:

$$I(t) = u_g \cdot C_{ash} \cdot n_{imp} \cdot \eta_{capt} \quad [kg/m^2 s] \tag{3.2}$$

The impaction efficiency of the particles flowing in the streamlines intercepted by a tube, was very well quantified and correlated by Rosner and Co-workers (1986 [86]), as being a function of the particle Stokes and Reynold's numbers. The value of the Stokes number needs to exceed 1/8 for particle in order to hit the cylindrical surface by the inertial impaction as shown schematically in Figure 3-3a

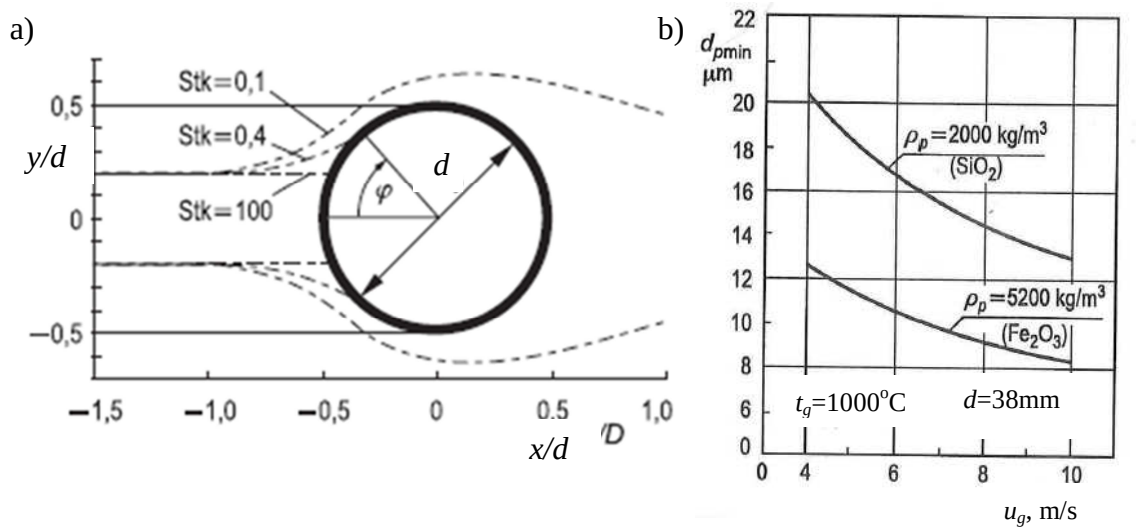

Figure 3-3. a) Particle trajectories in function of Stokes number [87], b) Minimal diameter of impacting ash particles in function of impaction velocity and density of mineral [87].

Assuming the Stokes number, *Stk* = 0.1 and after transforming the Stokes number function, we can obtain the formula describing the minimal ash particle diameter that can hit the cylindrical tube, as follows:

$$d_{p,\min} = \sqrt{\frac{1.8 \nu_g \rho_g d}{u_p \rho_p}} \tag{3.3}$$

where ρ_p is the particle density (kg/m^3), ρ_g is the gas density (kg/m^3), v_g is the gas kinematic viscosity (m^2/s), u_p is the velocity of the particle (m/s) and d is the diameter (m) of the cylinder, respectively. For the particle size of 20µm the value of the *Stk* is around 0.46 which corresponds to the impaction efficiency of about 0.2 [51]. Based on the derived functions for $d_{p,min} = f(u_p,\rho_p)$ as shown in Figure 3-3b, and for the assumed uniform size distribution of the arriving ash particles to the tube, it can be concluded that most of the arriving ash particles to

the tubes are of high density [87]. This is confirmed in practise, as usually more particles enriched in Fe_2O_3 are found in deposited material when firing coals.

The fly ash capture efficiency by the surface is associated with the physical state of the ash particles approaching the tube as well as the state of the tube surface itself, respectively. According to Sarofim [51] factors that govern the capture efficiency are incompletely quantified. These should include the kinetic energy of the impinging particles (Wibberley and Wall, 1982 [88]) but also the viscous dissipation, which is dependent upon the viscosity of the approaching molten particles as well as deposited material. Other relevant parameters are the surface tension, impact angle and impact velocity [89] which may all determine the particles energy to rebound [89, 90]. There a number of empirical formulas found in the literature which describe above mentioned phenomena [90]. Here, the relation of the capture efficiency with the fly ash sticking probability is analysed in some more detail, as it is the most commonly used. It combines the stickiness of the incoming ash particles with the stickiness of the deposit surface, as follows [51, 83, 84]:

$$\eta_{capt} = P_{stick}(T_p) + P_{stick}(T_s)\cdot\left(1-P_{stick}(T_p)\right) - K_e\cdot\left(1-P_{stick}(T_p)\right)\left(1-P_{stick}(T_d)\right) \qquad (3.4)$$

where T_p is the temperature of the particle (assumed to be equal to the temperature of the flue gas), T_d is the temperature of the deposit surface, P_{stick} is the sticking probability and K_e represents the erosion coefficient. The sticking probability is commonly expressed in as:

$$P_{stick}(T) = \begin{cases} \dfrac{\mu_{ref}}{\mu} & \mu > \mu_{ref} \\ 1 & \mu \le \mu_{ref} \end{cases} \qquad (3.5)$$

To assess the sticking probability, the reference critical viscosity μ_{ref} needs to be assigned above which the deposition of sticky fly ash particles is highly limited. In the literature there is not consistency in this matter and a value from a wide range between 10^4-10^8 Pa*s is chosen in different investigations. The typical flow viscosity of the slag is about 10^3 Pa*s and during the temperature drop the solidification occurs which may have individual character for the various ashes considered. In other works, Hansen *et al.* [83, 91] assumed, based on experiments, that the sticking probability increases linearly with the melt fraction in the fly ash approaching the tube banks. Although there large differences between the reference viscosity/adhesion criteria used, usually the assumed criteria have been found to agree well with the experimental results obtained for the different pilot-scale furnaces or deposition rigs

[90, 92, 93]. Nevertheless, the further, more fundamental investigations are still needed in this matter.

The theory behind the **condensation** of inorganic vapours or gas-to particle formation is very well developed, however when applying it into practise it becomes very complex, especially when the mixture of gases is considered [51, 85]. In a very simplified form, the mass flux of condensable species diffusing per unit surface area towards the outer surface of the tube can be calculated by the equation [82, 84]:

$$C(t) = k_{c,i} \cdot \frac{p_i - p_{s,i}}{p_g} \cdot \rho_g \quad [kg/m^2 s] \tag{3.6}$$

and the mass transfer coefficient of the ith component:

$$k_{c,i} = Sh \cdot D_i / d_t \, [m/s] \tag{3.7}$$

where ρ_g is the gas density (kg/m^3), p_g is the flue gas pressure (Pa), $p_{s,i}$ represent the saturation pressure of the ith component (Pa), $k_{c,i}$ is the mass transfer coefficient of the ith component (m/s), *Sh* is the Sherwood's number, D_i describes the diffusion coefficient (m^2/s), and d_t is the tube diameter (m). In the above formula, the mass transfer coefficient can be obtained based on the known correlations for the Sherwood's number valid for the cylinder in a cross flow [51]. Diffusion coefficients for binary mixtures can be relatively easily obtained, however this can be highly more problematic for the more complex gaseous mixtures. The concentrations of alkali vapors and their saturation pressures in wide temperature range can be calculated with the aid of phase equilibrium analysis tools or for less complex gaseous mixtures can be estimated using simple formulas as suggested by Tomeczek [84]:

$$\frac{p_s}{p_g} = \exp\left(A - B/T_g\right) \tag{3.8}$$

where the *A*, *B* are constants for a given salt and can be found in the literature [84]. With increasing temperature of the outer deposit surface, the saturation pressure increases which leads to decrease of the deposit growth due to condensation processes.

According to Sarofim [51] the turbulent deposition rate for particle deposition due to **thermophoresis forces** can be assessed from the same turbulent mass transfer coefficient as for the vapour, but including some corrections e.g. regarding the reduced diffusivity of the particles. In other studies, Baxter [82] adapted a functional form for the thermophoretic force which is based on applying a Knudsen number, expressed as a ratio of the gas mean-free-path to the particle diameter, as follows:

$$F_T = -6\pi\mu_g d_p f(Kn)\nabla T_g \tag{3.9}$$

where *f(Kn*) is a function of Knudsen number (Kn) and several material-specific properties. This functional form was derived based on the integration of particle-gas momentum exchange over the surface of particle, and was used also in other investigations with some success [82, 94].

The Brownian and eddy diffusion is in general a minor contributor to the overall deposition rate and its quantification is largely empirical [51, 81, 85]. The ash deposition rates derived by these transport mechanisms for submicron particles in a turbulent fluid can be found in studies performed by Wood *et al.* [95].

The shedding of deposits can be due to soot-blower activity but also due to natural gravity forces when deposits grow too much, or are heavily fused of low viscosity and thus are too heavy for the adhesive forces to support them, or else through the thermal expansion effects during the boiler shutdowns. The development of a 2D model for predicting natural shedding of deposits formed during straw firing was investigated by Zhou *et al.* [83] who also performed a parametric study on the impact of the local conditions and ash material properties change on the ash deposit formation.

An alternative to the already described approach used to assess the overall deposition rate was proposed by Yan *et al.* [75]. In this one-dimensional approach, the influence of a simple flow pattern inside the furnace is additionally included. Three different flow pattern zones are defined, namely: a fully turbulent core, a buffer layer and a boundary layer as shown in Figure 3-4. The major mechanisms considered in this study were the inertial impaction for larger particles, Brownian diffusion and thermophoresis for finer particles.

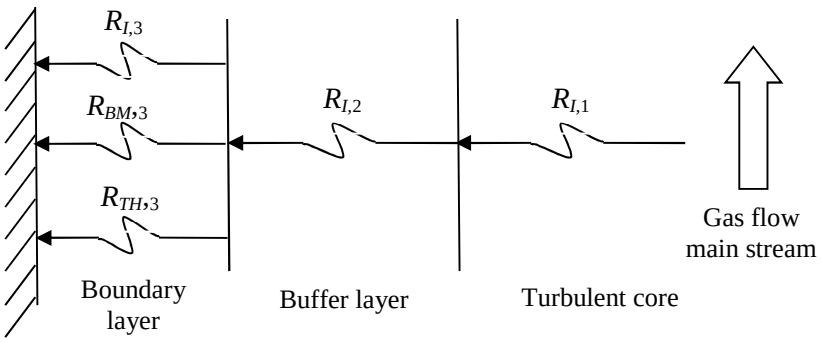

Figure 3-4. Diagram of main mechanisms for ash transport considered in a boiler's furnace [75].

In this model, it was assumed that in the boundary layer the Brownian motion and thermophoresis processes are the key contributors to the ash transport to the furnace walls. However, these processes can be neglected in the outer turbulent core flow and a buffer layer,

since the inertial impaction is dominant in these regions. Overall, the total resistance of ash transport R_{tot} can be defined based on the analogy with the well-known electric resistance formula, as follows [75]:

$$R_{tot} = \frac{1}{1/R_{I,3} + 1/R_{BM,3} + 1/R_{TH,3}} + R_{I,1} + R_{I,2} \tag{3.10}$$

where $R_{I,1}$, R_{I2} and $R_{I,3}$ are inertial resistances belonging to the turbulent core, buffer layer and boundary layer, respectively; $R_{TH,3}$ is the thermophoretic resistance in the boundary layer, and $R_{BM,3}$ the resistance for Brownian motion in the boundary layer. The details of these individual resistances are given elsewhere [75, 96]. The arrival velocity of ash particles is inversely proportional the total transport resistance R_{tot}. Ash arrival rate onto heat transfer surfaces (kg/m^{2}s) is obtained by multiplying ash arrival velocity (m/s) with the particulate burden in the furnace (kg/m^3 of gas).

3.3.3 Heat Transfer through Ash Deposits

The heat transfer controls the surface temperature of the ash deposit, determining the physical conditions at the deposit surface, e.g. when with increasing deposit temperature the liquid phase occurs. Furthermore, the deposit surface conditions influence the deposit build-up rate as well as the removal/shedding of deposits. Occurrence of partly molten deposits may lead to a more efficient particle capturing. However, once the deposits become completely molten they flow down the heat transfer surfaces. According to Mueller *et al.* [97], deposits may reach a steady state, a maximum layer thickness when the percentage of molten phase in the deposits surface does exceed 70%.

In this subsection the basic parameters affecting the heat transfer conditions during deposit build-up are briefly discussed. A more comprehensive review of the state-of-the-art modelling approaches was carried out by Zbogar *et al*. [98]. In general, the net radiative heat flux through the ash deposit layer can be expressed by the following equation:

$$\dot{q} = \frac{k_{eff}}{\delta_{eff}} \cdot (T_d - T_w) = \alpha \cdot (T_g - T_d) + \varepsilon_d \sigma_0 (T_g^4 - T_d^4), \quad [W/m^2] \tag{3.11}$$

where, (T_d-T_w) is the temperature gradient through the deposit layer ("*d*" denotes deposit and "*w*" wall/tube surfaces respectively), T_g is the flue gas temperature (K), δ_{eff} is the thickness of deposited material (m), k_{eff} express the effective thermal conductivity (varied between 0.5 to 2.0 W/m^2 depending on the porosity of deposits), ε_d is the deposit surface emissivity, σ_0 is the Stefan-Boltzmann constant and α is the convective heat transfer coefficient (W/m^{2}K).

The heat transfer parameters of prime interest related to the deposits are the effective thermal conductivity (which includes besides the conductivity also radiation through the deposit layer) and the surface emissivity of the deposit. The emissivity of ash deposits can significantly affect the heat absorption by the furnace walls, especially when enriched in calcium: then white and highly reflective deposits are formed [99]. In unsteady conditions, the heat transfer through a developing deposit layer is more complex, since the values of all critical parameters (such as the conductivity, porosity and emissivity) are changing during the deposit build-up process, due to the likely liquid phase presence which accelerates sintering of deposits.

The comprehensive literature study performed by Zbogar *et al.* [98] showed that there is still a need for a wide range of experimental data that would help in evaluating and improving the existing thermal conductivity models. Also, it is necessary to formulate more accurate models for the thermal conductivity of solid mixtures, in which potentially important sources of errors have been identified [98].

3.4 Importance of the Phase Equilibrium Analysis

The phase equilibrium modelling is a powerful tool of investigating the transformation and phase changes of chemical species in a multi-component system under specific temperature and pressure conditions. The thermodynamic state of system can be described by specifying temperature, T, pressure, p, the number of moles of each component, n_i, i = 1, . . . ,n_s in the system. The convenient energy function of these state variables is the Gibbs energy of the system $G = G\ (T,\ p,\ n_i)$, and the difference between two different states can be expressed as follows:

$$dG = -SdT + Vdp + \sum_{i=1}^{c} \mu_i dn_i \tag{3.12}$$

where, S is the system entropy, V is the system volume and μi is the chemical potential of component i. In terms of stimulus and response, the pressure difference drives the volume changes, temperature difference drives entropy changes and the chemical potential difference drives the mass transfer. Considering the system which is in thermal equilibrium (T=const), mechanical equilibrium (p=const) but not at chemical equilibrium hence allowing the mass transfer, the total Gibbs energy of a chemically reacting multi-component system at constant pressure and temperature is given by [100] :

$$G^T = \sum_i n_i \mu_i = \sum_i n_i \left(\mu_i^0 + RT \ln a_i \right) \tag{3.13}$$

where n_i is the number of moles of i, μ_i is the chemical potential of species i, μ_i^0 stands for the chemical potential at standard state for species i and a_i for the activity of pure species i. At the constant temperature and pressure, the Gibbs free energy of the reacting mixture reaches a minimum value (a stable state) resulting in the equilibrium composition [100].

$$G^T = \min \Rightarrow \left(dG^T\right)_{T,p} = 0 \qquad (3.14)$$

In order to minimise a set of the above obtained functions of the multicomponent chemical system the Lagrangian multiplier method is used [101].

Thermodynamic equilibrium analysis can be efficiently performed with the aid of FactSage™ thermochemical software and databases [102], or other commercially available tools, which are based on a minimisation of Gibbs free energy. Once the initial composition and pressure of the system are set, FactSage™ determines equilibrium concentrations of solid, liquid, and gas species over a specified temperature range. It should be noted, that the equilibrium concentrations are calculated independently at each temperature. Depending on the kinetics of the reactions occurred, these equilibrium concentrations may or may not be achieved.

There have been several studies reported in the literature in which the phase equilibrium calculations were utilised to investigate the ash deposition tendencies in solid fuel combustion systems [72, 103-106]. The general procedure scheme is schematically illustrated in Figure 3-5.

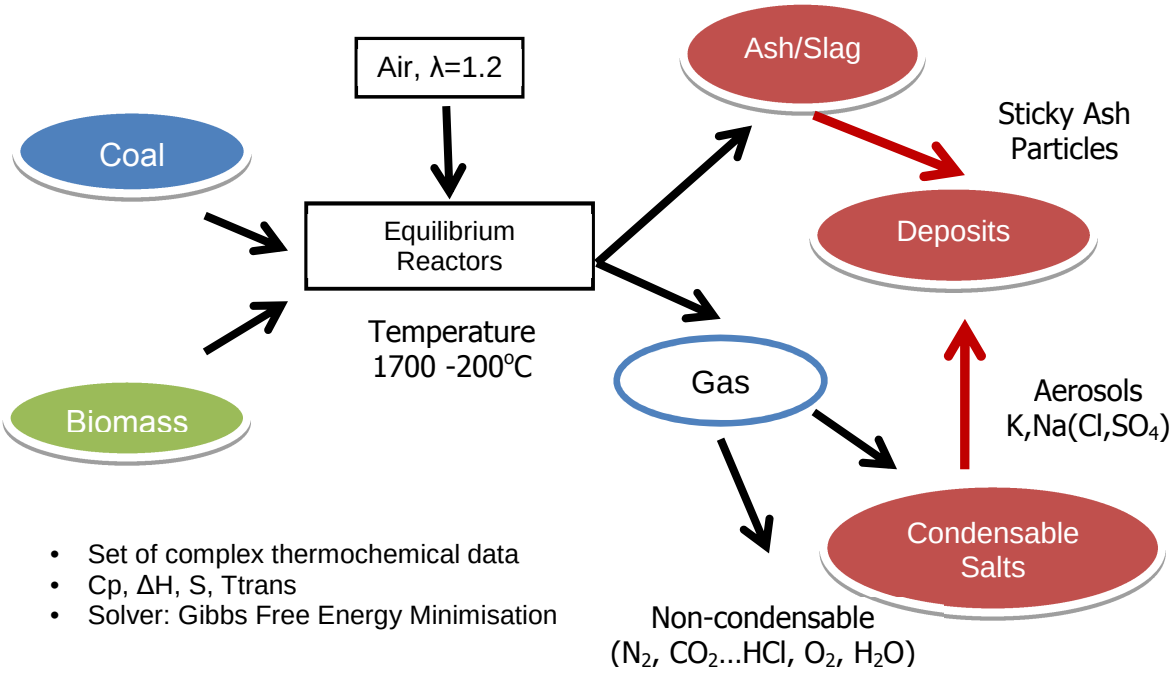

Figure 3-5. Application of the phase equilibrium analysis for the ash behaviour of solid fuels.

The available thermodynamic databases enables one to analyse, under high temperature conditions, the slag phase formation of complex alumino-silicates, but also the condensation (through the liquid/melt formation) of salts ((K, Na)(SO_4, CO_3, Cl, OH)) which are found commonly in solid fuels [102].

Due to the nature of the equilibrium analysis which does not consider kinetic as well as transport-mixing parameters, some additional approaches have been developed for various combustion systems. Gupta *et al.* (1998) [35] proposed the use of the availability coefficient which roughly describes the activity of the inorganic species under pulverised coal fired conditions. This coefficient utilises CCSEM and chemical fractionation fuel data, such as particle size distribution of the minerals and their association with the fuel matrix, to determine the minerals activities. Included minerals which encounter higher temperature and reducing atmosphere during coal combustion, therefore along with soluble salts and fine mineral matter have assigned the availability coefficient value of unity. Excluded minerals are assumed to be only partly reactive, and their availability coefficients are assessed based on the general formula, as follows [35]:

$$\mathrm{AC} = \frac{\sum n_i \left[1.0\left(r_i - \delta_i\right)^3 / r_i^3\right]}{\sum n_i} \tag{3.15}$$

where n_i is the mass fraction of excluded mineral in the size bin of radius r_i with δ_i its reactive thickness, and AC is the availability coefficient. The reactive thickness layer is assessed based on the experimental investigations: however according to Gupta it can be assumed to be less than 1.0μm [35]. The above defined AC coefficient determines the reactivity of the coal minerals when applying the phase equilibrium calculations.

In other studies, Zevenhoven *et al.* (2001) [106] used the data obtained from the chemical fractionation analysis of the fuel as an input to the phase equilibrium model applied to the thermal conditions of a fluidised bed boiler to investigate bed agglomeration risk and fouling. The fuel fraction that was leachable in water and acetate was expected to react with combustion products rapidly forming fly ash, thus approaching equilibrium, therefore, it was assumed to be a “reactive fraction” of inorganics (see Figure 3-6). The non-reactive fraction, which is leachable in hydrochloric acid or insoluble, was expected to form the bottom ash in FBC system. Both the fly ash and bottom ash behaviour was modelled based on the phase equilibrium calculations to identify equilibrium composition as well as melting temperatures of ashes, which were then successfully used to assess the bed agglomeration or fouling for various biomass fuels studied [105, 106].

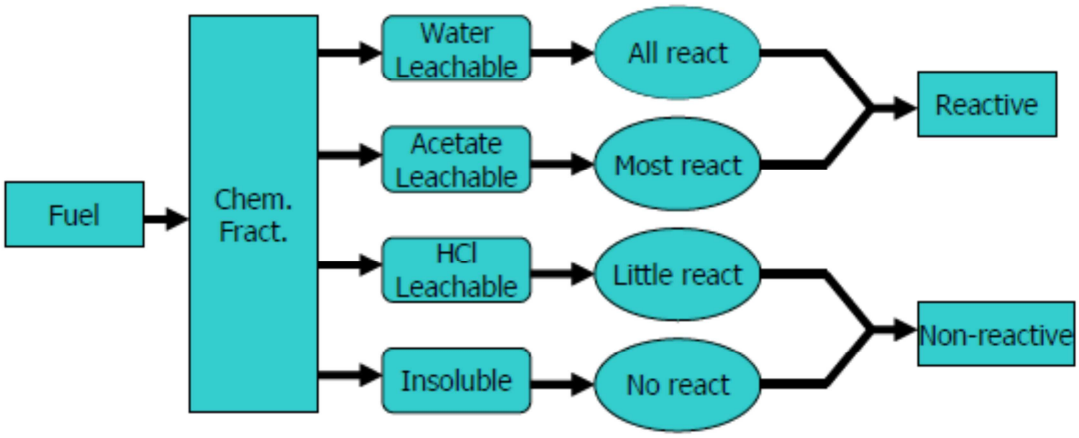

Figure 3-6. Chemical fractionation scheme for reactive and non-reactive ash fractions in fuel [104, 106].

Nutalapati (2007) [103] and Tortosa (2007) [104] used the modified phase equilibrium analysis schemes to investigate slagging and fouling in pulverised fuel fired boilers. This approach was based on laboratory investigations, which indicated that alkali ash compounds vaporise at elevated temperatures and can interact with the surface of nonreactive silica particles. This gives rise to low-melting temperature alkali silicates and contributes to the melt phase that occurs in the boiler. According to the obtained correlation trends presented in Figure 3-7, for the assumed the average thickness of the reacting layer of 0.3μm [103] and 10 μm size of non-reactive particles, this would correspond to around 15% on the volume or mass basis of the non-reactive particles. Such calculated percentage of non-reactive ash was assumed to reach equilibrium at high temperature (up to 1300°C) with water and acetate soluble inorganics (reactive ash).

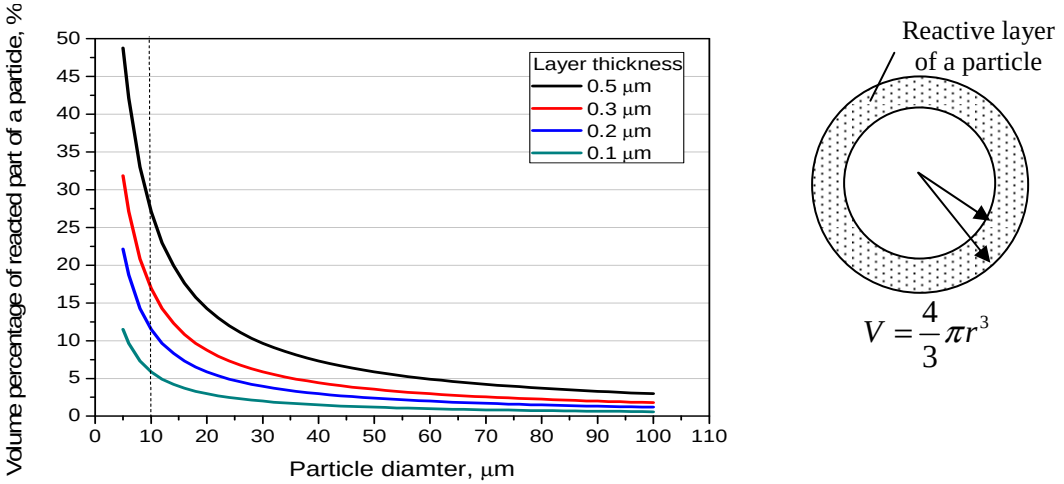

Figure 3-7. Volume percentage of reacted particle as a function of particle diameter and reactive layer thickness [103].

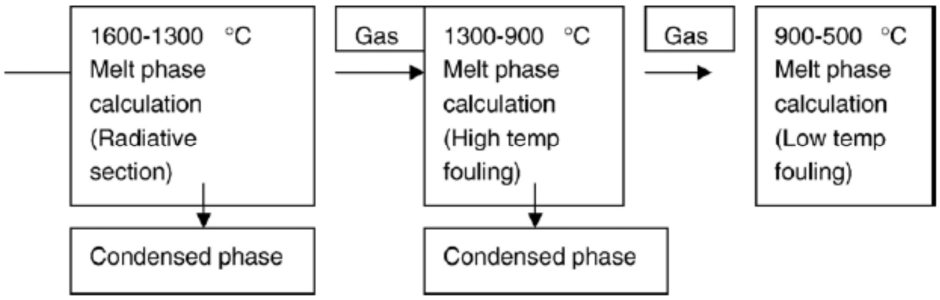

Figure 3-8. Nutalapati's simplified phase equilibrium algorithm for pf boiler conditions [103].

However, according to Nutalapati methodology, at the lower temperature range (below 1300^{o}C) only the fate of inorganic vapours is investigated as schematically shown in Figure 3-8. Two temperature ranges were defined in which the mass of the species condensed between 1300^{o}C and 900^{o}C; this was assumed to indicate fouling risk whereas the species able to condense between 900^{o}C-500^{o}C indicated low temperature fouling.

3.5 Towards Finding an Effective Predictive Furnace Model

Thermal conditions and flow pattern in a boiler furnace amongst the fuel characteristic are the key factors influencing the ash behaviour and deposition severity in boilers. Over the past 50 years several modelling approaches of different complexity have been developed that enable the assessment of boiler thermal performance including the impact of ash deposition. In general, two types of models can be distinguished, as follows:

- Zone based models are the precursors. These are relatively simple, flexible and thus rapid in response. In a one dimensional cases furnace is divided into one or several control volumes, in which radiation is the major mechanism of the heat transfer. Zone-based models are capable of predicting temperature distributions and heat fluxes within the zones. In multi-dimensional zone models the flow pattern is necessary to solve the total energy balance of the zones, which is simplified, prescribed or provided from the CFD calculations [107].

- Finite-difference models are able to calculate the flame temperature and other furnace variables in much finer resolution. Nowadays, these models are part of the computational fluid dynamic (CFD) commercial packages. They are able to predict flow, mixing, combustion, heat release and heat transfer based on the local conditions within the furnace and boiler. Its accuracy depends on the initial and boundary conditions, but also on grid fineness and turbulence model used [107].

They require large computational effort, therefore some other phenomena, such as i.e. ash deposition are typically simulated in post-processing calculations, when a converged steady-state solution is obtained.

3.5.1 Usefulness of the Zone-Based Models

The development of the zone method is largely due to the work (carried out in the 1950-60s) of Hottel, Cohen and Sarofim [108] who analysed the radiation heat transfer in an enclosure filled in with the flue gas. These methods over the years have been successively extended, and applied to the more complex geometries, ranging from a one-dimensional long-furnace model to multidimensional enclosures, and have been widely used in several industrial applications ranging from the gas-fired blast chambers [107] through to pulverised coal-fired furnaces [109, 110].

The concept of this method is based on a discretisation of the boundary surface and gas volume into a number of zones which are assumed to be of uniform temperature and have the radiation properties of the gas and surface. An energy balance is written for the each of zones, including the heat introduced with burning fuel, air and all the radiation arriving at the zone from all other zones within the furnace enclosure. In one-dimensional models the effect of the flow pattern may be neglected, opposite to multidimensional cases when the flow and heat release pattern is necessary to solve the total energy balance and has to be prescribed to obtain the mass transfer rates between each volume zone and other neighboring zones. The heat balance equations are solved iteratively for the gas temperature, which then allows the temperature distribution, heat flux on the heat surfaces and corresponding total values of radiation heat transfer between the zones to be determined.

According to the way radiative heat transfer is handled zone methods can be divided into three general groups: i) classical methods developed by Hottel and co-workers [108], ii) Monte Carlo probabilistic methods supporting Hottel's model when applied to the more complex geometries [111], and iii) simplified one-dimensional, Russian normative furnace models [112].

The classical method uses the precalculated radiative heat exchange coefficients for total energy balances, known as a directed flux areas (denoted as $\vec{GG}$, $\vec{GS}$, $\vec{SG}$ and $\vec{SS}$ for gas-gas, gas-surface, surface-gas and surface-surface radiation exchange, respectively). According to this theory, the radiation energy transfer between a pair of zones, e.g. between the gas volume enclosure (i) and surface (j) zones can be expressed as follows [107]:

$$Q_{i\leftrightarrow j} = \vec{G_i S_j}\,\sigma_0 T_{g,i}^4 - \overleftarrow{G_i S_j}\,\sigma_0 T_j^4 \tag{3.16}$$

where σ_0= 5.67*10^{-8}W/m^{2}K^4 is the Stefan-Boltzmann's constant and $T_{g,i}$ and T_j are temperatures of the gas and surface respectively. The thermal radiation balance of the surface zone is schematically shown in Figure 3-9a.

These direct flux areas (DFA), which are temperature dependent, include the effects of the total enclosure geometry, the non-grey absorption, the emissivity of combustion products and multiplied reflection. However, before DFA can be obtained, the more fundamental sets of exchange factors, namely direct exchange areas (DEA) have to be calculated. These exchange areas define the fraction of radiant heat transferred from one zone to another on the assumption that the surfaces of the surrounding enclosure are non-reflective [107]. Furthermore, these DEA are not temperature dependent, and can be easily applied for the basic zone shapes; their tabulated values are listed in [108]. More detailed description of the successive steps needed to transform the direct heat exchange areas into the direct heat flux areas can be found elsewhere [107].

The classical method described above is not flexible enough when dealing with more complex zone enclosures and handling the local dependencies of radiative properties. In such cases the use of Monte Carlo ray tracing method which is very versatile with respect to zone shape and arrangement can be very supportive as reported elsewhere [111]. This technique relies on algorithms of random sampling of a large number of discrete packages of energy (rays/beams) from each zone, which are then tracked to achieve a statistically significant measure of the distribution of the radiant heat (Figure 3-9b). However, in case of the multi-dimensional models the computer run time is more demanding since the computational effort of the exchange area calculations increases exponentially.

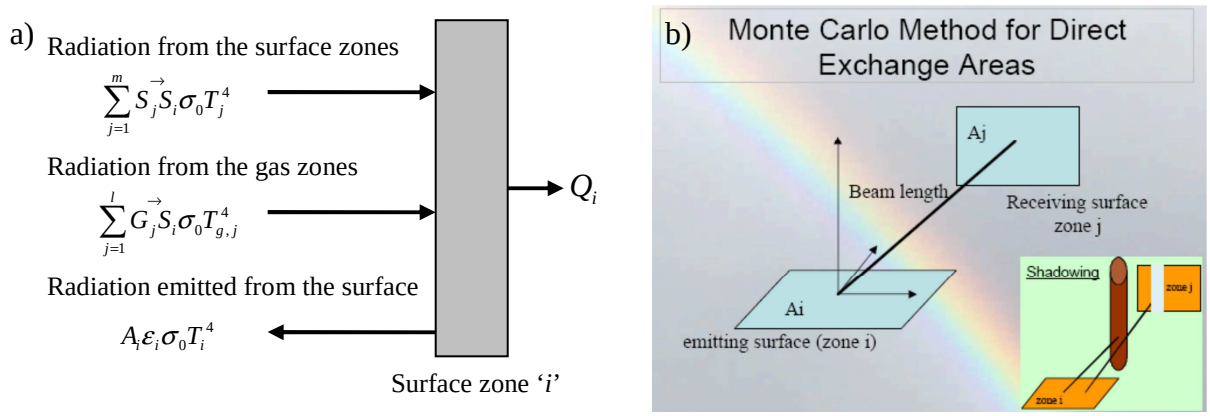

Figure 3-9. a) Thermal radiation balance of the surface, b) Monte Carlo method for calculating the direct exchange areas [113].

Although the Monte Carlo method is based on quite effective algorithms, the encountered difficulties with calculating the direct exchange areas for enclosures with participating media make this method more suitable for the gas-fired furnaces rather than pulverised fuel fired boilers. Nevertheless, a number of examples can be found in the literature that show the application of this method into large utility coal-fired boilers [114-119].

Lowe *et al*. (1975) [114] performed the sensitivity analysis of a zone method applied to a tangentially-fired pf boiler of 900 MW thermal input. The effects of different simple flow patterns variations, boiler load and ash content in coal were investigated. It was concluded that variations in the ash radiative properties has a dominating influence on the heat flux and temperature distributions, more relevant than the effect of flow pattern. Comparison of the simulation results with the measurements data gave relatively good agreement.

Blokh *et al.* (1992) [116] applied the 3D zone approach supported with Monte Carlo calculations to the brown-coal-fired pf boiler, with highly slagging tendencies. Although the flow pattern was assumed to be relatively simple, the more detailed ash deposits thermal resistance profile along the furnace determined from the measurements was included. The results obtained allowed to determine the rational conditions for burning slagging coals, and to develop an algorithm to evaluate degrees of smoke gas recirculation into different areas of the furnace chamber to obtain the highest intensity of heat exchange with minimum slagging of heating surfaces.

Hesselmann (1998) [117] developed algorithms to support the input data of the 3D zone model applied to a 300 MW_e pf boiler with the flow and axial heat release pattern provided by the CFD tools (Figure 3-10). The integration of CFD-based data within the zone model improved significantly model predictions of the heat fluxes as compared to real boiler data, and more realistic flame trajectories were obtained. Furthermore, this approach allowed more reliable and efficient studies on the impact of in-furnace NOx reduction methods on the boiler performance. However, in this work the uniform furnace deposition topography was assumed due to lack of proper data: thus a full validation of this model with respect to ash deposition impact could not be performed.

The different, more simplified/engineering concept of the one-dimensional zone model is illustrated by the Russian normative zone furnace method (standardised in 1973) [112]. In this approach, instead of the direct-exchange flux areas to handle the radiation heat transfer, the thermal efficiency factors are defined which express the ratio of absorbed to incident heat fluxes in the analysed zone. These factors, in a transparent way, describe the boundary conditions of the heat transfer inside the furnace, including the relation between the incident

heat flux, thermal resistance of the furnace walls and the radiative (absorptivity, emissivity) properties of deposits [120]. As a result, the impact of the ash deposition conditions or other sensitive parameters change on the heat fluxes and furnace performance can be potentially, relatively quickly, assessed.

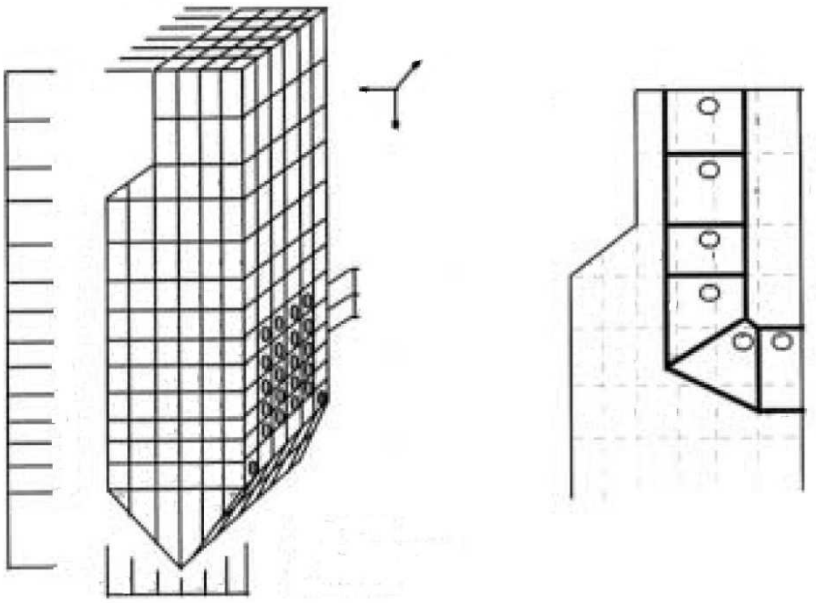

Figure 3-10. Three dimensional zone-based model of a pf boiler furnace including the platen superheater section [117].

Kuprianov *et al.* (2001) [119] applied the Russian normative method to determine the temperature and heat flux distributions for the furnace of a 500 MW_{th} pf boiler fired with high-ash, medium volatile bituminous coal under different operating conditions. In this work, Kuprianov proposed some improvements to the model by introducing more detailed thermal energy balances for the each burner row (now defined as a separate zone), and incorporating empirical correlations for the fuel burn-out profiles along the furnace height. This allows the simulation of the impact of staged combustion and reduced boiler loads of the individual burner tiers on the boiler performance. The numerical results were validated with some operational data obtained for different boiler's loads and fuel distribution patterns giving good agreement. Furthermore, the effect of various operating parameters, such as the effects of excess air and fuel particle size distribution were also studied to establish possible range of operating conditions that ensure the most efficient boiler operation.

The Russian zone method/model was successfully applied in a number of cases, and was recommended as a very powerful and efficient technique, to predict the thermal performance of combustion furnaces. These models vary in complexity depending on the number and arrangement of zones that subdivide the furnace. Some of them were also integrated with an on-line boiler performance monitoring tool [118]. Due to the uncomplicated nature of this

approach, the thermal characteristics of the furnace (temperature profiles, heat fluxes) can be obtained within a relatively short period of time and sufficiently accurate for engineering purposes [118, 119]. The advantages of this method are flexibility with respect to the furnace geometry and fuel type, including fuel mixtures, as well as potentially short computational time (a few minutes for a single case study) to optimise the model with respect to the fuel mixtures/air distribution.

As far as the accuracy of the zone-based method is concerned, according to literature reviews [119] this is estimated at about 3% (or 50°C for the temperature in burner zones) and 5% (or 60°C for the temperature at the furnace outlet) for various fuels and furnace types. For these industrial applications the predicted furnace characteristics are sufficiently accurate to be used for further calculations related to furnace design, retrofitting, or investigating the effects of fuel switching on thermal boiler performance.

3.5.2 Advanced CFD-based Modelling Approaches

Over the last two decades, a number of attempts have been made to apply more comprehensive CFD models to simulate ash deposition in boilers. Such advanced analysis is most useful when investigating the impact of the local boiler conditions on slagging and fouling. Different approaches have been explored in order to reduce computational efforts needed but also with respect to the mechanistic ash deposition sub-models used.

Richards (1993) [92] and Wang (1997) [121] coupled the comprehensive combustion code to predict the gas temperature and flow field fluctuations with the particle impaction and the sticking probability routines used in post processing mode. At an early stage, due to the large computational effort required, a 2D geometry of a pilot-scale furnace was investigated by Richard *et al.* [92] who used the stochastic flow trajectories approach and assumed the critical viscosity of less than 10^4 Pa*s to simulate fly ash particles impaction and deposition. At the later development stage, Wang and Harb [121] applied a statistical cloud particle model to assess the particle impaction rates for a 3D boiler geometry, which reduced significantly simulation time from the several months for individual particle tracking to several days. In this work, the deposit growth on the panel of the pilot scale furnace was accurately predicted, however the model predictions were not validated with full-scale boiler results due to lack of proper data. In other studies, Fan *et al.* (2001) [122] used also a stochastic flow trajectory approach applied to simulate ash deposition in a pulverised coal-fired boiler, however they assumed a higher critical viscosity of fly ash - 10^5 Pa*s. The

predictions of the deposit mass and thickness growth as function of the furnace height were obtained.

Lee *et al*. (2002) [89] used the individual particle tracking approach while investigating the ash deposition in the local area around a single heat exchanger tube for their computational domain. The deposition caused by a sticky sodium layer on the fly ash particles was investigated. A more detailed model was developed and validated which calculated the sticking probability based on the particle viscosity, surface tension, impact angle and velocity. Tomeczek *et al.* (2009) [123] also used more complex individual particle tracking approaches when simulating the ash bridging between tube banks. During the deposit build-up the grid was adjusted affecting the flow pattern around tube banks. In another study, Degereji *et at.* (2012) [90] performed 2D simulations of a 0.2 MW_{th} pilot-scale coal-fired furnace with individual tracking of 10 injection group of particles between 70-200μm, using a critical viscosity of 10^8 Pa*s. The predicted deposition rates agreed well with the experimental measurements on four different coals.

Currently, with increasing computer power, more comprehensive sub-models within boiler CFD post-processing simulations are being incorporated. These include the ash formation, ash transport, deposition and deposit growth mechanistic sub-model (Lee and Lockwood (1999) [124], Ma *et al*. (2007) [125], Losurdo *et al.* (2012) [126] as schematically illustrated in Figure 3-11. Besides the increased massive computational effort, these models require detailed data on inorganic speciation, derived from the CCSEM and chemical fractionation analyses, as input in order to simulate the mineral matter transformation process and fly ash formation.

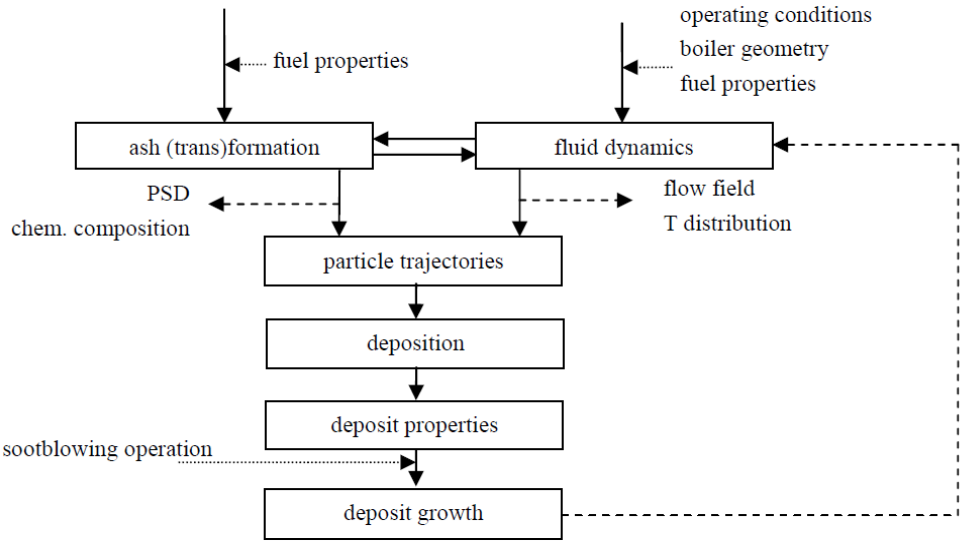

Figure 3-11. Scheme of a comprehensive CFD-based ash behaviour modelling approach [127].

Amongst CFD simulations performed for coal-fired boilers, only a few references can be found regarding the analysis of the ash deposition during biomass combustion. Kær *et al.* (2006) [94] simulated the ash deposition process in a 3D geometry of the straw-fired grate boiler. To calculate the ash deposition rate a velocity deposition approach was used that assumed additive contribution from impaction, themophoresis and condensation. As a sticking criterion the melt fraction of 15wt% in the ash was calculated with the aid of the phase equilibrium analysis, including two separate liquid phases, such as a molten salt and silicate slag [94]. In another study, Mueller *et al*. [97] also used 15 wt% melt fraction in the fly ash as a stickiness criterion when predicting ash deposition in biomass-fired fluidised bed boilers. In this approach, the CFD model was integrated with the phase equilibrium calculations that required input data derived from the chemical fractionation of the biomass fuels studied [97]. The model was successfully validated with entrained flow reactor experiments performed under well-defined conditions [128].

3.6 Concept of the Slagging and Fouling Advisory Tool

After reviewing many different approaches to the modelling of pulverised coal and biomass fuel combustion, and keeping in mind the necessity of high accuracy for the predictions, a short computational time and flexibility of the model with respect to the furnace geometry and fuels burning (including mixtures), a zone–based computational method was chosen to determine a midsection temperature profile throughout a pf boiler. The zone model of boiler is then aimed to be integrated with the improved thermo-chemical calculation-based schemes to be able to assess the slagging and fouling tendencies in different boiler regions when co-firing various coal/biomass blends. The simplified scheme of the slagging/fouling predictive tool is shown in Figure 3-12.

The concept of a generic slagging and fouling predictor originated from the previous research carried out by Cardiff University within PowerFlam1&2 European Project . In its original design a spreadsheet-based model was developed, designed to be run under Microsoft Excel (Cardiff University, Gralton T., PhD thesis, 2007 [54]). The spreadsheet uses a series of empirically derived correlations based on the FactSage thermodynamic calculations but also FLUENT derived, obtained for a number of coals and biomass fuels covering a large range of operating conditions. These correlations were implemented via the neural networks (NNT) into the spreadsheet. However, the flexibility of the model were limited since the NNT had to be learnt each time when different biomass ash chemistries were considered. It also

introduced other limitations associated with the further development of more sophisticated ash deposition models.

In light of the above, it was decided within this work, to attempt a development of the more complex 1D-zone model that could be directly integrated with the phase equilibrium module. In such approach, the highest flexibility of the phase equilibrium calculations should be achieved allowing the analysis of various fuel chemistries (only limited by thermo-chemical databases used) but also further modifications of equilibrium model.

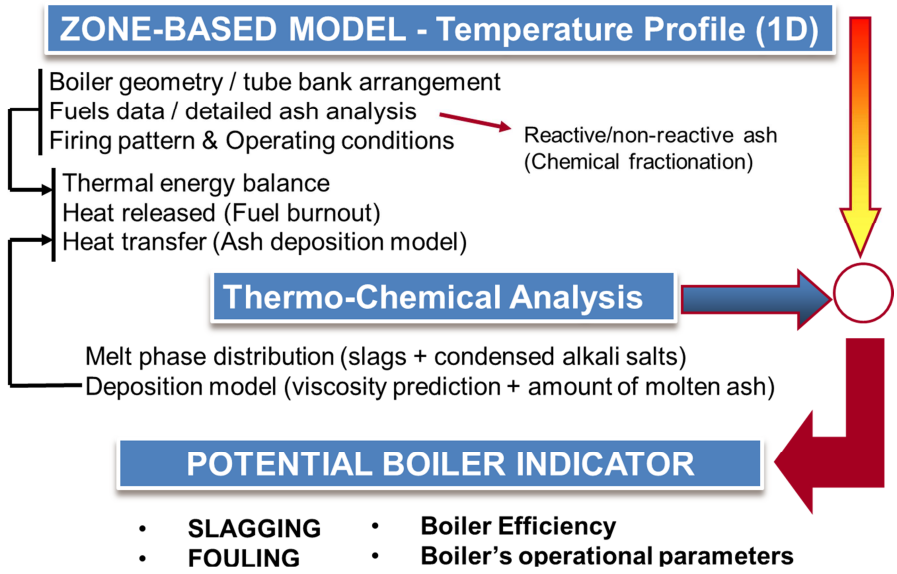

Figure 3-12. Simplified scheme of the proposed slagging/fouling predictive tool.

Furthermore, the improved modelling approach should be capable of predicting the impact of fuel switching and related slagging/fouling risk on the various associated heat transfer and thermodynamic parameters of the system, such as e.g. boiler efficiency and steam temperatures.

3.7 Summary

In this Chapter various methodologies of different complexity that have been developed over the decades for predicting ash behaviour but also thermal performance of boilers were presented and discussed. It was observed that in practice, during the boiler designed stage or boiler operation, when evaluating slagging/fouling propensities of fuels the less accurate standard methods are still in use along with the indices which have been reported to give unreliable predictions for more complex fuel blends. Nowadays, in the scientific community very comprehensive modelling approaches generally dominate: these models integrate the mechanistic ash-related sub-models within the CFD simulations. The predictions obtained from these models have been validated mostly for the pilot-scale furnaces or rigs fired with

coals. The question arises if these highly comprehensive models can be ever validated with data derived from large scale boilers?

Despite the apparent advantages associated with CFD tools, in day-to-day decision making, it is more useful for the boiler operators and managers to have available generic models capable of giving first order, reliable predictions. In order to meet these needs the development of an integrated package of methodologies was proposed which is based on coupling of the simplified zone-based model of a boiler with thermo-chemical phase equilibrium calculations capable of analysing more complex ash chemistries to assess their slagging/fouling tendencies. The development of the proposed model as well as its validation are the goals of the next Chapters.

4

THERMAL PERFORMANCE ANALYSIS OF A LARGE SCALE PF BOILER

In this Chapter, the development of an improved one–dimensional zonal furnace model of a large utility pulverised fuel boiler is investigated. The model has been improved by adding the convective section as well as including the water/steam cycle for performing more comprehensive thermal analysis of the system. Additionally, the functions describing the impact of deposits resistance and emissivity on the local heat transfer conditions were derived and implemented. The first sections deal with relevant theoretical background of the heat transfer process to obtain a set of proper energy balance equations for the zones placed in the different boiler's regions. Some method assumptions and limitations are discussed. The model enables the assessment of the local heat transfer conditions within the zones, determining a midsection temperature and heat flux profiles throughout a boiler. Associated changes in boiler efficiency as well as various heat transfer and thermodynamic parameters of the system can be also analysed. The developed model has been applied to the large 235 MW_e wall-fired pf boiler fired with blends of bituminous coal and biomass fuels of different quality. The effects of changes in the ash and moisture contents in the fuels on heat transfer conditions and boiler performance are analysed for different biomass types and co-firing shares. The sensitivity of the model is analysed for various operational conditions, including simulated severe furnace slagging. The open and clear structure of this approach gives the possibility for adapting the ash deposition module which development is described in more detail in the next Chapter.

4.1 Introduction

Amongst the most crucial factors influencing the ash deposition severity in pulverised fuel fired boiler are the nature of fuel fired, aerodynamics and thermal conditions, of which the last one affects almost every other physical or chemical process taking place [129].

The amount of heat absorbed in the furnace which is dominated by radiation represents around 40% of the total thermal energy released during combustion. Slagging of the furnace may disturb the heat exchange rate distribution between the furnace and convective section leading to the production of lower steam mass flows and higher temperatures at the furnace exit, resulting in overheating of the heat exchangers (higher steam temperatures), or extending the ash deposition to the convective pass of the boiler.

The major parameters that determine thermal conditions in the radiant and convection sections of a pulverised fuel-fired boiler are shown in Figure 4-1.

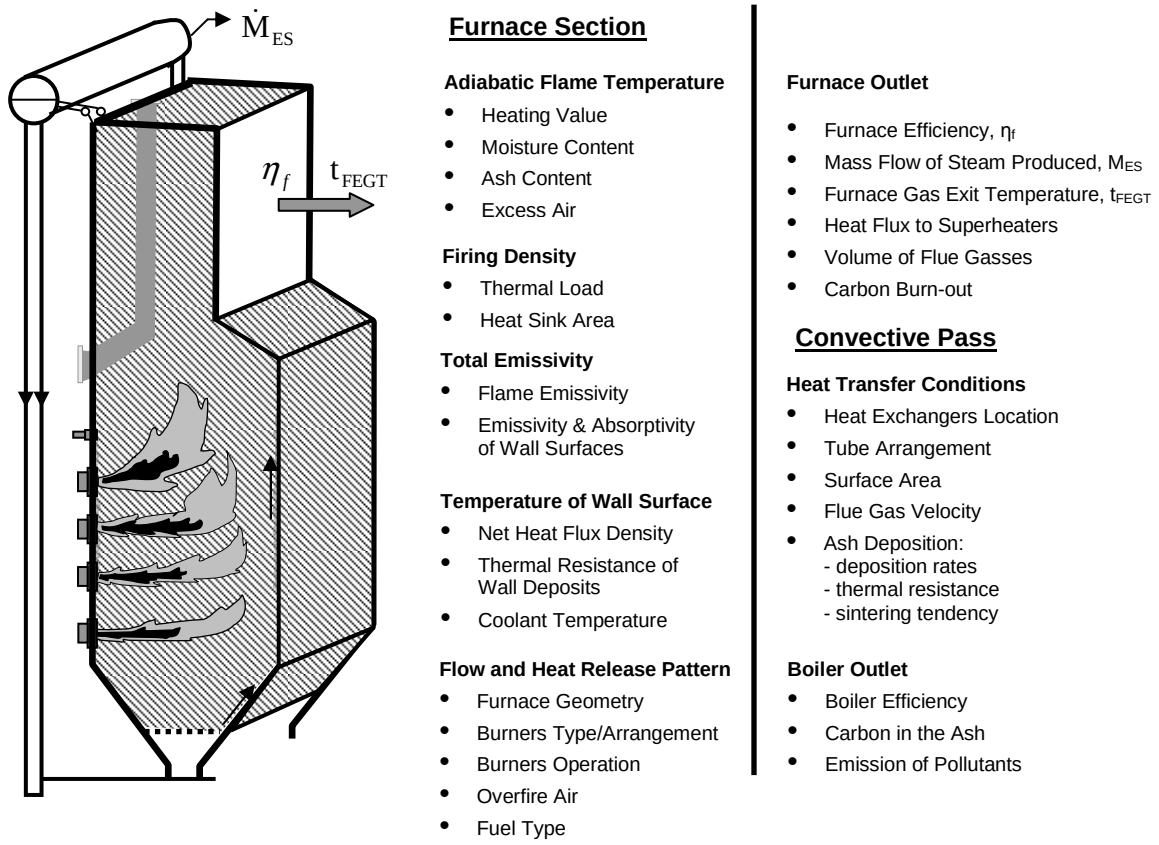

Figure 4-1. Factors influencing thermal performance of pf boiler.

In order to minimise slagging and fouling issues, the furnace should be designed to achieve a proper thermal load of the heat-exchange surfaces along the furnace height. Furthermore, aerodynamics in the furnace should prevent impingement of flames on the water

wall and ensure uniform distribution of heat flux on the water walls. With respect to the fuel ash quality, the furnace exit gas temperature (FEGT) should be kept below the softening temperature of ashes (usually in the range of 1050-1250^{o}C) to avoid deposit build-up on the platen superheaters, and other heat exchange surfaces entering the convective sections [115, 129, 130].

Besides slagging furnace issues, the variations in radiative properties of flue gasses mainly occur when co-firing high moisture and high/low ash content biomass fuels: this may also affect significantly the heat transfer within the furnace. Furthermore, convective heat transfer will be influenced by higher volumes, and thus velocities of the flue gas produced when utilising lower quality, low calorific and wet solid fuels.

The impact of fuel quality on the thermal performance of a boiler can be relatively simply and accurately conducted with the aid of one-dimensional zone modelling methods. In this Chapter the use of an extended version of such zone methods is investigated, with the purpose of analysing the effects of biomass co-firing and ash deposition on thermal performance of a pf boiler.

4.2 Concept of Improved 1D-Zonal Modelling Approach

A comprehensive extended version of the Russian standard one-dimensional zonal furnace model is proposed with the conceptual scheme shown in Figure 4-2. The proposed modelling concept consists of the following general modules:

- Furnace section module which utilises the furnace model constructed based on the mathematical principles of the Russian standard zone method [112]. It is capable of assessing heat flux and temperature distribution along the furnace height for a wide range of boiler thermal loads. This model can be relatively simply extended to simulate the effects of fuel/air distribution variations, fuel burn-out [119] as well as the impact of furnace slagging on thermal furnace performance. As a result, the furnace thermal efficiency can be predicted, including the mass flow of steam generated and the flue gas temperature entering the convective pass of the boiler.

- Convective section module which is based on thermal balancing of heat exchangers placed in the convective pass of boiler. To each of the heat exchangers one zone is assigned. The heat transfer/exchange between the flue gas and heating media is assessed. The proper heat transfer coefficients are included which take into account the effects of tube banks arrangement, thermal and flow conditions as well as thermal

deposit resistance. Along with the parallel calculations conducted with the aid of the furnace section module, the impact of fuel switching on the overall boiler thermal performance and efficiency can be analysed.

- Ash deposition module aims at delivering information to the furnace and convective section modules, regarding the thermal resistivity of the ash deposited in different boiler's zones. These data can be assessed either by the use of reliable ash deposition models, or else by the direct measurements of heat fluxes change during the ash deposit build-up process (i.e. on the furnace walls) and recalculation of the deposit resistivity [131]. The development of the ash deposition predictive methodology that utilises phase equilibrium calculations is the aim of the next Chapter.

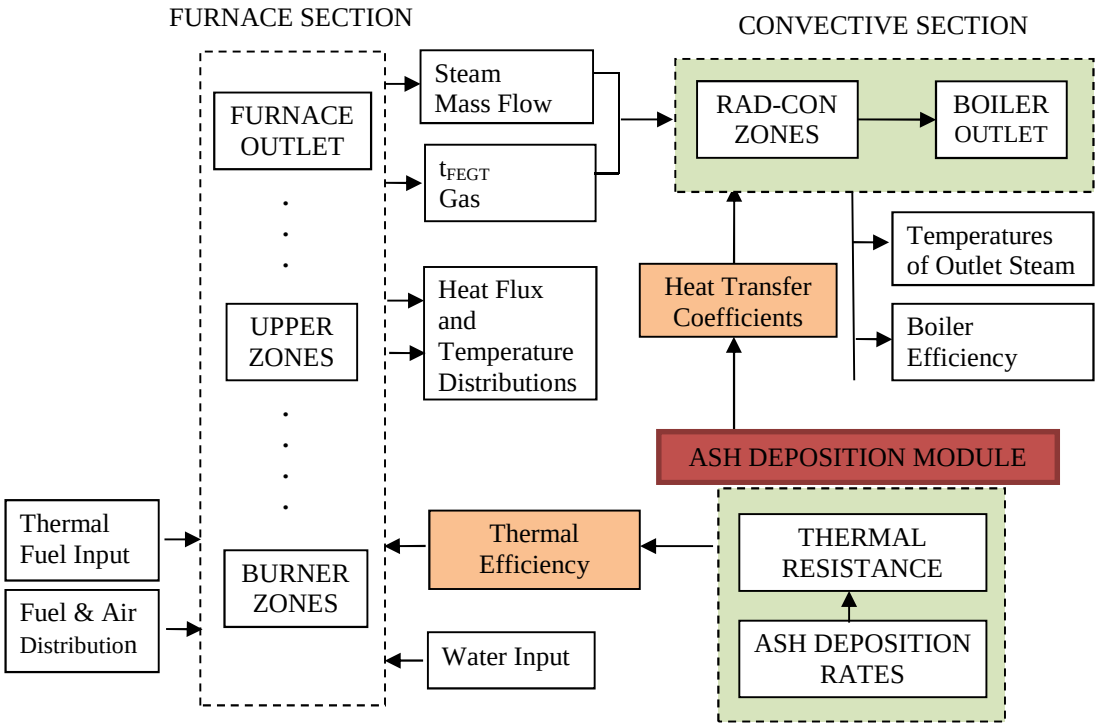

Figure 4-2. Conceptual scheme of the used zone modelling approach.

The model output includes boiler performance information with respect to boiler/furnace thermal efficiency, amount of steam generated, temperatures of superheated/reheated steam, spray-water injection flows, and other related thermodynamic data. Most importantly, with the aid of ash deposition model, the effect of deposit resistance on thermal performance can be investigated.

4.3 Zone Modelling Procedure

This section deals with presenting the theoretical background regarding the construction of a one-dimensional zone furnace model for pulverised coal/biomass fired boilers.

4.3.1 Radiant Heat Exchange

Before the whole set of thermal energy balances is presented and discussed, first the analysis of the heat exchange between the flame zone and furnace walls in a single zone in the furnace will be analysed in more details. In this approach it is assumed that the whole furnace is occupied by a flame with the surface of A_{fl} and emissivity ε_{fl} (Figure 4-3). The furnace enclosure consists of diffuse grey surfaces surrounding a grey gas. The assumed greyness of the gas means that its emissivity does not depend on the wavelength but only on the temperature and gas composition (CO_2, H_2O concentrations). For diffuse grey surfaces, the radiant energy is emitted or reflected in all directions.

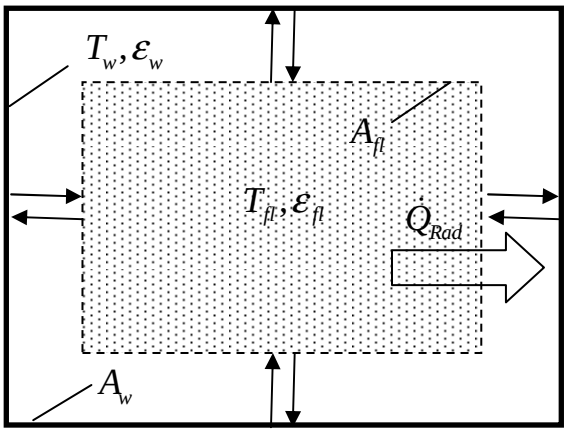

Figure 4-3. Gas enclosure in radiant zone of the furnace.

The rate of radiative heat transfer from the flame towards the furnace walls can be calculated from the following formula:

$$\dot{Q}_{Rad} = \frac{\sigma_0 A_{fl}\left(T_{fl}^4 - T_w^4\right)}{\frac{1}{\varepsilon_{fl}} + \frac{1-\varepsilon_w}{\varepsilon_w}\frac{A_{fl}}{A_w}} \tag{4.1}$$

where $\sigma_0 = 5.67*10^{-8} W/m^2K^4$ – Stefan-Boltzmann's constant.

Taking into account that the flame fills up the whole furnace zone, therefore it can be assumed that the surface of the flame is equal to the surface of the wall ($A_{fl} = A_w$).

$$\dot{Q}_{Rad} = \frac{\sigma_0 A_w \left(T_{fl}^4 - T_w^4\right)}{\frac{1}{\varepsilon_{fl}} + \frac{1}{\varepsilon_w} - 1} \tag{4.2}$$

Since not all incident radiation from the flame is absorbed by the water-walls, part of it is reflected (as shown in Figure 4-4).

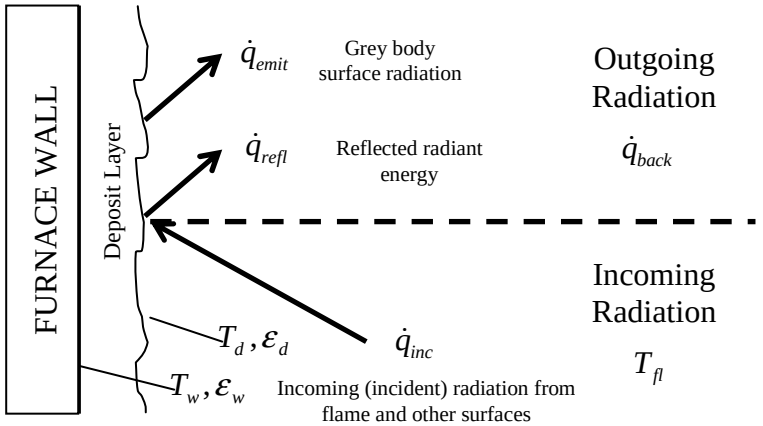

Figure 4-4. Energy distribution at the surface.

Moreover, taking into account that the wall surfaces emit also the energy, the net heat flux which is absorbed by the water-wall can be given by the formula:

$$\dot{q}_{rad} = \frac{\dot{Q}_{Rad}}{A_w} = \dot{q}_{inc} - \dot{q}_{back} \tag{4.3}$$

$$\dot{q}_{back} = \dot{q}_{emit} + \dot{q}_{refl} = \varepsilon_w \sigma T_w^4 + \left(1 - \varepsilon_w\right) \dot{q}_{inc} \tag{4.4}$$

After introducing the thermal efficiency factor, which is defined as the ratio of the heat flow rate absorbed by the furnace water-walls to the incident heat flow rate:

$$\psi = \frac{\dot{q}_{rad}}{\dot{q}_{inc}} = \frac{\dot{q}_{inc} - \dot{q}_{back}}{\dot{q}_{inc}} = 1 - \frac{\dot{q}_{back}}{\dot{q}_{inc}} \tag{4.5}$$

the outgoing radiation from the surface, as a part of incident flux, can be expressed as

$$\dot{q}_{back} = \left(1 - \psi\right) \dot{q}_{inc} \tag{4.6}$$

Submitting expression (4.4) into (4.6), one obtains

$$\varepsilon_w \sigma_0 T_w^4 + \left(1 - \varepsilon_w\right) \dot{q}_{inc} = \left(1 - \psi\right) \dot{q}_{inc} \tag{4.7}$$

and then

$$\varepsilon_w \sigma_0 T_w^4 = \varepsilon_w \dot{q}_{inc} - \psi \dot{q}_{inc} \tag{4.8}$$

After substitution and proper transformations

$$\dot{q}_{rad} = \psi \dot{q}_{inc} = \frac{\varepsilon_w \varepsilon_{fl} \sigma_0 T_{fl}^4 - \varepsilon_w \varepsilon_{fl} \sigma_0 T_w^4}{\varepsilon_{fl} + \varepsilon_w - \varepsilon_w \varepsilon_{fl}} \tag{4.9}$$

$$\psi \dot{q}_{inc} = \frac{\varepsilon_w \varepsilon_{fl} \sigma_0 T_{fl}^4 - \varepsilon_{fl} \left(\varepsilon_w \dot{q}_{inc} - \psi \dot{q}_{inc} \right)}{\varepsilon_{fl} + \varepsilon_w - \varepsilon_w \varepsilon_{fl}} \tag{4.10}$$

Performing further transformations a formula for the emissivity of the flame can be derived as follows:

$$\varepsilon_{fl} = \frac{1}{1 + \frac{1}{\psi} \left(\frac{\sigma_0 T_{fl}^4}{\dot{q}_{inc}} - 1 \right)} \tag{4.11}$$

Furthermore, from the definition of the furnace emissivity, we obtain

$$\varepsilon_{furn} = \frac{\dot{q}_{inc}}{\sigma_0 T_{fl}^4} \tag{4.12}$$

which leads then to the expression for correlating the emissivity of the flame and furnace chamber, as follows:

$$\varepsilon_{fl} = \frac{1}{1 + \frac{1}{\psi} \left(\frac{1}{\varepsilon_{furn}} - 1 \right)} \tag{4.13}$$

$$\varepsilon_{furn} = \frac{\varepsilon_{fl}}{\varepsilon_{fl} + \psi \left(1 - \varepsilon_{fl} \right)} \tag{4.14}$$

Finally, the rate of heat transfer transferred by radiation to the water-walls with the surface area A_{furn} and flame temperature T_{fl} can be calculated from the following expressions.

$$\dot{Q}_{Rad} = \dot{q}_{rad} A_{furn} = \dot{q}_{inc} \psi A_{furn} = \varepsilon_{furn} \sigma_0 T_{fl}^4 \psi A_{furn} \tag{4.15}$$

4.3.2 Furnace Deposit Boundary Conditions

By definition, the thermal efficiency factor of the furnace walls expresses the ratio of the heat flow rate absorbed by the furnace water-walls to the incident heat flow rate in a given zone. After transformation of equation (4.8), the general formula, which characterizes the heat transfer efficiency by radiation between the flame and furnace walls (or the heat exchange surfaces) covered by deposit layer, can be obtained as follows [110]:

$$\psi = \frac{\dot{q}_{rad}}{\dot{q}_{inc}} = \varepsilon_d \left(1 - \frac{\sigma_0 T_d^4}{\dot{q}_{inc}} \right) \tag{4.16}$$

The thermal efficiency factors of the furnace walls reflect the slagging conditions in the furnace zones. A simple relation can be found between the thermal resistance of the deposit

layer and thermal efficiency factors. Considering a flat layer of deposits, the heat conducted through deposit layer and absorbed by water-walls is as follows:

$$\dot{q}_{abs} = \frac{\lambda_{eff}}{\delta_d}\left(T_d - T_w\right) = \psi \dot{q}_{inc} \tag{4.17}$$

Note that the heat exchange between deposit and tube's outer layer takes into account the conductive and radiative heat transfer in the deposit layer which is often expressed for simplicity by the effective conductance λ_{eff} coefficient. The above correlations (4.17) , can be transformed to the form which expresses the thermal deposit resistance (R_d), as follows:

$$\frac{\delta_d}{\lambda_{eff}} = \frac{\left(T_d - T_w\right)}{\psi \dot{q}_{inc}} = R_d \tag{4.18}$$

Further transformation of equation (4.16) enables extraction of the temperature of the deposit surface as:

$$T_d = \left(\frac{\varepsilon_d - \psi}{\varepsilon_d \sigma}\dot{q}_{inc}\right)^{0.25} \tag{4.19}$$

The final relation between the thermal resistance and thermal efficiency factor that includes also the emissivity of deposits (ε_d) can be expressed by [120]:

$$R_d = \left[\left(\frac{\varepsilon_d - \psi}{\varepsilon_d \sigma_0}\dot{q}_{inc}\right)^{0.25} - T_w\right] \Big/ \left(\psi \dot{q}_{inc}\right) \tag{4.20}$$

As can be seen, this above correlation in a very flexible way reflects boundary conditions of the deposit layer and can be used to assess the temperature of deposit surfaces by:

$$T_d = T_w + \dot{q}_{inc}\psi\left(\frac{1}{\alpha_s} + R_d\right) = T_w + \varepsilon_{furn}\sigma_0 T_{fl}^{\ 4}\psi\left(\frac{1}{\alpha_s} + R_d\right) \tag{4.21}$$

To give a wider perspective on how the thermal efficiency factors and the correlated temperature of deposit vary within the incident flux range, the corresponding curves were generated for different thermal resistance of furnace wall deposits (with the assumed emissivity of deposits, $\varepsilon_d = 0.75$) as shown in Figures 4-5ab. These calculations were performed for cases starting from the operationally clean surface (2.5 m^2K/kW) and following severe slagging conditions in the furnace. The corresponding thermal resistances for various slagging conditions on platen superheaters are presented in Table 4-1. As can be seen, in the most intense heat zones (such as burner regions) due to the high incident heat fluxes (600-700 kW/m^2K), the ash deposits accumulated in time can relatively easily and quickly reach

their melting temperature. This may result in a significant drop of thermal efficiency of heat exchange surfaces, shifting the gas temperature peak towards the higher levels of the furnace and accelerating ash deposition.

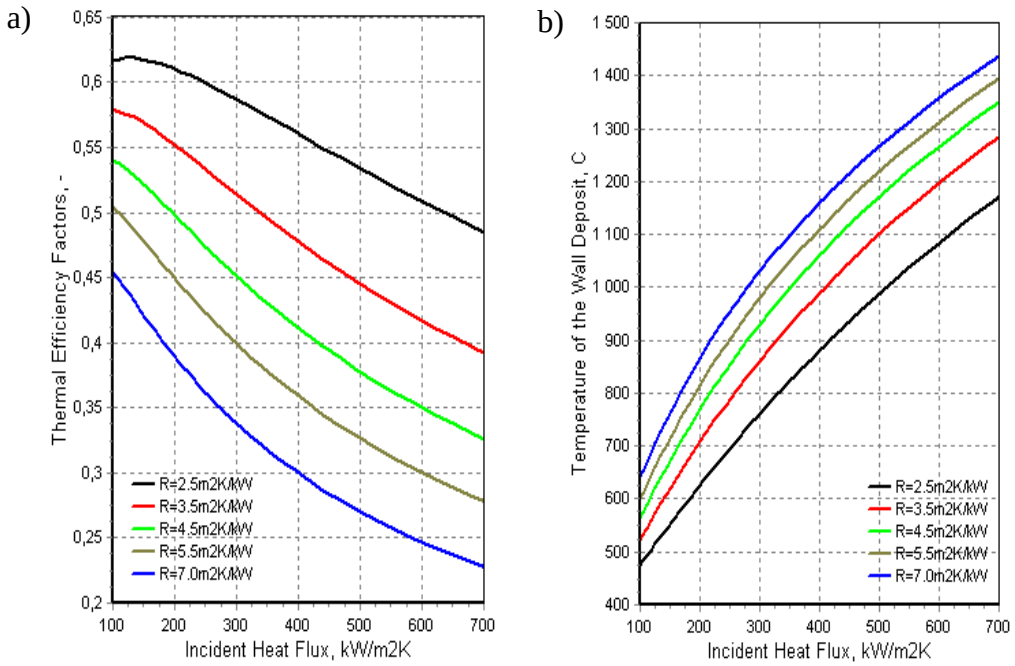

Figure 4-5. Thermal efficiency factors and temperature of the wall deposits distribution as a function of the incident heat flux for different thermal resistances assumed (Tw=320°C, ε_d=0.75).

Table 4-1. Assessment of thermal resistances of heat exchange surfaces under various slagging conditions [120, 132].

Slagging conditions	Furnace Walls	Platen SH,temp.1300°C
Operationally clean surface, (m^2K/kW)	2.5	6.45
Slightly contaminated surface, (m^2K/kW)	3.5	12.9
Contaminated surface, (m^2K/kW)	4.5	17.2
Surface covered with slag, (m^2K/kW)	5.5	21.5

The presented correlations in this subsection describe the boundary conditions of the heat transfer with the presence of an ash deposition layer. However, it should be noted that these thermal and radiative properties of deposits can change during the deposit growth and may depend on both the physical state (amount of molten phase, porosity, texture) and the chemical composition of the deposit as well as its temperature. Furthermore, once the growing deposits reach their melting temperature, the overall process of further ash deposition may slow down, since all the new particles transported to the molten surface will be not

captured. Under these extreme conditions the steady state deposit layer can be reached, and its thickness can be estimated by [115]:

$$\delta_{FT} = \frac{\lambda_{eff}\left(T_{FT} - T_w\right)}{\varepsilon_d \dot{q}_{inc} - \varepsilon_d \sigma_0 T_{FT}^4} \tag{4.22}$$

For typical values of the ash fluid temperature T_{FT} =1500K, the temperature of the outer surface of the wall T_w =750K, deposit emissivity ε_d=0.7, and deposit conductivity λ_{eff} =0.8*10^{-3} kW/mK, the estimated thickness of molten deposit layer is around 8mm [115]. Furthermore, analysing equation 4.22, it can be generally concluded, that the steady-state fused deposits in the most intense heat flux regions will be thinner than those accumulated in less heat loaded zones within the furnace.

4.3.3 Thermal Energy Balances in the Zones

Before deriving a set of equations used to describe the thermal energy balances in specific boiler zones, first the following general assumptions need to be introduced:

- Combustion flue gas and flame are assigned a single temperature T_i.
- The gas is grey and the ash particles are dispersed uniformly in the flue gas influencing gas emissivity.
- The Weighted-Sum-of-Gray-Gases Model (WSGGM) is used to describe emissivity of combustion flue gas (see Appendix I).
- The surface of deposit is grey.
- Radiation is the dominant way of heat transfer.
- Convection from the gases to the deposit on the wall panels is negligible.
- Due to the one-dimensional nature of the calculations and relatively large zone volumes assumed, flow pattern details are neglected.
- The heat release from the burning fuel along the furnace height is described by simple empirical fuel burn-out characteristics being a function of basic fuel properties, such as the amount of combustible matter, size of fuel particles and ash content, as described in subsection 4.3.6.

Zone-based models are based on dividing the furnace into a series of control volumes across which the energy balance equations are written, which results in a system of algebraic non-linear equations in terms of the outlet temperature of each zone, allowing the radiative heat flux distribution to be predicted [107, 108, 119]. Depending upon the zone location, the

heat streams can be delivered into the furnace zones by burning fuel ($\dot{Q}_{\mathrm{B}}$), by preheated air ($\dot{Q}_{\mathrm{Air}}$), and by heat from flue gas entering from the previous zone ($\dot{Q}_{\mathrm{FG},i}$), as shown in Figure 4-6. In some specific cases, i.e. for the first zone, part of the heat delivered is emitted to the furnace bottom ($\dot{Q}_{\mathrm{EM},out}$). Such case occurs at the furnace outlet zone which emits radiation towards surfaces placed in the platen superheater zone.

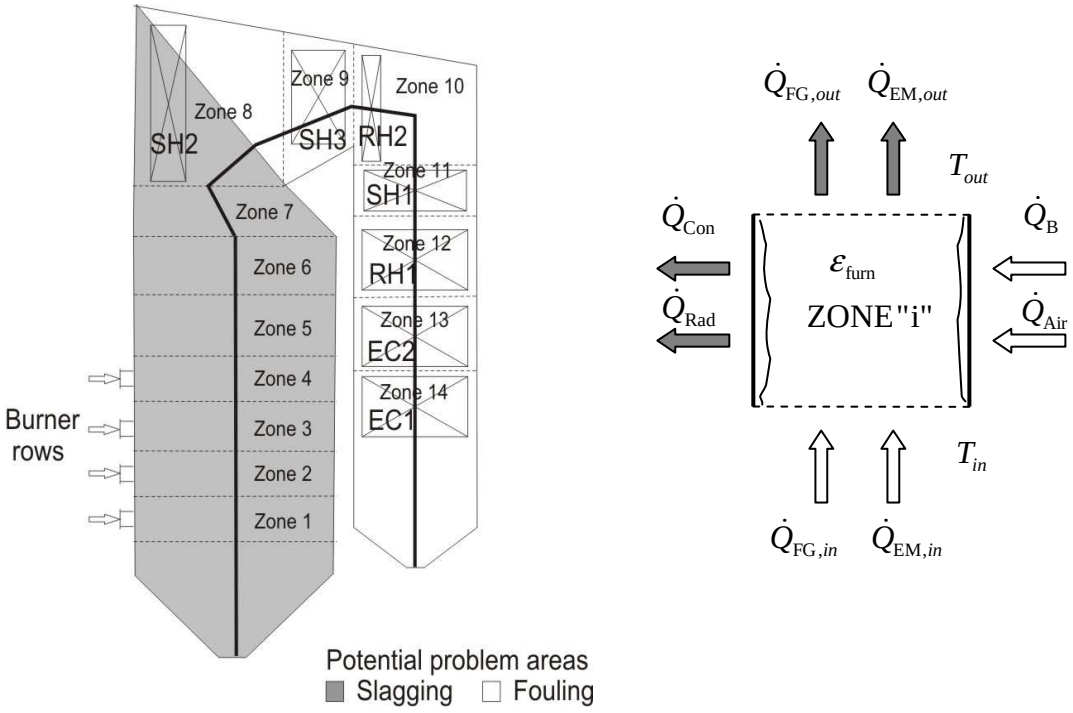

Figure 4-6. Thermal energy balance of the zones in the boiler's furnace [133].

In each zone in the furnace heat is absorbed by wall furnace tubes, especially by radiation ($\dot{Q}_{\mathrm{Rad}}$). Convection ($\dot{Q}_{\mathrm{Con}}$) is usually neglected in the furnace but is considered when the platen superheater is situated at the outlet of the furnace. The general steady state thermal balance of a zone in the furnace, excluding inter-zone radiation, can be written as follows:

$$\dot{Q}_{\mathrm{FG},in}+\dot{Q}_{\mathrm{B}}+\dot{Q}_{\mathrm{Air}}-\dot{Q}_{\mathrm{Rad}}-\dot{Q}_{\mathrm{Con}}-\dot{Q}_{\mathrm{FG},out}=0 \tag{4.23}$$

$$\dot{Q}_{\mathrm{FG},in}=\sum_{1}^{i-1} n_{\mathrm{B}}\cdot\dot{M}_{\mathrm{B}}\left(Vc_{p,t_{in}}\right)t_{in} \tag{4.24}$$

$$\dot{Q}_{\mathrm{B}}=\left(n_{\mathrm{B},i}\beta_i+\sum_{1}^{i-1} n_{\mathrm{B}}\Delta\beta_i\right)\dot{M}_{\mathrm{B}}\cdot\mathrm{LHV}+n_{\mathrm{B},i}\dot{M}_{\mathrm{B}}i_{\mathrm{B}} \tag{4.25}$$

$$\dot{Q}_{\mathrm{Air}}=n_{\mathrm{B},i}\cdot\dot{M}_{\mathrm{B}}\dot{q}_{\mathrm{Air}} \tag{4.26}$$

$$\dot{Q}_{Rad} = \varepsilon_{furn}\sigma_0 \left[0.5\left(T_{in}^4 + T_{out}^4\right)\right](\psi A_w) \tag{4.27}$$

$$\dot{Q}_{\mathrm{Con}} = \alpha_k \left[0.5\left(t_{in} + t_{out}\right) - t_d\right] A_k \tag{4.28}$$

$$\dot{Q}_{\mathrm{FG},out} = \sum_1^i n_{\mathrm{B}} \cdot \dot{M}_{\mathrm{B}} \left(Vc_{p,t_{out}}\right) t_{out} \tag{4.29}$$

where $\dot{M}_B$ is a total fuel mass flow rate, and n_{B} represents the current fraction of the total fuel supply delivered into the zones until i ; $\left(Vc_{p,t_{in}}\right)$ and $\left(Vc_{p,t_{out}}\right)$ are the average specific heats of the flue gases of 1 kg fuel burnt at the related zone temperatures (*in, out* denote the inlet and outlet of current zone), β - the current fuel burn-out fraction of the fuel at the actual furnace level; $\Delta\beta = \beta_i - \beta_{i-1}$ is a degree of fuel burn-out in a specified zone i from the combustion of the fuel introduced into previous zones; LHV is the lower heating value of the fuel, kJ/kg; i_{B} is the sensible heat of fuel delivered into the zone, kJ/kg; $\dot{q}_{Air}$ is the heat transferred with air into the current zone per kg fuel with a specified air excess ratio λ ; T and t are the temperatures of flue gases (in $^{\mathrm{o}}$C and K, respectively); σ_0 is the Stefan-Boltzmann constant; ε_{furn} is the emissivity of the furnace; A_w *and* A_k are the radiative and convective heat exchange surfaces areas of the zone (in m^2); ψ is the thermal efficiency factor of the surfaces; α_k is the convective heat transfer coefficient and t_d is the temperature of surface deposit.

After transformation of the thermal energy balance equation the following general formula is obtained for the temperatures at the outlet of the zone in the furnace [110, 112, 133]:

$$t_{out,i} = \frac{2\left(n_{\mathrm{B},i}\beta_i + \sum_1^{i-1} n_{\mathrm{B}}\Delta\beta_i\right)\dot{M}_{\mathrm{B}} \cdot \mathrm{LHV} + 2n_{\mathrm{B},i}\dot{M}_{\mathrm{B}} i_{\mathrm{B}} + 2n_{\mathrm{B},i} \cdot \dot{M}_{\mathrm{B}}\dot{q}_{\mathrm{Air}}}{2\sum_1^i n_{\mathrm{B}} \cdot \dot{M}_{\mathrm{B}}\left(Vc_{p,t_{out}}\right) + \alpha_{\mathrm{k},i}A_{\mathrm{k},i}} +$$

$$+ \frac{2\sum_1^{i-1} n_{\mathrm{B}} \cdot \dot{M}_{\mathrm{B}}\left(Vc_{p,t_{in}}\right) - \alpha_{\mathrm{k},i}A_{\mathrm{k},i}}{2\sum_1^i n_{\mathrm{B}} \cdot \dot{M}_{\mathrm{B}}\left(Vc_{p,t_{out}}\right) + \alpha_{\mathrm{k},i}A_{\mathrm{k},i}} t_{in,i} + \frac{2\alpha_{\mathrm{k},i}A_{\mathrm{k},i}}{2\sum_1^i n_{\mathrm{B}} \cdot \dot{M}_{\mathrm{B}}\left(Vc_{p,t_{out}}\right) + \alpha_{\mathrm{k},i}A_{\mathrm{k},i}} t_{\mathrm{d,i}} - \tag{4.30}$$

$$- \frac{\varepsilon_{furn}\sigma_0}{2\sum_1^i n_{\mathrm{B}} \cdot \dot{M}_{\mathrm{B}}\left(Vc_{p,t_{out}}\right) + \alpha_{\mathrm{k},i}A_{\mathrm{k},i}} \left[\left(T_{in,i}^4 + T_{out,i}^4\right)\right](\psi A_w)_i$$

In order to solve the above thermal balance of the zone, other associated equations are needed, which describe the emissivity of the furnace, thermal efficiency factors as well as the temperature of deposit in a given zone, as follows:

$$\varepsilon_{furn} = f(\psi, \varepsilon_{fl}) \rightarrow eq.4.14$$

$$\psi = f(R_d, \varepsilon_w, T_d, q_{inc}) \rightarrow eq.4.20$$

$$T_d = f(T_{w,} R_d, \psi, q_{inc}) \rightarrow eq.4.21$$

The sensitivity analysis of the impact of the thermal resistivity (R_d) as well as the emissivity of the deposit (ε_d) on the heat flux and temperature distributions along the furnace height is performed in subsection 4.4.5.

The obtained thermal balance equations for zones in the furnace can vary, and are dependent on specific conditions of heat release and transfer in each zone. In the burner zones each burner row is considered as a separate zone into which fuel flows at the given rate and the degree of fuel burn-out achieved in the previous zone is also considered. A more detailed procedure for estimating the fuel burn-out rate along the height of the furnace is described in subsection 4.3.6.

The thermal energy balance equations derived for the specific zones, which may also include inter-zone radiative heat transfer can be found in Appendix I. All other related correlations used to calculate flue gas composition, emissivity and enthalpy are also included in Appendix I.

The temperature profiles and heat fluxes along the furnace height, obtained by the zone method can be used to assess the amount of the heat absorbed by the furnace walls. Thus, the mass flow of steam generated can be estimated with the support of the mass and energy balance written on the water/steam side. Moreover, the effects of a change in the rate of heat radiated from the furnace and absorbed directly by the platen superheaters, as well as the other aerodynamics-related factors (such as velocity of flue gasses, heat exchangers geometry) influencing the intensity of heat transfer can be easily evaluated if these parameters are introduced into thermal balance equations. The mass and energy balance scheme, for both the gas and water/steam sides, allowing for such an evaluation is illustratively shown in Figure 4-7. The division of all individual heat sinks of the thermal boiler's system cycle into control volumes (zones) for balance calculations needs to be made. This schematic includes the complete boiler's cycle for saturation of live steam, starting with water preheating in the economiser, following by boiler evaporator control volume and subsequent 3-stages of live

steam superheating (zones 11, 8 and 9) with the spray- water injections to control the temperature of the outlet live steam. The steam cycle for reheated steam is also included.

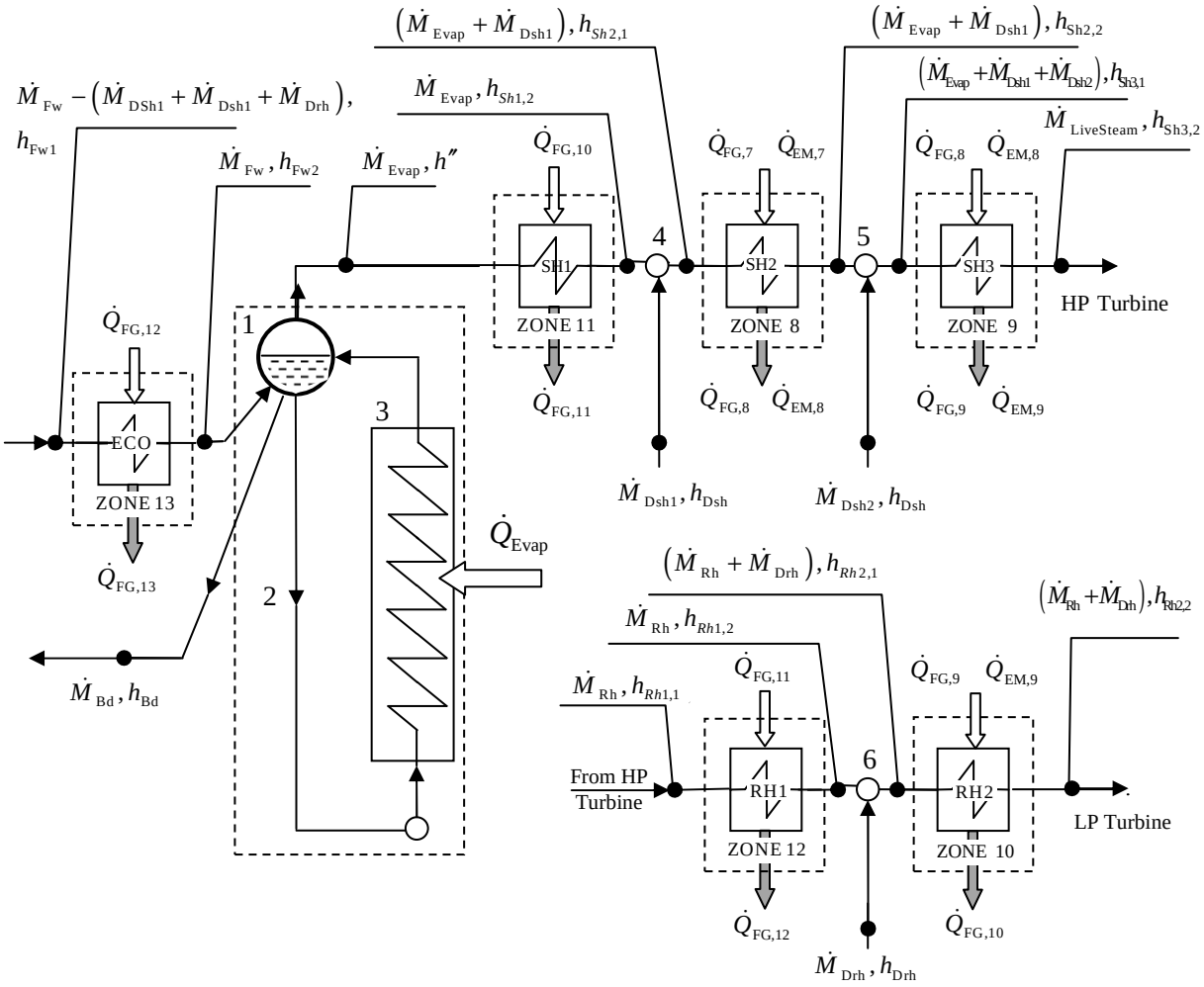

Figure 4-7. Illustrative scheme of control volumes for mass and thermal balance of boiler evaporator, water economizer (ECO), subsequent 3-stages of live steam superheating (SH1, SH2 and SH3) [134] and 2-stages of steam reheating (RH1 and RH2): 1-drum, 2-downcomers , 3-evaporator, 4- 1st stage and 5-2nd stage superheater spray attemperator, 6-1st stage reheater spray attemperator.

The mass flow rate of the steam produced in a boiler ($\dot{M}_{Evap}$) can be estimated based on the overall radiative heat ($\dot{Q}_{Evap}$) transferred from the combustion chamber to the surrounding water-walls in the furnace. Taking into account the heat absorbed by the second superheater stage ($\dot{Q}_{SH2}$) which is placed inside the furnace, it can be calculated from the expressions:

$$\dot{M}_{\mathrm{Evap}} \approx \frac{\dot{Q}_{\mathrm{Evap}}}{h''(p_d) - h_{\mathrm{Fw2}}} - \dot{M}_{\mathrm{Bd}} \frac{h'(p_d) - h_{\mathrm{Fw2}}}{h''(p_d) - h_{\mathrm{Fw2}}} \tag{4.31}$$

$$\dot{Q}_{\mathrm{Evap}} = \left(\dot{Q}_{\mathrm{Ad}} - \dot{M}_{\mathrm{B}} \left(Vc_{p,t_{\mathrm{fegt}}}\right) t_{\mathrm{fegt}}\right) - \dot{Q}_{\mathrm{SH2}} \tag{4.32}$$

where the mass balance of boiler evaporator is described as

$$\dot{M}_{\mathrm{Fw}} - \left(\dot{M}_{\mathrm{Dsh1}} + \dot{M}_{\mathrm{Dsh2}} + \dot{M}_{\mathrm{Drh}}\right) = \dot{M}_{\mathrm{Evap}} + \dot{M}_{\mathrm{Bd}} \tag{4.33}$$

According to Kefa [21] the heat loss through blow-down can be neglected as the blow-down water ($\dot{M}_{Bd}$) in large condensing power plants does not exceed of 2% of the main steam flow. The mass flows of the spray-water in subsequent stages of the attemperators $\dot{M}_{\mathrm{Dsh1}}, \dot{M}_{\mathrm{Dsh2}}$ and $\dot{M}_{\mathrm{Drh}}$ can be estimated based on the algorithm described in subsection 4.3.4. In the above equations, $h''(p_d)$, h_{Fw2} are the enthalpies of the saturated steam at drum pressure and feed-water after the economizer, respectively; $\dot{Q}_{\mathrm{Ad}}$ is the theoretical combustion heat (under adiabatic conditions) of the coal/air mixture introduced into the combustion chamber, given by the formula:

$$\dot{Q}_{\mathrm{Ad}} = \dot{M}_{\mathrm{B}} \left(Vc_{p,t_{\mathrm{ad}}}\right) t_{\mathrm{ad}} \tag{4.34}$$

Finally, the adiabatic temperature of combustion t_{ad} can be calculated iteratively as follows:

$$t_{\mathrm{ad}} = \frac{\dot{M}_{\mathrm{B}} \left(LHV + i_{\mathrm{B}}\right) + \dot{M}_{\mathrm{B}} \dot{q}_{\mathrm{Air}}}{\dot{M}_{\mathrm{B}} \left(Vc_{p,t_{\mathrm{ad}}}\right)} \tag{4.35}$$

Based on both the adiabatic temperature of combustion, whose value is directly related with the fuel and does not depend on furnace thermal conditions, and the furnace exit gas temperature (predicted by zonal method), the overall furnace thermal efficiency can be assessed with the formula:

$$\eta_{\mathrm{F}} = \frac{\dot{M}_{\mathrm{B}} \left(Vc_{p,t_{\mathrm{ad}}}\right) t_{\mathrm{ad}} - \dot{M}_{\mathrm{B}} \left(Vc_{p,t_{\mathrm{fegt}}}\right) t_{\mathrm{fegt}}}{\dot{M}_{\mathrm{B}} \mathrm{LHV}} \tag{4.36}$$

Extending the above methodology to the convective pass of the boiler, and consequently, incorporating within the iterative procedure more thermal balance equations written for the next neighboring zones (each zone represents one heat exchanger), the subsequent zone outlet gas temperatures can be calculated, as well as the parameters of the heating media. As an example, the thermal energy balance for the ZONE 11, which corresponds to the first-stage of live steam superheating, can be expressed as:

$$\begin{aligned} &\dot{M}_{\mathrm{B},10}\left(Vc_{p,t_{10}}\right) t_{10} - \dot{M}_{\mathrm{Evap}} \cdot \left(h_{\mathrm{Sh1,2}} - h''\right) - \dot{M}_{\mathrm{B},11}\left(Vc_{p,t_{11}}\right) t_{11} = 0 \;\Rightarrow\; t_{11} = ? \\ &\dot{M}_{\mathrm{Evap}} \cdot \left(h_{\mathrm{Sh1,2}} - h''\right) - k_{\mathrm{Sh1}} A_{\mathrm{Sh1}} \Delta T_{\log} = 0 \;\Rightarrow h_{\mathrm{Sh1,2}}\left(t_{\mathrm{Sh1,2}}, p_{\mathrm{Sh1,2}}\right) \;\Rightarrow\; t_{\mathrm{Sh1,2}} = ? \end{aligned} \tag{4.37}$$

where the flue gas enthalpy drop, and thus the outlet flue gas temperature from the zone (t_{11}) can be obtained from the first equation, simultaneously in solving the second formula to

obtain steam outlet temperature ($t_{Sh1,2}$). Here, the heat transfer conditions are determined by the logarithmic temperature difference between flue gas and steam, surface area of heat exchanger A_{Sh1} and the overall heat exchange coefficient which depends, on fluid (gas and steam) properties, flow direction and turbulence given for specific types of heat exchangers, and thermal resistances of the tube and deposit materials.

Since all parameters of importance (flue gas emissivity, enthalpies, and deposit radiative properties) directly depend on the temperature, an iterative technique is used for convergence of the results. The Newton-Raphson method can be applied, which proved to be a highly efficient technique and widely used in solving non-linear radiation equations. In this method each non-linear function is differentiated with respect to each master unknown to form the Jacobian matrix. A set of linear equations is formed from the Jacobian matrix that can be solved to approximate a solution to the nonlinear equations. By iteratively solving successive sets of linear equations, a solution to the nonlinear equations can be found. More details regarding this method can be found elsewhere [107].

Once all unknown parameters are calculated, as a final assessment of thermal performance, the boiler efficiency can be directly estimated:

$$\eta_B = \frac{\dot{Q}_N}{\dot{Q}_{Fuel}} = \frac{\dot{M}_{Evap}\left(h_{Sh3,2} - h_{Fw1}\right) + \left(\dot{M}_{Dsh1} + \dot{M}_{Dsh2}\right)\left(h_{Sh3,2} - h_{Dsh}\right)}{\dot{M}_B \mathrm{LHV}} + \\ + \frac{\dot{M}_{Rh}\left(h_{Rh2,2} - h_{Rh1,1}\right) + \dot{M}_{Dsh3}\left(h_{Rh2,2} - h_{Dsh3}\right)}{\dot{M}_B \mathrm{LHV}} \tag{4.38}$$

$$\dot{M}_{Rh} \approx 0.95 \cdot \dot{M}_{LiveSteam} = 0.95 \cdot \left[\dot{M}_{Evap} + \left(\dot{M}_{Dsh1} + \dot{M}_{Dsh2}\right)\right] \tag{4.39}$$

4.3.4 Variations in Steam Parameters

The steam produced in the evaporator, in general, is passing through one or more primary superheating sections, where it is raised to some intermediate temperature, after continuing to flow through the secondary and final stage of superheating.

The heat exchange areas of the superheaters / reheaters are usually oversized to achieve the required full steam temperatures for lower boiler's loads (typically up to 60 % of full load). As a consequence, the additional mass flow of spray-water needs to be injected via the attemperators in order to cool down the overheated steam to the designed parameters.

As an example, the mass flow of spray-water needed after the first stage of steam superheating can be derived from the following thermal balance of SH1 section, as shown in Figure 4-8:

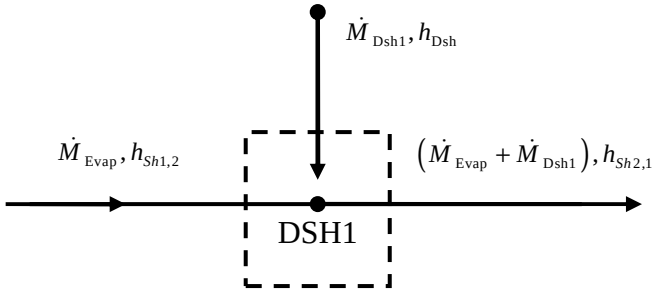

Figure 4-8. Thermal balance of the 1st stage superheater spray attemperator DSH1.

$$\dot{M}_{Evap}\left(h_{Sh1,2} - h_{Sh2,1}\right) = \dot{M}_{Dsh1}\left(h_{Sh2,1} - h_{Dsh}\right) \tag{4.40}$$

$$\dot{M}_{Dsh1} = \dot{M}_{Evap}\frac{\left(h_{Sh1,2} - h_{Sh2,1}\right)}{\left(h_{Sh2,1} - h_{Dsh}\right)} \tag{4.41}$$

In the above equations, the steam enthalpy ($h_{Sh2,1}$) and thus its temperature after ($t_{Sh2,1}$=?) spray-water injection needs to be known or determined. The steam superheating process and the algorithm used to calculate the cool-down to intermediate steam temperatures (after spray-water injections) is schematically presented in Figure 4-9.

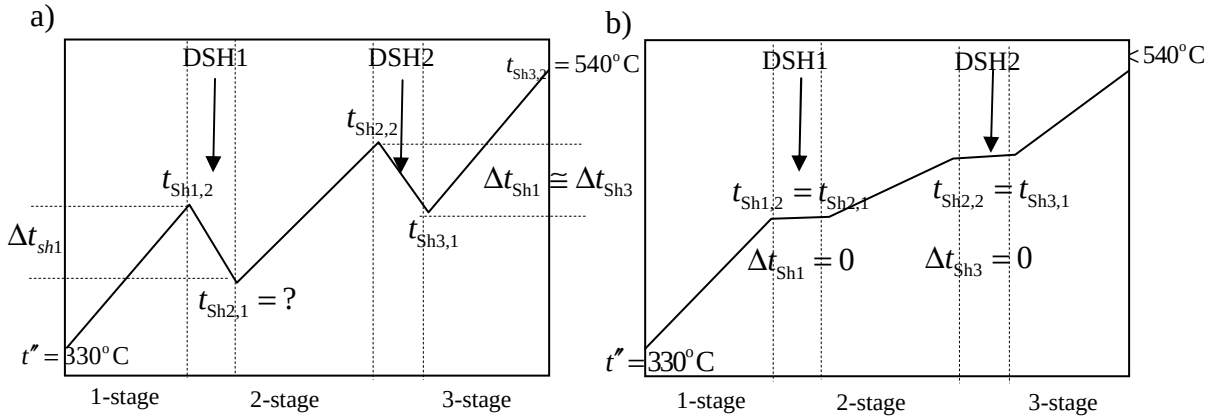

Figure 4-9. Illustrative increase of steam temperature during three-stage of superheating.

The algorithm used is based on the assumption of the same temperature drop of superheated steam when spray-water is injected by the first (DSH1) and second (DSH2) attemperators. The outlet temperature of the steam passed through the first superheating stages ($t_{Sh1,2}$) and the inlet steam temperature to the third superheating section ($t_{Sh3,1}$) can be determined from the thermal balances of the SH1 and SH3 superheaters when including flue gas side, for the known inlet t''=330^{o}C and outlet ($t_{Sh3,2}$=540^{o}C) steam temperatures, respectively. To determine the temperature at the inlet to SH2, ($t_{Sh2,1}$=?) the mentioned above assumption is used, according to which:

$$\left(t_{Sh1,2} - t_{Sh2,1}\right) = \left(t_{Sh2,2} - t_{Sh3,1}\right) \tag{4.42}$$

and then:

$$t_{\mathrm{Sh2,1}} = \left(t_{\mathrm{Sh1,2}} + t_{\mathrm{Sh3,1}}\right) - t_{\mathrm{Sh2,2}} \tag{4.43}$$

The remaining steam temperature at the SH2 outlet ($t_{\mathrm{Sh2,2}}$) is derived from the thermal balance equation written for the SH2 superheater.

During the operation of the boiler under specific conditions, e.g. partial boiler loads, or increased ash deposition, the outlet nominal temperature may not be obtained or reduced mass flows of water-spray injections can be expected, as shown schematically in Figure 4.8-b. A similar algorithm can be applied for reheat steam. Although the spray-water injections into superheaters do not affect significantly the efficiency of the unit, spraying in reheaters is generally not desirable, because of reducing effects on the overall thermal cycle efficiency.

4.3.5 Overall Heat Transfer Coefficient

The overall heat transfer coefficient expresses the rate of heat transferred (in kW/m^{2}K) from flue gasses through the subsequent layers of the tubes and deposit material to the water/steam. Its value is determined by the heat exchanger type and localisation within the boiler, including the heat exchanger geometry, the tube arrangement (staggered, in-line tube banks, tube walls), fluid flow directions and turbulence conditions. Other critical parameters include the local temperature gradients and fluids/materials physical properties (such as e.g. medium viscosity, medium/tube (deposit) material conductivity, thickness of deposit layers etc.). Assuming negligible value of the thermal resistance of the tube metal (due to its very high thermal conductivity), the overall coefficient of heat transfer can be given by [132, 135]:

$$k_{\mathrm{SH1}} = \frac{\alpha_g}{1 + \left(R_d + \frac{1}{\alpha_s}\right)\alpha_g} \tag{4.44}$$

$$\text{or} \quad k_{\mathrm{SH1}} = \psi_{\mathrm{Con}} \cdot k_{SH1\_Clean} = \psi_{\mathrm{Con}} \frac{\alpha_g}{1 + \frac{\alpha_g}{\alpha_s}} \tag{4.45}$$

where α_g is the combined radiation and convective heat transfer coefficient of flue gases; α_s - is the convective heat transfer coefficient of water/steam, R_d – is the thermal resistance of the ash deposit, and ψ_{Con} is the thermal efficiency factor [136] of a convective heat-exchange surface, defined as a quotient of overall heat transfer coefficients in real and ideal-clean conditions. More details of the applied into model formulas can be found in Appendix 1.

The key point is associated with a proper estimation of the thermal deposits resistance growth in time, which is affected by the fouling tendency of the ash in given conditions. Usually, due to the complex nature of the ash deposition process these coefficients are derived from experimental lab-scale tests or boiler's trials, with a limitation to certain conditions. Some of the more interesting empirical correlations which link the thermal efficiency factor of convective surface with the ash quality have been found by Pronobis [136]. These correlations have been derived from experimental tests carried out in pulverised fuel fired Polish steam boilers and are valid for heating surfaces covered with loose or slightly sintered deposits (for exact formulas see Appendix 1).

4.3.6 Fuel Burn-Out Rate Assessment

Proper calculation of the thermal balance in the boiler furnace requires the assessment of the fuel burn-out degree over the furnace chamber height. The basic equation which determines the one-dimensional fuel burnout profiles, related to the total fuel burn-out in the furnace (q_{UBC}) can be determined by a simple relationship [119]:

$$\beta_j = \frac{\overline{H}_j}{\overline{H}_j + 0.01 q_{\mathrm{UBC}}} \cdot \frac{1}{1 - 0.01 q_{\mathrm{UBC}}} \tag{4.46}$$

Where $\overline{H}_j$ is the relative height from the bottom plane of the first zone to the top plane of the arbitrary j^{th} zone, and q_{UBC} is the value of heat energy loss due to unburned carbon which can be derived from experimental trials or alternatively calculated by the following formula proposed by Kouprianov, which has been validated for coals with an accuracy of 2-4%:

$$q_{\mathrm{UBC}} = 0.52 C_f C_b C_{sr} \left[1.5 + C_a (\lambda)^{1.2}\right] \frac{\left(\mathrm{Ash}^{\mathrm{ar}} n_{90}\right)^{0.9}}{\left(\mathrm{VM}^{\mathrm{daf}}\right)^{1.5}} \tag{4.47}$$

C_f, C_b, C_{sr}, and C_a are the fuel, burner, ash removal and air empirical factors which are determined by the boiler and fuel type as described in [119], λ is the excess air ratio, $\mathrm{Ash}^{\mathrm{ar}}$ is the ash content of the fuel, n_{90} is the dust fineness and $\mathrm{VM}^{\mathrm{daf}}$ is the volatile content. According to the literature, this formula gives good assessment of heat loss for burning pure coals. However, the temperature dependent kinetic parameters are not included within this empirical correlation, limiting its predictions e.g. for partial boiler loads. Some indicative degrees of fuel burn-out over the furnace height are presented in Table 4-2.

Applying above correlations for biomass co-firing cases leads to larger uncertainties. This simple model without including the temperature effect on fuel conversion may be not sufficient for solid fuels with relatively wide range of moisture, high amount of volatiles, and

wide particle size distribution dominating with larger particles. In most cases, when co-firing higher shares of biomass, better degrees of fuel burn-out are predicted, which is not always true with operational boiler data [137, 138]. In theory, the higher amount of volatile matter is important because it counteracts the generally larger size of the biomass particles. Overall, for an equal particle size, the burn-out in case of biomass is higher than for coal. In addition, when coal/woody biomass blends are considered, due to the fact that biomass is much harder to grind than coal, more pressure is also exerted on the coal particles resulting in much finer particles then when coal is milled alone.

Table 4-2. Degree of fuel burn-out in different zones over the furnace height [110, 119].

	Zone location over the furnace height *Hi*/*Hf*					
Type of fuel fired	0.15	0.20	0.30	0.40	0.50	1.00
Anthracite, semi-anthracite	0.72-0.86	0.86-0.90	0.92-0.95	0.93-0.96	0.94-0.97	0.96-0.97
Black coals	0.90-0.94	0.92-0.96	0.95-0.97	0.96-0.98	0.98-0.99	0.98-0.995
Brown coals	0.91-0.95	0.93-0.97	0.96-0.98	0.97-0.98	0.98-0.99	0.99-0.995
Natural gas, Fuel oil	-	-	0.94-0.96	0.96-0.98	0.97-0.99	0.995

Furthermore, as it has been proved by sensitivity studies performed by Kouprianov, it is not expected that the differences in biomass burn-out will significantly change the temperature profile and affect ash behaviour. Therefore, in order to make predictions more comparable, a constant value of UBC equally to 5% is assumed for all co-firing cases, and the heat loss (q_{UBC}) is given by

$$q^{*}_{\mathrm{UBC}} = \frac{\mathrm{Ash}^{ar}}{(100-\mathrm{UBC\%})} \cdot \mathrm{UBC\%} \cdot \frac{32.762}{\mathrm{LHV}}, \% \qquad (4.48)$$

However, it should be kept in mind that heat loss related with unburnt fuel contributes to a drop in overall boiler efficiency and the increased carbon content in the fly ash (above 5%) influencing the quality of the ash used for sale.

4.4 Results and Discussion – Model Sensitivity Analysis

In this subsection, the results obtained from the application of the zone-based model into the 235 MW_e wall-fired pulverised fuel boiler are presented and discussed. The model response sensitivity is tested for various operational conditions, including the impact of firing poorer quality fuels on the thermal performance of the boiler. The investigated cases include:

- Boiler load change.
- Fuel distribution and air excess change.

- Impact of moisture and ash content change in fuel (fuel switching)
- Deposits resistance and emissivity.

All presented cases, except the last one, are investigated for clean heat-exchange surfaces to give a base-reference-line for further comparison, when the ash deposition effects will be included.

4.4.1 The 235 MW_e PF Wall-Fired Boiler

The zonal method presented in this work is applied to the E.ON operated Genk-Langerlo 235 MW_e pulverised coal-fired boiler, fired with typical bituminous coal and different blends of biomass (see Table 4-7). This unit was built and put into service in 1972-1974, and was originally designed for fuel oil firing and generated 300 MW_e with a steam cycle of 130 bar, 540°C/540°C [139, 140]. The general layout of the investigated boiler with some major operational data are presented in Figure 4-10 and Table 4-3. More information regarding the boiler geometry and steam cycle are included in Appendix I.

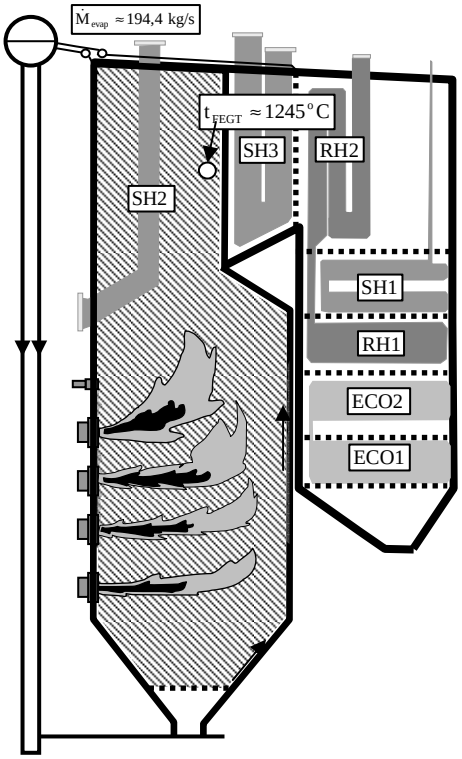

Figure 4-10. Boiler layout with basic parameters.

Table 4-3. Main data for Langerlo boiler.

Thermal Input	618 MW_{th}
Electrical Output	235 MW_e
Steam Raised	194.4 kg/s (700 t/h)
Coal mass flow for LHV=28.0MJ/kg	30.15 (108.5) kg/s (t/h)
Superheated Steam	540°C / bar
Reheated Steam	540°C / bar
t_{FEGT}	1245°C

The boiler is of the natural circulation two-pass type. In 1985-1986, two of these identical units, installed in Genk-Langerlo (Belgium), were converted to coal and natural gas firing, after the oil crisis. During this fuel transit process the furnaces of the existing boilers was not drastically changed. However, the nominal gross power capacity of boiler had to be de-rated to 235 MW_e .

The front-wall fired furnace of the investigated boiler consists of four burner rows with each having four low-NOx coal burners, with secondary overfire ports above the main burner zone. In the upper part of the furnace the platen "L-type" and final pendant superheater are located, which along with a primary superheater in the convective section, are integral parts of the three stage steam superheating process. Double stage reheaters are placed in a back-pass of the boiler and at the end of the originally constructed flue gas path two tube-type economisers are located .

4.4.2 The Effect of Boiler Load Change

As a reference fuel, the medium volatile and intermediate-ash subbituminous Colombian Coal has been selected. The proximate analysis of reference coal is shown in Table 4-4.

Table 4-4**.** Fuel reference data.

Fuel	LHV, kJ/kg (ar)	FC, % (ar)	VM, % (ar)	Moisture, %	Ash, %
Colombian Coal (CO1)	26080	48.17	34.03	9.00	8.80

The maximum (235 MW_e), and two intermediate stages of boiler loads (Table 4-5) are simulated for combustion of the reference fuel. The goal is to check whether the predicted thermal performance parameters corresponds sufficiently well with operational/design basic data, in particular if the steam nominal outlet parameters are achieved for the 50 %MCR partial load (approximately 60% of thermal fuel load).

As non-deposition cases are investigated in this section, the boundary conditions were set up as for a clean surface condition, given by: the surface emissivity equals to 0.75; the thermal resistance of furnace walls - 2.5 m^2K/kW and platen superheater (SH2) - 6.45 m^2K/kW, respectively.

Table 4-5. Operational parameters for different boiler's loads.

Gross power output	90 MW_e	120 MW_e	165 MW_e	235 MW_e
Applicable Load Range	Minimum	Intermediate 1	Intermediate 2	Maximum
% Load	38 % MCR	50 % MCR	70 % MCR	100 % MCR
Fuel Heat Input	1025 GJ/h	1310 GJ/h	1715 GJ/h	2225 GJ/h
Temp. of SH/RH Steam	<540/ < 540	540 / 540	540 / 540	540/540

The temperature profile predicted for the maximum boiler load shows good agreement with the one obtained from CFD simulation performed by van Ormelingen and Co-workers [141], as shown in Figure 4-11. The CFD-AIOLOS code used in these simulations, developed

at the University of Stuttgart was intensively validated, in particular with respect to the three-dimensional temperature distributions, which were compared with acoustic pyrometry measurements giving satisfactory results [142].

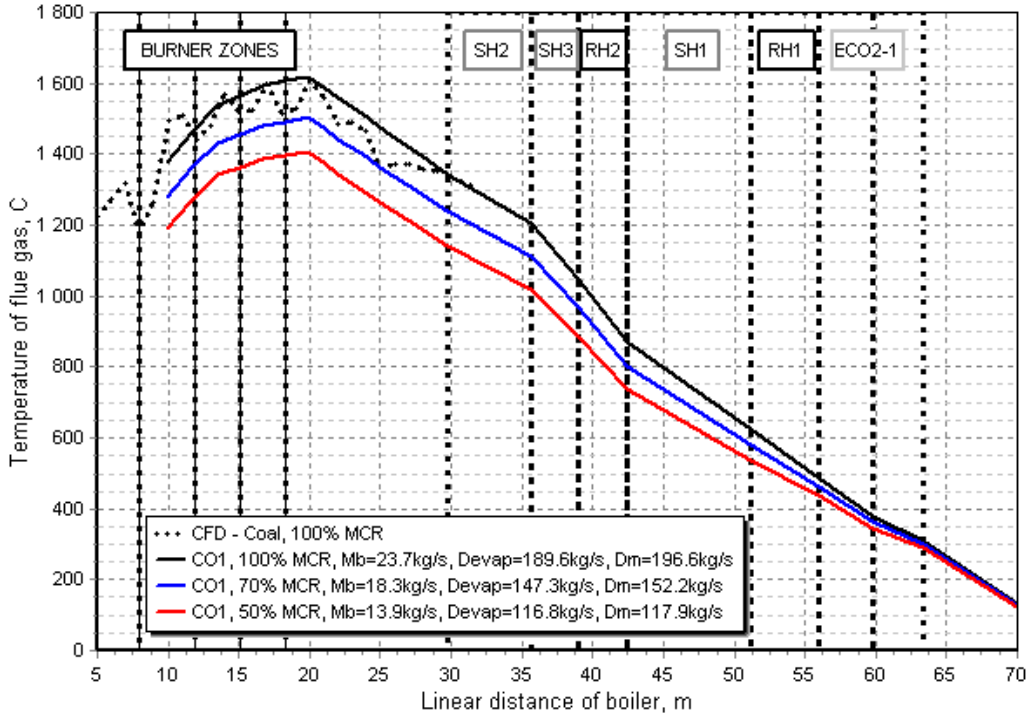

Figure 4-11. Predicted gas temperature profiles for different boiler loads - pure coal combustion case: Mb- fuel mass flow, Dm - Livesteam mass flow Dm=Devap+DSH1+DSH2.

The maximum flue gas temperature was predicted at the outlet of the burner zones (1615^{o}C), whereas the temperature of gas entering the convective section (after platen superheater) was slightly above 1200^{o}C. The higher differences in results obtained from the zonal and CFD models appeared at the 25m level of the furnace, when over fire air is introduced. This additional air, on the one hand ensures more complete combustion and on the other hand dilutes the flue gas, and overall leads to a decrease in temperature in this region. Although the over fire air effect is not included within the zonal model, these large temperature variations are reduced in the furnace outlet giving satisfactory comparison with CFD predictions. The simulations performed for lower boiler loads give reasonable profiles, and the steam outlet temperatures up to 50 %MCR load are obtained for both the superheated and reheated steam (540^{o}C). Furthermore, the mass flows of raised steam ($\dot{M}_{Evap}$=D$_{evap}$), as shown in Figure 4-12 correspond quite well with design operational boiler data and spray-water injection flows ($\dot{M}_{Dsh1}$=DSH1, $\dot{M}_{Dsh2}$=DSH2 and $\dot{M}_{Drh}$=DSH3) and are comparable to those of typical pulverised fuel fired boilers of such capacity.

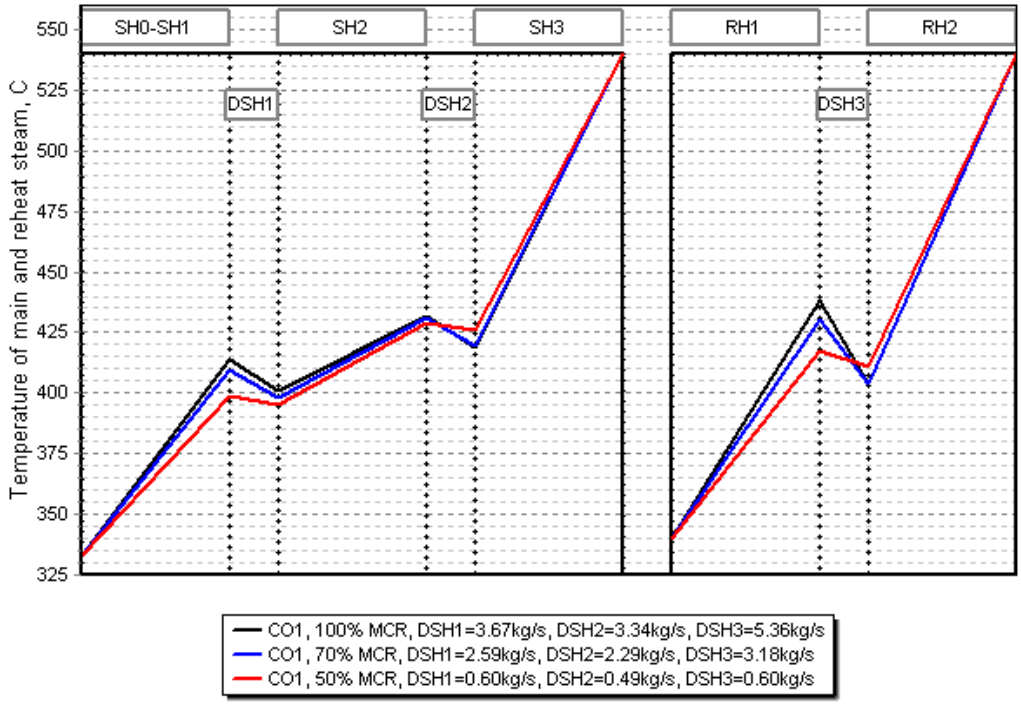

Figure 4-12. Predicted variations in steam parameters for different boiler loads and coal combustion case.

4.4.3 The Effect of Fuel Distribution and Air Excess Change

The investigated cases for analysing the effects of fuel distribution and total air excess changes are shown in Table 4-6. Simulations were carried out for full boiler load, clean surface properties and Colombian Coal as a reference fuel.

Table 4-6. Operational parameters settings for studying the effects of fuel distribution and air excess ratio.

	Change in Fuel Distribution					
Case	Load, %	B1	B2	B3	B4	α
1fd	100	0.25	0.25	0.25	0.25	1.1
2fd	100	0.35	0.30	0.20	0.15	1.1
3fd	100	0.50	0.50	0.00	0.00	1.1
4fd	100	0.15	0.20	0.30	0.35	1.1
	Change in Total Air Excess Ratio					
1ea	100	0.25	0.25	0.25	0.25	1.1
2ea	100	0.25	0.25	0.25	0.25	1.2
3ea	100	0.25	0.25	0.25	0.25	1.3

where B indicates the ratio of total fuel introduced into given burner tier

The predicted temperature profiles are presented in Figure 4-13, whilst the relative changes in furnace efficiency and mass flows of steam produced are shown in Figure 4-14.

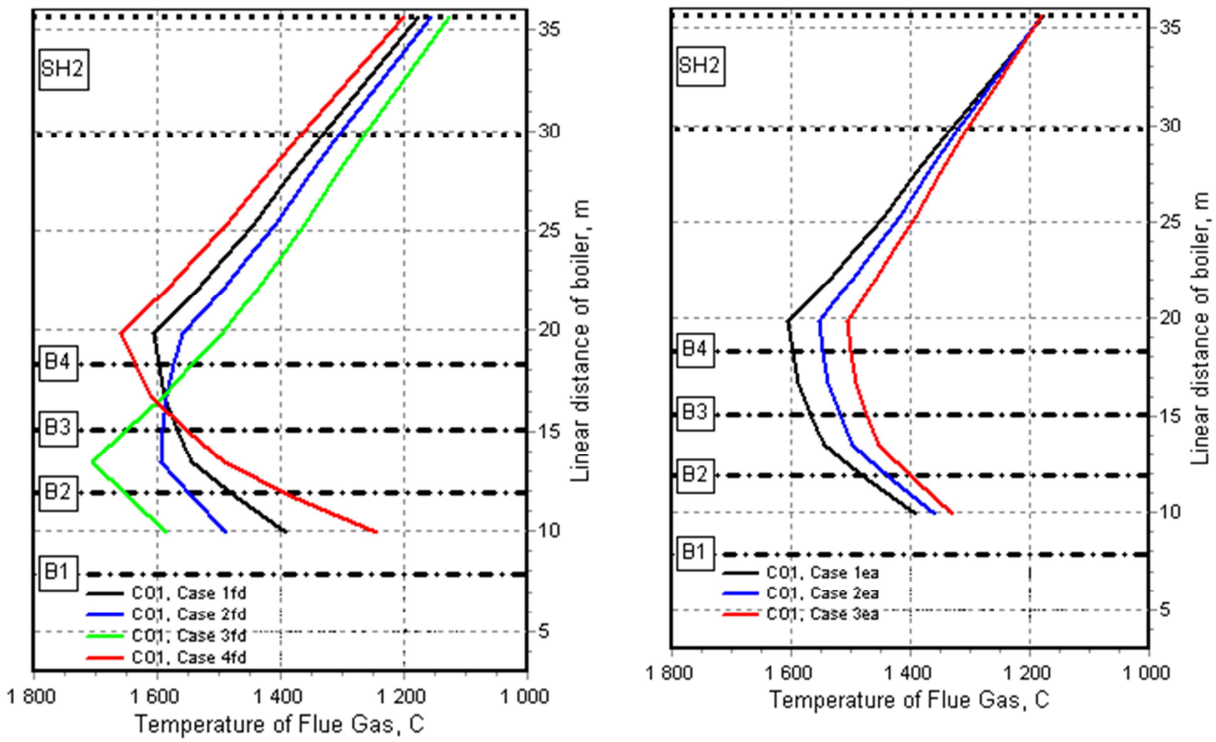

Figure 4-13. Predicted temperature profiles for different fuel distribution and excess air ratio cases.

Analysing the results obtained it can be concluded that overloading the lower part of the furnace "case 3fd" as well as increasing total air excess in the furnace ("case 3ea") have the greatest impact on thermal performance. However, while the "case 3fd" leads to increase the furnace efficiency the raise in air excess ratio clearly contributes to the efficiency drop (for λ=1.3,up to 6% efficiency decrease or 15% relative change to the reference case) as shown in Figure 4-14.

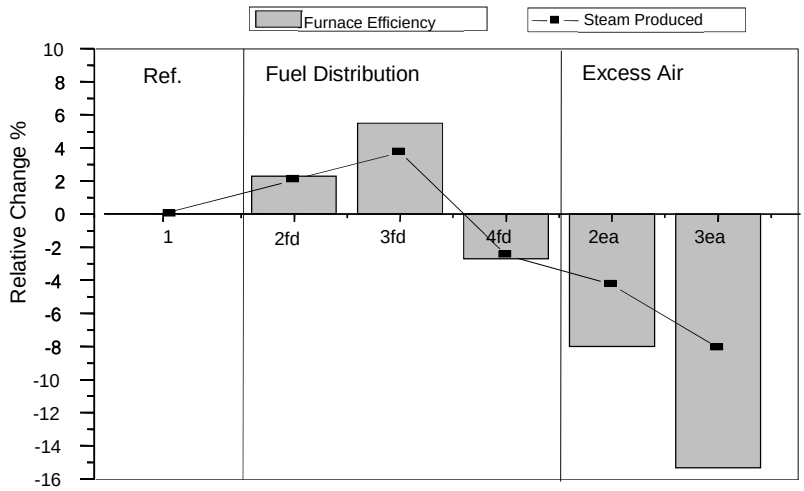

Figure 4-14**.** The effects of fuel distribution, excess air on relative change in boiler furnace efficiency and mass flows of steam produced.

Moreover, the furnace efficiency improvement related to shifting firing densities towards lower furnace levels, may lead to a significant increase of local heat fluxes in these regions, and cause both tube overheating and increased slagging risk.

4.4.4 The Effect of Fuel Switching

The amount of incombustible matter, such as ash and moisture, can significantly vary in low calorific biomass/waste fuels changing the thermal performance of the boiler. These fuel quality variations may mainly affect the radiative heat transfer, which depends on the radiative properties of combustion gases and solid particulates produced by burning of solid fuels. Furthermore, a relatively low adiabatic flame temperature may also influence the flame stability and fuel conversion in the furnace.

In this subsection, the zonal model responses are tested concerning the co-firing of substitute fuels with extreme and intermediate values of ash and moisture presence, namely sawdust (low-ash, high-moisture), olive residue (intermediate ash and moisture) and sewage sludge (high-ash), respectively. The reference Colombian coal with up to 40% thermal biomass substitution as considered. The slagging/fouling effects on thermal boiler performance are not evaluated here but are part of larger discussion in the following subsections. The proximate and ultimate analysis of the investigated fuels and some basic thermal properties of the flame are presented in Table 4-7.

Analysing the fuels' thermal properties, it can be noticed regarding the low-ash sawdust as an example, that increasing the moisture input in general dilutes the flue gas and leads to a drop in adiabatic temperature, slightly improving the emissivity of flue gas. The same effect can be also visible in comparison of the 40% wet sawdust with the high –ash (48%) sewage sludge as fuels. Although, the sewage sludge has the lowest calorific value amongst the fuel investigated, its adiabatic flame temperature is slightly above the value calculated for 40% wet sawdust (Figure 4-15a).

Moreover, despite the low LHV which usually results in increased volume of flue gas produced for the same fuel thermal input, the high concentration of fly ash in sewage sludge may significantly improve the radiative heat transfer in the furnace. The contribution of the fly ash particles to the total flame emissivity for co-firing coal-sawdust and coal-sewage sludge blends, calculated based on the WGSM model at 1300^{o}C, is shown in Figure 4-15b. Further discussion in relation to the obtained thermal boiler characteristics is continued later on in this subsection.

Table 4-7. Investigated fuels data.

Fuel property	**Colombian Coal– CO1**	**Sawdust SD2/SD2wet**	**Olive Residue – OR3**	**Sewage Sludge – SL1**
LHV,(ar) kJ/kg	26080	17630 / 10480	16400	9100
Proximate analysis (% as received basis)				
Volatile Matter (VM)	34.03	77.43 / 49.94	66.24	36.72
Fixed Carbon (FC)	48.17	14.85 / 9.58	14.92	2.75
Moisture	9.00	6.98 / 40.00	9.00	11.72
Ash	8.80	0.74 / 0.48	9.84	48.81
Ultimate Analysis (% dry ash free)				
C	81.0	50.46	46.76	48.44
H	5.50	6.62	5.95	10.54
N	1.70	0.21	1.37	6.71
S	0.70	0.07	0.06	1.95
Cl	0.01	0.01	1.00	0.50
O	11.10	42.65	34.20	32.35
Thermal Properties of the Flame, ^{o}C				
Adiabatic Flame Temp, ^{o}C	2090	1992 / 1677	1969	1721
Emissivity (Gas+Ash)	0.612	0.484 / 0.506	0.682	0.948

Emissivity of flame was calculated at 1300^{o}C for mean beam length.

The flue gas temperature profiles as well as other boiler thermal performance parameters variations predicted for pure coal firing and blends with wet sawdust, sewage sludge and olive residues, up to 40% thermal co-firing ratio are presented in Figures 4-16..4-19.

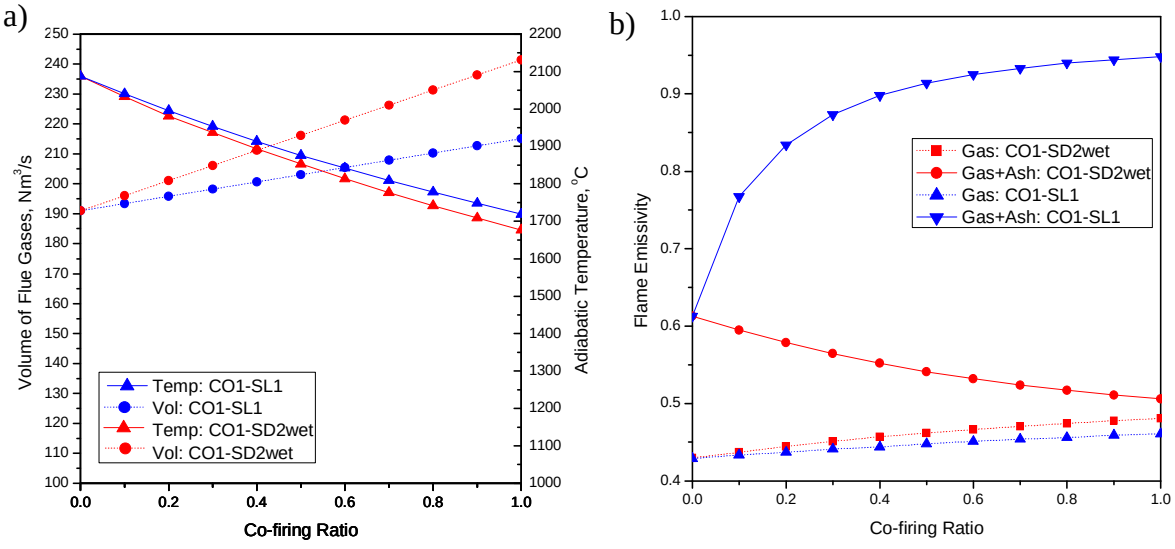

Figure 4-15**.** Calculated volumes of flue gas produced and thermal properties of flame for various co-firing ratios.

Simulations were carried out for full boiler load with operational parameters given in Table 4-8. The results show a lower gas temperature for co-firing in the furnace and, correspondingly, a slightly higher level in the convective section of the boiler compared with pure coal combustion. This is due to the different radiative properties and lower adiabatic temperatures of the gaseous combustion products for biomass that affect the combustion and heat transfer. The temperature rise in the convective section for sawdust co-firing cases is due to the lower heat absorption in the furnace, which is indicated by decreased furnace efficiency. In other words, the heat transfer is shifted towards the convective section of boiler, and as a consequence lower mass flows of steam are produced.

Table 4-8. Operating conditions set-up for biomass co-combustion simulations.

Operating Conditions	Value	Deposit Properties	Value
Thermal input	618 MW (100%)	Thermal Resistance of the Water/Wall Deposit	2.5 m^2K/kW
Uniform Fuel Distribution	4 x 0.25		
Fuel Fineness, n_{90}	15%	Thermal Resistance of the SH2 Deposit	6.45 m^2K/kW
Unburned Coal in Ash, UBC	5.0%		
Total Air Excess, α	1.1	Emissivity of Deposit	0.75

This is opposite to the results obtained for sewage sludge co-firing, for which an increase in furnace efficiency and mass flows of generated steam was observed up to approximately 10th% co-firing share. The raised values of these parameters (above the nominal related with pure coal combustion) were achieved also for higher biomass rates (up to 40th%).

The lowest impact on thermal furnace characteristics and the amount of the steam produced was observed for cases with olive residues co-firing. This could be explained by the comparable content of ash and moisture in comparison with coal fired, and slightly lower adiabatic flame temperature.

Analysing the effects of co-firing on steam temperature variations, it must be highlighted that sawdust co-firing generates more instabilities. As already mentioned earlier, less efficiency in steam production and increased temperatures in the convective section as well as larger flue gas velocities are all factors influencing positively the heat transfer conditions downstream the furnace, and are responsible for such a sensitivity to steam temperature changes. As a consequence higher spray-water injections are required to cool down the temperatures to the nominal level. Overall, co-firing high percentages of wet sawdust may lead to a significant drop in boiler efficiency (up to 2.8% for 40th%), lower steam generation,

and higher steam parameter variations, which results in steam overheating and increased spray-water injection.

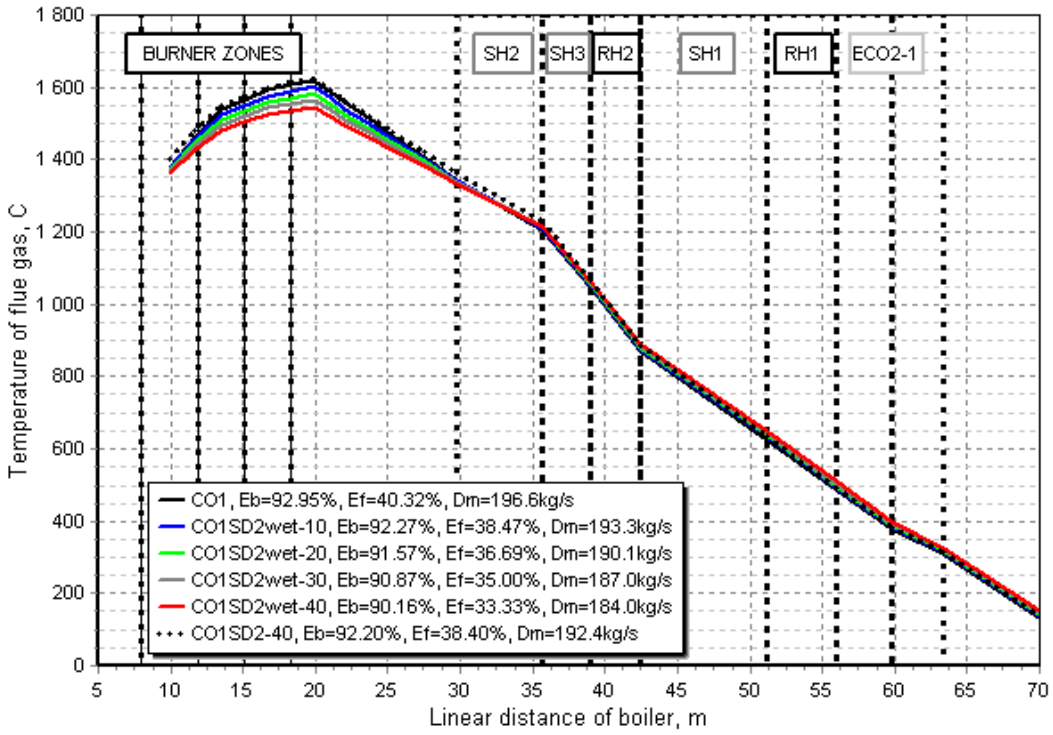

Figure 4-16. Predicted gas temperature profiles for sawdust co-firing with Colombian coal.

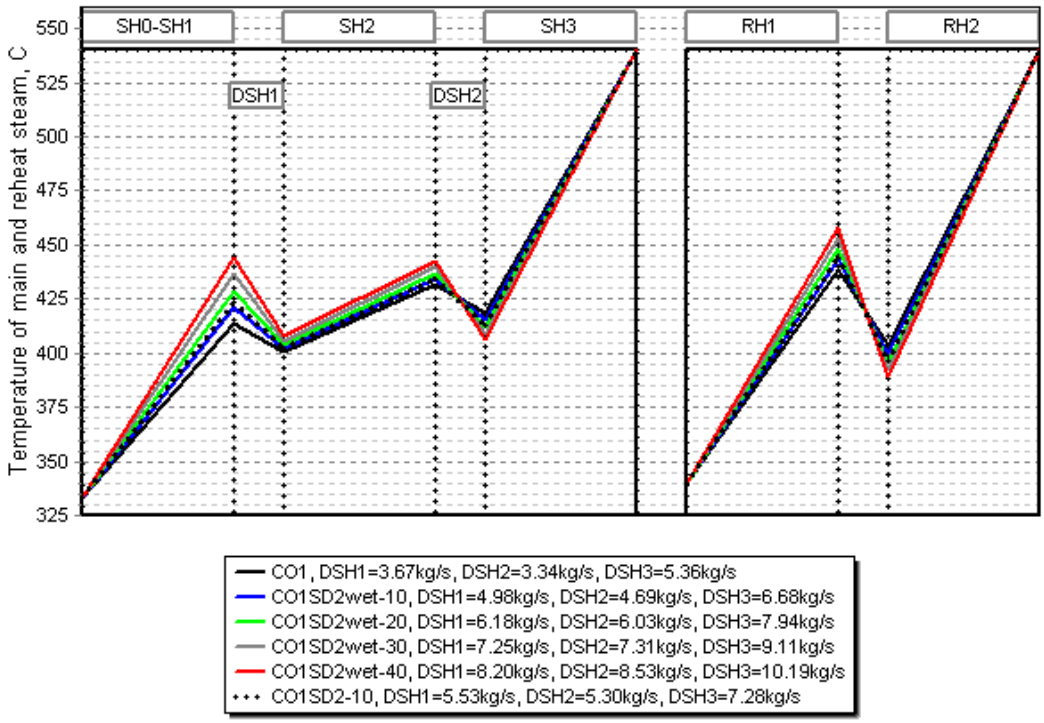

Figure 4-17. Predicted variations in steam parameters for sawdust co-firing with Colombian coal.

Co-firing of a high-ash, dried sewage sludge may improve radiative heat transfer in the furnace and thermal boiler performance. However, the increase in heat absorption leads to corresponding higher heat fluxes, and thus temperature of the furnace wall as well. This, in turn may enhance the risk of slagging of sewage sludge ashes: this is a well-known phenomenon due to their low fusion temperatures.

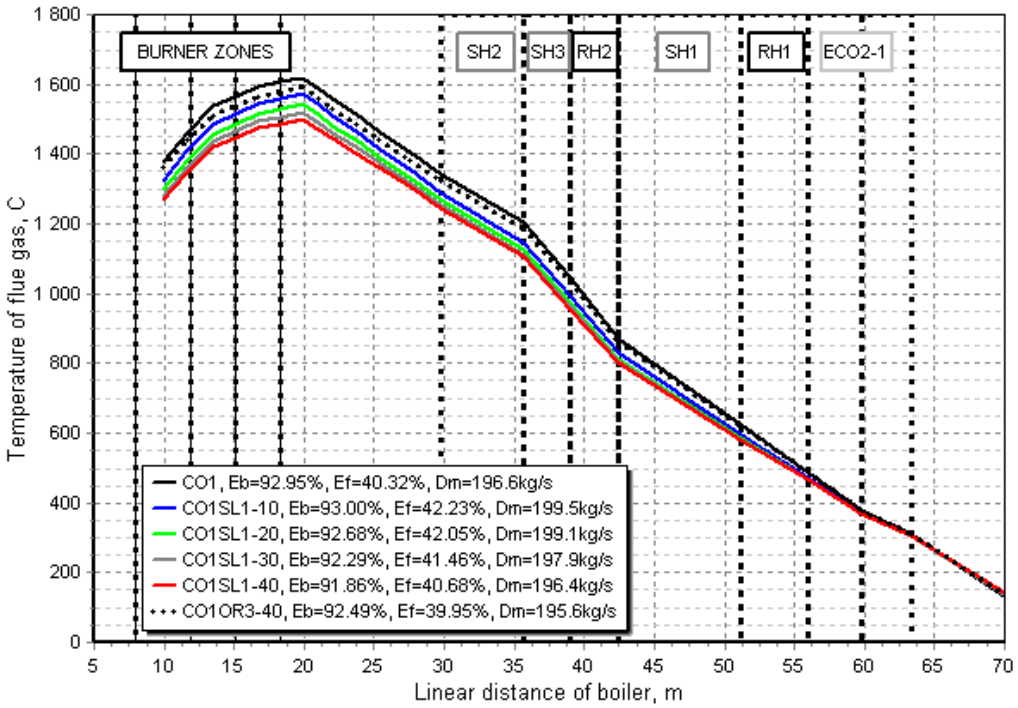

Figure 4-18. Predicted gas temperature profiles for sewage sludge co-firing with Colombian coal.

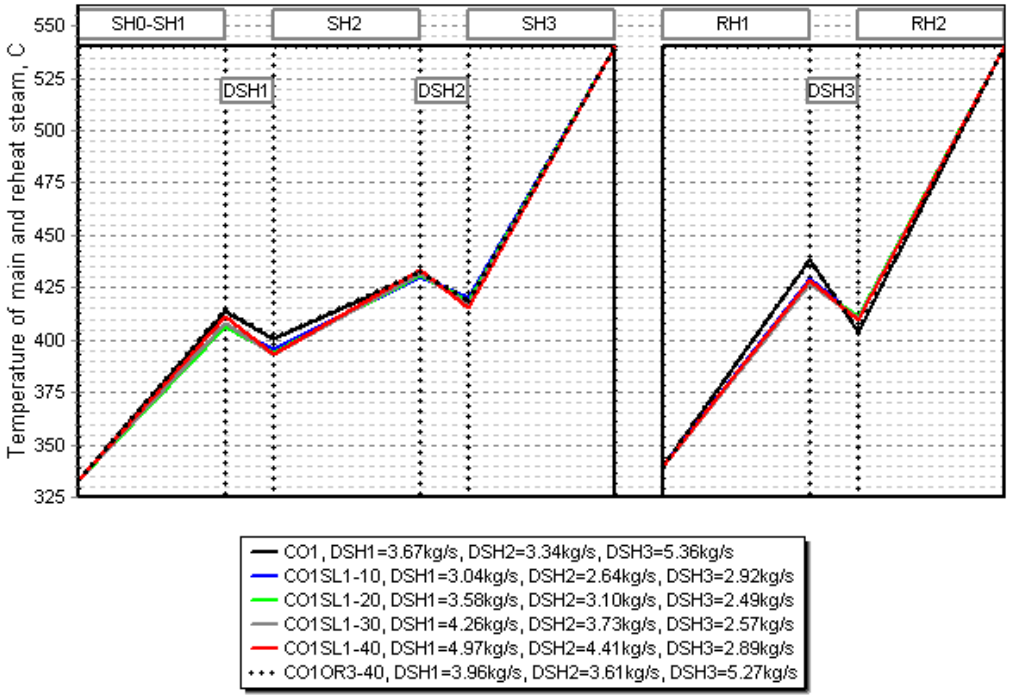

Figure 4-19**.** Predicted variations in steam parameters for sewage sludge co-firing with Colombian coal.

4.4.5 The Effect of Slagging Conditions Change

Slagging conditions can be simulated by varying the thermal resistance of the furnace wall deposits over the height of the furnace. As the risk of slagging is highly dependent on the incident heat flux falling on the walls, which reaches its maximum at the outlet of the burner zones, the following proportional correlations can be assumed for studying model sensitivity:

$$R_{loc} = R_{\max} \frac{\dot{q}_{inc,loc}}{\dot{q}_{inc,\max}} \tag{4.49}$$

The "curve shapes" of deposit resistance distributions obtained by eq. 4.49 have been found in coal-fired pf boilers utilising slagging coals [116]. In the above formula is an attempt to relate these slagging conditions directly with the heat load of furnace walls. $R_{\max}$ expresses here the maximum resistance corresponding to the maximum heat incident in this region $q_{inc,max}$ with respect to the conditions when the steady-state deposit layer is reached (described by eq. 4.22, for an ash fusion temperature of 1350^{o}C). Since the emissivity of the deposits is dependent on the temperature and molten state of deposits (among other parameters such as texture and chemistry), the simple correlation proposed by Williams *et al.* [143] can be used:

$$\varepsilon_d = K - 3 \cdot 10^{-4} T_d \tag{4.50}$$

where the parameter K varies depending on the type of deposits, see Table 4-9.

Table 4-9. Parameters used to describe the emissivity of coal ash deposits [143].

Type of deposit	Particle diameter (mm)	K
Glassy	-	1
Sintered	-	0.9
Powder	120	0.85
	33	0.75
	6.5	0.65

All simulated cases describing the extreme and intermediate states of surface conditions, performed to analyse the model sensitivity are summarised in Table 4-10. The reference "operationally clean conditions" is described by a constant thermal resistance of R=2.5 m^{2}K/kW and emissivity equal to 0.75, while severe slagging conditions is defined by cases 3a-3c. The effects of non-linear emissivity distribution along the furnace height (given by eq. 4.50, and assumed sintered deposits, K=0.9) were taken into account in the last case (3c) as a comparison to the assumed constant emissivity values in case 3a. In addition, the intermediate cases were also performed for the average values of deposits resistances that correspond to the non-linear deposit distribution profiles (eq. 4.50). Based on the above, it was possible to

evaluate the effects of a commonly used uniform deposits topography assumption on thermal furnace performance in comparison with more realistic deposits distribution patterns.

Table 4-10. Parameters describing the cases for study the effects of thermal resistance and emissivity of deposits.

	Change in the Wall Thermal Resistance Distribution Model				
Case	Resistance model type		Surface conditions	Emissivity model type	
1	Linear	R_{const}=2.5	Operationally Clean	Linear	ε_{const}=0.75
2a	Non-linear	R_{max}=4.5	Contaminated	Linear	ε_{const}=0.75
2b	Linear	R_{ave}=3.1	Contaminated	Linear	ε_{const}=0.75
3a	Non-linear	R_{max}=5.22	Max. Thickness – Covered with slag	Linear	ε_{const}=0.68
3b	Linear	R_{ave}=3.61	Contaminated	Linear	ε_{const}=0.68
3c	Non-linear	R=5.22	Covered with slag	Non-Linear	ε_{var} (0.52-0.73)

According to the obtained predictions, the maximum furnace exit temperature difference between clean and slag covered furnace walls (cases 1 and 3c) was around 70^{o}C (raised from 1200^{o}C, see Figure 4-21d), leading to a drop in furnace efficiency up to approximetaly 2.7%.

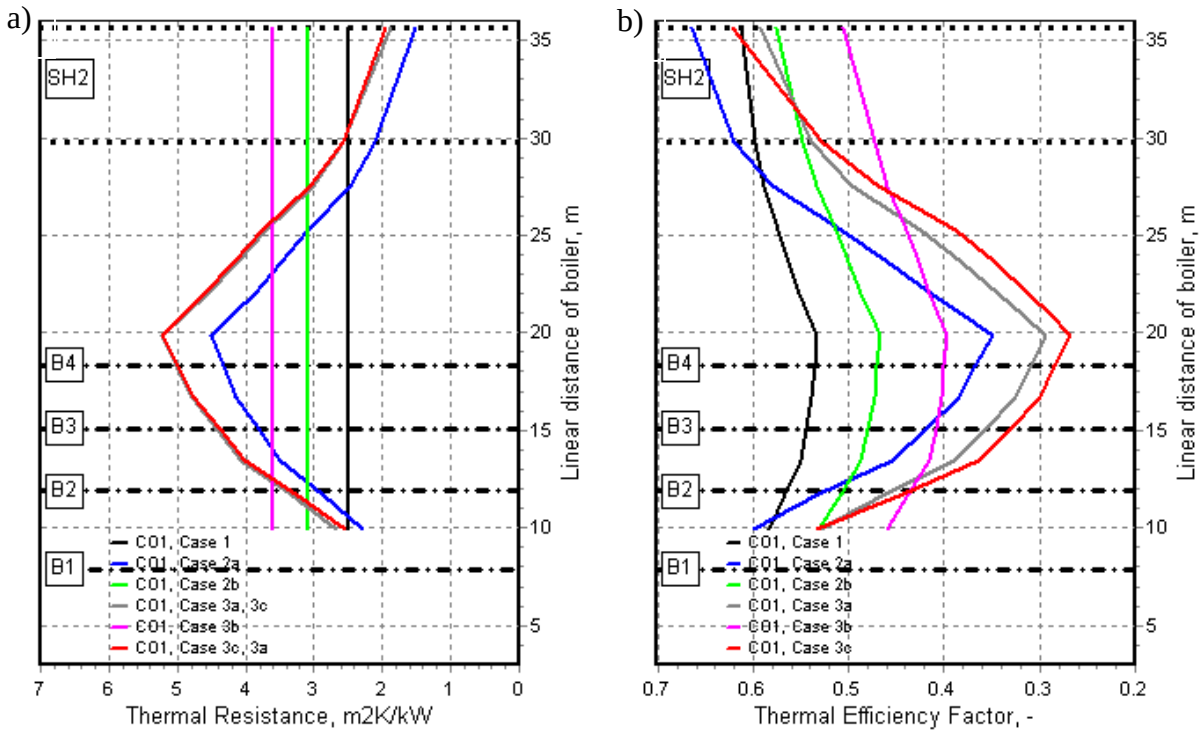

Figure 4-20. Assumed thermal resistance profiles and corresponding calculated thermal efficiency factors over the furnace height.

A similar efficiency fall was noticed with an increased excess air ratio in the furnace (λ=1.2) or is achieved for co-firing of around 15% of high-moisture (40%) sawdust in a non-ash deposition case (Figure 4-16).

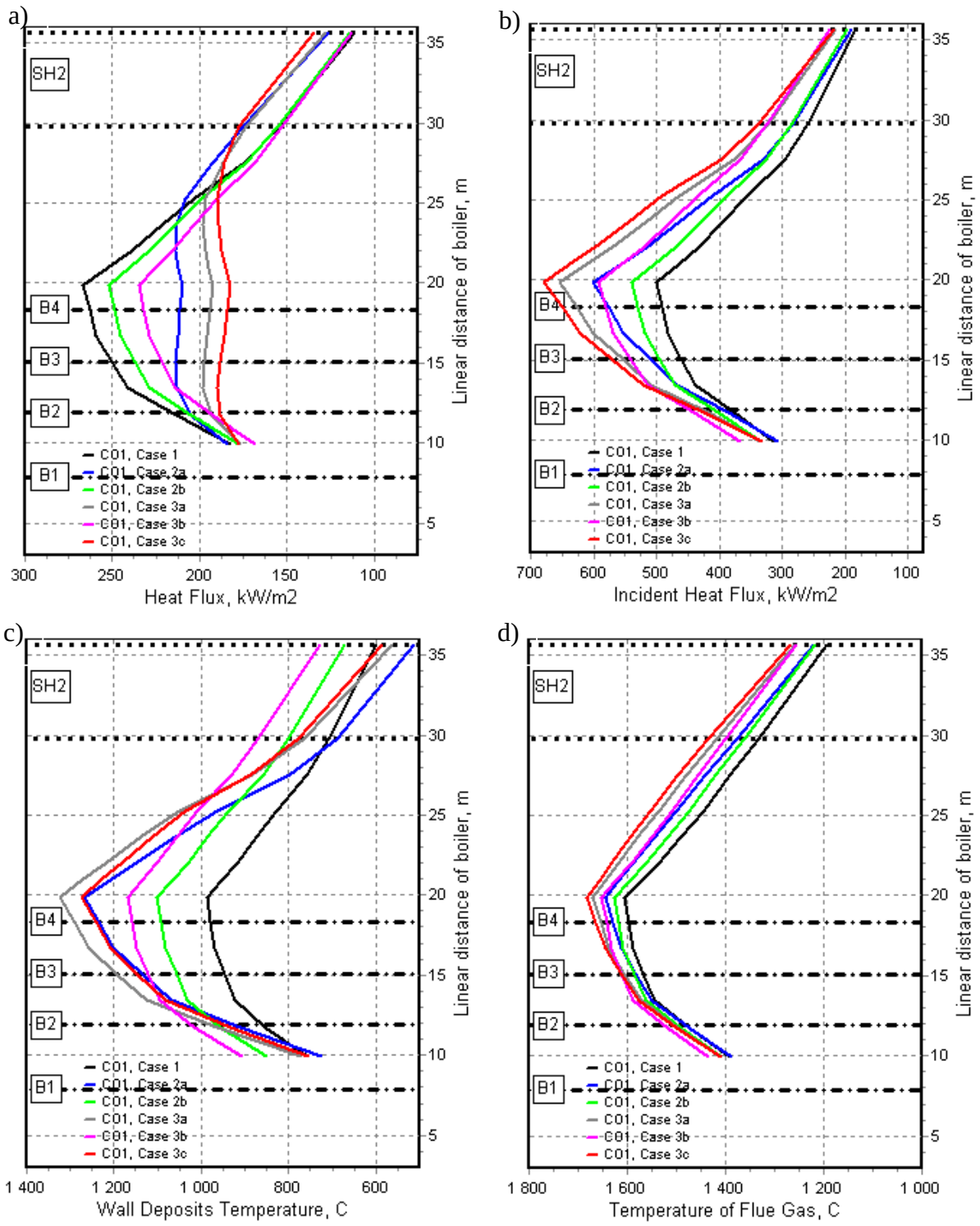

Figure 4-21. Predicted distributions of the heat fluxes and the temperatures of flues gas and wall deposits for assumed thermal resistance deposits profiles.

Moreover, it was observed that when the deposits resistance exceeds 3.65 m^2K/kW (Figure 4-20a) and the thermal efficiency factors fall below 0.4 (Figure 4-20b) a significant decrease in heat flux absorbed by furnace walls may occur, producing “concave shape” heat flux profiles

(Figure 4-21a). This results in shifting the heat absorption process towards upper levels of the furnace and increasing the temperature of the furnace wall deposits above 1100^{o}C. Such a high deposits temperature may lead to the acceleration of the ash sintering process, making deposits difficult to remove.

Furthermore, the simulations revealed that a decrease in emissivity of deposits that have the same thermal resistance (cases 3a, 3c Figure 4-20a and Table 4-10) may result in lowering its outer surface temperature as shown in Figure 4-21c. It is due to the lower heat absorbed by the furnace walls in these zones (Figure 4-21a, cases 3a, 3c), which in consequence, lead to higher heat fluxes to the zones located upstream and overall drop in furnace efficiency.

4.5 Summary

In this chapter a one-dimensional zonal model has been defined and applied to a pulverised fuel fired boiler to analyse the effects of biomass co-firing on thermal boiler performance. Although the developed model is able to give quantitative predictions, it is primarily designed to assess the relative changes of heat exchange efficiency and associated thermodynamic parameters caused by the variations in radiative properties of co-firing fuels as well as the varying resistance of the deposits layers.

The results revealed that the increased ash content in secondary fuels does not change significantly thermal efficiency of the boiler and for certain ratios may even slightly improve boiler performance, e.g. for sewage sludge. However, in case of co-firing with large shares of high-moisture fuels, such as wet sawdust, the boiler efficiency may drop up to 2.8% for a 40% coal substitution.

The conducted sensitivity analysis proved that the deposit resistance pattern is the most important factor that influences all other key parameters, such as furnace efficiency, furnace exit gas temperature as well as mass flow of steam produced. If slagging of the furnace walls occurs, due to the reduced heat absorption in the furnace a relatively low mass flow of steam is evaporated and undesirably high flue gas temperatures may appear entering the convective pass of the boiler (up to 70^{o}C higher than for non-slagging cases). As a consequence, the temperature of the superheated steam increases and to maintain the present constant temperature of the live steam, the mass flow of spray-water injection to the attemperators must be increased. Another factor that has a significant influence on slagging behaviour is the incident heat flux falling on the furnace walls. Overloading of the boiler with incident heat fluxes above 550 kW/m^2 can result in severe furnace slagging.

In order to reduce major uncertainties caused by the unknown slagging and fouling patterns in the furnace, a proper ash deposition model needs to be developed. This would be still a challenge for the one-dimensional approaches since simulating the near-wall boundary ash transport phenomena in the furnace is limited. More realistic results could be obtained for superheaters / reheaters placed perpendicularly to the major flow trajectories. Nevertheless, the combination of a one–dimensional zone method with other on-line monitoring tools, such as heat flux sensors located on the furnace walls may significantly support input data into such a predictor. Despite the mentioned few limitations, the used approach with the aid of the proper ash deposition mechanistic models (which is the focus of the next chapter) is well-suited as engineering tool for simulation and performance analysis of boilers.

5

DEVELOPMENT OF A SLAGGING AND FOULING PREDICTIVE APPROACH

The development of a slagging and fouling predictive methodology integrated within the zone based thermal model of pf boiler is of major focus in this Chapter. It is aimed to develop a reliable model for coal blends but also capable of predicting the effects of biomass on the ash deposition. Due to the non-additive behaviour of the ashes the improved phase equilibrium-based approach which is more adjusted to the conditions existing in the pulverised fuel fired boilers is investigated. In such a thermo-chemical equilibrium model the effects of different activity of certain ash-forming species should be taken into account. Furthermore, the ash deposition related criteria should be carefully evaluated. Two major slagging and fouling mechanisms are investigated including the deposition of molten sticky ash on the heat transfer surfaces placed at the furnace outlet and salts deposition in the convective pass of a boiler. In this Chapter the model development is described and the model sensitivity analysis is performed.

5.1 Introduction

Although many ash behavior indices and prediction techniques are available, most of them have been developed for addressing slagging/fouling during coal combustion, and are valid only for specific, narrow fuels types (i.e. slagging index B/A for eastern bituminous US coals). Empirically derived indices fail when it comes to investigate blends composed of fuels of different ash composition. It is due to the non-additive behaviour of such ash mixtures caused by the non-linear ash melting characteristics but also due to time and contact-limited interactions between inorganic species under conditions existing in pulverised fuel boilers. The recent progress in a development of phase equilibrium analysis gives the possibility to investigate the ash behaviour of more complex fuel blends, including coal/biomass mixtures. However, due to the nature of the phase equilibrium analysis the proper predictive algorithms based on the phase equilibrium calculations need to be developed, and then critically evaluated.

This chapter is divided into two sections. In the first part, the theory behind the developed model will be presented to outline and discuss the important criteria and assumptions within methodology that has been applied to assess the behaviour of ash forming elements during conditions in pf boilers. In this section, proper slagging/fouling indices are defined. In the second part, the sensitivity analysis of the predictive model is performed for the thermal conditions of the 235 MW_e pf boiler which was analysed in the previous Chapter. The used assumptions, regarding the ash stickiness criteria are evaluated, including the effects of biomass co-firing. Finally, the impact of coal blend ash quality on the ash deposition severity is investigated when co-firing with high alkalis content biomass such as straw.

5.2 Model Development

The aim is to develop a reliable slagging/fouling predictive methodology for large scale pulverised boilers fired with coal/biomass blends. The considered approach is based on the integration of a one-dimensional zone based thermal model used to determine midsection temperature profile throughout a boiler with the phase equilibrium analysis applied to assess fuels slagging/fouling tendencies for corresponding thermal conditions and investigated boiler configuration. The zone based boiler model has been described and evaluated in the previous Chapter. This section is focused on adapting the phase equilibrium calculations for predicting slagging/fouling propensities of coal/biomass blends when co-firing in pf boilers. It is aimed

to derive more universal slagging/fouling indices that can be applied to rank fuel blends composed of the fuels of different chemistry and origin of inorganic species.

5.2.1 Conceptual Approach Layout

In a very general term, the ash behaviour for coal is dictated by minerals, in case of biomass by simple salts and organically associated with biomass ash-forming elements. Minerals undergo transformation and melting under high temperature whereas ash-forming in biomass systems vaporise and subsequently condense forming aerosols/sub-micron particles, or else interact with minerals affecting their melting characteristics. Such different behaviour of inorganic species originating from coal and biomass, should be reflected by different, separate phase equilibrium pathways that need to be specified for conditions existing in pf boilers [81]. The general procedure for evaluating behaviour of ash-forming matter from biomass/coal co-firing with the aid of phase equilibrium predictions is shown in Figure 5-1.

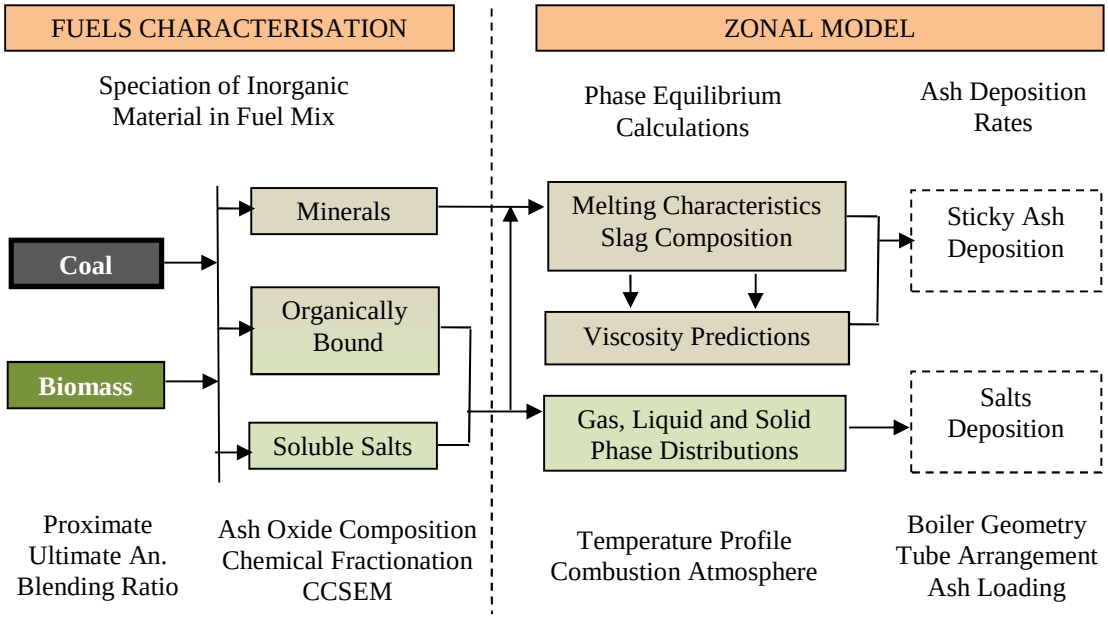

Figure 5-1. Procedure scheme for assessing inorganics behaviour with the aid of equilibrium calculations.

In the first instance, the speciation of inorganic material in coal and biomass needs to be done. The first group of inorganics consist of minerals (mostly silicates/clays but also some carbonates, pyrites and others) that can be either excluded or included within the fuel matrix. Due to short residence time of minerals in the most heat intense zones (1-3 sec), such minerals can be partially fused or completely molten captured in the slag (more likely for included minerals due to higher temperatures and reducing conditions presence). The second group consists of alkali salts and organically associated metals (mainly found in biomass) that are assumed to achieve equilibrium in the furnace, and are released into the gas phase during

combustion. A combination of Computer-Controlled Scanning Microscopy- CCSEM (best for coals), chemical fractionation and pH-based extraction methods can be used to determine speciation of inorganic species in solid fuels [35, 81]. The usefulness of bulk ash composition in determining the average fly ash composition over the CCSEM method is discussed in section 5.2.2.

Depending on the group to which the inorganic species belong to, different phase equilibrium calculation schemes are performed. For the minerals, their melting characteristics and slag viscosities are calculated with relation to the temperature profile along the furnace height determined by zonal method. The amount slag produced and its viscosity are regarded as major criteria for assessing the stickiness of ash particles approaching the tube banks. Then separate equilibrium calculations are carried out for the stream of alkali salts and organically associated metals which are expected to be released into the gas phase, followed by aerosols and solids formation during sub-cooling process in the convective section of a boiler [81].

Moreover, the procedure includes the interactions between streams of minerals and the remaining part of the ash-forming elements which are released into the gas phase. Such interactions, taking place at furnace conditions, may lead to recapturing of some part of e.g. alkali metals by Al-Si based fly ash, reducing alkali salts formation in the convective pass of a boiler. However, this positive effect of alkalis capture may influence formation of a sticky layer on the ash particles and cause increase slagging and fouling propensity [88, 103].

5.2.2 Phase Equilibrium Model

Based on the above outline the conceptual modelling approach is developed with three phase equilibrium modules being defined which include different pathways of ash behaviour modelling, as follows:

- Slagging and high-temperature fouling module (EQ1) to investigate ash deposition on the heat-exchange surfaces placed at the furnace outlet, and caused by sticky, partially fused, silicate-based ash particles (see section 5.2.2.2).
- Low temperature fouling module (EQ2) to analyse condensation of ash-forming elements in a temperature range typical for convective section of a boiler (see section 5.2.2.3).
- Inorganics interactions phase equilibrium (EQ3) module to investigate alkali metals capture at the furnace caused by the silicate-based ash particles. This module is connected with EQ1 and EQ2 modules to analyse phase equilibrium

interactions between silicate-based ash and alkali metals at specific limited rate (see section 5.2.2.4). It is run first to give input data to the other related modules EQ1 and EQ2.

As reviewed in more detail in Chapter 3, due to the nature of the phase equilibrium analysis, which is not related to the kinetics of the process, the various improved phase equilibrium schemes were developed [35, 81, 88, 103, 104, 106]. It is generally agreed that the soluble inorganics, such as simple salts and organically associated elements, can be used as an input to the phase equilibrium calculations to analyse low temperature fouling, which is specifically applicable for fluidised bed conditions as studied by Zevenhoven and Hupa [105, 106]. Interactions of alkali metals with the reactive ash, likely to occur at the high temperatures of the pf boiler furnaces, and their effects on the salts condensation was thermodynamically investigated by Nutalapati *et al.* [103]. However, in this work the effects of inorganics interactions on the ash viscosity change was not analysed.

Improved phase equilibrium schemes for slagging and HT fouling were investigated by Gupta *et al.* [35] who proposed the use of activity coefficients for certain minerals groups, of which the included minerals, identified by CCSEM method, were assigned the highest activities. The major drawback of such approach is that by CCSEM only a small raw fuel sample is analysed and the minerals data may be not fully representative. Furthermore such analysis in not commonly available.

Akiyama *et al.* [144] performed phase equilibrium calculations based on the bulk ash composition of coal blends, achieving good correlation between the predicted slag phase percentages and deposition severity observed in practise. The use of the bulk ash composition is supported by the investigations of the fly ash samples taken from the pf coal-fired boilers which revealed the high interactions between coal minerals. Most of the Ca-, Fe- carbonates and oxides were found to be transformed into the alumina-silicates [145]. When co-firing with straw, the formation of Ca-Si- and K-Al-based deposits were reported, and potassium to alumina-silicates conversion was found to be dependent on the coal ash content and quality [8, 46, 146].

Overall, the bulk ash composition appears to be a good indicator of the fly ash composition, and can be potentially used in a proper constructed phase equilibrium schemes to assess slagging and high temperature fouling tendencies of ashes. Although several practical advantages of the bulk ash composition arose, their universal applicability should be validated across a wider spectrum of coal/biomass blends analysed.

5.2.2.1 Model Assumptions and Design

Based on the considerations the previous sections the following general assumptions are made and applied in the model:

- The melting behaviour alumina-silicate- based slag is determined by the bulk oxide composition of the ash elements able to form alumina-silicates, present in the coal and biomass fuels. However, specific conditions apply when the additional effects from the organically bound and simple salts are considered.
- The behaviour of organically associated ash-forming elements and easily soluble salts: **Coals:** the most severe case is considered in which all of these elements are captured by slag. Typically their concentrations are less than 5-10% of the total ash content for a high rank coals. **Biomass fuels:** these elements are the major part of the inorganics. In case of the soluble alkalis, they are assumed to partly interact with the alumino-silicate ash particles and produce sticky, molten outer layer on the particles, according to the Nutalapati model [103] (section 5.2.2.4). Unreacted with the Al-Si ash alkalis remain in the gas phase and form salts which condense in the convective section. Other elements are assumed to form submicron solids which are fully captured by generated slag.

More specific assumptions are assigned to each phase equilibrium modules which are described in the following subsections. The connections between defined phase equilibrium modules as well as the temperature ranges of calculations for particular equilibrium modules are shown in Figure 5-2.

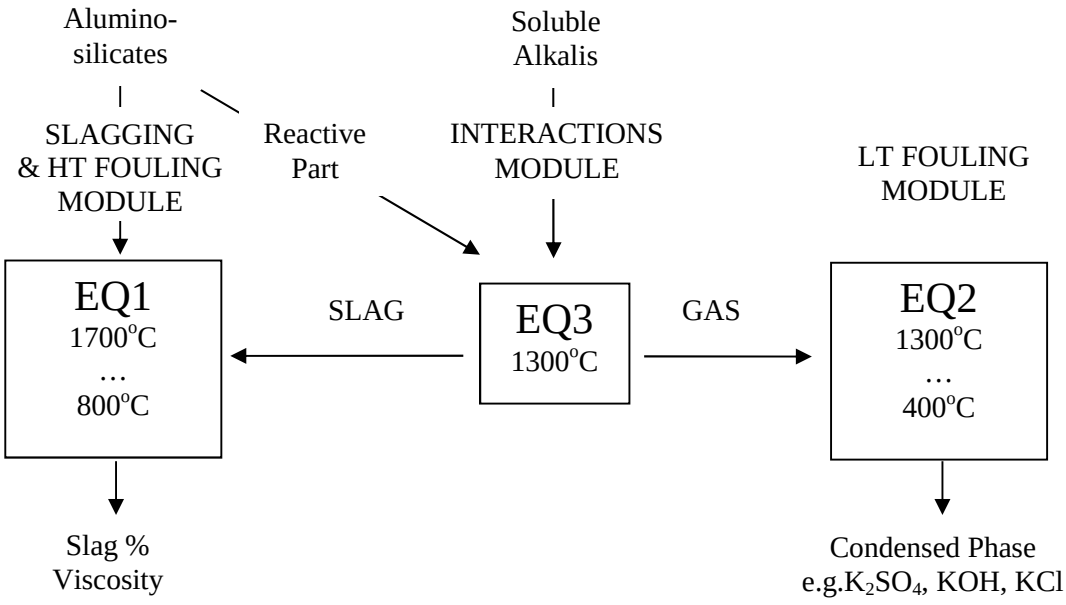

Figure 5-2. Scheme of the mass stream connections between the phase equilibrium modules.

The phase equilibrium calculation modules were built with the aid of SimuSage™ package of thermodynamic libraries and procedures (for Delphi programming language), which utilise FactSage™ thermo-chemical data and phase equilibrium solver (ChemApp) [102, 147]. The phase equilibrium analysis is conducted based on the minimisation of total Gibbs free energy of a system of chemical compounds. The use of SimuSage™ allows, in a flexible and controllable way, constructing the simulated thermodynamic process with the use of thermodynamic blocks and mass flow connectors between them [147]. The non-equilibrium processes can be investigated by limiting or excluding certain compounds/phases which are not expected achieve thermal equilibrium at the specific temperature ranges. More details regarding the current model construction by SimuSage™ can be found in Appendix II.

5.2.2.2 Slagging and HT Fouling Equilibrium Module

This module (EQ1) is designed to determine the melting characteristics of bulk ash composition at the specified temperature range between 1700-800^{o}C and atmosphere of the flue combustion gases. Apart from the information about the slag percentage distribution over the temperature range, the composition of slag can be also obtained which is used then to calculate the slag phase viscosity characteristic. The data derived from this module are used to assess the slagging and high temperature fouling propensities of fuel blends as described in section 5.2.3.

Thermo-chemical (FactSage™ 5.4) databases used:

- Liquid/glass solution: The FToxid-slag-A database has been used, which contains the system of six components Al_2O_3-CaO-FeO-Fe_2O_3-MgO-SiO_2, fully optimised and evaluated together at all compositions from 25^{o}C to above the liquidus temperatures. Additional oxides such as Na_2O or K_2O have been also considered, although, the optimisations are less precise for their high concentrations in a slag mixture [102].
- Solid solutions: Complex alumino-silicates (wollastonite, olivine, mulite).
- Stoichiometric compounds:
    - solid compounds of corresponding silicates, alumino-silicates and oxides.
    - gas compounds adequate to describe combustion atmosphere.

  Complete list of compounds considered can be found in Appendix II.

Input data into EQ1:

- To create the proper combustion atmosphere the elemental analysis of fuels (C, H, O, N, S, Cl) as well as the air excess (λ=1.2) were introduced into the equilibrium calculations.
- Ash bulk chemistry of minerals, described by Si, Al, Fe, Ca, Mg, Na, K elements. Other elements were not investigated due to limitations of the liquid/glass solution databases [102].
- Organically bound elements. These are assumed to be fully (or almost complete) captured by slag to simulate the most severe conditions.
- Data output from the EQ3 module, in terms of the amount of alkalis captured by the reactive part of the ash.

Viscosity model:

- Several models have been reported for the estimation of slag viscosities [148, 149], but the modified Urbain equation (Kalmanovitch model) has been found to be the most accurate in a range of viscosity up to 10^3 Pa*s where complete molten slags are expected. To increase its accuracy for a lower temperature range, where slags solidification is likely, the slag composition changes are calculated based on the equilibrium model which were introduced according to reference [148]. This approach is in good agreement with results obtained by other empirical viscosity models (i.e. Senior model [149]) and is valid for a lower temperature ranges but limited to slag composition of silicates.

5.2.2.3 LT Fouling Equilibrium Module

The module EQ2 is constructed to assess the fate of ash-forming elements that have been released into the gas phase in the furnace and are entering the convective section of a boiler. The focus is mostly on the alkali salts formation, including aerosols at the temperature range between 1300-400^{o}C. However, the alkali earth metals behaviour, especially sulphation of the calcium, magnesium oxides can be also assessed based on the phase equilibrium conditions. Although, there are no further kinetic parameters introduced for the sulphation process, the maximum concentration of SO_2 (g) in the flue gases generated in pf boilers, are close to those predicted by the phase equilibrium calculations at temperatures between 1000-900^{o}C [79]. Based on predictions obtained by this module the tendencies to form alkali aerosols can be assessed and compared for various fuels mixtures.

Thermo-chemical (FactSage™ 5.4) databases used:

- Liquid solution: Salt melt (SALT-F): (K, Na)(SO_4, CO_3, Cl, OH).
- Solid solutions:
  - $(Na, K)_2(SO_4, CO_3)$ (ss)
  - (Na, K)(Cl) (ss)
- Stoichiometric compounds:
  - solid compounds of corresponding salts and oxides.
  - gas compounds of corresponding salts and oxides, and combustion atmosphere.

Complete list of compounds considered can be found in Appendix II.

Input data into EQ2:

- The elemental analysis of fuels (C, H, O, N, S, Cl) as well as the air excess (λ=1.2).
- Organically associated and easily soluble elements, described by K, Na, Ca, Mg, P elements chemistry. Impact of P is limited due to incomplete thermo-chemical data [102]. The input in particular includes:
  - Data output from the EQ3 module, in terms of the amount of alkali metals not captured by the reactive ash and still remaining in the gas phase.
  - Part of organically associated elements that were assumed not to be captured by slag. Input of these elements should be calibrated with the experimental results. Here, it is not investigated, therefore the input from this elements is assumed to be equal 0.

5.2.2.4 Interactions Equilibrium Module

This phase equilibrium module (EQ3) is designed to investigate the high temperature interactions between the part of the alumino-silicate based ash and alkali metals which were recognised as easily soluble and thus very reactive. Part of these alkalis are expected to be captured by the ash. The alkali metals capture efficiency can be determined as defined in section 5.2.4.

This assessment is based on laboratory investigations, which revealed that alkali vapours can interact with the outer surface of silica/clay mineral particles [88] producing low temperature melting alkali silicates/clays. Taking this as a basis, in the model developed it was assumed (according to Nutalapati *et al.* [103]) that all the ash particles are spherical, are of 10μm diameter, and at high temperatures (assumed to be 1300°C) whilst the same

proportion of particles are reacting [88, 103]. Furthermore, the average thickness of the reacting layer was assumed to be 0.1μm which corresponds to around 5% in volume or mass basis for 10μm sized silicate/clay particles [88, 103].

Thermo-chemical (FactSage^{TM} 5.4) databases used:

- Liquid/glass, solid solutions and stoichiometric compounds as defined in the EQ1-Slagging and HT Fouling Equilibrium Module.
- Phase equilibrium calculation performed at the temperature of 1300^{o}C.

Input data into EQ3:

- The elemental analysis of fuels (C, H, O, N, S, Cl) as well as the air excess (λ=1.2).
- Alkali metals such as K and Na which are easily soluble and/or organically associated (assessed based on the chemical fractionation analysis).
- The reactive part of ash (according to Nutalapati *et al*. [103] model) described by Si, Al, Fe, Ca, Mg, Na, K elements being part of minerals originated mostly from coals but also can be from biomass which are then identified as a not soluble (thus less reactive) fraction according to the chemical fractionation. Other elements were not investigated due to limitations of the liquid/glass solution databases [102].

Output data from EQ3

- The predicted by the EQ3 amount of alkalis captured by the reactive ash analysis is introduced into the EQ1 module which utilise this data to analyse the effects of captured alkalis on the viscosity and slag generation changes (formation of a sticky layer) remaining in the gas phase, uncaptured alkalis are introduced into the EQ2 module to calculate the amount of condensed salts.

5.2.3 Deposition of Sticky Ash Particles

In this subsection, the slagging and high temperature fouling deposition rate and indices are defined. Slag and high-temperature fouling deposits are formed by the inertial impaction of relatively large, sticky, partially fused, silicate-based ash particles, and dominate on heat-exchange surfaces placed at the furnace outlet of pulverised-fuel fired boilers. Depending on the temperature at the furnace exit and nature of the fuel fired the slagging/fouling can be extended from the platen superheater to reheater/superheater surfaces suspended over the furnace box or entering the convective pass of a pf boiler.

The slag and viscosity distributions calculated by the EQ1 phase equilibrium module, are used to formulate proper indicators that allows ranking fuels according to their slagging/fouling performance.

5.2.3.1 Formulation of Ash Deposition Rate

The ash deposition rate of sticky, partially fused, large ash particles resulting from the inertial impaction on the upstream side of the tube banks of heat exchangers can be determined using the following simplified formula [84, 121, 150, 151]:

$$I_d = u_g \cdot C_{ash} \cdot \frac{A_{tube}}{A_{total}} \cdot P_{stick}(T) \cdot \phi(T) \quad [kg/m^2 s] \tag{5.1}$$

The ash deposition rate defined above is assumed to be proportionally dependent upon such parameters as the velocity of the flue gas u_g (m/s), ash concentration (C_{ash}, kg/m^3), the ratio of cross-sections areas of the heat exchanger and duct (A_{tube}/A_{total}) [84] which express the probability of the ash particles hitting the surface. Other parameters are more ash quality related and include the sticking probability (P_{stick}) [150] and ratio of molten slag (ϕ) in the ash particles approaching to the tube banks. The effects related with the deposit layer stickiness or erosion of deposit layer are not included here as the onset of the ash deposition process is investigated. The sticking probability of the impacting fly ash particles is commonly calculated by using a method similar to that of Walsh *et al.* [150] and is expressed by:

$$P_{stick}(T) = \begin{cases} \dfrac{\mu_{ref}}{\mu} & \mu > \mu_{ref} \\ 1 & \mu \le \mu_{ref} \end{cases} \tag{5.2}$$

where, μ represent the viscosity at the local gas temperature and μ_{ref} is the reference critical viscosity. Deposition may occur if the critical viscosity criterion is met at the estimated gas local temperature. According to the literature [84, 121, 150, 151] the reference value for critical viscosity vary significantly and the most likely values lies between 10^3 – 10^5 Pa*s. Such a wide range of the reference critical viscosities is a major drawback of this method. Difficulties in determining the reference stickiness of ash particles can be associated with the different melting/solidification curves and viscosity changes for slags of various composition. The impact of ash quality and the reference critical viscosity changes on the predicted ash deposition rates throughout the boiler are investigated in section 5.3.

5.2.3.2 Formulation of Slagging and HT Fouling Indices

The assessment of the ash deposition rate as outlined in the previous section may include large uncertainties associated with:

- Not including the melting history of the impacting particles due to the phase equilibrium calculations of the local molten slag ratio, which is temperature dependent.
- Not well defined sticking probability functions, especially the reference critical viscosity.
- Not well defined function describing probability of the ash particles hitting the surface.

In order to decrease the above mentioned uncertainties, the alternative slagging and high temperature fouling indices are considered, which are based on the following postulations regarding the melting history of the ash and its viscosity:

- Instead of the use of the local molten slag ratio (ϕ), the average values are calculated. However, the slagging tendency is assessed by taking the slag average values calculated for a higher temperature range whereas HT fouling correspondingly for a lower temperature range as schematically shown in Figure 5-3 (for details see Appendix I-6).

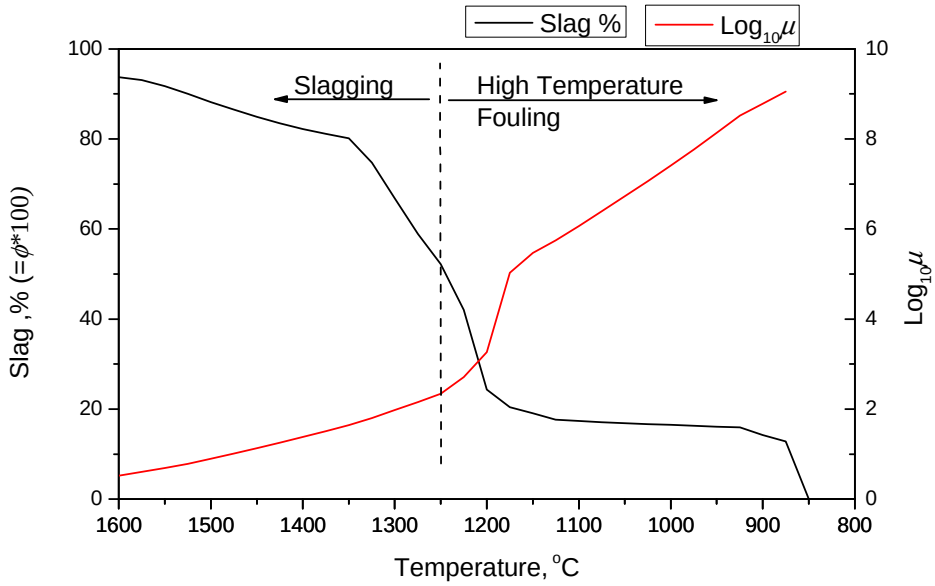

Figure 5-3. Slag % and slag viscosity regions for slagging and HT fouling assessment.

- The sticking probability, as defined in section 5.2.3.1. is not taken into account. However, it is assumed that the ash deposition rate is inversely proportional to the slag phase viscosity ($\log_{10}\mu$) at the specific reference temperature related to the location of

the given heat exchanger and represents the viscosity of the deposit outer surface. To make a general comparison, not strictly boiler related, the viscosity calculated at 1250^{o}C can be used, which was found to be a good indicator for slagging/fouling [16, 64].

Overall the slagging/HT fouling fuel tendencies can be assessed by the following general form:

$$I_{SL(HTF)} = A \cdot \left(C^{*}_{ash} \cdot \frac{\bar{\phi}_{SL(HTF)}}{Log_{10}\mu_{Temp}} \right) + B \qquad (5.3)$$

where C^{*}_{ash} (g/kg flue gas) is the ash concentration, $\bar{\phi}_{SL(HTF)}$ is the average slag ratio at the slagging (SL) or HT fouling (HTF) defined temperature ranges, respectively; $\log_{10}\mu_{Temp}$ is the viscosity factor calculated for the viscosity at the reference temperature; and *A* and *B* are the calibration coefficients, used to adjust predictions to the known slagging/fouling severity scale of a given heat-exchanger when assuming linear correlation.

The ($\bar{\phi}_{SL(HTF)}/\log_{10}\mu_{Temp}$) ratio can be further used to determine the ash stickiness criteria as discussed in section 5.3.5. The major difference between this ratio and the sticking probability defined in section 5.2.3.1, is that it includes viscosity calculated for the specific reference temperature whereas the sticking probability is calculated for the reference critical viscosity which is assumed to be constant for all coal ash chemistries.

The usefulness of such above formulated ash deposition indices lies in the conviction that the three major ash quality parameters, such as the viscosity, average slag ratio and ash burden determine mostly the ash deposition severity, and those parameters can be relatively simply obtained with the use of developed model. Once the deposition indices are calibrated to the known slagging/fouling observations, they can be further applied to investigate more complex fuel blends to optimise their composition.

All of the abovementioned indices are critically analysed in more detail based on the slagging/fouling observation examples presented in the various subsections.

5.2.4 Salts Condensation-Based Indices

Based on the results derived from the phase equilibrium calculations performed by modules EQ2 and EQ3, the following indices can be defined to assess the likelihood of low temperature fouling due to salts condensation in a convective pass of a boiler:

- Alkali metals capture efficiency index. This is expressed as a mass ratio of the captured alkali metals (Na, K) by active part of silicate-based ash (assessed during the

phase equilibrium calculations by the module EQ3 at 1300^{o}C) to the mass input of alkali metals to the module EQ3 (easily soluble alkalis). The higher capture efficiency, the lower availability of alkalis for fouling in convective pass of boiler.

- Alkali aerosols formation tendency, which can be assessed based on the predicted molten alkali salts concentrations distributed over the temperature range. For a relatively higher alkali salt concentrations in the flue gas, the formation of molten salts phase is expected to occur at the higher temperature ranges. Correspondingly, this may indicate the increased tendency of aerosols formation for the fuel analysed.
- Apart from the above defined indices, the predicted concentrations of salts in the flue gas related to the 1 kg of fuel fired can be also used as indicators.

5.3 Model Sensitivity Analysis – Results and Discussion

In this section the responses of the developed model on various ash quality related parameters as well as model assumptions are tested. The model is applied to the thermal conditions of the Langerlo 235 MW_e pf boiler configuration analysed in more details in the previous Chapter 4. The following effects are investigated:

- The impact of different coal ash chemistry (in terms of CaO, Fe_2O_3 and K_2O, Na_2O content) on melting and slag viscosity characteristics.
- The impact of assumed ash reference critical viscosity on the ash deposition rates predictions.
- The effects of increasing co-firing of alkalis-rich biomass with coal on the predicted ash deposition rates (for assumed different interactions rates of silica-based ash). The corresponding condition changes of various salts formation in the convective pass of the boiler are also analysed.
- The impact of coal quality on slagging and fouling when co-firing with alkalis-rich biomass. The proposed new slagging and HT fouling indices, as defined in sec. 5.2.3.2, are tested to identify the optimal coal/biomass blends.

5.3.1 Investigated Fuels

Three different ash quality bituminous coals and one typical high-alkali content biomass type were chosen in this investigation, namely South African (SA3), Australian (AL1) Colombian (CO1) coals and straw (DS2), respectively. The more detailed oxide ash

composition as well as proximate and ultimate analyses of investigated fuels are shown in Table 5-1.

Table 5-1. Proximate, ultimate and ash oxide analyses of the investigated fuels (on as received basis).

Fuel Name	SA3[a]	CO1[b]	AL1[c]	DS2[d]
VM, %	22.28	34.03	28.3	68.49
FC, %	58.21	48.17	43.7	13.15
Moisture, %	5.2	9.0	3.3	12.4
Ash, %	14.31	8.8	24.7	5.96
LHV, MJ/kg	25.58	26.08	22.17	14.67
C, %	66.74	66.58	57.67	40.38
H, %	3.79	4.52	3.53	5.26
N, %	1.52	1.40	1.08	0.51
O, %	8.04	9.06	9.17	34.9
S, %	0.38	0.58	0.51	0.11
Cl, %	0.02	0.06	0.04	0.48
SiO_2, % in the ash	44.6	61.8	48.2	34.0
Al_2O_3, % in the ash	34.2	21.1	31.6	0.94
TiO_2, % in the ash	1.1	0.9	1.2	0.06
Fe_2O_3, % in the ash	4.4	**6.6**	7.9	0.65
CaO, % in the ash	**9.4**	2.2	3.8	7.3
MgO, % in the ash	1.1	2.1	1.5	2.0
K_2O, % in the ash	**0.6**	**2.4**	**0.4**	**29.8**
Na_2O, % in the ash	0.2	1.1	0.2	0.85
P_2O_5, % in the ash	1.3	0.2	0.5	0.5
SO_3, % in the ash	3.1	1.6	2.9	4.74
SUM, %	100	100	98.2	80.8
IDT_{oxy}, ^oC	1350	1250	>1480	1015
HT_{oxy}, ^oC	1360	1305	>1480	1170
FT_{oxy}, ^oC	1400	1410	>1480	1240
B/A	0.17	0.17	0.20	1.16
B/A*Sd	0.09	0.11	0.08	-
B/A*Na_2O	0.03	0.19	0.04	-

a) South African coal, S21 [24], b)Typical Colombian coal , c) Typical Australian Coal – Liddell Seam [38], d) Danish Straw.

South African coal (SA3) is the intermediate ash content coal with a low alkali metals presence and relatively increased calcium content. Australian coal (AL1) similarly to SA3 is poor with alkali metals, however has the highest ash content and is slightly enriched in iron. Colombian coal (CO1) has the lowest ash content amongst coals investigated, but is the most

enriched in the alkalis metals and has the increased silica presence. The calculated indices based on the B/A ratios indicated the low slagging and fouling tendencies for the all coals. However, the increased Na_2O% content in the CO1 ash (above 1.0%) classified this coal as a highly fouling. In terms of the ash melting tendencies, the lowest ash fusion temperatures measured at oxidising atmosphere (AFT) were reported for the CO1 ash, followed by the SA3 and AL1 ashes. It is expected that the AFT for the AL1 coal ash obtained under reducing conditions should be lower due to not being fully oxidised, thus giving reduced melting of iron in the slag [135].

Straw was chosen for the sensitivity model investigation, as it is a good example of the biomass that includes a high content of alkali metals as well as a relatively increased amount of calcium. These elements are mostly organically associated or in form of easily soluble salts, thus highly reactive. Furthermore, straw contains a realtively high ash concentration as compared with e.g. low ash content woody biomass. Therefore, the models are expected to be more senistive for the effects of straw co-firing with coal with itermediate co-firing biomass shares up to 20th%. As far as melting tendency of the straw ash is concerned, the reported ash fusion temperatures are shown to be relatively lower, due to the high ratio of K_2O% to SiO_2% in the ash, as compared with the coals investigated.

5.3.2 Melting and Slag Viscosity Characteristics

The ash melting and viscosity characteristics predicted by the phase equilibrium module EQ1 for the investigated coals are shown in Figures 5-4 and 5-5.

For a better interpretation of the results, the temperature scale is divided into two, slagging temperature range (1600-1250^{o}C) and high temperature (HT) fouling range (1250-800^{o}C).

In the slagging temperature region, the melting of the investigated ashes is influenced mostly by such oxides as CaO, Fe_2O_3, SiO_2 and Al_2O_3 whereas in the HT fouling region by the presence of SiO_2, Na_2O and K_2O. The example slag composition in those two regions for SA3 coal is shown in Figure 5-6.

Two coals, namely SA3 and AL1, whose oxide compositions differ only in terms of CaO and Fe_2O_3 content, revealed overall similar melting curve shapes with some visible differences at the slagging region. It was observed that, the higher CaO concentration in the SA3 coal ash caused the increased slag levels between 1600-1420^{o}C whereas for AL1 coal ash, the raised Fe_2O_3 content in the ash led to higher slag percentages at the lower temperature range of slagging region between 1420-1250^{o}C. The decrease slag levels with a temperature

drop for SA3 coal was related to a solidification of Ca-Si/Al phase from the slag, whose chemistry is dominated by the ternary Al_2O_3-SiO_2-CaO oxides system.

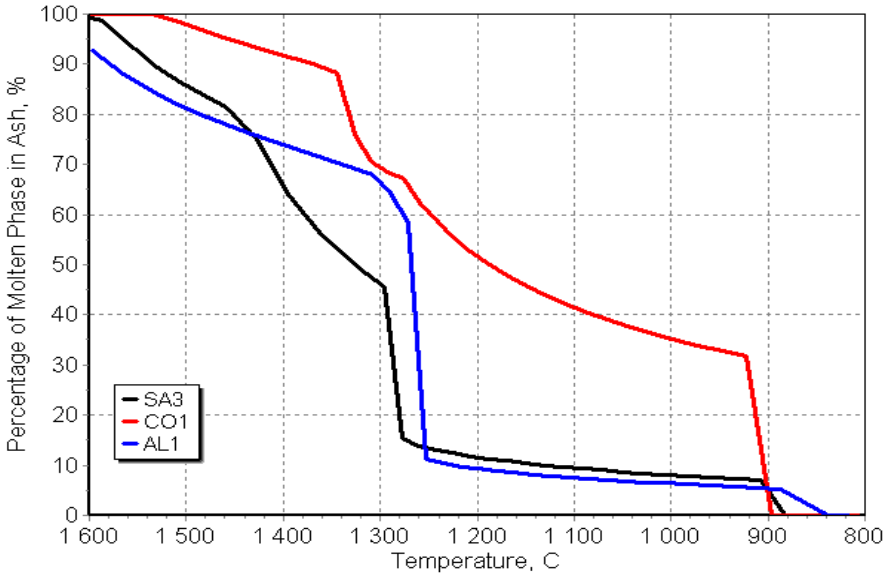

Figure 5-4. Ash melting characteristics for South African (SA3), Colombian (CO1) and Australian (Al1) coals.

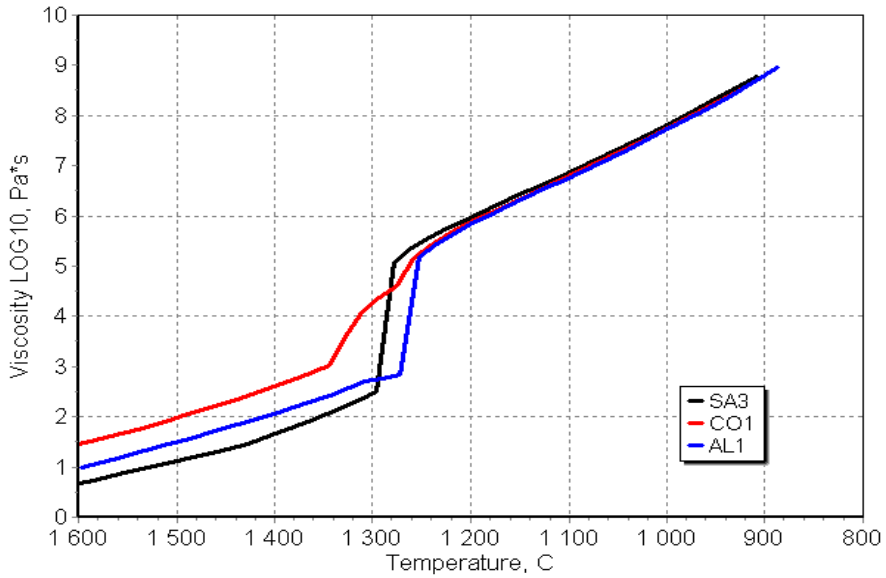

Figure 5-5. Calculated viscosities of slags obtained for South African, Colombian and Australian coal.

In case of CO1 coal, due to significantly lower contents of Al_2O_3, higher SiO_2 and intermediate content Fe_2O_3 oxides, as compared to the other investigated coals, the highest levels of slag was calculated to be at the slagging region. Furthermore, CO1 coal revealed also the highest slag levels in the HT fouling temperature range, due to the increased silica and alkali metals presence in the ash, as compared with the SA3 and AL1 coals.

Analysing the obtained viscosity curves it can be seen that the slag viscosity increases gradually with a temperature drop and those changes are associated with the corresponding

melting curve development. Moreover, it was noticed that, for the investigated ashes, the viscosity changes in the slagging temperature range are mostly influenced by the high CaO content in the slag which leads to lower viscosities (Figure 5-6). In the HT fouling region the differences in calculated viscosities are significantly lower for the investigated coals, and the slag chemistries are mainly dominated by the oxides of silica, alumina, sodium and potassium.

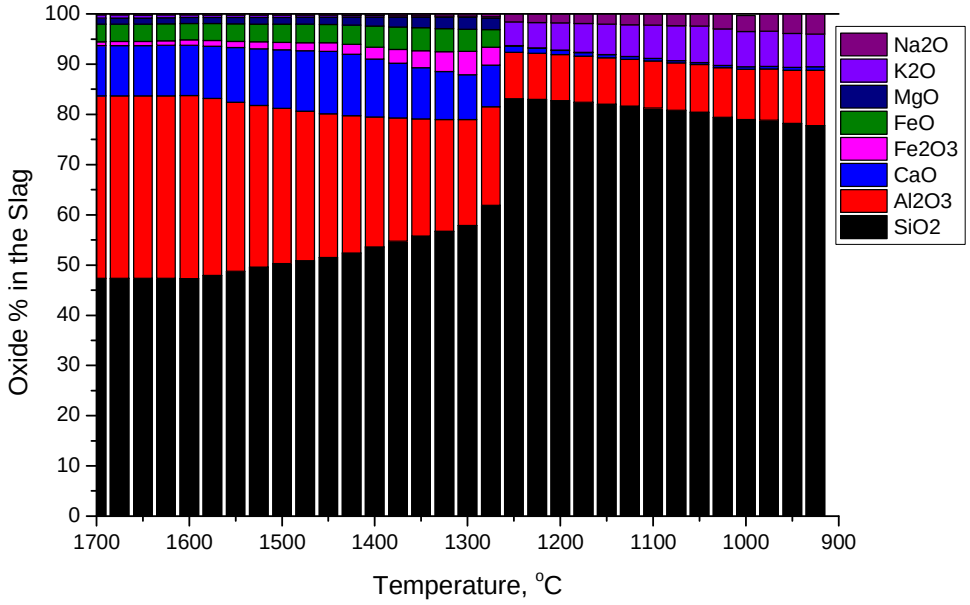

Figure 5-6. Phase equilibrium calculated composition of the slag for South African coal.

5.3.3 Evaluation of Ash Sticking Probability Criterion

In this subsection, the impact of the assumed reference viscosity value on the sticking probability distributions (as defined in section 5.2.3.1) and the predicted ash deposition rates are evaluated. The calculations are performed for the ash of CO1 coal that revealed the highest percentage of a slag presence over the widest temperature range amongst the investigated coals. The temperature dependent slag ratio is the key parameter that determines the ash deposition rate of sticky ash particles impacting the heat exchangers.

The influence of two boundary reference critical viscosities from the range of 10^3 Pa*s to 10^5 on the predicted ash deposition distribution is shown in Figure 5-7. The temperature scale on the X-axis is transformed to a corresponding linear distance within the boiler with highlighted zone areas of the heat-exchangers adequate for the Langerlo pf boiler (investigated in Chapter 4). At the entrance to the SH2 platen superheater section, the flue gas temperature was predicted to be around 1350^{o}C whereas for the SH3 zones reached approximately 1250^{o}C (Figure 4-11, Chapter 4).

As far as the ash impact is concerned, the simulations revealed that changing the reference viscosity value from 10^3 Pa*s to 10^5 leads to significant shifting of sticking probabilities of the CO1 coal ash, as shown in Figure 5-7a. This caused extension of the ash deposition from the SH2 platen superheater zone towards the heat-exchangers entering the convective section of the boiler, SH3 and RH2, respectively (Figure 5-7b). The rapid increases of the predicted ash deposition rates at the entrance to the subsequent heat-exchangers sections are related with the changes of their cross-section areas.

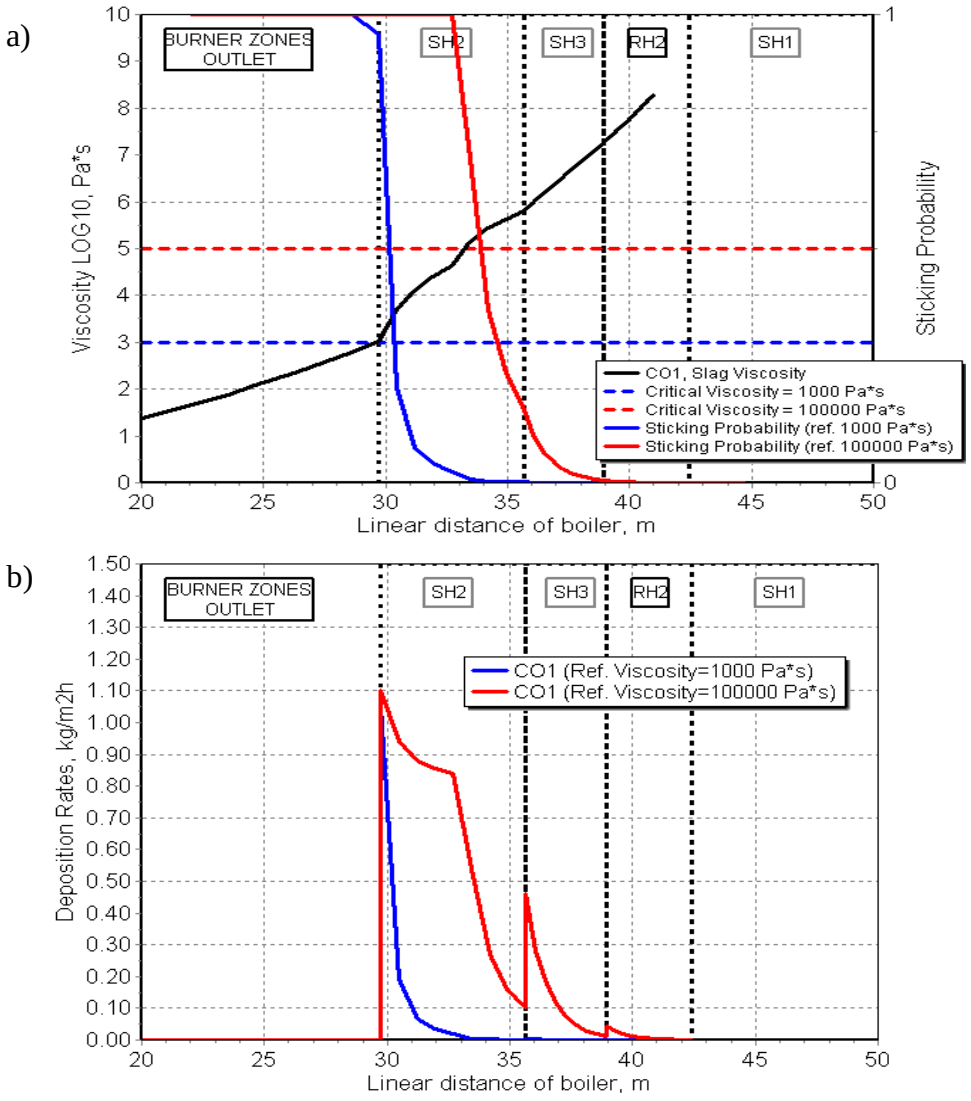

Figure 5-7. Predicted viscosity, corresponding sticking probability functions and their effects on the predicted ash deposition rates obtained for two reference viscosity values 10^3 and 10^5 Pa*s, and CO1 coal.

Overall, the predcitions obtained for CO1 coal, and for the assumed reference viscosity value of 10^5 Pa*s apear to be in most agreement with the operational experiences citied in the literature releated with the fouling performance of high alkalis content coals [10, 145, 152].

5.3.4 Impact of Co-firing Alkalis Rich Biomass with Coal

The capture efficiency of the biomass originated potassium by the alumino-silicate based coal ash determines the slagging and fouling when co-firing high alkali content biomass with coal. The quality of coal ash, in terms of increased ash content as well as a high relative amount of alumino-silicate to alkali metals in the ash, is the major factor affecting the capture process efficiency. In this analysis, the low alkalis and itermediate ash content SA3 coal was chosen to investigate the impact of straw co-firing on the coal ash behaviour up to 20th% coal subsitution. All alkalis present in straw were assumed to be easilly soluble. The set of cases considered in the sensitivity analysis in summarised in Table 5-2.

Table 5-2. Sensitivity parameters for studying the effects of co-firing rate and mass % of reactive ash.

	Change in Straw Co-firing Rate			
Case	Legend in Figures	SA3 th%	DS2 th%	Mass % of Reactive Ash
1cr	SA3	100	0	5.0
2cr	SA3DS2-10th%	90	10	5.0
3cr	SA3DS2-20th%	80	20	5.0
	Change in Ash Reactivity			
1ar	SA3DS2-20th%-5REA	80	20	5.0
2ar	SA3DS2-20th%-10REA	80	20	10.0
3ar	SA3DS2-20th%-20REA	80	20	20.0

Note: Reactive ash mass % calculated for assumed 10μm partcile diameter.

Besides the change in straw co-firing rate, the impact of the assumed mass % of ash reactivity was investigated, varying from the 5% to 20% of total ash amount for the assumed conditions as defined in section 5.2.2.4. The detailed input of the elements into the particular EQ for the cases considered is summarised in Appendix I-4.

5.3.4.1 Ash Deposition Rates up to 20th% Straw Co-firing

To investigate the effects of the sensitivity parameters change on the ash deposition severity, three types of characteristic were generated and compared including the slag phase, viscosity and the ash deposition rate distributions for all investigated cases as shown in Figure 5-8. The performed analysis revealed that with the increasing straw co-firing rate from 0th% to 10th% and 20th% coal substitution a slightly higher slag levels in the zones upstream of the platen superheater (SH2) and the more increased slag levels at the HT fouling region between SH2-RH2 zones were predicted. These changes are associated with the raised CaO % and SiO_2 % in the slag at higher temperature zones and the increased K_2O content in the slag at the lower temperature range, respectively.

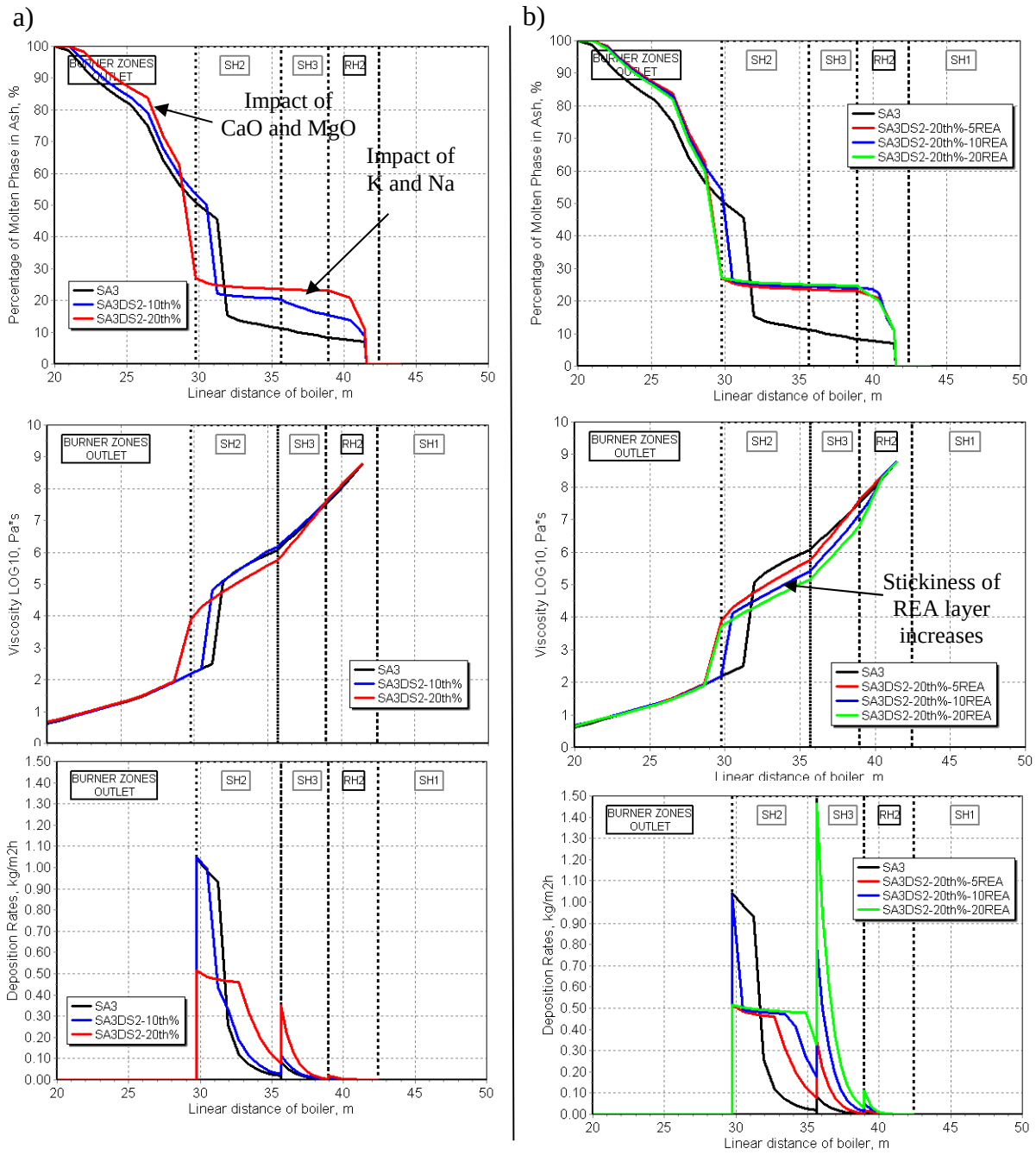

Figure 5-8. Predicted impact of straw co-firing with coal on ash slag and viscosity distributions as well as ash deposition rates: a) 5% mineral mass (REA) interacting with alkali metals, b) 5%, 10% and 20% of REA.

As a consequence, this further led to the slag viscosity changes and lowering their values at the HT fouling region. Interesting effects were identified at the temperature range between 28 and 32 meters of linear distance inside of the boiler (see Figure 5-8a). In this region, the slag percentages dropped with increasing co-firing ratio of straw which was affected by the solidification of Ca-Si/Al phases predicted by phase equilibrium considerations. This effect accordingly influenced the viscosity increase which reached the critical reference value (10^5 Pa*s) earlier, before the platen superheater zone. As a result, the lower local ash deposition

rates were predicted for the ash impacting the surface placed at the entrance to the platen superheater. After this region, for the increased straw co-firing shares higher ash deposition rates were obtained.

The effects of increasing the reactive layer of ash particles towards alkali metals capture when co-firing 20th% straw are presented in Figure 5-8b. As expected, the higher reactive mass of particles leads to more interaction, which resulted in a slight increase of slag phase and more significant viscosity drop leading to a rise in the predicted local ash deposition rates at the HT fouling region.

The impact of other coals with different ash chemistries, including coal blends with miscanthus, on the predicted ash deposition characterisics for this boiler was analysed separately in a paper [153].

5.3.4.2 Salts Formation in a Convective Section of Boiler

The impact of the analysed sensitivity parameters on the potassium capture efficiency and K_2SO_4(s) concentrations is summarised in Figure 5-11. The example potassium distributions over the temperature range of the boiler convective section predicted for the 20th% coal substitution and two ash reactivity considered cases, 1ar (5%REA) and 3ar (20%REA) are presented in Figures 5-9 and 5-10, respectively.

Analysing potassium distributions, according to equilibrium calculations, at the furnace conditions the most stable gaseous species are KOH(g) and KCl(g). With decreasing temperature, K_2SO_4(g) forms, and then subsequently the available quantities of potassium in the gas phase condense to form a liquid K_2SO_4(l) phase as shown in Figure 5-9. The remaining gaseous chlorine is predicted to be more stable in the form of HCl(g) for the investigated straw co-firing shares. The assumed higher ash reactivity results in reducing the levels of potassium available for condensation. Consequently, the amount of liquid phase is affected which is shown by the movement of the onset of condensation temperature towards lower ranges.

The performed sensitivity analysis revealed that for the assumed constant mass % of the reactive ash, an increase in straw co-firing share (2cr-3cr cases) does not affect the potassium capture efficiency. The capture efficiency was observed to be more sensitive to the changes in the ash reactivity (1ar-3ar cases, Figure 5-11) as well as ash concentration (section 5.3.5.2).

Moreover, as expected, with increasing straw co-firing share a proportionally higher concentrations of maximum K_2SO_4(s) levels were predicted. These levels were significantly reduced when a higher mass % of the ash reactivity was assumed.

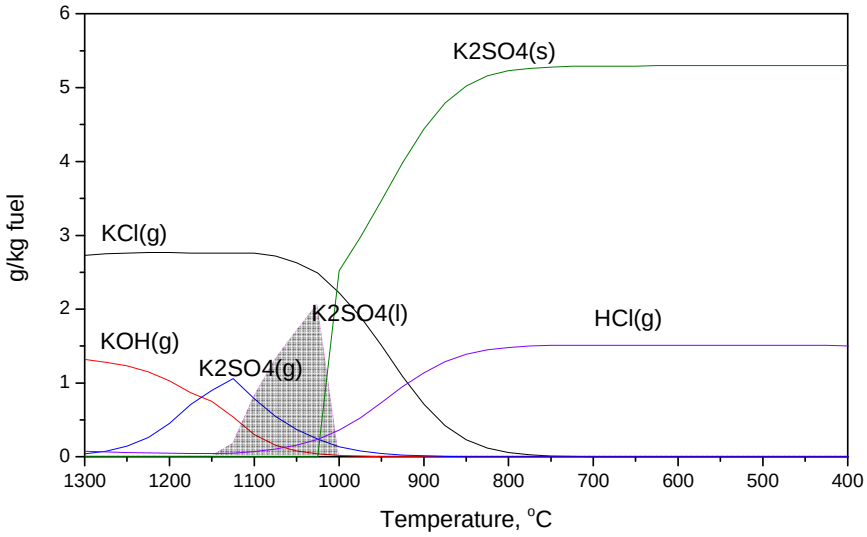

Figure 5-9. Potassium distribution predicted for co-firing SA3 coal with 20th% - 5REA case.

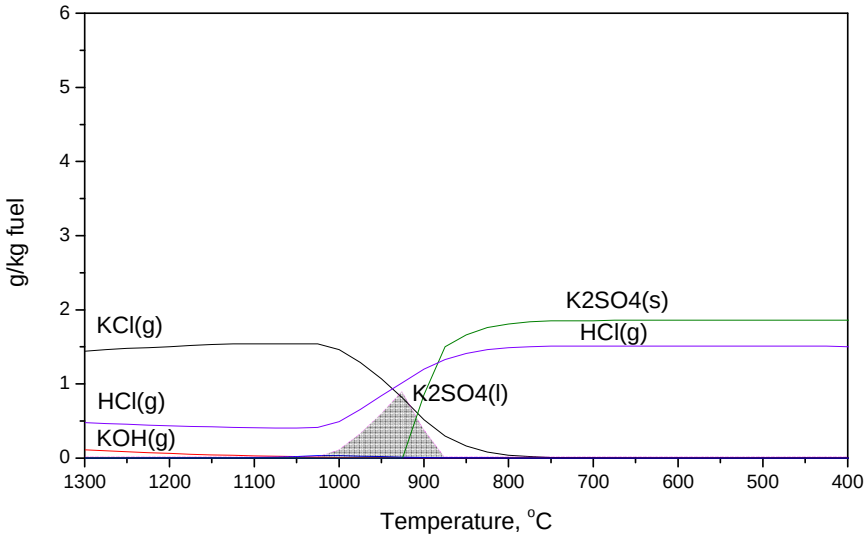

Figure 5-10. Potassium distribution predicted for co-firing SA3 coal with 20th% - 20REA case.

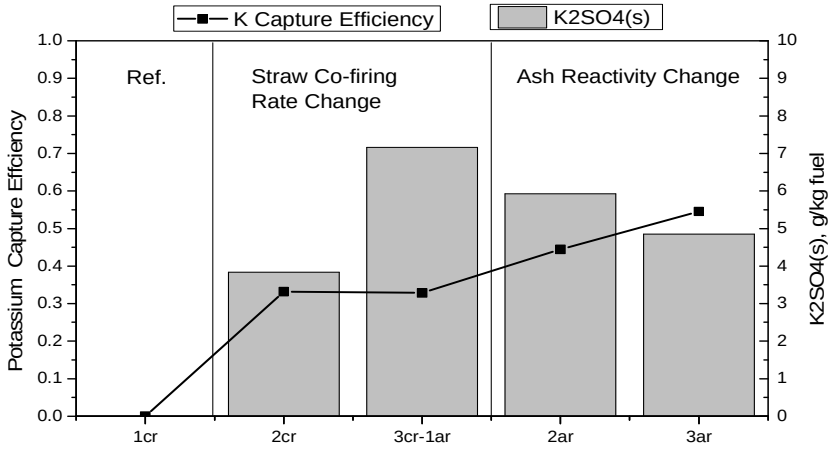

Figure 5-11. Impact of the straw co-firing rate and ash reactivity change on the potassium capture efficiency and the max K_2SO_4(s) concentration in the convective pass of the boiler.

5.3.5 Optimisation of Coal/Biomass Blends – Impact of Coal Quality

In this section, the impact of coal quality on slagging and fouling when co-firing with alkali-rich biomass is analysed. The aim is to identify the fuel flexibility widows when investigating the blends composed of three coals, namely SA3, CO1 and AL1 co-fired with straw (DS2) for the 20th% coal substitution case. To indicate changes in the slagging/fouling severity the proposed slagging and HT fouling indices are used as defined in section 5.2.3.2.

Amongst the fuels investigated the SA3 and AL1 coals are good quality coals with low slagging/fouling tendencies according to the B/A based indices as well as the AFT results summarised in Table 5-1. The blends of the CO1 and straw are expected to increase slagging/fouling.

5.3.5.1 Slagging and HT Fouling Indices

In the defined slagging and HT fouling indices there are three key parameters, the average slag ratios in specific temperature ranges, the viscosity at the reference temperature (1250^{o}C) and ash burden (g/kg flue gas). The first two parameters, or more precisely the ratio between them, is assumed to determine the stickiness conditions of the particles impacting the heat transfer surface. In order to make the results more comparable, the normalised ratio of these parameters is introduced according to the formula:

$$\left(\frac{\bar{\phi}_{SL(HTF)}}{Log_{10}\mu_{Temp}}\right)_{\text{Norm}} = \frac{\left(\frac{\bar{\phi}_{SL(HTF)}}{Log_{10}\mu_{Temp}}\right) - \left(\frac{\bar{\phi}_{SL(HTF)}}{Log_{10}\mu_{Temp}}\right)_{\text{Critical}}}{\left(\frac{\bar{\phi}_{SL(HTF)}}{Log_{10}\mu_{Temp}}\right)_{\text{Max}} - \left(\frac{\bar{\phi}_{SL(HTF)}}{Log_{10}\mu_{Temp}}\right)_{\text{Critical}}} \qquad (6.4)$$

where: Max denotes the maximum stickiness ratio amongst all calculated cases, and Critical denotes the critical stickiness ratio. The critical stickiness ratio was assessed by calibration of this ratio to the values obtained for the non-slagging/fouling coals, such as SA3, AL1. For the slagging region, the average slag ratio ($\bar{\phi}_{SL}$) was around 0.66 whereas the viscosity (at 1250^{o}C) was equal to $\log_{10}\mu$=5.8, which gives the critical slagging stickiness ratio ($\bar{\phi}_{SL/}\log_{10}\mu_{Temp}$) of 0.114. Considering the HT fouling, the corresponded parameters were: the slag ratio $\bar{\phi}_{HTF}$=0.095 and the critical HT fouling stickiness ratio =0.016. More detailed calculation results are summarised in Appendix I-6 (Table I-13 and Table I-14).

The normalised stickiness ratios predicted for the pure coal blends and co-fired with the 20th% straw share (1ar case, Table 5-1) obtained for the slagging and HT fouling conditions

are compared in Figure 5-12. On the ternary diagrams the white areas show the non-slagging or non-HT fouling fuel blends thermal ratios windows whereas the coloured shadows indicate increasing stickiness ratio tendencies.

a) **Platen Superheater Slagging**

SA3-CO1-AL1 Coal Blend **SA3-CO1-AL1+20th% Straw**

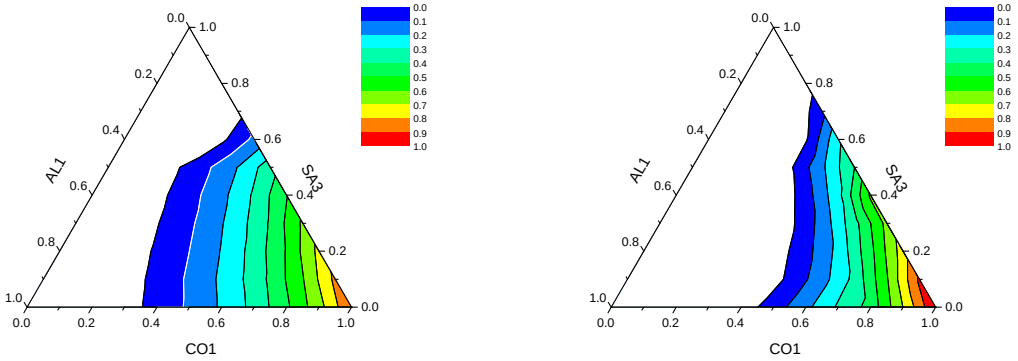

b) **High Temperature Fouling**

SA3-CO1-AL1 Coal Blend **SA3-CO1-AL1+20th% Straw**

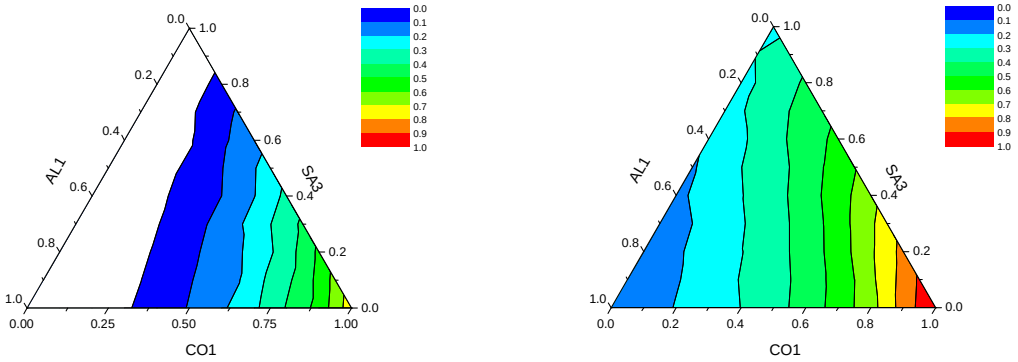

Figure 5-12. Predicted impact of straw co-firing with coal on normalised stickiness ratios for pure coal blend and 20th% straw co-firing: a) Platen superheater slagging , b) HT fouling region.

Analysing firstly the results obtained for the ternary blends of coal without straw impact, as expected, the increased ratio of CO1 in blends led to raised slagging and HT fouling stickiness ratios. To meet the non-ash deposition conditions (“white areas” on the diagrams) the thermal ratio of CO1 coal should be below 0.3 in a coal blend. The impact of AL1 and SA3 coals on reducing CO1 coal effects is predicted to be comparable.

When analysing the influence of 20th% straw co-firing with the set of coals considered, the different predictions were obtained between the slagging and HT fouling regions. The impact of straw co-firing on slagging condition change was predicted to be not significant for the 20th% coal substitution. The non-slagging operational windows slightly increased for

AL1 coal and decreased for SA3 coal shares in a blend with straw. The positive effect of AL1 coal and the increasing negative impact of CO1 coal were identified. These positive/negative observations are shifted also to the HT fouling regions. However, the impact of straw co-firing is here much more visible. In this case, for the 20th% straw share, the increased HT fouling was predicted for the all coal blends considered.

The highest impact on increasing stickiness ratio showed blends dominated by the CO1 coal whereas the blends composed of the high shares of SA3 and AL1 coals reduced significantly the straw effects. The blends with dominating AL1 coal revealed the most positive influence on reducing slagging/HT fouling tendencies. Although the overall ash burden increases for blends with AL1 coal as shown in Figure 5-13a, the predicted low stickiness ratios affected mostly the slagging/HT fouling indices which remain low for these blends. The effect of ash burden on the HT fouling index predictions (1ar case, Table 5-1) is presented in Figure 5-13b.

SA3-CO1-AL1+20th% Straw

a) **Ash burden, g/kg flue gas** b) **HT Fouling Index**

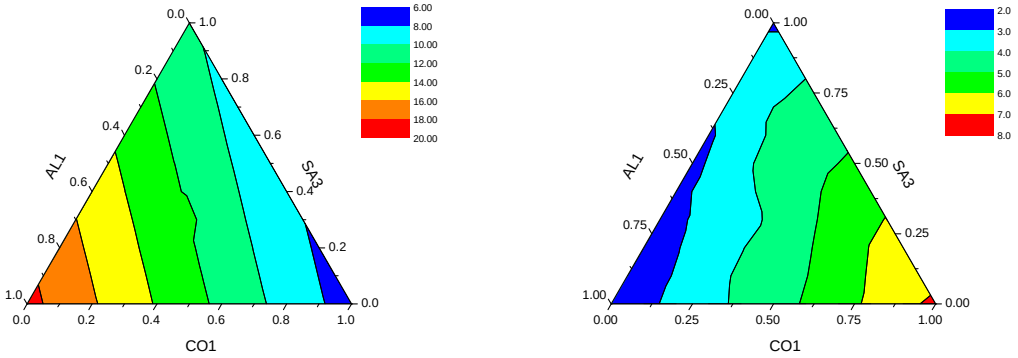

Figure 5-13. Coal co-firing with 20th% straw: a) Ash concentration g/kg flue gas, b) Predicted high temperature fouling index (normalised stickiness ratio multiplied by the ash burden).

The results showed that even though the lowest ash content of CO1 coal, the blends composed of this coal still maintain their high HT fouling tendencies which are mostly influenced by the high stickiness ratios.

5.3.5.2 Alkalis Capture Efficiency

The impact of coal ash blends quality on the potassium capture efficiency and the predicted K_2SO_4(s) maximum concentrations (g/kg fuel) found in the temperature range of the convective section of the boiler co-fired with the 20th% straw share (1ar case, Table 5-1) are shown in Figure 5-14.

SA3-CO1-AL1+20th% Straw

a) **Potassium Capture Efficiency** b) **K_2SO_4(s) g/kg fuel**

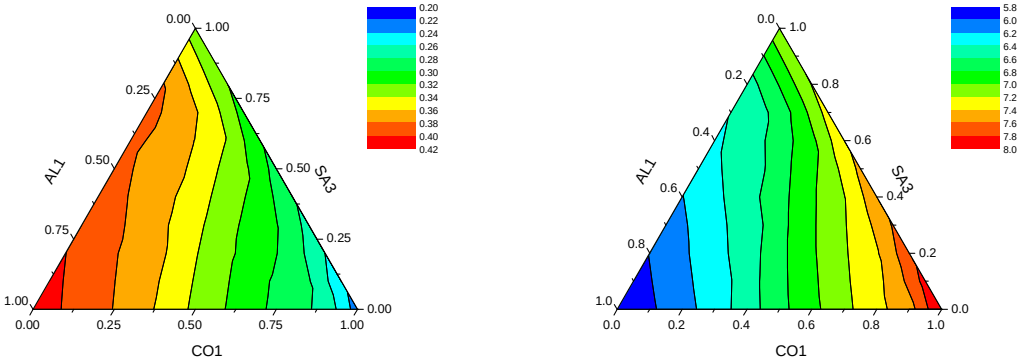

Figure 5-14. Predicted impact of 20th% straw co-firing with coal: a) Potassium capture efficiency – 5% of fly ash mass (REA) interacting with alkali metals, b) Corresponded max K_2SO_4(s) concentrations in a convective pass.

As can be seen, the potassium capture efficiencies agreed well with the predicted HT fouling tendencies analysed in the previous sub-section. The highest efficiencies have been predicted for the AL1-coal dominated blends, due to their high content of the ash, enriched in SiO_2 and Al_2O_3 and low Na_2O, K_2O percentages. Blends composed of the SA3 coal revealed it to be a relatively less efficient in capturing alkalis as compared with the AL1 coal.

The remaining flue gas alkalis formed salts in the convective section of the boiler. As expected, the simulations revealed the highest K_2SO_4(s) concentrations predicted for the CO1-coal dominated blends due to their relatively lower propensities to capture alkali metals from the flue gas.

5.3.5.3 Agreement with the Observations found in the Literature

Although is it difficult to compare directly the obtained model predictions with the slagging/fouling observations reported in the literature, the general tendencies can be noticed, mainly derived from the Danish experience in straw co-firing straw with coal in large scale pulverised fuel fired boilers [7, 8, 46, 145, 146].

Visual inspection after one week co-firing of 20th% straw with Canadian, high-S coal at the Amager Power Station (250 MW_e pf boiler) revealed less deposition formed at the platen superheater region and increased deposition of the tertiary superheater as compared with the pure coal firing [7]. The lowest sensitivity of the platen superheater sections on the ash deposition effects from the straw as compared with the reheat exchangers were also predicted by the current phase equilibrium-based model.

Co-firing up to 20th% straw with US and South American coals at Midtkraft-Studstrup (MKS) Power Station, Unit 1 of 150 MW_e capacity, revealed increased deposition tendencies of platen superheater and other sections entering the convective pass of the boiler. However, in the platen superheater region the reduced tenacity of deposit was observed over time probably due to shedding of the deposits [8, 46].

Other results obtained from the straw co-firing campaign undertaken at the MKS Power Station, Unit 4 of 300 MW_e capacity, strongly indicated the high impact of the coal content and quality on the alkali metals behaviour. During straw co-firing with a South African coal much more improved conversion of K from straw into insoluble K-Al silicates was observed as compared with co-firing lower ash content Colombian coal for which increased K_2SO_4(s) concentration was detected in the ash [146].

In the all above reported experiences, it was generally agreed that the quality of coal, especially their ash content was the major parameter that controlled the potassium behaviour which was either captured by the alumino-silicates or converted into potassium sulphates. Furthermore, decreasing the furnace gas exit temperature by reducing boiler load mitigated the ash deposition severity revealing the high correlation of the thermal boiler conditions with slagging and fouling.

5.4 Summary

In this chapter the development of a slagging and fouling predictive model is described. The model is based on the phase equilibrium analysis and utilises three separate phase equilibrium schemes assigned to the modules in order to assesses the ash deposition caused by the different mechanisms, such as slagging and HT fouling, condensation of salts and inorganics interactions phenomena. The model is based on the assumption of including the slag percentage in the bulk ash approaching the tube banks, the slag viscosity and ash concentration as the major factors affecting the ash deposition severity. The ash deposition rate as well as the proper slagging and fouling rate and indices assigned to the specific boiler regions were defined. Due to the one-dimensional nature of the model and associated simplification of a flow pattern, only the assessment of ash deposition rate by inertial impaction on the heat exchangers surfaces placed perpendicularly to the major flow trajectories were attempted. Furthermore, the near furnace wall-boundary deposition likely to occur by thermophoresis or diffusion was not investigated, as it is known to have minor impact when co-firing with relatively lower levels of biomass, i.e. when the coal share dominates.

The effects of various model criteria to determine the stickiness of the ash particles were critically evaluated. It was revealed that the model predictions are very sensitive to the assumed reference critical value which is not well defined in the literature. Furthermore, the predicted local slag phase percentages corresponding to the temperature profile of the boiler may also lead to misinterpretation of the obtained results. To overcome mentioned uncertainties, the average slag ratios determined separately for the slagging and high temperature fouling temperature ranges were introduced. Moreover, instead of the reference critical viscosity value being constant for all cases, the slag viscosity at the specific reference temperature was proposed to be calculated to determine the stickiness of particles.

As far as straw co-firing is concerned, the predictions revealed that an increase in coal ash blend quality, expressed by the higher alumina-silicates presence in the fuel caused higher potassium capture efficiencies by the fly ash avoiding salts condensation in the convective pass of the boiler. Furthermore, the interacting mass of the particles influenced mostly the viscosity at the lower temperature range by decreasing its value, and thus enhancing the stickiness and increasing the local ash deposition rate. The impact of straw co-firing with a lower ash quality coal was much more significant and caused higher deposition especially at the heat exchange section placed at the HT fouling region.

The model responses, in general corresponded well with the findings reported for straw co-firing cases in the literature. However, the developed approach needs to be validated for a wider spectrum of fuel blends. This is carried out in the next Chapter of this thesis.

6

VALIDATION OF THE DEVELOPED SLAGGING AND FOULING PREDICTIVE APPROACH

In this Chapter an attempt is made to validate the developed slagging and fouling predictive approach based on the field observations derived from the industrial scale pf coal-fired 2.5 MW_{th} furnace well as a large pf 518 MW_e utility boiler fired with coal/biomass blends. A wide range of different quality trade coals and their blends are investigated. Furthermore, the impact of co-firing more complex biomass blends, up to 30wt% coal substitution, on slagging and fouling is analysed. The investigated biomass mix includes the mixture composed of the meat and bone meal, wood pellets and the biomass mix pellets produced on site at the power plant consisting of the sewage/paper sludge, and other wood residues. The gathered ash deposition observations are compared with the model predictions and conventional slagging/fouling indices. Correspondingly, the assumptions related with the used modelling approach are discussed with respect to the fuels investigated. Additionally, with the aid of the developed model, the fuel mix optimisation is performed to identify the biomass share flexibility windows for blends which ensure the most reliable operation of the boiler without severe slagging and fouling when co-firing 30wt% of biomass considered.

6.1 Introduction

Based on the carried out literature review in Chapters 1-3, the conventional predictive slagging and fouling indices fail when coal blends of different quality and their blends with biomass are considered. In this Chapter the predictive potential of the new developed indices is evaluated.

The goal is to answer the research question stated at the beginning of this thesis, which is as follows: *Is it possible to assess successfully the slagging/fouling tendencies of complex coal/biomass fuel blends with the aid of the models based on the phase equilibrium analysis? How detailed fuel data are required for such analysis?* Basically, it is aimed to check if the assumptions made to define the new slagging/fouling indices are correct, in terms of correlating the slagging/fouling severity with the ash burden, average slag percentages and viscosity of the surface predicted for the bulk ash composition of blended fuels. In case of biomass co-firing, the interest is in investigating the impact of the assumed interaction conditions between coal and biomass ash-forming matter on the predictions with known slagging/fouling observations.

To meet the stated objectives the predicted results are compared and discussed with the field observations gathered from the industrial-pilot scale coal-fired pf furnace and large scale utility pf boiler fired with complex coal/biomass blends.

6.2 IFRF-ECN Campaign to Characterise Behaviour of the Battle Coals

The slagging and fouling observation data used here to validate the developed predictive model originate partly from the past tests/research programs carried out by the IFRF and ECN in 1999 [69]. One of the major tasks of this collaborative research program was to evaluate the slagging and fouling tendencies of the imported, cheaper coals, some of them being of the low-quality (so called “battle“ coals), which were aimed to be fired in Dutch pf boilers. The majority the imported coal is originated from South Africa, Colombia, Australia, Indonesia, Russia, Poland and the United States.

During the IFRF-ECN “battle coals” investigation campaign, the semi-quantitative slagging/fouling assessment was performed for the selected single coals as well as binary blends which were fired in a 2.5 MW_{th} IFRF boiler furnace simulator. It was then supported by the ash deposition tests conducted under well-controlled conditions with the use of the ECN’s lab-scale combustion simulator to provide more mechanistic ash-related information,

which could allow the further interpretation of the observations made from the semi-industrial scale trials.

During the one hour trials for each tested fuel, the ash and deposit samples were collected for the off-line analysis and evaluation, by the air-cooled slag sampling probe located in the recirculation zone of the burner to simulate near-burner slagging at a gas temperature of 1300-1400^{o}C. Another, fouling probe was placed in the flue gas exit channel to simulate fouling at the gas temperature of 1100-1200^{o}C [69]. These tests were simultaneously performed under well-known conditions of the ECN simulator, established for the full-scale pf boiler equipped with the low-NOx burners. Ash deposition probes were inserted into the simulator to collect particles and deposits at different residence times: this included the near-burner area (at the 20 ms residence time) to study slagging under reducing and high-temperature conditions as well as at high residence times of around 2000 ms to assess fouling at the flue gas exist areas [69].

The collected samples were analysed by the SEM-EDX method to obtain information regarding the thickness, orientation and composition of the ash layer on the deposition surface. The results were expressed in a form to allow the ranking of the slagging and fouling propensities of investigated coals/blends, and were compared with the predictions obtained by the commonly used predictive ash deposition indices which in many cases failed. The results obtained are summarised in Table 6-3, and discussed in more detail in section 6.4.1.

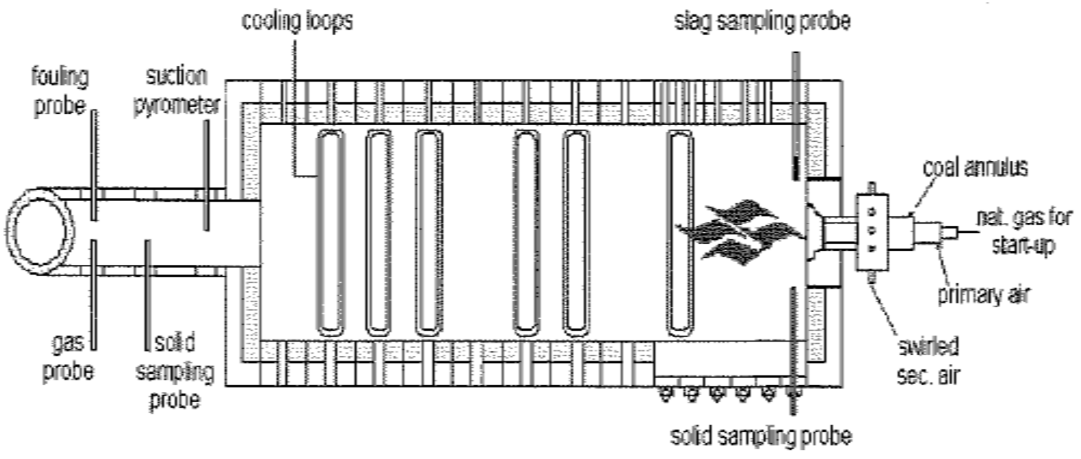

Figure 6-1. Schematic of the semi-industrial 2.5 MW_{th} furnace used during IFRF-ECN slagging/fouling trials [69].

6.3 Biomass Co-firing at the Maasvlakte 518 MW_e PF Boilers

The Maasvlakte Power Plant (MPP) owned by E.ON Benelux, was commissioned in June 1975 and was at that time fired by natural gas/oil, further converted into burning coal in 1988. The plant consists of two pulverised fuel tangentially-fired sub-critical steam boilers, each with a capacity of 518 MW_e. Both units are equipped with SCR DeNOx, electrostatic fly-ash filters and desulphurisation installation. The boiler layout showing the heat-transfer surface arrangements as well as the major boiler operational parameters are shown in Figure 6-2 and in Table 6-1.

6.3.1 Boiler Layout and Fuels Portfolio

Co-firing of biomass with coal has been practised at Maasvlakte since 1998 approaching the levels of around 10% monthly average level of coal substitution (on mass basis) after 2001. Suitable location of the MPP, close to energy port Rotterdam, makes this power plant attractive for importing coals and biomass of various sources. The portfolio of biomass fuels used for co-firing includes a wide range of wastes, food and agricultural solid/liquid residues of varied ash composition and slagging/fouling propensities.

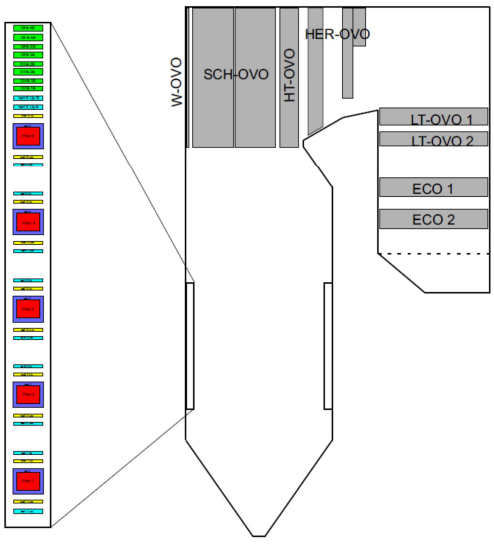

Table 6-1. Maasvlkate PF Boilers data [154].

Thermal Input	1272 MWth
Electrical Output	518 MWe
Steam Raised	444.4 kg/s (700 t/h)
Coal mass flow for LHV=25.0 MJ/kg	50.9 (183) kg/s (t/h)
Superheated Steam	540°C / 180 bar
Reheated Steam	540°C / 42 bar
Firing pattern	Tangentially fired
t_{FEGT}	1238°C
Boiler Efficiency	93.4%

Figure 6-2. Layout of the Maasvlakte boiler with the shown major operational parameters.

At the Maasvlakte Power Plant the blends of different quality trade bituminous coals are fired that fit to the designed fuel blending windows based on the basic fuel properties, in general limited by the levels of the pollutants emission allowed. On the average, most of the coal mix is composed of the various sources of Colombian coals, South African coals, followed by the lower relative percentages of the Russian, Indonesian, US-high sulphur and

other multisource coals. The individual coal ratios in coal blend may vary over the longer operational periods depending upon the current prices of the trade coals.

As far as the co-firing of biomass fuels is concerned, three major substitute fuels dominate in the current co-firing strategy at Maasvlakte, including: the meat and bone meal (MBM), woody biomass (WP) and biomass mix pellets (BMP) which are produced on-site at the power plant, and are composed of the sewage/paper sludge, bleaching clay and other wood residues. Moreover, the Maasvlakte Power Plant has experience in co-firing the chicken litter and various liquid fuels such as heavy hydrocarbon-based as well as the animal fat [154].

Blending of such a variety of fuel types may have a positive or negative impact on the overall slagging and fouling occurred in the boiler.

6.3.2 Slagging/Fouling Observations Methodology

The slagging/fouling assessment of the fuel blends is performed based on the long-term experience and slagging/fouling observations reported periodically since 2008 with the current time interval of around once per week.

The scheme of the heat transfer surfaces arrangements at the furnace outlet along with a drawn example of ash deposits found in the boiler are presented in Figure 6-3. As typical for the pf boilers design, the heat-exchange sections exposed on the high temperature and the flue gas radiation have higher distances between the flat panels, which also favours minimising the build-up of deposits bridging the individual tube's panels. As the temperature of the flue gas cools down when entering the convective pass, the distance between tube's panels is designed to be lower to achieve better heat-transfer via the convection mechanism.

A four-grade scale is applied to assess the severity of the slagging/fouling occurring, starting from: 0 – no deposition occurred on the individual tube panel; 1 – presence of low thickness deposits; 2 – high thickness deposits occurred on the individual tube panel, and 3 – severe deposition occurred, observed by the formation of the deposit bridges growing between the individual tube panels. For the all platen superheater/reheaters placed at the upper part of the furnace, the individual slagging/fouling severity points are summarised to obtain the overall deposition index. More detailed examples of such assessment are shown in a confidential report [155].

Co-firing of good ash quality fuels should not lead to the increase of ash deposition. However, this risk of the high temperature fouling still exists; therefore the boiler is

additionally equipped with the soot-blowing system to remove periodically the deposited material.

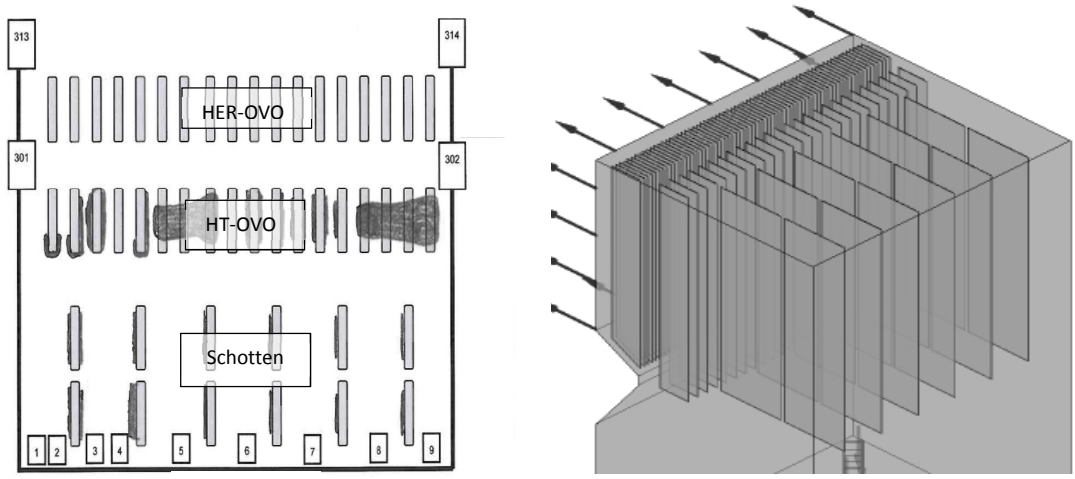

Figure 6-3. Scheme of the heat-exchange surface arrangement in the upper part of the furnace [155, 156].

6.4 Results and Discussion - 2.5 MW_{th} PF Furnace

In this section the coal blends investigated during the experimental IFRF-ECN campaign are analysed with the use of developed slagging and fouling predictive model. It is expected to give more understanding on the observed differences between measured ash deposition tendencies and predicted slagging/fouling propensities of fuels when utilising conventional indices. The flexibility of the new proposed indices in terms of their applicability for different coal ash chemistries/mineralogy is aimed to be tested. The obtained model predictions are then calibrated to the ash deposition severity scale applied during the experimental IFRF-ECN campaign.

6.4.1 Investigated Coals, IFRF-ECN Campaign

Various quality coals are tested originating from the worldwide sources, namely South African (SA), Egyptian (EG) , Indonesian (IN), Russian (RU), Polish (PL) and Candanian (CA) coals. Amongts these coals, the selected binary blends of SA-EG, EG-IN and IN-RU coals were investigated [69]. The blending coals had properties which would not allowed them to be burnt as a single fuel, mainly due to the sulphur and ash content. For instance for the IN-RU blend, the high ash and high sulphur RU coal was counterbalanced by the low ash, low sulphur IN coal.

Ash content, calorific value, oxide composition along with the slagging and fouling assessement carried out during the IFRF-ECN camapign for the investigated coals and their blends are summarised in Table 6-2 and 6-3. Based on these results, it can be seen that besides the ash chemistry, ash burden was another important factor that influenced slagging and fouling severity during the experiemental trials.

Table 6-2. Ash composition of the invesigated IFRF-ECN coals [69].

IFRF-ECN INVESTIGATION – COALS AND COAL BLENDS												
Coal	LHV MJ/kg	S % daf	Ash %	SiO_2 %	Al_2O_3 %	Fe_2O_3 %	CaO %	MgO %	Na_2O %	K_2O %	P_2O_5 %	SO_3 %
SA	25.8	0.8	17.14	45.8	32.0	5.6	**8.0**	1.2	0.2	0.7	1.2	4.1
SA60-EG40	26.8	1.6	13.58	40.1	27.1	8.7	**6.8**	1.1	0.2	0.7	1.0	13.2
EG	28.2	2.7	8.24	22.2	12.0	**18.4**	2.9	0.6	0.3	0.5	0.2	**41.7**
EG61-IN39	29.4	1.8	5.70	24.0	13.3	**17.7**	3.9	1.0	0.7	0.7	0.2	**37.3**
IN	31.3	0.3	1.73	37.8	23.3	**12.4**	**11.0**	4.2	**3.9**	1.8	0.2	4.7
IN36-RU64	27.3	2.0	16.14	40.9	20.6	**9.1**	**5.4**	1.5	**1.0**	2.1	1.2	17.4
RU	25.1	3.0	24.25	41.0	20.5	9.0	5.2	1.4	0.9	2.1	1.2	17.9
PL	26.6	0.9	16.33	46.6	26.1	9.0	5.0	3.5	0.6	**2.9**	0.5	4.9
CA	21.0	0.3	26.21	61.4	21.8	5.0	4.7	1.5	**2.6**	2.4	0.1	0.0

Table 6-3. Slagging and fouling assessment of the investigated IFRF-ECN coals [69].

IFRF-ECN INVESTIGATION – COALS AND COAL BLENDS						
Coal	Slagging Assessment				Fouling Assessment	
	Experimental	B/A	B/A*Sd	T25, ^oC	Experimental	B/A*Na2O
IN	Low (0.5)	**0.54 (H-S)**	0.15 (L)	1231 (H)	Low	2.1
SA	Low-medium (1.0)	0.20	0.13 (L)	1396 (M)	Low	0.04
EG	Low-medium (1.0)	**0.64 (H-S)**	**1.58 (M)**	1183 (H)	Low	**0.20**
SA60-EG40	Medium (1.5)	0.26	0.35 (L)	1364 (M)	Low	0.06
EG61-IN39	High (2.5)	**0.62 (H-S)**	**1.04 (M)**	1192 (H)	Low	**0.48**
PL	High (2.5)	0.29	0.21 (L)	1384 (M)	Low	0.17
IN36-RU64	Severe (3.5)	0.31	**0.63 (M)**	1392 (M)	Medium-high	0.32
RU	Very severe (4.5)	0.30	**0.68 (M)**	1399 (M)	Severe	0.27
CA	Very severe (4.5)	0.19	0.04 (L)	1543 (L)	High-severe	0.50

Slagging: B/A: 0.4-0.7 (high-severe "**H-S**"); **B/A*Sd:** <0.6 (low "**L**"); 0.6-2.0 (medium "**M**"); 2.0-2.6 (high "**H**"); >2.6 (severe "**S**"); **T25**: >1400^{o}C (low "**L**"); 1400-1245^{o}C (medium "**M**"); 1245-1120^{o}C (high "H"); >1120^{o}C (severe "**S**");
Fouling: B/A*Na_2O: <0.2 (low "**L**"); 0.2-0.5 (medium "**M**"); 0.5-1.0 (high "**H**"); >1.0 (severe "**S**").

For instance, the low ash IN coal, enriched in iron, calcium and alkali metals content in the ash, expressed by a relatively high B/A ratio, and notorious for the low melting point ash, revealed both the low slagging and fouling tendency during the experimental tests. This could be associated with the very low ash content of this coal and the aerodynamic conditions around the slag sampling probe which had a relatively low projected area as compared with the furnace dimensions. Similarly, based on the conventional indices applied, the EG coal also

revealed a high slagging severity. However, due to the intermediate ash content of the EG coal it was ranked within the low-medium category according to measurements.

Interesting results were obtained for the blend composed of the EG61-IN39 coals which has slightly reduced ash content due to the IN coal impact. For this blend the increase in slagging tendency was observed during the trials.

In general, it was observed that coals with increased ash content had correspondingly higher slagging/fouling tendencies with some exceptions e.g. for the SA coal which has a relatively low B/A ratio and was assessed as a low-medium slagging coal.

The use of conventional indices completely failed when evaluating the slagging potential of the CA coal. This coal was identified to cause very severe slagging based on experiments, which was opposite to the index predictions indicating the low slagging risk. Based on these results, it was revealed that the conventional indices underestimate the impact of alkali metals on slagging prediction. It was especially visible for the ashes with the low B/A index values, such as in case of the CA coal ash, which was additionally found to be enriched in both the sodium and potassium metals.

6.4.2 Predicted Melting and Slag Viscosity Characteristics

To give more insights into behaviour of the investigated coal ashes the phase equilibrium calculations were performed, being part of the developed predictive methodology. The predicted slag ratios in the bulk ash over the wide temperature range as well as the corresponded slag viscosity for the investigated coals are summarised together in Figure 6-5 and 6-6.

According to the calculations, the SA and EG coals revealed the most benign slag distributions whereas for the IN and CA coals the highest levels of slag were predicted. Polish and Russian coals showed intermediate melting characteristics amongst coals investigated. Blending of SA and EG coals led to a minor increase in the slag percentages in the ash due to the impact of EG coal whose ash revealed a slightly higher melting tendency, but a lower ash content as compared with the SA coal. The impact of increased percentage (36wt%) of the low ash but with a high slagging propensity IN coal in a blend with RU coal was even less significant due to a considerable difference in the ash contents of these two coals. A similar blending ratio of IN coal with EG coal led to a higher sensitivity of the results, due to the three times less ash content of the EG coal as compared with the RU coal.

As far as slag viscosity characteristics are concerned, the lowest viscosities, in a temperature range below 1300^{o}C, were predicted for the Indonesian coal, followed by the

Canadian, Polish and Russian coals. Blending with Indonesian coal affected the overall slag blend viscosity by lowering its value which was observed to be the most significant for the blend of EG61-IN39 coals.

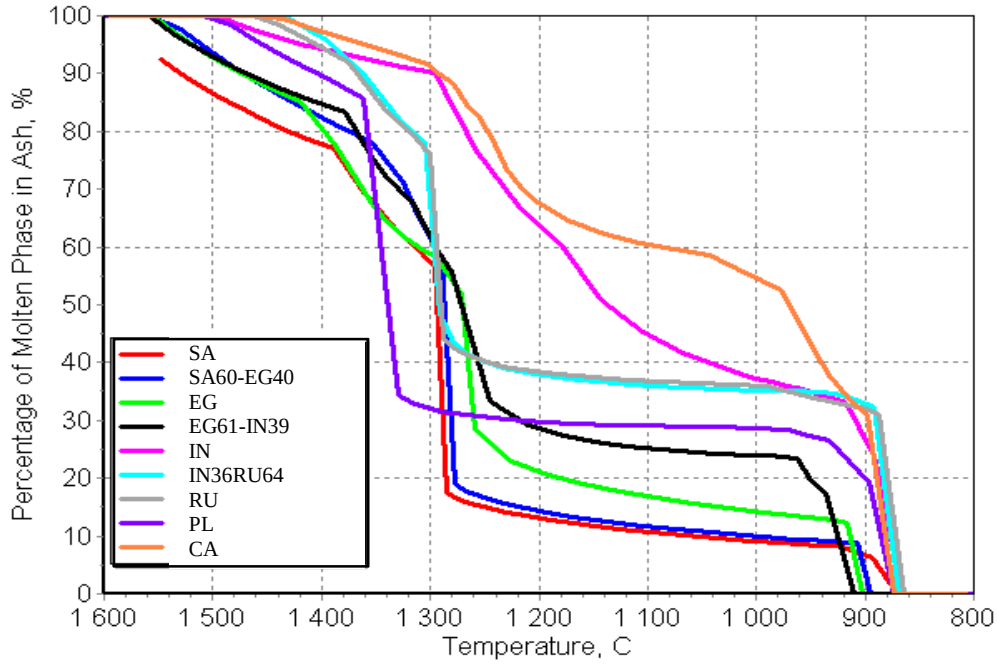

Figure 6-4. Slag % distributions over the temperature range 1600-800°C, calculated for the IFRF-ECN coals.

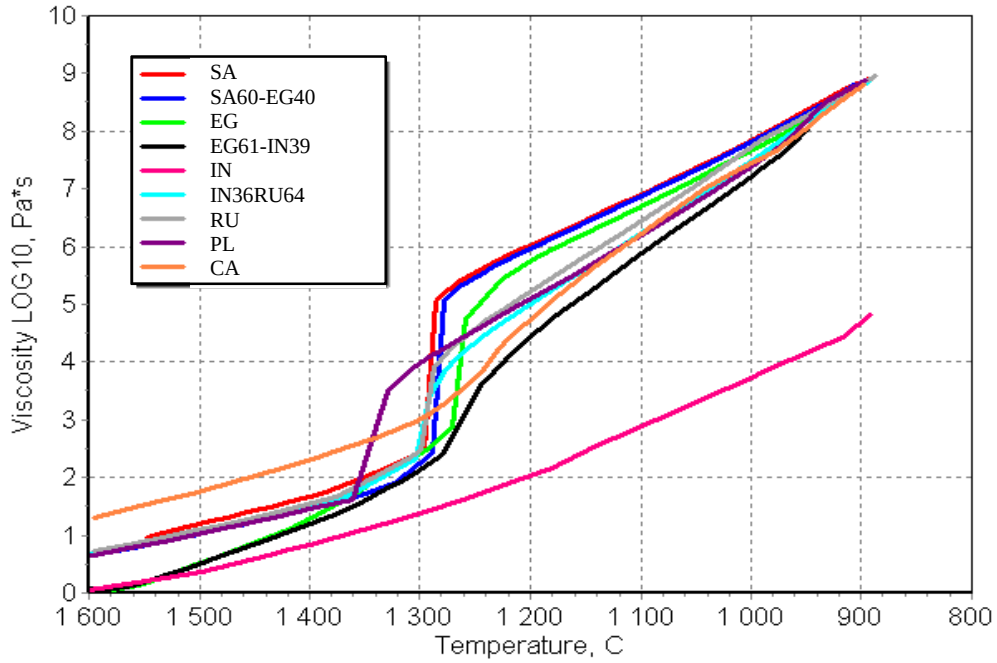

Figure 6-5. Slag viscosity distributions over the temperature range 1600-800°C, calculated for the IFRF-ECN coals.

An interesting tendency was observed for the Canadian slag viscosity characteristic which revealed the highest viscosity levels above 1350°C whilst achieving relatively low levels at the lower temperature range. It is due to the low calcium and iron content (thus low B/A ratio) as well as the increased potassium and sodium levels in the ash of the CA coal as compared with the other investigated coals.

The impact of blending the IN coal having the low viscous slag with the EG coal on the overall slag blend viscosity was predicted to be a quite significant. Such coal blends may reveal the elevated slagging risk which is agrees with the field observations gathered during the IFRF-ECN slagging trials.

6.4.3 New Slagging Index vs. Field Observations

The predicted for the investigated coals/blends ash-deposition related parameters, such as the average values of slag ratio at the slagging temperature range (above 1250°C), the slag viscosity at 1250°C, and the calculated ash burden, were used then to determine the slagging severity based on the new slagging index as defined in Chapter 5.

To identify more clearly the impacts of slag ratio and surface viscosity on the ash deposition, the following graphs have been produced. On the first one – Figure 6-6, the effects of the ash loading and the average slag ratio in the ash is included, and the predicted ash deposition severity is compared with the observed slagging tendencies. The second graph, Figure 6-7 presents additionally the impact of the deposit surface viscosity on the ash deposition severity.

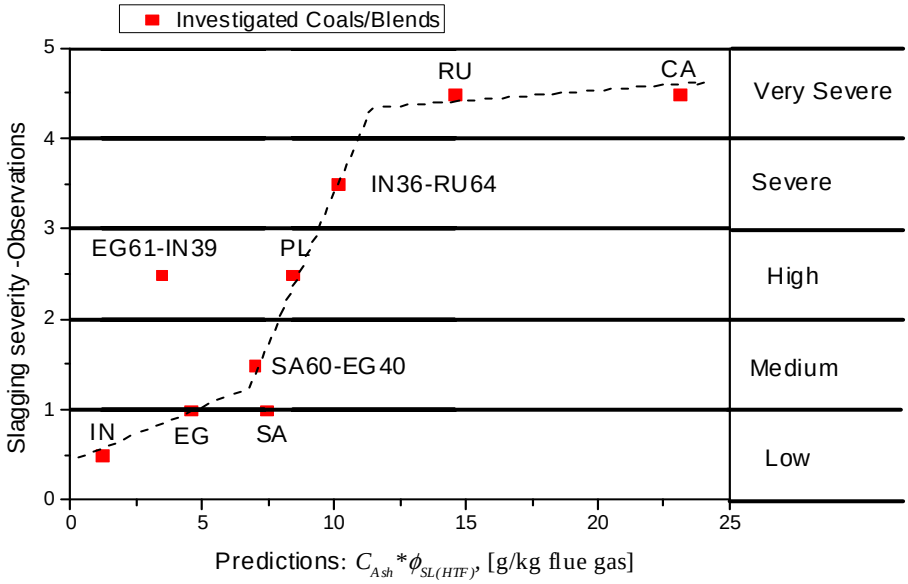

Figure 6-6. Comparison of the prediction (part 1) with the slagging observations for the IFRF-ECN coals.

Amongst the investigated coal ashes, for two of them, namely for the South African coal and EG61-IN39 coal blend the observed slagging severity tendencies differ from those predicted based only on the ash loading and slag ratio parameters.

In case of the EG61-IN39 coal blend, the slagging observations did not match the general predictive trend which would indicate far less benign slagging severity, in a range of low-medium risk, as compared with the observed high slagging severity for this coal blend. This mismatch can be associated with another important factor such as the low viscosity of slag at the temperature corresponding to the deposit surface layer (around 1250^{o}C), which was not included within this predictive index. The low slag viscosity for the EG61-IN39 coal blend was confirmed by the phase equilibrium calculations (see Figure 6-5). Therefore, it is very likely that additional mass of non-molten fly ash approaching the tube was captured by the sticky deposit layer and contributed to the deposit build-up process.

For the South African coal, the predictions were slightly more severe in comparison with the field observations which revealed a low-medium slagging risk for this coal. This can be associated with a relatively low stickiness ratio of the SA ash (see Chapter 5), whose slag ratio levels were predicted to be the lowest, and slag viscosity the highest from the investigated coals. Considering also the intermediate ash content of the SA coal, this ash can have the increased erosion potential.

When including additionally the slag viscosity parameter within the index, the improved linear correlation between the predictions and slagging observations within the index range of 1-3, has been obtained as shown in Figure 6-7.

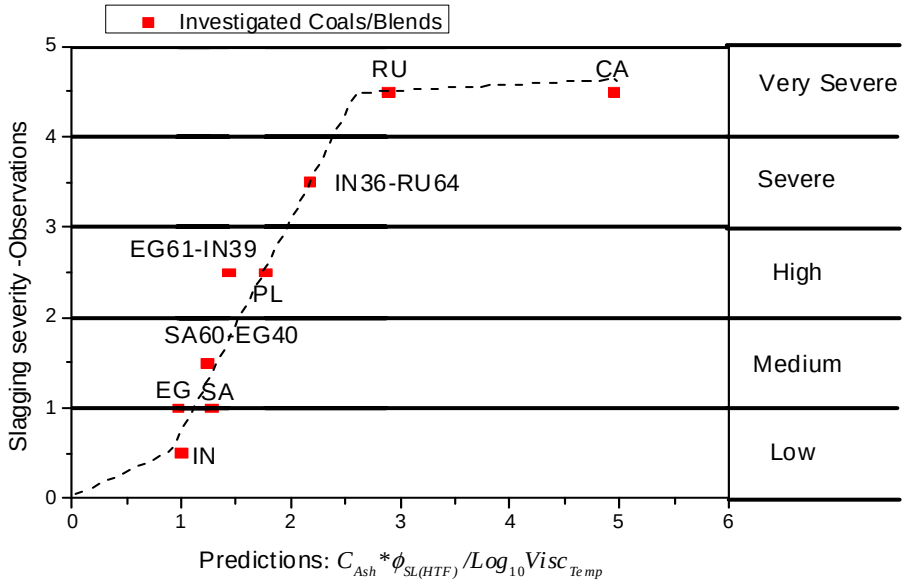

Figure 6-7. Comparison of the predictions (part 2) with the slagging observations for the IFRF-ECN coals.

This was followed by the calibration of the prediction scale to the field observations. For the assumed linear relationship, the following calibrated formula (with the determination coefficient of R^2=0.92) valid for the slagging severity assessment, based on the investigated pf furnace, has been obtained:

$$I_{SL} = 2.0137 \cdot \left(C_{ash} \cdot \frac{\bar{\phi}_{SL}}{Log_{10}\mu_{Temp}} \right) - 1.0622 \qquad (6.1)$$

where C_{ash} is the ash burden (g/kg flue gas), $\bar{\phi}_{SL}$ is the average slag ratio for the slagging temperature range (<1250^{o}C, see section 5.2.3.2 Chapter 5) and $\log_{10}\mu_{Temp}$ is the viscosity factor calculated for the slag viscosity at the reference temperature (1250^{o}C).

6.5 Results and Discussion – Maasvlakte PF Boiler

In this section the developed predictive methodology is validated against the slagging/fouling observations derived from the MPP pf boiler. It is aimed to perform such an analysis for the selected operational periods during which the different quality coals and biomass fuels were fired altering the ash deposition severity.

Currently, the biomass percentages are around 10wt% coal substitution (on monthly average basis) with some temporary operational days when higher biomass shares were fired approaching 20wt%. The validation part is followed by performing an example of the fuel blends optimisation analysis to identify fuel blends flexibility windows with non-severe slagging/fouling propensity when co-firing biomass mix shares up to 30wt%.

6.5.1 Investigated Operational Periods

From the long reported history of slagging and fouling observations (since 2008, see confidential report [155]) two shorter operational periods have been selected for conducting a more detailed analysis:

- **<u>Period A (one month long: May 2009).</u>** In this period, in general, the **good ash quality coal blends** were co-fired with **biomass mix of lower ash quality** and increased co-firing shares typically above 10wt%, especially during the first half of the month. After the mid-month the biomass ash quality improved and lower co-firing percentages were experienced. During the whole period the bulk ash of the coal blend was of low alkali metals content. The measured IDT ash fusion temperatures were relatively high for all the coal ashes within the blend [155]. The ash content of biomass mix was a relatively

high compared to coal blend. The temporary biomass mix quality drop was identified to be associated with the impact of the BMP ash composition change, which was enriched in calcium in the ash [155].

- **Period B (three months long: Jan 2011 – March 2011).** In the second half of this period a significant **drop in coal ash quality** has been identified whilst **a good quality of biomass mix** input was maintained over the whole analysed operational time. Although, the biomass co-firing ratios have been found to vary considerably on a daily basis, they were typically below 10wt% with the identified short-term (daily) peaks of around 15wt% coal substitution. The drop in coal ash quality was indicated by the relatively low IDT ash fusion temperatures of the all coals within the blend, which was associated with the increased alkali metals presence in the bulk ash. During this operational period when a high slagging/fouling was observed the boiler shutdown was reported and the heat transfer surfaces cleaned. The biomass ash quality has been found to not change significantly over the whole investigated period. More details can be found in a confidential report [155].

Amongst the all considered biomass fuels co-fired at Maasvlakte Power Plant, the MBM showed the most stable ash chemical composition whilst the BMP revealed the highest variations mostly regarding the ash content and calcium concentration in the ash. This due to varied origin of the biomass residues of which the BMP are composed, being a mixture of the composted sewage/paper sludge, bleaching clay and other wood residues.

The individual co-firing ratios of the coal and biomass fuels in the overall fuel mix as well as their ash chemical composition variations during the investigated periods can be found in a confidential report [155].

6.5.2 Discussion on the Biomass Mix Inorganic Species Activity

In order to perform more reliable phase equilibrium calculations which are part of the developed slagging and fouling predictive methodology, the preliminary assessment of the inorganic species activity based on the inorganic speciation is needed, particularly in relation to biomass fuels.

In general the procedure follows the assumptions defined in section 5.2.2.1, Chapter 5. According to them, as far as coals are concerned the bulk ash composition is used as the input into the model, assuming alumino-silicate chemistry of the fly ash. Part of the alumino-

silicates is assumed to be more reactive towards capturing the alkali metal released into the gas phase from the biomass, based on the Nutalapati [103] model (see section 5.2.2.4).

In case of the biomass fuels, all the ash-forming elements which are easily soluble, or are organically associated (i.e. alkali metals) are very reactive, thus can interact with alumino-slicate-based fly ash based on the conditions specified in section 5.2.2. The key point is related with identification of the less reactive minerals/salts present in biomass materials which would behave as inert during fuel combustion and do not affect slagging and fouling.

In the biomass mix co-fired with coal blend at Maasvlakte boilers, typically more than one third mass of the biomass stream consist of the meat and bone meal. A dominate percentage of the MBM ash (> 85%) is composed of the hydroxyapatite $Ca_5(PO_4)_3(OH)$, a constituent of the bones. This mineral appears to be a very stable during combustion (eventually releasing -OH part) and influence the high fusion temperatures (HT= 1700^oC, Table 2-3) of the MBM ash. Furthermore, according to reported experiences with MBM co-firing, the hydroxyapatite was a majority of the ash found in the bottom ash in pf boilers, contributing to the coarser, heavier ash fraction, and not affecting the slagging increase [157]. In light of the above, it was assumed to exclude the calcium and phosphorous originated from the MBM from the input into slagging and HT fouling phase equilibrium module. The dominating impact of the MBM on slagging/fouling is thus expected to come from the relatively high contents of the reactive sodium and potassium elements.

Biomass mix pellets produced on site at the Maasvlakte Power Plant are dominated by the alumino-silicates derived from the bleaching clay but also from the composted sewage/paper sludge which additionally contribute to the large extent of calcium and eventually smaller presence of the phosphorous in biomass mix. The increased content of very reactive (organically bound) calcium in the BMP ash, originated most likely from the higher shares of the paper sludge, is the key factor which may influence the slagging and fouling. Within this work, the 20% part of the identified calcium in the BMP was assumed to not interact with alumino-silicate fly ash. This is based on the findings which revealed a high ability of the BMP enriched in Ca, to produce sub-micron CaO particles, which were further sulphated to form $CaSO_4$ in the DeNOx catalyst region [154].

Regarding the wood originated biomass, such as wood pellets or forest residues, which are enriched in calcium, the similar approach as for the BMP (in terms of 20% non-interacting Ca with alumino-silicate ash) was applied. Other elements, derived from the extraneous minerals, mostly S-Al-based were introduced into slagging and HT fouling phase equilibrium module as defined in 5.2.2 section.

6.5.3 Slagging / HT Fouling Predictions vs. Field Observations

In this subsection the slagging/fouling observations are compared with the model predictions obtained for the specific fuel blends fired during the investigated periods.

However, before analysing more complex fuel blends, first the impact of a single biomass types co-fired with coal is simulated to give more understanding of the model behaviour when increasing co-firing share of biomass with specific ash chemistry. Therefore, firstly the slagging and viscosity predictions were performed for co-firing the reference coal blend with MBM (for 0wt%, 10wt%, and 20wt% shares), followed by the simulations of co-firing the same coal blend and co-firing shares with the BMP pellets (enriched in calcium in the ash). The predicted slag % distribution in the ash and the slag viscosity over the wide temperature range are shown in Figure 6-8.

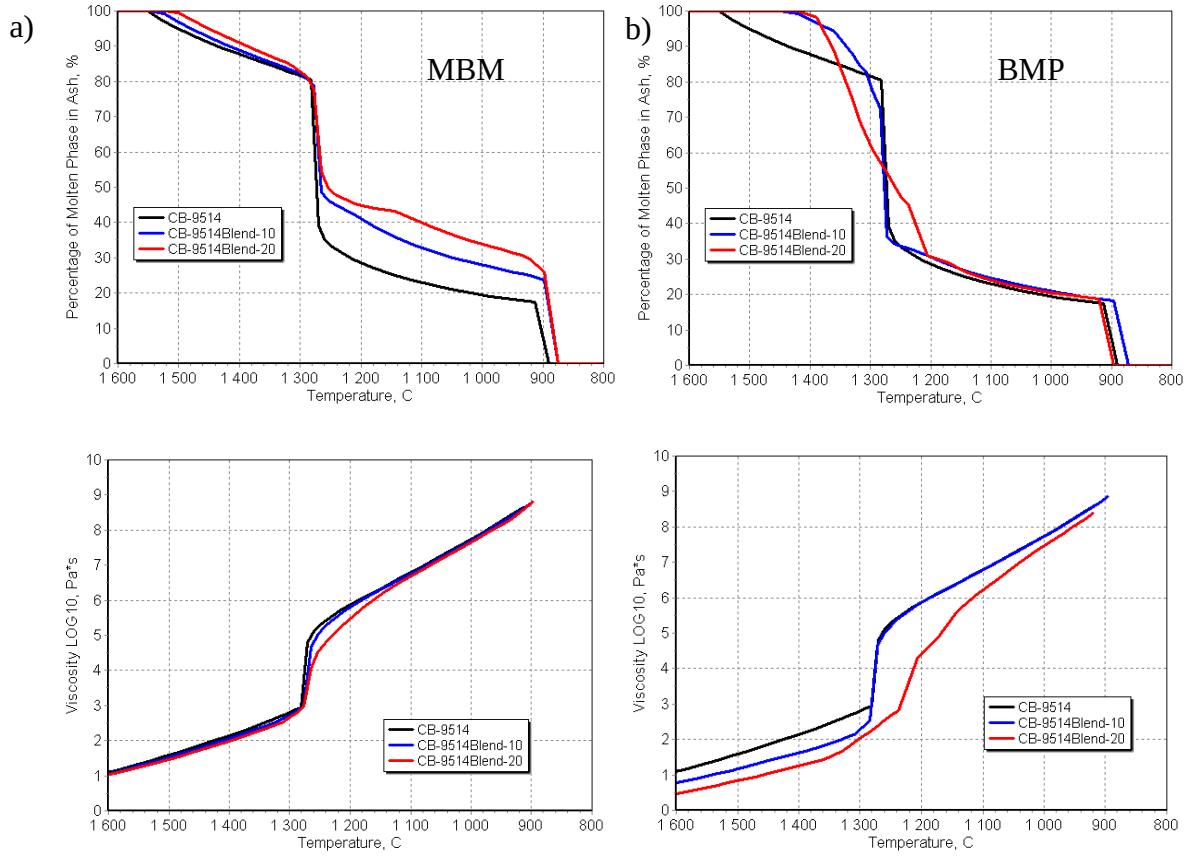

Figure 6-8. Predicted slag % and corresponded slag viscosity distributions for: a) MBM co-fired with coal for 0wt%, 10wt%, 20wt% coal substitution, b) BMP co-fired with coal for 0wt%, 10wt%, 20wt%.

It is clear according to the model, that co-firing of the meat and bone meal with coal would affect mostly the high temperature fouling propensity of the overall blend when increasing co-firing shares of MBM. It is showed by the raised slag % at the lower temperature ranges which was not observed to be so significant above 1300^{o}C, therefore

indicating the low impact on slagging propensity change. It is associated with the capturing of sodium and potassium originated from the MBM by molten alumino-silicates which led to the decreasing of the melting temperature of the ash as well as caused the rise in the slag % occurring at the lower temperature range. The effect of the MBM co-firing up to 20wt% share on the slag viscosity change was observed to be minor.

In case of the BMP co-firing, the impact is more complex. In general, according to the predictions, as seen in Figure 6-8b, the slag % increased as compared with the pure coal firing case, reaching 100% in the total ash at around 1400^{o}C for both 10wt% and 20wt% co-firing ratios. Correspondingly, the significant drop of the slag viscosities were predicted, which overall can result in the rise of the slagging severity in the platen superheater region. Furthermore, the performed analysis revealed that 10wt% co-firing of the BMP would not change significantly the HT fouling tendency of such blend, as the differences between the predicted viscosity and slag % are minor as compared with pure coal firing. However, the situation can change dramatically when higher co-firing rates of the BMP are considered. For instance, as shown in Figure 6-8b, the 20wt% coal substitution has already led to the drop of the slag viscosity at the lower temperature ranges which can lead to severe fouling. In comparison with the MBM co-firing, the impact of the BMP enriched in Ca content in the ash, can be more severe and lead to both the slagging and fouling when higher BMP co-firing shares are considered.

A comparison of the obtained predictions with the slagging/fouling observations gathered during two investigated periods is shown in Figure 6-9. Additionally, in Figure 6-10 the results for co-firing were compared with the predictions obtained for the corresponding pure coal blends firing cases to highlight more clearly the impact of biomass mix on the ash deposition severity. More detailed data of the fuel blends, regarding the ash compositions, individual shares of coals and biomass co-firing ratios within the blends during the investigated periods are summarised in a confidential report [155].

The scale of the predictions was calibrated to the field observations. Slagging index was calculated for the platen superheater section (Schotten) and HT fouling index was assessed for the heat transfer sections entering the convective pass of the boiler as defined in 5.2.3.2 (Chapter 5). These included the calculation of the average slag ratios and the reference slag viscosities for the corresponded temperature ranges. Moreover, it is important to note, that the calculated slagging/HT fouling indices (“Deposition Index” in Figures 6-9, 6-10) did not include the effects of the ash burden on the ash deposition due to some uncertainties related with this assessment. The operational periods between the subsequent field observations were

relatively long and not equal (from a few days to two weeks). The boiler load also changed which also would affect the real ash burden found between the field observation intervals. Another uncertainty was related with the unknown soot-blowing activity during the investigated periods. Therefore, it was postulated that predicting average slag ratios as well as the slag viscosity would at least give some insights, and correspondence with the history of ash deposition giving the reliable first order predictions. This could be supported with the observed relatively low overall average ash content changes within the blends fired during the investigated operational periods.

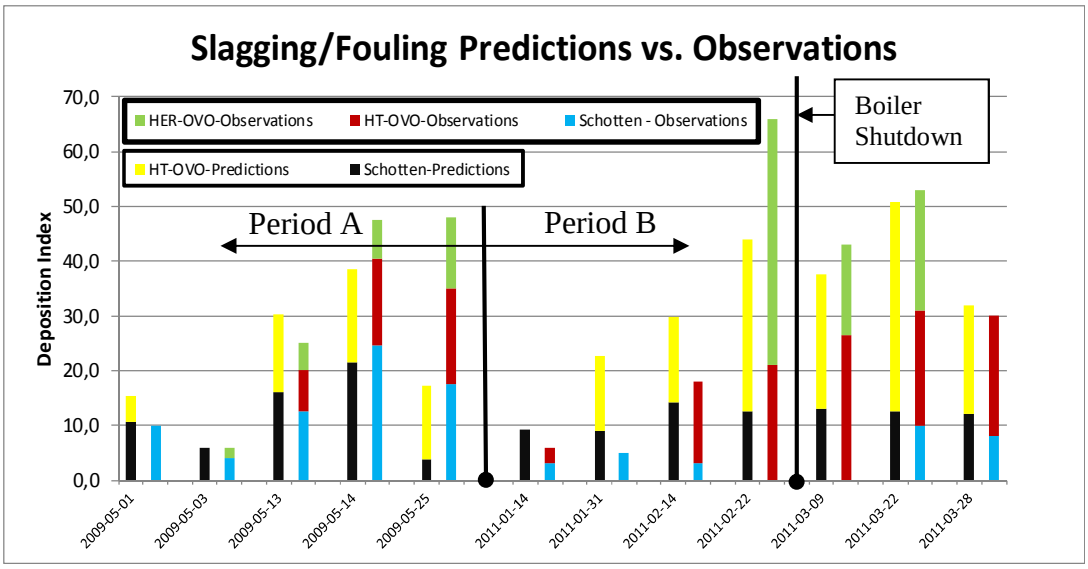

Figure 6-9. Comparison of the predicted slagging/fouling tendencies with the field observations gathered for two operational periods when co-firing biomass with coal: Period A – good quality coal co-fired with a lower quality biomass, Period B – lower quality coal co-fired with good quality biomass.

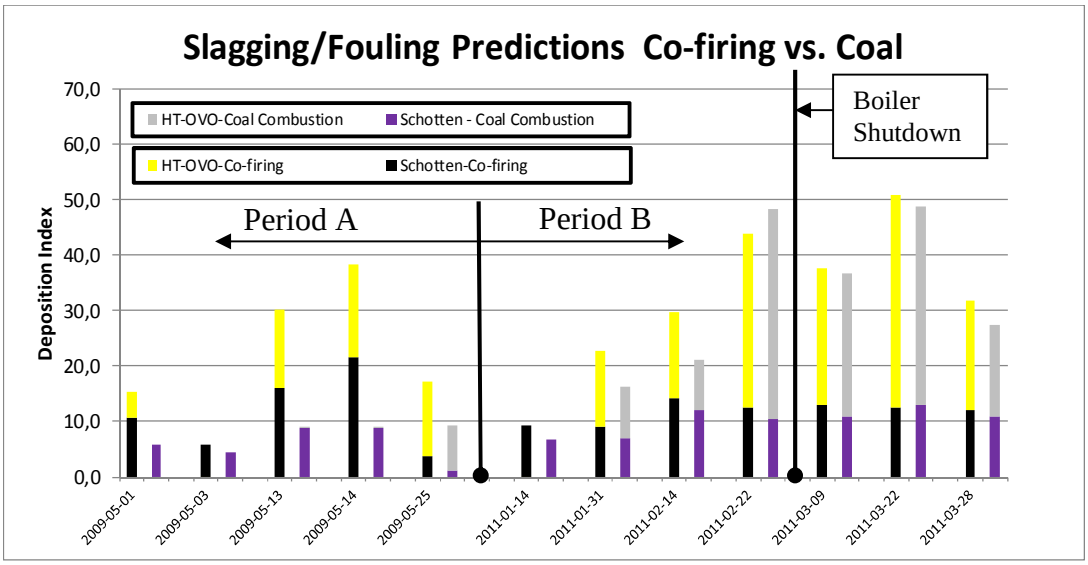

Figure 6-10. Comparison of the predicted slagging/fouling tendencies obtained for biomass co-firing and pure coal firing cases, related to the two investigated periods.

According to the predictions, it was noticed that the impact of biomass co-firing on increasing ash deposition was more significant in the first analysed "Period A" whereas the quality of coal in the second period ("Period B") affected dominantly the slagging/fouling performance. The predictions obtained corresponded well with the field observations, allowing the identification of the differences in deposition severity between the platen superheater and further heat transfer surface placed at the furnace outlet. This is especially visible for the cases when increased shares of Ca-rich biomass mix pellets were co-fired with coal during the Period A.

During the Period B, after 22/02/2011 the boiler shutdown was reported during which the heat transfer surfaces were cleaned. However, after this intervention the observed ash deposition severity quickly re-occurred, indicating a high slagging/fouling propensity of fired alkali rich coal blend in this period.

The performed analysis confirmed that for the assumptions made regarding the bulk ash composition simulation and behaviour of the more reactive biomass ash-forming elements (as discussed in more detail in section 6.5.2 – Chapter 6 and also in section 5.2.2.1 Chapter 5) relatively good first order predictions have been obtained for the investigated co-firing rates and biomass fuels considered.

6.5.4 Fuel Blend Optimisation when Co-firing up to 30wt% Biomass Share

The optimisation of the overall fuel blend composition to minimise slagging and fouling is a further objective of this work. It is aimed to find the safe operational fuel flexibility windows that allow the operation of boiler without severe slagging/fouling. Within the co-firing strategy of the MPP there is a drive to possibly increase co-firing rates of lower ash quality fuels in a total biomass mix whilst reducing co-firing percentages of less ash-troublesome but expensive wood pellets.

The optimisation process is performed with the aid of the same modelling approach as already presented and validated for the co-firing cases analysing in the previous subsections. The maximum co-firing rate in this study is considered to approach 30wt% for the biomass mix composed of the mixture of the meat and bone meal, wood pellets and biomass mix pellets enriched in calcium in the ash (the worst scenario).

The slagging and HT fouling predictions obtained for the three co-firing ratios: 10wt%, 20wt% and 30wt% in a blend with a good quality coal blend (as fired in the first mid of May 2009, Figure 6-9), are shown in the ternary diagrams in Figure 6-11. The severity of

slagging/fouling predictions was calibrated based on the field observations from the validation part of the model (section 6.5.3), and includes the joint index of the slagging severity of the platen superheater as well as the HT fouling severity assessment of the further heat exchange surfaces that enter the convective pass of the boiler. As already mentioned in a previous section, such calibrated indices did not include the effects of the ash burden on the ash deposition severity predictions as it has been found to be less relevant for the operating conditions of the MPP boilers co-fired with biomass shares below 20wt% coal substitutions, as discussed in the previous sub-section.

The low slagging/fouling fuel flexibility windows correspond to the blue areas in the ternary diagrams, the medium slagging/fouling fuel ratios go through the yellow shadows, and high to severe slagging/fouling is defined by red to dark coloured index isolines.

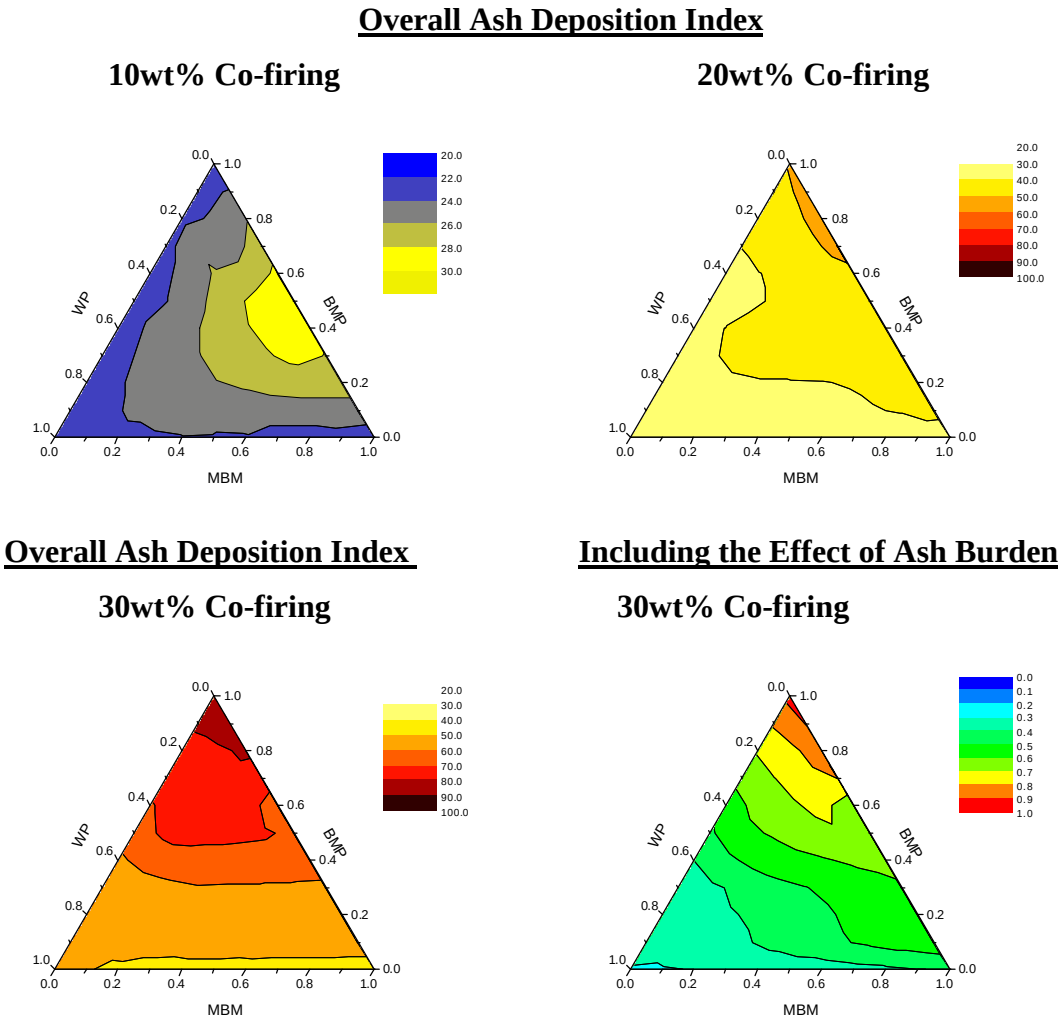

Figure 6-11. Predicted overall ash deposition index (for the Schotten and HT-OVO sections) when co-firing 10wt%, 20wt% and 30wt% biomass blend composed of the wood pellets (WP), meat and bone meal (MBM) and biomass mix pellets (BMP).

The obtained modelling results revealed highly non-linear trends of the predictions indicating different optimal fuel blending windows for the 10wt%, 20wt% and 30wt% coal substitutions.

As far as 10wt% co-firing rate is concerned, the overall (joint) ash deposition index was predicted to be the most severe for the biomass mix composed of the half mass of the BMP and MBM biomass fuels (0.5 BMP-0.5 MBM, yellow field in Figure 6-11). In this blend, the BMP was predicted to affect primarily slagging of the platen superheater whilst co-firing the MBM led to increased HT fouling of the next heat transfer sections. This has been already discussed in more detail when analysing predictions shown in Figure 6-8. Adding wood pellets clearly mitigates the ash deposition risk obtaining low slagging/fouling indications for the WP mass ratio which exceed 0.4 in biomass mix (blue shadow areas).

Increasing co-firing share to 20wt% coal substitutions led to the rise in the overall ash deposition index indicating medium severity. In biomass mix blend, the BMP revealed to have the highest impact on the ash deposition, followed by the MBM and WP.

For co-firing 30wt% of biomass mix considered, the fuel flexibility windows for the non-severe ash deposition conditions have been narrowed significantly, dominated by the effects from the high slagging BMP. Moreover, for such a relatively high co-firing rate of fuels whose individual ash contents differ considerably, the differences in the ash burden also affect the slagging/fouling severity. This is especially visible when predicting the impact of co-firing low ash content wood pellets within the investigated biomass mix. Although, based on the joint ash deposition index, the impact of MBM and WP was predicted to be comparable for the 30wt% co-firing case, the significantly higher ash content of MBM as compared with WP indicated higher slagging/fouling risk for MBM, as shown in Figure 6-11.

As far as the low temperature fouling is concerned, the alkalis remaining in the gas phase which were not captured by the alumino-silicate fly ash under the high temperature conditions at the furnace can form alkali salts able to condense during the flue gas cooling in a convective pass of boiler. The predicted (via the phase equilibrium model) alkali sulphates concentrations (as a sum of Na_2SO_4(s) and K_2SO_4(s)) in the flue gas downstream of the furnace obtained for the 30wt% co-firing ratio are shown in Figure 6-12a. Additionally, the overall efficiencies of the alkalis capture by the fly ash, predicted for the corresponded biomass mix ratios, are presented in the ternary diagram in Figure 6-12b.

30wt% Co-firing

a) **K_2SO_4(s) + Na_2SO_4(s), g/kg fuel** b) **Alkalis Capture Efficiency**

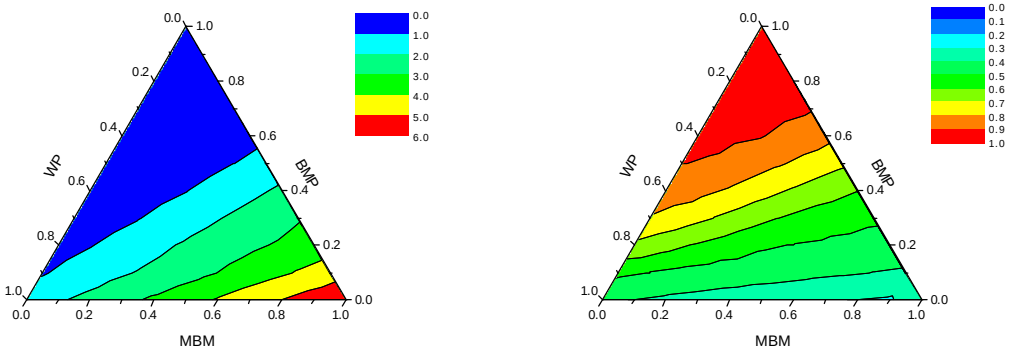

Figure 6-12. Predicted alkali sulphates concentrations (g/kg fuel) in the flue gas downstream the furnace when co-firing investigated fuel blends composed of the 30wt% of biomass mix.

The predictions showed that with increasing the MBM share in the 30wt% biomass mix the higher concentrations of the alkali sulphates in the flue gas occurred. This may result in a further deposition of the alkali salts aerosols on the tube banks in the convective pass of boiler and formation of a sticky deposit layer accelerating deposition of the non-molten ash particles. Regarding the predicted alkali capture efficiencies, the mixtures dominated by the BMP revealed the highest efficiency ratio which approached the unity for the 100% BMP share in the 30wt% co-firing blend. This was related to relatively high concentrations of alumino-silicates present in the BMP, originated mostly from bleaching clay.

6.6 Summary

In this Chapter a critical validation of the developed slagging and fouling predictive model has been attempted against the experimental observations derived from the industrial-scale pf coal-fired furnace and the large scale 518 MW_e pf boiler.

Various imported coals and their blends of different ash melting tendencies and ash content were analysed. The results obtained from the IFRF-ECN campaign showed that the assessed by the conventional indices slagging/fouling severity did not match the corresponding field observations. Performed within this thesis, more detailed modelling of the ash melting and slag viscosity changes revealed additional information that improved the understanding of the observed differences in the ash behaviour which led to a better predictions. It was proved that the ash deposition severity is proportional to the average slag ratio in the ash, ash burden as well as the slag viscosity at the reference (deposit surface) temperature.

The validation of the developed predictive methodology applied to the large scale pf boiler fired with coal/biomass blends gave also relatively good agreement. The ash deposition severity was predicted well for the platen superheater section and the other heat transfer surfaces entering convective pass of the analysed boiler. It was again confirmed that the coal ash quality has the crucial impact on reducing slagging/fouling when co-firing with biomass.

Furthermore, the model validation analysis revealed that the use of the bulk ash composition of coal ash, including blends as well as other related assumptions related with the behaviour of the more reactive biomass ash-forming elements were sufficient within the methodology to give reliable first order predictions for the investigated cases.

The fuel blend optimisation process was performed for the good quality coal blend co-fired with up to 30wt% of lower quality biomass mix composed of the mixture of the high alkalis content meat and bone meal, low ash-wood pellets, and biomass mix pellets enriched in organically associated calcium. The non-additive behaviour of the fuel blends has been identified. The performed modelling analysis showed that amongst the biomass considered, the BMP has the highest impact on slagging occurrence and gradually produces more severe HT fouling conditions when increasing biomass co-firing ratios. In case of co-firing the MBM dominated biomass blends, these influence primarily the HT fouling of the heat-transfer section placed at the entrance to the convective pass of the boiler: as well as this can lead to enhanced alkali salt aerosols formation able to condense downstream of the furnace. Ash deposition severity can be mitigated by co-firing wood pellets with coal, mostly due to its low ash content. However, with increasing co-firing share the impact of WP on the overall slagging and HT fouling tendency becomes more severe.

7

CONCLUSIONS

In this final Chapter, the summary of the conclusions obtained from this research work is presented. Some relevant recommendations are given for further research, highlighting the potential areas for improvements in the modelling methodology, which in the Author's opinion are of importance.

7.1 Overall Conclusions

The major focus of this research was to develop a reliable slagging and fouling predictive methodology which should enable in a relatively short time the optimisation of the complex coal/biomass fuel blends to minimise slagging and fouling as well as to assess the direct impact of the fuel quality on pulverised fuel fired boiler performance. Based on the literature review focused on the fuel ash behaviour, predictive methodologies and most importantly from the obtained findings regarding the development and model validation stages the following conclusions can be drawn:

Chapters 1 – Introduction, and Chapter 2 – Understanding slagging and fouling:

- Co-firing of a good ash quality biomass with coal in the existing pulverised fuel fired boilers is the most efficient, and cost-effective methodology for biomass utilisation towards reducing CO_2 emissions from the power generation sector.
- Currently, the Power Utilities are exploring new areas of utilising the variable quality, cheaper coal blends whilst increasing the biomass shares of different origin in a total blend to achieve more profitable operation, i.e. obtained from the biomass co-firing subsidies. Combustion of such fuel blends may lead to more severe slagging and fouling issues.
- Generally, for coals it is established that the increased iron and calcium contents in the ash lead to higher slagging whereas fouling is associated with the raised sodium levels in coal.
- As far as the biomass fuels are concerned, the most ash-troublesome biomass types are those enriched in potassium and silica, such as herbaceous biomass, but also phosphates rich solid biomass residues which decrease the melting temperatures of the ashes. Woody biomass, due to its generally low ash content and increased calcium presence, appears to be the best choice when considering large co-firing shares.
- Inertial impaction is a dominant mechanism of ash deposition during coal combustion when coarser fly ash particles are formed. When co-firing with biomass, the fraction of sub-micron ash and aerosols increases, and other ash deposition mechanisms such as condensation and diffusion become more important.

- Ash deposition cannot be completely avoided. The best way to minimise this operational problem when switching to fuel blends for which the boiler was not originally designed is to optimise the composition of the fuel mixture and ensure proper boiler operation. The use of fuel additives may be an additional option; however, increased operational costs occur depending upon the fuel quality and additive type used whose effects need to be still further investigated.

Chapter 3 – Review of slagging/fouling predictive methods:

- The slagging/fouling indices developed over the past half-century are mostly applicable and valid for specific coal groups and fail when used for the more complex coal and coal/biomass blends composed of the different ash chemistries.
- The standard ash fusion temperature test, which is still in use nowadays for assessing slagging/fouling propensities of the fuels, is widely criticised in the literature due to its subjective nature and large reported uncertainties. This led to more intensive development of other non-standard experimental methods; however they are not widely applied in practice.
- In the field of the slagging/fouling modelling, over the last few decades the combinations of various mechanistic and phase equilibrium based models have been developed. There have been a number of attempts made to incorporate these sub-models into the more compressive, but very time consuming 3D-CFD approaches. Less complex zone-based models, precursors of the CFD tools appear to be less investigated in the field of slagging/fouling, especially when coupled with the phase equilibrium models.
- Based on the various approaches reviewed, the integration of a one-dimensional zone based model capable to assess the heat transfer conditions throughout the pf boiler with the improved thermo-chemical phase equilibrium calculation algorithms to investigate the possible non-additive behaviour of blended fuel ashes was proposed.

Chapter 4 – Development of the improved one-dimensional thermal zone model for the pulverised fuel fired boilers:

- The Russian standard zone furnace model has been successfully improved by extending the zonal approach to the convective section of the boiler and including a steam cycle for performing a more comprehensive thermodynamic analysis of the

system. Moreover, more transparent formulas describing the effects of fireside deposition were incorporated into the model.

- The improved model is capable of predicting, for burning a wide quality of coal/biomass blends, the midsection temperature profile throughout the boiler, the heat fluxes inside the furnace, and the related boiler performance parameters, such as furnace/boiler efficiency and the parameters of the heating media.
- The performed sensitivity analysis of the model which was applied to the wall-fired 235 MW_e pf boiler revealed that co-firing of high moisture content biomass with coal can lead to lower heat absorption in the furnace and a relatively high flue gas volume produced. This resulted in the shifting of the heat transfer towards the convective section of the boiler. As a consequence lower steam flows were generated and steam overheating occurred which caused a drop in boiler efficiency. The increase in ash content to certain levels may result in improvements to the radiative heat transfer inside the furnace. Moreover, the resistivity and emissivity of the wall-ash-deposits revealed to have a relatively high influence on the predicted heat transfer characteristics of pf boiler furnace.
- To support input data into the predictive model it is proposed to combine it with the on-line monitoring system of the boiler, including additionally for instance heat flux sensors located on the furnace walls at different levels. These would improve the model predictions of the thermal performance and better identify when slagging conditions may occur in the furnace.

<u>Chapter 5 – Development of a slagging/fouling predictive approach based on the improved phase equilibrium calculation schemes:</u>

- The phase equilibrium-based algorithms adjusted to investigate the ash behaviour under pulverised fuel fired boiler conditions were successfully designed and integrated within the zone methodology.
- The developed predictive algorithms utilise three separate phase equilibrium schemes assigned to the modules in order to assess the ash deposition caused by the different mechanisms, such as slagging and HT fouling, condensation of salts and inorganics phenomena.

- The sensitivity analysis of the various ash deposition-related parameters and criteria were performed, indicating that the average slag ratio, the slag viscosity at the reference temperature of the deposit surface as well as ash burden are the most reliable parameters defining the slagging and high temperature fouling tendencies.
- The phase equilibrium interactions analysed between alumino-silicate fly ash and alkali metals in the gas phase, cause a viscosity decrease of the bulk ash slag, thus raising its stickiness which resulted in the overall increase of the ash deposition rate.

Stated research question: *How the quality of coal ash would affect the slagging and fouling when co-firing of coal with biomass?*

- The performed coal blends optimisation analysis revealed that the coal ash content and chemistry/mineralogy are of a great importance in understanding how to mitigate slagging and fouling when co-firing high alkali content biomass fuels, such as straw. The lowest ash deposition tendencies were projected were co-firing high alumino-silicate content coals with straw. The predicted ash behaviour tendencies for coal/straw blends were in good agreement with the reported experience found in the literature.

Chapter 6 – Validation of the developed predictive methodology:

Stated research question: *Is it possible to assess successfully the slagging/fouling tendencies of complex coal/biomass fuel blends with the aid of models based on the phase equilibrium analysis? How much detailed fuel data are required for such analysis?*

- The developed slagging and fouling predictive approach has been critically validated with the slagging/fouling observation data derived from the semi-industrial pf 2.5 MW_{th} coal-fired furnace and a large scale 618 MW_e pf boiler fired with various quality imported coals and complex biomass blends up to 20wt%.
- The obtained results revealed that the slagging/fouling tendencies of coal blends can be successfully assessed with the use of the developed predictive methodology. The bulk ash analysis data of coal blends are sufficient for obtaining the first order predictions.
- The developed methodology was capable of predicting ash deposition on the platen superheater as well as the surfaces belonging to the heat exchangers entering the convective pass of the boiler.

- The impact of co-firing good quality coal blends with the increased percentages of poor ash quality biomass (up to 20wt% coal substitution) was found to be comparable, or even lower in comparison with co-firing of poorer ash quality coals that contained increased sodium levels (above 1.5% in the ash).
- As far as co-firing more complex fuel blends of coal with biomass is concerned, more detailed speciation of the ash-forming elements in biomass fuels may be required to estimate their reactivity/interactions needed for the phase equilibrium calculations. Although, the current assumptions made for the investigated fuel blends have led to predictions which agreed quite well with the field observations. More experimental work is needed to improve understanding of interactions between coal and biomass inorganic species to support the developed phase equilibrium algorithms.

Chapter 6 – Optimisation of biomass mixture when co-firing with 30wt% coal substitution:

- Based on the previous validation of the model the optimisation of the coal/biomass blends were performed for a higher biomass co-firing share up to 30wt%.
- Ternary diagrams were used to display the predicted results and identify fuel flexibility windows when co-firing three different biomass type streams with coal, such as a high alkalis content meat and bone meal, low ash content wood pellets and enriched in calcium biomass mix pellets produced on site at the investigated power plant.
- The performed analysis identified highly slagging fuel mixtures which were dominated by the biomass mix pellets whereas a low temperature fouling was associated with co-firing the increased percentages of the meat and bone meal.

Appendix II – Slagging Prediction Tool – Software Development:

- The developed predictive methodology and algorithms has been integrated into a user-friendly software package, that additionally includes an extended fuel database for coals and biomass fuels (see Appendix II).
- The software is designed to allow the user to make a quick comparison of the predicted slagging/fouling indices and other thermodynamic parameters of the system obtained for a wide range of analysed fuel blends.

- The developed prediction tool can support the day-to-day decision making of managers and operators, to help remove much of the uncertainty associated with decisions related to fuel characteristics and operating procedures. Such a tool is most useful in determining the optimum fuel-blending strategies in order to avoid the elevated ash deposition in the boiler and ensure the most efficient boiler operation.

7.2 Recommendation for the Future Work

Zone-based model improvement:

- The impact of deposits chemistry and its physical properties on the deposit emissivity and radiative heat transfer in the furnace should be investigated. It is important; in particular, for the fireside deposits enriched in CaO, having a highly reflective nature. These deposits can originate from firing high calcium content coals, such as western U.S. Powder River Basin coal. A procedure to assess the impact of the ash chemistry on deposit emissivity, supported with derived proper correlations should be incorporated into the model.
- A more sophisticated fuel burn-out sub-model which takes into account time-temperature history of particles and physical properties of fuels could more accurately assess the impact of biomass co-firing on the boiler efficiency losses and the temperature change at the furnace outlet.
- The assessment of the residence time of particles in the individual boiler zones can be further investigated. Such an investigation for a one-dimensional furnace model was carried out by van der Lans [158]. Determining the residence time of particles can be helpful when incorporating the kinetics data of combusted fuel particles, or to assess the kinetics of transforming minerals/salts at high temperature zones of the boiler.
- The current 1D model could be potentially extended to the 2D geometry to obtain a more detailed gas temperature distribution within the furnace. In such case the flow pattern could be taken from CFD models.

Slagging/fouling predictive approach:

- The interaction kinetics between coal mineral matter (alumino-silicates) and biomass ash-forming elements, such as K, Ca, P under pf boiler conditions should be investigated in more detail. This would require more experimental investigations performed under well controlled conditions commensurate with that existing in pulverised fuel fired boilers.

- The incorporation of the P-based thermodynamic data into the phase equilibrium calculations could be better explored. The impact of phosphorous can be significant when burning materials such as agricultural/animal/domestic residues. Preliminary investigations in this field were carried out by Wu *et al.* [159].
- Regarding the ash formation models, the aerosols and sub-micron ash formation models which include the homogenous and heterogeneous condensation mechanisms adequate for biomass co-firing cases, could be potentially studied in more detail. This was partly investigated by Doshi *et al.* [81], and some algorithms based on the phase equilibrium calculations were proposed in this work.
- Considering the development of ash formation sub-models, the predictive methodology could be extended to include the fouling assessment in the high-dust DeNOx SCR catalyst region, in which sub-micron ash particles and aerosols play important roles in the masking and poisoning of the vanadium based SCR catalysts.
- In relation to the ash transport/deposition sub-models, besides the inertial impaction and condensation also other mechanisms such as thermophoresis and diffusion could be further investigated to be included within the methodology, i.e. following up the one-dimensional simplified approach proposed by Yan *et al.* [75], applicable for the furnace wall conditions.
- The impact of predicted ash deposition rates throughout the boiler on the parameters of the heating media, and boiler efficiency could be further assessed. However, this will require the investigation of reliable approaches allowing the assessment of the deposit resistivity which is correlated with the thickness and conductivity of the deposit layer under given thermal conditions. More details regarding such investigations can be found in ref. [92].
- The mechanisms involved in the corrosion caused by molten salts, chlorine/sulphur induced corrosion could be potentially further investigated with the aid of the phase equilibrium analysis, and derived algorithms incorporated into the predictive methodology.
- The deposit strength is often more important to boiler operation than the rate of deposition. During the operation of pulverised fuel boilers the deposits must not be highly sintered as otherwise removal by soot-blowing systems is difficult. The development of deposit strength is related to the presence of viscous liquid phases which accelerate the sintering process as well as the chemistry of the deposits (i.e.

highly sintered deposits are found to be enriched in sodium alumino-silicates). Some preliminary experimental and phase equilibrium modelling investigations have been done by the author, and published in a journal paper (see Appendix III) [60]. It is postulated that based on the phase equilibrium analysis, the strength of deposits can be assessed which could be further implemented within the developed methodology.

- The data and parameters derived from the phase equilibrium calculations parameters, such as the slag phase and viscosity distributions obtained for specific fuel blends, can be potentially correlated with the CFD-based algorithms to investigate the impact of 3D flow pattern details on slagging/fouling topography within the boiler.

Further validation of the predictive model:

- Although the developed predictive model has been validated for some more complex coal/biomass blends and the promising preliminary results have been obtained, a further more comprehensive validation is suggested. This should include a study of slagging/fouling observations gathered from longer operation of a boiler. Moreover, more objective, short-term trials including measurements of the ash deposition rates and heat fluxes in different boiler regions would be very helpful in further validation studies.
- During this PhD research work professional contacts have been established that have evolved into further model validation collaborative projects. These include a collaboration with the *Maasvlakte Power Plant* (E.ON Benelux, The Netherlands) for which the model has been already been successfully tested against some slagging/fouling observations. Further model evaluation could well continue via cooperation with the *Electric Power Research Institute* (EPRI, USA), which has expressed interest in model testing for various boiler configurations firing bituminous/sub-bituminous coal blends.

7.3 Outlook

Co-firing of coal with biomass is regarded as a short term measure towards reducing CO_2 emission from the power generation sector. However, in a longer time perspective firing biomass in dedicated high efficient power energy units of a small capacity is expected to play an important role. In large scale boilers, co-firing of coal/biomass blends in an oxidising

atmosphere with CO_2 recirculation and CO_2 sequestration is likely to be important in the future both for pf combustion and pressurised gasifiers.

Although the developed predictive model is aimed at assessing the slagging/fouling risk when co-firing biomass with coal in large pf utility boilers, it can be also potentially applied or further develop for other boiler types, or to investigate the impact of other process conditions on the ash deposition. These may include for example the study of the ash agglomeration and fouling in fluidised bed combustors or gasification systems when utilising biomass/waste fuels of lower quality.

Besides the generation of heat/energy from biomass, the utilisation of low rank coals which are of order 50% of the world's resources is expected to increase in forth-coming years or decades. Nowadays, e.g. in the USA the blending of bituminous coals with the poorer quality, cheaper PRB coals is very common. According to the US energy utilities experience, the assessment of slagging/fouling tendencies for such coal blends is very challenging due to the highly non-additive ash behaviour of these coals.

An application of the zone based furnace models to investigate the oxy-fuel combustion conditions on the heat transfer and boiler performance is another field that could be investigated, also in view of the impact of the enriched O_2/CO_2 atmosphere on slagging and fouling. Finally, the zone-based model can be also used as a design tool to determine the optimal furnace geometry and the heat-transfer surfaces arrangement to achieve the most efficient heat-transfer inside the furnace.

REFERENCES

[1] BP. (2012). BP Statistical Review of World Energy. Available at: www.bp.com/statisticalreview.

[2] IEA. (2012). Key World Energy Statistics

[3] Department of energy and climate change. [accessed September 2012]; Available from:http://www.decc.gov.uk/en/content/cms/meeting_energy/renewable_ener/renew_obs/renew_obs.aspx.

[4] Hansson, J., Berndes, G., Johnsson, F. and Kjärstad, J. (2009). Co-firing biomass with coal for electricity generation—An assessment of the potential in EU27. *Energy Policy* **37:**1444-1455.

[5] IEA-ETSAP and IRENA (2013). Biomass Co-firing-Technology Brief. Available at: www.irena.org/Publications.

[6] Hansen, L. A., Nielsen, H. P., Frandsen, F. J., Dam-Johansen, K., Hørlyck, S. and Karlsson, A. (2000). Influence of deposit formation on corrosion at a straw-fired boiler. *Fuel Processing Technology* **64:**189-209.

[7] Pedersen, L. S., Nielsen, H. P., Kiil, S., Hansen, L. A., Dam-Johansen, K., Kildsig, F., Christensen, J. *et al.* (1996). Full-scale co-firing of straw and coal. *Fuel* **75:**1584-1590.

[8] Wieck-Hansen, K., Overgaard, P. and Larsen, O. H. (2000). Cofiring coal and straw in a 150 MWe power boiler experiences. *Biomass and Bioenergy* **19:**395-409.

[9] Gibb, W. H. (1996). The UK Collaborative Research Programme on Slagging Pulverised Coal-Fired Boilers: Summary of Findings. In: Baxter, L. and DeSollar, R. (eds.) *Applications of Advanced Technology to Ash-Related Problems in Boilers*. Springer US, pp. 41-65.

[10] Raask, E. (1985). Mineral impurities in coal combustion : behaviour, problems, and remedial measures. Washington ; London: Hemisphere.

[11] Miles, T. R., Baxter, L. L., Bryers, R. W., Jenkins, B. M. and Oden, L. L. (1996). Alkali deposits found in biomass power plants. U.S. Department of Energy.

[12] Rayaprolu, K. (2013). Boilers - A practical reference. CRC Press. Taylor & Francis Group.

[13] Stultz S. C., Kitto J. B. (2005). Chapter 14 - Burners and combustion systems for pulverized coal, in Steam - its generation and use. 41st Edition. The Babcock & Wilcox Company.

[14] Piotrowska, P. (2012). Combustion properties of biomass residues rich in phosphorus. PhD Thesis, *Åbo Akademi University*.

[15] Frandsen, F., J. (2011). Ash Formation, Deposition and Corrosion When Utilizing Straw for Heat and Power Production. Doctoral Thesis, *Technical University of Denmark*.

[16] Couch, G. (1994). Understanding slagging and fouling in pf boilers. IEA-CCC Report.

[17] Barnes, I. (2009). Slagging and fouling in coal-fired boilers. London, UK.

[18] Bryers, R. W. (1996). Fireside slagging, fouling, and high-temperature corrosion of heat-transfer surface due to impurities in steam-raising fuels. *Progress in Energy and Combustion Science* **22:**29-120.

[19] Hatt, R. M. (1990). Fireside deposits in coal-fired utility boilers. *Progress in Energy and Combustion Science* **16:**235-241.

[20] Reinartz, E. (2006). Technical and economic analysis of supercritical pf plant suitable for Greek lignite. RWE Power International.

[21] Kefa, C. and Jestin, L. (2000). Boilers and burners. New York: Springer, p. 563.

[22] Spliethoff, H. and al, e. (2013). Intelligent monitoring and selective cleaning control of deposits in pulverised coal boilers. Luxembourg: Publications Office of the European Union.

[23] Stach, E., Mackowsky, M.-T., Teichmuller, M., Taylor, G. H., Chandra, D. and Teichmuller, R. (1982). Stach's textbook of coal petrology. Berlin-Stuttgart, p. 535.

[24] Barratt, D. J. and Roberts, P. T. (1991). Coal quality and combustion performance. Amsterdam: Elsevier, p. 638.

[25] IFRF Online Combustion Handbook, Type of ash-forming elements association in solid fuels. Available at: www.handbook.ifrf.net

[26] Van Loo, S. and Koppejan, J. (2008). The handbook of biomass combustion and co-firing. London: Earthscan, p. 442.

[27] Livingston, W. R. (2005). A review of the recent experience in Britain with the co-firing of biomass with coal in large pulverised coal-fired boilers. itsui Babcock, Renfrew, Scotland, Presented at IEA EXco Workshop on Biomass Co-firing, Copenhagen.

[28] Burvall, J. (1997). Influence of harvest time and soil type on fuel quality in reed canary grass (Phalaris arundinacea L.). *Biomass and Bioenergy* **12:**149-154.

[29] Lewandowski, I. and Heinz, A. (2003). Delayed harvest of miscanthus—influences on biomass quantity and quality and environmental impacts of energy production. *European Journal of Agronomy* **19:**45-63.

[30] Beck, J., Brandenstein, J., Unterberger, S. and Hein, K. R. G. (2004). Effects of sewage sludge and meat and bone meal Co-combustion on SCR catalysts. *Applied Catalysis B: Environmental* **49:**15-25.

[31] Zhang, L., Ito, M., Sato, A., Ninomiya, Y., Sakano, T., Kanaoka, C. and Masui, M. (2004). Combustibility of dried sewage sludge and its mineral transformation at different oxygen content in drop tube furnace. *Fuel Processing Technology* **85:**983-1011.

[32] Benson, S. A., Jones, M. L. and Harb, J. N. (1993b). Ash Formation and Deposition. In: Smoot, L.D. (ed.) *Fundamentals of Coal Combustion for Clean and Efficient Use;*. Elsevier: New York, pp. 299-373.

[33] Zevenhoven, M., Yrjas, P. and Hupa, M. (2010). Ash-Forming Matter and Ash-Related Problems.*Handbook of Combustion*. Wiley-VCH Verlag GmbH & Co. KGaA.

[34] Werkelin, J., Skrifvars, B.-J., Zevenhoven, M., Holmbom, B. and Hupa, M. (2010). Chemical forms of ash-forming elements in woody biomass fuels. *Fuel* **89:**481-493.

[35] Gupta, R. P., Wall, T. F., Kajigaya, I., Miyamae, S. and Tsumita, Y. (1998). Computer-controlled scanning electron microscopy of minerals in coal—Implications for ash deposition. *Progress in Energy and Combustion Science* **24:**523-543.

[36] Ferens, W. (2005). Zachowanie się substancji mineralnej w czasie spalania paliw stałych (Mineral matter behaviour during combustion of solid fuels). Wroclaw Univeristy of Technology. Report No 23/2005.

[37] Mechel. (2010). Coal and coal concentrate. Iron ore concentrate. Coke, coking products and coke breeze. *Russian Sibirginsky TKO, p.27*.

[38] Singer, J. G. (1991). Combustion Fossil Power - A reference book on fuel burning and steam generation. Fourth Edition ed. Combustion Engineering, INC.

[39] BCURA. The BCURA Coal Sample Bank: A Users Handbook.

[40] Savat, P. (2002). Trends in the combustion of substitute fuels. Laborelec. In: *TOTeM 22. Combustion trends for power generation industries.* Laborelec, Linkebeek, Belgium.

[41] Vuthaluru, H. B. and French, D. (2008). Ash chemistry and mineralogy of an Indonesian coal during combustion: Part II — Pilot scale observations. *Fuel Processing Technology* **89:**608-621.

[42] Wigley, F., Williamson, J. and Riley, G. (2007). The effect of mineral additions on coal ash deposition. *Fuel Processing Technology* **88:**1010-1016.

[43] Grammelis, P. and Karampinis, E. (2011). Co-combustion trials at Kardia TPS. In: *BIOCLUS Int. Workshop "Energy crops and their co-firing potential"*. Ptolemaida, Greece.

[44] Laursen, K. and Frandsen, F. (2002). Classification System for Ash Deposits Based on Sem analyses. In: Gupta, R.P. and Wall, T.F. and Baxter, L. (eds.) *Impact of Mineral Impurities in Solid Fuel Combustion*. Springer US, pp. 205-216.

[45] Wigley, F. and Riley, G. (2008). Coal-biomass ash deposition during deeply-staged combustion. Final report for BCURA - B78.

[46] Andersen, K. H., Frandsen, F. J., Hansen, P. F. B., Wieck-Hansen, K., Rasmussen, I., Overgaard, P. and Dam-Johansen, K. (2000). Deposit Formation in a 150 MWe Utility PF-Boiler during Co-combustion of Coal and Straw. *Energy & Fuels* **14:**765-780.

[47] ECN. *Phylis2 fuel database*. Available from: http://www.ecn.nl/phyllis2/Biomass/View/1303.

[48] Plaza, P. (2007). Prognozowanie zagrożeń związanych żużlowaniem, popieleniem i aglomeracją popiołów w paleniskach kotłów energetycznych użytkujących paliwa węglowe i biopaliwa stałe (Predicting slagging, fouling and bed agglomeration of coals and biomass fuels fired in utility boilers). Wroclaw, Poland: Wroclaw University of Technology, Poland.

[49] Kupka, T., Mancini, M., Irmer, M. and Weber, R. (2008). Investigation of ash deposit formation during co-firing of coal with sewage sludge, saw-dust and refuse derived fuel. *Fuel* **87:**2824-2837.

[50] Biomass conversion of coal plant. (2011). Committee on Climate Change. Mott MacDonald: UK.

[51] Sarofim, A. F. and Helble, J. J. eds. (1994). *Mechanisms of ash and deposit formation*. The Impact of ash deposition on coal fired plant. Engineering Foundation Conference. Taylor & Francis.

[52] McLennan, A. R., Bryant, G. W., Bailey, C. W., Stanmore, B. R. and Wall, T. F. (2000). An Experimental Comparison of the Ash Formed from Coals Containing Pyrite and Siderite Mineral in Oxidizing and Reducing Conditions. *Energy & Fuels* **14:**308-315.

[53] Frandsen, F. J. (1998). Fly ash and deposit chemistry, in *Performance prediction in advanced coal fired boilers*. Demark University of Technology.

[54] Rees-Gralton, T.M. (2007). *The development of a prediction tool for utility boiler performance*. 2007, PhD thesis, *Cardiff Univeristy*.

[55] Aho, M., Vainikka, P., Taipale, R. and Yrjas, P. (2008). Effective new chemicals to prevent corrosion due to chlorine in power plant superheaters. *Fuel* **87:**647-654.

[56] Wall, T. F., Creelman, R. A., Gupta, R. P., Gupta, S. K., Coin, C. and Lowe, A. (1998). Coal ash fusion temperatures—New characterization techniques, and implications for slagging and fouling. *Progress in Energy and Combustion Science* **24:**345-353.

[57] López, C., S, Unterberger, S., Maier, J. and Hein, K. R. G. (May 18-22, 2003). Overview of Actual Methods for Characterization of Ash Deposition. In: *ECI Conference on Heat Exchanger Fouling and Cleaning: Fundamentals and Applications.* Santa Fe, New Mexico, USA.

[58] Hansen, L. A., Frandsen, F. J., Dam-Johansen, K., Sørensen, H. S. and Skrifvars, B.-J. (1999). Characterization of Ashes and Deposits from High-Temperature Coal−Straw Co-Firing. *Energy & Fuels* **13:**803-816.

[59] Kahraman, H., Bos, F., Reifenstein, A. and Coin, C. D. A. (1998). Application of a new ash fusion test to Theodore coals. *Fuel* **77:**1005-1011.

[60] Plaza, P., Ferens, W., Griffiths, A., J, Syred, N. and Rybak, W. (2010a). Predicting slagging/fouling propensities of solid fuels with the aid of experimental and modelling techniques. *Archivum Combustionis* **30:**10.

[61] Frenkel, J. (1945). Viscous flow of crystalline bodies under the action of surface tension. *Journal of Physics (Moscow)* **9:**7.

[62] Skrifvars, B.-J., Backman, R. and Hupa, M. (1998). Characterization of the sintering tendency of ten biomass ashes in FBC conditions by a laboratory test and by phase equilibrium calculations. *Fuel Processing Technology* **56:**55-67.

[63] Skrifvars, B. J., Öhman, M., Nordin, A. and Hupa, M. (1999). Predicting Bed Agglomeration Tendencies for Biomass Fuels Fired in FBC Boilers: A Comparison of Three Different Prediction Methods. *Energy & Fuels* **13:**359-363.

[64] Wall , T. F., Gupta, S., Gupta, R., Bryant, G., Elliott, L., Al-Otoom, A. and Browning, G. (2000). Ash formation, fusibility, deposit formation: Predictive techniques for utility boilers. IFRF 15th ToTEM Meeting, Technical Univeristy of Denmark, Denmark.

[65] Zelkowski, J. (2004). Kohlecharakterisierung und Kohleverbrennung. Essen: VGB PowerTech. Service GmbH.

[66] Attig, R. C. and Duzy, A. F. eds. (1969). *Coal ash deposition studies and application to boiler design*. American Power Conference.

[67] Winegartner, E. C. (1974). Coal Fouling and slagging parameters.

[68] Benson, S. A., Hurley, J. P., Zygarlicke, C. J., Steadman, E. N. and Erickson, T. A. (1993a). Predicting ash behavior in utility boilers. *Energy & Fuels* **7:**746-754.

[69] Korbee, R., Eenkhoorn, S., Heere, P. G. T., Visser, H. J. M., Comans, R. N. J. and Kiel, J. H. A. (October 1999a). Combustion characteristics of low quality battle coals – Mineral matter transformations. ECN, The Netherlands.

[70] Robinson, A. L., Junker, H. and Baxter, L. L. (2002). Pilot-Scale Investigation of the Influence of Coal−Biomass Cofiring on Ash Deposition. *Energy & Fuels* **16:**343-355.

[71] Krause, H. H. (1986). High temperature corrosion problems in waste incineration systems. *Journal of Materials for Energy Systems* **7:**322-332.

[72] Becidan, M., Houshfar, E., Khalil, R. A., Skreiberg, Ø., Løvås, T. and Sørum, L. (2011). Optimal Mixtures To Reduce the Formation of Corrosive Compounds during Straw Combustion: A Thermodynamic Analysis. *Energy & Fuels* **25:**3223-3234.

[73] Beer, J. M., Sarofim, A. F. and Barta, L. E. (1992). From coal mineral properties to fly ash deposition tendencies. In: Benson, S.A. (ed.) *Inorganic Transformations and Ash Deposition During Combustion*. Engineering Foundation Press.

[74] Wilemski, G., Srinivasachar, S. and Sarofim, A. F. (1992). Modeling of mineral matter redistribution and ash formation in pulverized coal combustion. In: Benson, S.A. (ed.) *Inorganic Transformations and Ash Deposition During Combustion*. Engineering Foundation Press.

[75] Yan, L., Gupta, R. P. and Wall, T. F. (2001). The implication of mineral coalescence behaviour on ash formation and ash deposition during pulverised coal combustion. *Fuel* **80:**1333-1340.

[76] Yan, L., Gupta, R. P. and Wall, T. F. (2002). A mathematical model of ash formation during pulverized coal combustion. *Fuel* **81:**337-344.

[77] Monroe, L. S. (1989). An experimental and modeling study of residual fly ash formation in combustion of a bituminous coal. PhD Thesis, Massachusetts Institute of Technology, USA.

[78] Yamashita, T. ed. (2002). *Modeling of ash formation, deposition and sintering behavior in entrained-bed coal gasification*. 12th Annual Conference on Clean Coal Technology. Japan Coal Energy Center. Tokyo, Japan.

[79] Christensen, K. A., Stenholm, M. and Livbjerg, H. (1998). The formation of submicron aerosol particles, HCl and SO2 in straw-fired boilers. *Journal of Aerosol Science* **29:**421-444.

[80] Christensen, K. A. and Livbjerg, H. (2000). A Plug Flow Model for Chemical Reactions and Aerosol Nucleation and Growth in an Alkali-Containing Flue Gas. *Aerosol Science and Technology* **33:**470-489.

[81] Doshi, V., Vuthaluru, H. B., Korbee, R. and Kiel, J. H. A. (2009). Development of a modeling approach to predict ash formation during co-firing of coal and biomass. *Fuel Processing Technology* **90:**1148-1156.

[82] Baxter, L. L. and DeSollar, R. W. (1993). A mechanistic description of ash deposition during pulverized coal combustion: predictions compared with observations. *Fuel* **72:**1411-1418.

[83] Zhou, H., Jensen, P. A. and Frandsen, F. J. (2007). Dynamic mechanistic model of superheater deposit growth and shedding in a biomass fired grate boiler. *Fuel* **86:**1519-1533.

[84] Tomeczek, J., Palugniok, H. and Ochman, J. (2004). Modelling of deposits formation on heating tubes in pulverized coal boilers. *Fuel* **83:**213-221.

[85] Baxter, L. (2000). Quantitative description of ash deposit formation in boilers. Review. In: *TOTeM 15. Ash and Deposit Formation in Utility Boilers*. Technical University of Denmark, Denmark.

[86] Rosner, D., E. (1986). Transport processes in chemically reacting flow systems. Boston: Butterworths, p. 540.

[87] Pronobis, M. (2009). Modernizacja Kotłów Energetycznych (Modernisation of Utility Boilers). p. 362.

[88] Wibberley, L. J. and Wall, T. F. (1982). Alkali-ash reactions and deposit formation in pulverized-coal-fired boilers: experimental aspects of sodium silicate formation and the formation of deposits. *Fuel* **61:**93-99.

[89] Lee, B. E., Fletcher, C. A. J., Shin, S. H. and Kwon, S. B. (2002). Computational study of fouling deposit due to surface-coated particles in coal-fired power utility boilers. *Fuel* **81:**2001-2008.

[90] Degereji, M. U., Ingham, D. B., Ma, L., Pourkashanian, M. and Williams, A. (2012). Prediction of ash slagging propensity in a pulverized coal combustion furnace. *Fuel* **101:**171-178.

[91] Hansen, L. (1998). Melting and sintering of ashes. Thesis PhD, Department of Chemical Engineering, Technical University of Denmark.

[92] Richards, G. H., Slater, P. N. and Harb, J. N. (1993). Simulation of ash deposit growth in a pulverized coal-fired pilot scale reactor. *Energy & Fuels* **7:**774-781.

[93] Huang, L. Y., Norman, J. S., Pourkashanian, M. and Williams, A. (1996). Prediction of ash deposition on superheater tubes from pulverized coal combustion. *Fuel* **75:**271-279.

[94] Kær, S. K., Rosendahl, L. A. and Baxter, L. L. (2006). Towards a CFD-based mechanistic deposit formation model for straw-fired boilers. *Fuel* **85:**833-848.

[95] Wood, N. B. (1981). The mass transfer of particles and acid vapour to cooled surfaces. *Journal Institute of Energy* **76:**8.

[96] Im, K. H. and Chung, P. M. (1983). Particulate deposition from turbulent parallel streams. *AIChE Journal* **29:**498-505.

[97] Mueller, C., Selenius, M., Theis, M., Skrifvars, B.-J., Backman, R., Hupa, M. and Tran, H. (2005). Deposition behaviour of molten alkali-rich fly ashes—development of a submodel for CFD applications. *Proceedings of the Combustion Institute* **30:**2991-2998.

[98] Zbogar, A., Frandsen, F. J., Jensen, P. A. and Glarborg, P. (2005). Heat transfer in ash deposits: A modelling tool-box. *Progress in Energy and Combustion Science* **31:**371-421.

[99] Zygarlicke, C. J., McCollor, D. P. and Crocker, C. R. (1999). Task 3.2. - Ash emissivity characterization and prediction. Energy & Environmental Research Center, Univeristy of North Dakota.

[100] Smith, J. M., Abbott, M. M. and Ness, H. C. (2001). Introduction to chemical engineering thermodynamics. McGraw-Hill, 6 ed. Boston.

[101] Koukkari, P. and Pajarre, R. (2011). A Gibbs energy minimization method for constrained and partial equilibria. *Pure and Applied Chemistry* **83:**12.

[102] Bale, C. W., Bélisle, E., Chartrand, P., Decterov, S. A., Eriksson, G., Hack, K., Jung, I. H. *et al.* (2009). FactSage thermochemical software and databases — recent developments. *Calphad* **33:**295-311.

[103] Nutalapati, D., Gupta, R., Moghtaderi, B. and Wall, T. F. (2007). Assessing slagging and fouling during biomass combustion: A thermodynamic approach allowing for alkali/ash reactions. *Fuel Processing Technology* **88:**1044-1052.

[104] Tortosa Masiá, A. A., Buhre, B. J. P., Gupta, R. P. and Wall, T. F. (2007). Characterising ash of biomass and waste. *Fuel Processing Technology* **88:**1071-1081.

[105] Zevenhoven-Onderwater, M., Blomquist, J. P., Skrifvars, B. J., Backman, R. and Hupa, M. (2000). The prediction of behaviour of ashes from five different solid fuels in fluidised bed combustion. *Fuel* **79:**1353-1361.

[106] Zevenhoven-Onderwater, M., Backman, R., Skrifvars, B.-J. and Hupa, M. (2001). The ash chemistry in fluidised bed gasification of biomass fuels. Part I: predicting the chemistry of melting ashes and ash–bed material interaction. *Fuel* **80:**1489-1502.

[107] Tucker, R. J. (1991). Modelling of gas-fired furnaces and boilers. London: British Gas, p. 444.

[108] Hottel, H. C. and Sarofim, A. F. (1967). Radiative transfer. New York ; London: McGraw-Hill, pp. 520.

[109] Díez, L. I., Cortés, C. and Campo, A. (2005). Modelling of pulverized coal boilers: review and validation of on-line simulation techniques. *Applied Thermal Engineering* **25:**1516-1533.

[110] Blokh, A. G. and Viskanta, R. (1988). Heat transfer in steam boiler furnaces. Washington: Hemisphere Pub. Corp, pp. 283.

[111] Lawson, D. A. and Ziesler, C. D. (1996). An accurate program for radiation modelling in the design of high-temperature furnaces. *IMA Journal of Mathematics Applied in Business & Industry* **7:**8.

[112] Kouznetsov, N. V., Mitor, V. V., Dubovsky, I. E. and Karasina, E. S. (1973). Thermal calculation of steam boilers: Normative Method [in Russian]. Moscow: *Energiya*.

[113] Tucker, R. J., Ward, J., Chong, A. and Tan, C. K. (2009). Developments in the Application of ZONE Modelling for furnace efficiency improvements. Presentation. In: *British-French Flame Joint Meeting.* Lille, France.

[114] Lowe, A., Wall, T. F. and Stewart, I. M. (1975). A zoned heat transfer model of a large tangentially fired pulverized coal boiler. *Symposium (International) on Combustion* **15:**1261-1270.

[115] Richter, W., Payne, R. and Heap, M. P. (1986). Influence of Thermal Properties of Wall Deposits on Performance of Pulverized Fuel Fired Boiler Combustion

Chambers.*Mineral Matter and Ash in Coal*. Vol. 301. American Chemical Society, pp. 375-393.

[116] Blokh, A. G., Zhuravlev, Y. A. and Tinkova, S. M. (1992). An analysis of radiant heat transfer in furnace chambers burning slagging coals. *International Journal of Heat and Mass Transfer* **35:**2849-2853.

[117] Hesselmann, G. (1998). Modelling of pulverised coal fired furnaces with advanced combustion system by integrated performance programs. Mitsui Babcock Energy Limited, Renfrew, Scotland.

[118] Karasina, E. S., Livshits, B. N., Chudnovskii, B. R. and Talanker, A. E. (2010). Experience gained from using a computer program implementing the 3D zone-wise method for calculating heat transfer in the furnace chambers of the coal-fired boilers of 350- and 575-MW power units. *Thermal Engineering* **57:**897-900.

[119] Kouprianov, V. I. (2001). Modeling of thermal characteristics for a furnace of a 500 MW boiler fired with high-ash coal. *Energy* **26:**839-853.

[120] Alekhnovich, A. N. (2007). The thermal efficiency factor of furnace waterwalls as applied to the standard method for thermal calculation of boilers. *Thermal Engineering* **54:**698-704.

[121] Wang, H. and Harb, J. N. (1997). Modeling of ash deposition in large-scale combustion facilities burning pulverized coal. *Progress in Energy and Combustion Science* **23:**267-282.

[122] Fan, J. R., Zha, X. D., Sun, P. and Cen, K. F. (2001). Simulation of ash deposit in a pulverized coal-fired boiler. *Fuel* **80:**645-654.

[123] Tomeczek, J. and Wacławiak, K. (2009). Two-dimensional modelling of deposits formation on platen superheaters in pulverized coal boilers. *Fuel* **88:**1466-1471.

[124] Lee, F. C. C. and Lockwood, F. C. (1998). Modelling ash deposition in pulverized coal-fired applications. *Progress in Energy and Combustion Science* **25:**117-132.

[125] Ma, Z., Iman, F., Lu, P., Sears, R., Kong, L., Rokanuzzaman, A. S., McCollor, D. P. (2007). A comprehensive slagging and fouling prediction tool for coal-fired boilers and its validation/application. *Fuel Processing Technology* **88:**1035-1043.

[126] Losurdo, M., Spliethoff, H. and Kiel, J. (2012). Ash deposition modeling using a visco-elastic approach. *Fuel* **102:**145-155.

[127] Stam, A. F., Livingston, W. R., Cremers, M. F. G. and Brem, G. (2010). Review of models and tools for slagging and fouling prediction for biomass co-combustion. IEA Bioenergy Task 32: Biomass Combustion and Cofiring.

[128] Tran, H., N, Mao, X., Kuhn, D. C. S., Backman, R. and Hupa, M. (2002). The sticky temperature of recovery boiler fireside deposits. *Pulp & Paper-Canada* **103:**5.

[129] Su, S. H. I., Pohl, J. H., Holcombe, D. O. N. and Hart, J. A. (2001). A Comparison of Thermal Condition between Pilot- and Full-Scale Furnaces for Studying Slagging and Fouling Propensity in PF Boilers. *Combustion Science and Technology* **165:**129-150.

[130] Richter, W. (1985). Scale-up and advanced performance analysis of boiler combustion chambers. Winter Annual Meeting. Florida.

[131] Xu, M., He, X., Azevedo, J. L. T. and Carvalho, M. G. (2002). An advanced model to assess fouling and slagging in coal fired boilers. *International Journal of Energy Research* **26:**16.

[132] Kruczek, S. (2001). Boilers – Construction and Calculations [in Polish]. Wrocław, Poland: Oficyna Wydawnicza Politechniki Wrocławskiej.

[133] Plaza, P., Griffiths, A. J., Syred, N. and Rees-Gralton, T. (2009). Use of a Predictive Model for the Impact of Cofiring Coal/Biomass Blends on Slagging and Fouling Propensity†. *Energy & Fuels* **23:**3437-3445.

[134] Taler, J., Trojan, M. and Taler, D. eds. (2009). *Assessment of ash fouling and slagging in coal fired utility boilers*. *International Conference on Heat Exchanger Fouling and Cleaning VII.* Austria.

[135] Kakac, S. (1991). Boilers, evaporators, and condensers. New York: Wiley, p. 835.

[136] Pronobis, M. (2006). The influence of biomass co-combustion on boiler fouling and efficiency. *Fuel* **85:**474-480.

[137] Grammelis, P., Skodras, G. and Kakaras, E. (2006). Effects of biomass co-firing with coal on ash properties. Part I: Characterisation and PSD. *Fuel* **85:**2310-2315.

[138] Lester, E., Snape, C. and Malmgren, A. (2007). The effect of biomass on PF combustion efficiency and ash during coal/biomass co-combustion. The University of Nottingham and RWEnpower, UK.

[139] Lagerlo Boiler operational data pack, Laborelec. (2002).

[140] van Ormelingen, J. J., Jensen-Holm, H. and Hvid, S. L. (2003). *Experience from erection and operation of two SCR denitrification units at Electrabel's Langerlo Power Station*. Combined Power Plant Air Pollutant Control MEGA Symposium. Washington, USA.

[141] van Ormelingen, J., Berreth, A. and Risio, B. (2001). *CFD-study of a 235 MW_e coal fired boiler to predict the influence of secondary fuels on slagging, fouling, CO corrosion and NOx formation*. In. *IJmuiden, The Netherlands.*

[142] Risio, B. (2008). Modelling of deposit formation for pulverized fuel boilers. In: *15th DVV Colloquium & TOTeM 32.* Freising, Germany.

[143] Williams, A., Hampartsoumian, E., Hainsworth, D. and Taylor, J. M. (2001). *The radiant emissivity of some materials at high temperatures, review*. *Journal of the Institute of Energy* **74**:9.

[144] Akiyama, K., Pak, H., Tada, T., Ueki, Y., Yoshiie, R. and Naruse, I. (2010). Ash Deposition Behavior of Upgraded Brown Coal and Bituminous Coal. *Energy & Fuels* **24:**4138-4143.

[145] Laursen, K., Frandsen, F. and Larsen, O. H. (1998). Ash Deposition Trials at Three Power Stations in Denmark. *Energy & Fuels* **12:**429-442.

[146] Sander, B. and Wieck-Hansen, K. (October 17-21, 2005). Full-scale investigations on alkali chemistry and ash utlization by co-firing of straw. In: *14th European Biomass Conference and Exhibition.* Paris, France.

[147] Petersen, S., Hack, K., Monheim, P. and Pickartz, U. (2007). SimuSage – the component library for process modeling and its applications. *International Journal of Materials Research* **98:**8.

[148] van Dyk, J. C., Waanders, F. B., Benson, S. A., Laumb, M. L. and Hack, K. (2009). Viscosity predictions of the slag composition of gasified coal, utilizing FactSage equilibrium modelling. *Fuel* **88:**67-74.

[149] Senior, C. L. and Srinivasachar, S. (1995). Viscosity of Ash Particles in Combustion Systems for Prediction of Particle Sticking. *Energy & Fuels* **9:**277-283.

[150] Walsh, P. M., Sayre, A. N., Loehden, D. O., Monroe, L. S., Beér, J. M. and Sarofim, A. F. (1990). Deposition of bituminous coal ash on an isolated heat exchanger tube: Effects of coal properties on deposit growth. *Progress in Energy and Combustion Science* **16:**327-345.

[151] Baxter, L. L. (1993). Ash deposition during biomass and coal combustion: A mechanistic approach. *Biomass and Bioenergy* **4:**85-102.

[152] Floris, F., Pasini, S., Partesotti, C. and Quattroni, G. (1988). A Laboratory-scale furnace to study ash deposition and fouling due to pulverized Coal combustion. In: *American Flame Research Committee.* Pittsburgh, Pennsylvania.

[153] Plaza, P., Syred, N. and Griffiths, A., J. (2010b). Slagging and fouling prediction tool for large utility pulverized fuel co-fired boilers. *Archives of Energetics* **40:**9.

[154] Plaza, P. and de Jong, W. (November 2012). Direct impact of co-firing of biomass with coal on catalytic SCR DeNOx performance at the Maasvlakte Power Station – Energy from Biomass Project-Phase 1. Delft University of Technology, The Netherlands.

[155] Plaza, P., de Jong, W. and de Vries, H. (September 2013). Strictly Confidential Report on Analysis of Slagging and Fouling Data of Maasvlakte Power Plant - Unit 1. Delft University of Technology, The Netherlands.

[156] Schmitt, M. (31.08.2012). CFD results of Maasvlakte Boiler - presentation. Maasvlakte Power Station: DNV KEMA, E.ON Benelux.

[157] Senneca, O. (2008). Characterisation of meat and bone mill for coal co-firing. *Fuel* **87:**3262-3270.

[158] van der Lans, R. P., Glarborg, P., Dam-Johansen, K., Knudsen, P., Hesselmann, G. and Hepburn, P. (1998). Influence of coal quality on combustion performance. *Fuel* **77:**1317-1328.

[159] Wu, H., Castro, M., Jensen, P. A., Frandsen, F. J., Glarborg, P., Dam-Johansen, K., Røkke, M. *et al.* (2011). Release and Transformation of Inorganic Elements in Combustion of a High-Phosphorus Fuel. *Energy & Fuels* **25:**2874-2886.

APPENDICES

Nomenclature

a	emissivity weighting factor	-
A	area	m^2
b	weighting factors	
E	depth	m
El	chemical element	-
h	enthalpy	kJ/kg
H	height	m
L	effective thickness of the radiating gas layer	m^2
LHV	low heating value	kJ/kg
M	mass of component per kg fuel	kg/kg
$\dot{M}$	mass stream	kg/s
n	fraction	-
p	sum of partial pressures	-
R	thermal resistance	m^2K/W
S	width	m
t, T	temperature	^oC, K
W	moisture	%
V	volume of the component per kg fuel	Nm3/kg
Vc	average specific heat of the flue gas	$kJ/(kg^oC)$
α	convective heat transfer coefficient	W/m^2K
β	fuel burnout fraction	-
ε	emissivity	-
λ	air excess ratio	-
μ	viscosity	Pa*s
ρ	density	kg/m3
ψ	thermal efficiency factor	-

Subscripts

a	parent fuel	-
b	substitute fuel	-
c	blend	-
d	deposit	-
EM	emitted	-
fa	fly ash in the flue gas stream	-
FG	flue gas	-
p	constant pressure	-

Superscripts

ar	as received	-
in	inlet	-
mass	mass	-
mol	mole	-
out	outlet	-
th	thermal	-
0	theoretical (stoichiometric)	-

Appendix I – Basic Calculations

I-1. Fuel Blend

Mass ratio of the parent fuel in the fuel blend:

$$n_a^{mass} = \frac{\dot{M}_a}{\dot{M}_a + \dot{M}_b} \tag{I-1}$$

Thermal ratio of the parent fuel:

$$n_a^{th} = \frac{\dot{M}_a \cdot \mathrm{LHV}_a^{ar}}{\dot{M}_a \cdot \mathrm{LHV}_a^{ar} + \dot{M}_b \cdot \mathrm{LHV}_b^{ar}} \tag{I-2}$$

Low heating value is assessed by using the Mendelejew's formula:

$$\mathrm{LHV}_i^{ar} = 339.15 \cdot \mathrm{C}^{ar} + 1030 \cdot \mathrm{H}^{ar} - 108.9\left(\mathrm{O}^{ar} - \mathrm{S}^{ar}\right) - 25.1 \cdot \mathrm{W}^{ar}, \quad kJ/kg \tag{I-3}$$

Recalculation of the mass ratio from the known thermal ratio of the parent fuel:

$$\frac{n_b^{mass}}{n_a^{mass}} = \frac{\left(1 - n_a^{th}\right)/\mathrm{LHV}_b^{ar}}{n_a^{th}/\mathrm{LHV}_a^{ar}} \Rightarrow \frac{n_b^{mass}}{n_a^{mass}} + 1 = \frac{\left(1 - n_a^{th}\right)/\mathrm{LHV}_b^{ar}}{n_a^{th}/\mathrm{LHV}_a^{ar}} + 1 \tag{I-4}$$

$$\Downarrow$$

$$\frac{n_b^{mass} + n_a^{mass}}{n_a^{mass}} = \frac{\left(1 - n_a^{th}\right)/\mathrm{LHV}_b^{ar} + n_a^{th}/\mathrm{LHV}_a^{ar}}{n_a^{th}/\mathrm{LHV}_a^{ar}}$$
$$\frac{1}{n_a^{mass}} = \frac{\left(1 - n_a^{th}\right)/\mathrm{LHV}_b^{ar} + n_a^{th}/\mathrm{LHV}_a^{ar}}{n_a^{th}/\mathrm{LHV}_a^{ar}} \tag{I-5}$$

$$n_a^{mass} = \frac{n_a^{th}/\mathrm{LHV}_a^{ar}}{\left(1 - n_a^{th}\right)/\mathrm{LHV}_b^{ar} + n_a^{th}/\mathrm{LHV}_a^{ar}} \tag{I-6}$$

The composition of the blend is calculated assuming the additive behaviour between parent and substitute fuel:

$$i_c = \frac{\left(n_a^{mass} \cdot i_a\right) + \left(n_b^{mass} \cdot i_b\right)}{\left(n_a^{mass} + n_b^{mass}\right)} \tag{I-7}$$

Thus, the low heating value of fuel blend is determined as follows:

$$\mathrm{LHV}_c^{ar} = \mathrm{LHV}_a^{ar} \cdot n_a^{mass} + \mathrm{LHV}_b^{ar} \cdot \left(1 - n_a^{mass}\right), \quad kJ/kg \tag{I-8}$$

I-2. Flue Gas Properties Formulas

The stoichiometric reactions resulted from combustion of the wet solid fuel fired are shown in Table I-1 whereas the calculation of the flue gas products is presented in the following formulas.

Table I-1. Stoichiometric reactions of solid fuel combustion.

C 1 kmole 12.010 kg 12.010 kg	+	O_2 1 kmole 32.0 kg 22.39 Nm3	=	CO_2 1 kmole 44.010 kg 22.26 Nm3
2C 2*12.010 kg	+	O_2 2*16.0 kg	=	2CO 56.020 kg
$2H_2$ 2 kmole 4.032 kg 4.032 kg	+	O_2 1 kmole 32.0 kg 22.39 Nm3	=	$2H_2O$ 2 kmole 36.032 kg 44.80 Nm3
S 1 kmole 32.066 kg 32.066 kg	+	O_2 1 kmole 32.0 kg 22.39 Nm3	=	SO_2 1 kmole 64.06 kg 21.89 Nm3
O_2 32.0 kg		–		O_2 22.39 Nm3
N_2 28.016 kg		–		N_2 22.39 Nm3
H_2O 18.016 kg		–		H_2O 22.39 Nm3

Theoretical (stoichiometric) volume of air required to burn 1 kg fuel:

$$V_{Air}^{0} = \frac{V_{O_2}^{0}}{0.21} = \left(\frac{22.39}{12.01} \cdot \frac{C^{ar}}{100} + \frac{22.39}{4.032} \cdot \frac{H^{ar}}{100} + \frac{22.39}{32.07} \cdot \frac{S^{ar}}{100} - \frac{22.39}{32.00} \cdot \frac{O^{ar}}{100} \right) / 0.21 \left[Nm^3/kg \right] \quad \text{(I-9)}$$

Recalculated theoretical mass of air:

$$M_{Air}^{0} = \rho_{Air} \cdot V_{Air}^{0} = 1.293 \cdot V_{Air}^{0} \left[kg/kg \;\; fuel \right] \quad \text{(I-10)}$$

Air excess coefficient, defined as the ratio actual air volume to the theoretical air:

$$\lambda = \frac{V_{Air}}{V_{Air}^{0}} \quad \text{(I-11)}$$

Flue gas composition:

Volume of the nitrogen in the flue gas:

$$V_{N_2} = 0.79 \cdot \lambda \cdot V_{Air}^{0} + \frac{1}{\rho_{N_2}} \frac{N^{ar}}{100}, \quad Nm^3/kg \;\; fuel, \; \rho_{N_2} = 1.2505 \;\; kg/m^3 \quad \text{(I-12)}$$

Volume of the SO_2 produced: $V_{SO2} = \frac{21.89}{32.07} \cdot \frac{S^{ar}}{100}, \quad Nm^3/kg \; fuel$ (I-13)

Volume of the oxygen in a flue gas: $V_{O_2} = (\lambda - 1) \cdot 0.21 \cdot V_{Air}^{0}, \quad Nm^3/kg \; fuel$ (I-14)

Volume of the water vapour oxygen in a flue gas is assessed based on the hydrogen and moisture contents in the fuel and moisture in the combustion air:

$$V_{H_2O} = \frac{44.80}{4.03} \cdot \frac{H^{ar}}{100} + \frac{22.39}{18.02} \cdot \frac{W^{ar}}{100} + 0.0161 \cdot \lambda \cdot V_{Air}^{0}, \quad Nm^3/kg\ fuel \tag{I-15}$$

Volume of the CO_2 produced: $V_{CO2} = \frac{22.26}{12.01} \cdot \frac{C^{ar}}{100}, \quad Nm^3/kg\ fuel$ (I-16)

Volume of the dry flue gas produced:

$$V_{FG,dry} = V_{N_2} + V_{CO_2} + V_{SO_2} + V_{O_2}, \quad Nm^3/kg\ fuel \tag{I-17}$$

Volume of the wet flue gas produced:

$$V_{FG,wet} = V_{FG,dry} + V_{H_2O}, \quad Nm^3/kg\ fuel \tag{I-18}$$

Mass concentration of the fly ash in the flue gas stream, where n_{fa}= 0.85 is the ratio of the total ash in the fuel:

$$C_{ash}^{*} = \frac{0.01 \cdot Ash^{ar} \cdot n_{fa}}{1 - 0.01 \cdot Ash^{ar} + 1.306 \cdot \lambda \cdot V_{Air}^{0}} \cdot 1000, \quad g/kg\ \ flue\ \ gas \tag{I-19}$$

Molar ratios of the flue gas components in the flue gas:

$$n^{mol}{}_{RO_2} = n^{mol}{}_{CO_2} + n^{mol}{}_{SO_2} = \frac{V_{CO_2} + V_{SO_2}}{V_{FG,wet}}; \quad n^{mol}{}_{H_2O} = \frac{V_{H_2O}}{V_{FG,wet}}; \tag{I-20}$$

$$n^{mol}{}_{O_2} = \frac{V_{O_2}}{V_{FG,wet}}; \quad n^{mol}{}_{N_2} = \frac{V_{N_2}}{V_{FG,wet}} \tag{I-21}$$

The flue gas compositions calculated for two cases: a) combustion of Colombian coal (CO1) and b) co-firing of CO1 coal with 20th% of wet sawdust are summarised in Tables I-2 and I-3.

Table I-2. Flue gas products resulted from combustion of Colombian coal (CO1).

Coal (CO1)	V_i [Nm^3/kg wet fuel]	M_i [kg/kg wet fuel]	$n^{mol}{}_i$ - mole fraction [-]
Total air required (for λ=1.2)	8.192	10.682	-
N_2	6.483	8.239	0.741
CO_2	1.234	2.440	0.141
H_2O	0.746	0.666	0.085
SO_2	0.004	0.012	0.00045
O_2	0.287	0.409	0.033
Total amount of the wet flue gas	8.754	11.766	1.000

Table I-3. Flue gas products resulted from co-combustion of Colombian coal (CO1) with wet sawdust (SD2).

Coal + 20%th wet Sawdust	V_i [Nm^3/kg wet fuel]	M_i [kg/kg wet fuel]	$n^{mol}{}_i$ - mole fraction [-]
Total air required (for λ=1.2)	6.369	8.304	-
N_2	5.039	6.403	0.712
CO_2	0.974	1.926	0.242
H_2O	0.840	0.727	0.119
SO_2	0.003	0.007	0.001
O_2	0.223	0.318	0.041
Total amount of the wet flue gas	7.079	9.381	1.000

The average specific heat of the flue gas is calculated as follows:

$$Vc_{p,t}(\lambda,t)=V_{N_2}(\lambda)\cdot c_{p,N_2}(t)+V_{H_2O}(\lambda)\cdot c_{p,H_2O}(t)+V_{CO_2}(\lambda)\cdot c_{p,CO_2}(t)+ V_{O_2}(\lambda)\cdot c_{p,O_2}(t)+0.01\cdot Ash^{ar}\cdot n_{fa}\cdot c_{p,Ash}(t),\quad [kJ/(kg\cdot t)] \tag{I-22}$$

and the enthalpy of the flue gas:

$$h_{FG}(\lambda,t_{FG})=Vc_{p,t_{FG}}(\lambda,t_{FG})\cdot t_{FG},\quad kJ/kg \tag{I-23}$$

To calculate the specific heats of individual flue gas components the polynomial expressions were used being a function of temperature (in Celsius), as follows (see Table I-4):

$$c_{p,i}=b_{i,0}+\sum_{j=1}^{J} b_{i,j}t^j \tag{I-24}$$

where J is the order polynomial in temperature t (^{o}C) for the specific heat calculation.

Table I-4. Weighting factors for the specific heat functions.

Gas component, i	$b_{i,0}$	$b_{i,1}$	$b_{i,2}$	$b_{i,3}$
c_{p,N_2}	1.29775	0.10463*10^{-4}	1.2558*10^{-7}	-4.1863*10^{-11}
c_{p,H_2O}	1.49079	1.08808*10^{-4}	1.7499*10^{-7}	-5.8330*10^{-11}
c_{p,CO_2}	1.61306	10.58839*10^{-4}	-5.5424*10^{-7}	11.5810*10^{-11}
c_{p,O_2}	1.30359	2.08294*10^{-4}	-0.3289*10^{-7}	-0.19933*10^{-11}
$c_{p,Ash}$	0.73949	7.44816*10^{-4}	-11.0696*10^{-7}	72.0135*10^{-11}

Figure I-1 shows the plotted flue gas enthalpies in function of flue gas temperature and air excess (λ=1.2) calculated for pure coal combustion (CO1) and two co-firing cases: 20th% and 40th% wet sawdust (SD2) shares.

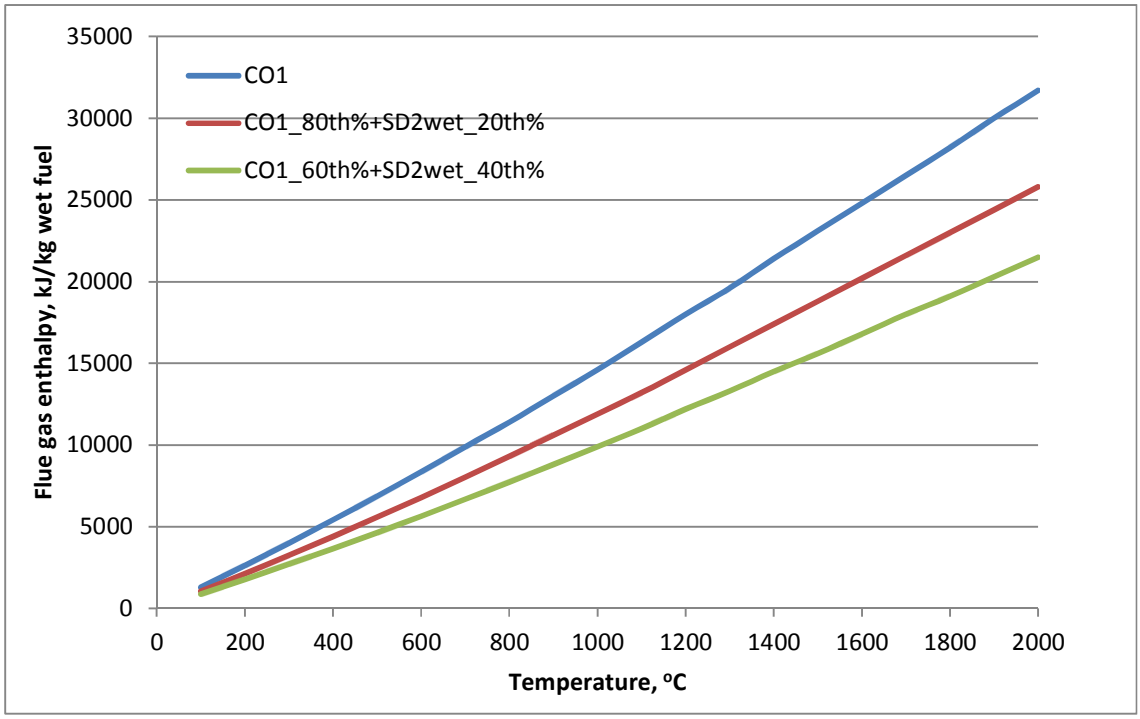

Figure I-1. Flue gas enthalpies distribution (λ=1.2): a) pure coal (CO1) combustion, b) 20th% wet sawdust co-firing, c) 40th% wet sawdust co-firing.

The weighted sum-of-grey-gasses model (WSGGM):

Non-greyness of the combustion products can be assessed with a weighted grey gas approach. This can be obtained by representing the emissivity of real gas as a weighted sum of the emissivities of a number of grey gases and one clear gas for considering the transparent windows in the spectrum. In this study the approach with three grey gases (+one clear gas) for a mixture of CO_2 and H_2O was adapted, and the emissivity of the flue gas was calculated as follows:

$$\varepsilon_{gas} = \sum_{i=0}^{3} a_i(T)\left[1 - e^{-k_i pL}\right] \qquad \text{(I-25)}$$

where a_i is the emissivity weighting factor for ith grey gas at T(K), k is the absorption coefficient, p is the sum of partial pressures of the absorbing gases and L is the path length (or the effective thickness of radiating gas layer).

$$a_i = b_{i,0} + \sum_{j=1}^{J} b_{i,j} T^j \qquad \text{(I-26)}$$

where j is the order polynomial in temperature T (K) for emissivity.

Table I-5. Absorption coefficients and weighting factors for the WSGGM model.

Grey gas, i	Absorption coefficient (k_i)	$b_{i,0}$	$b_{i,1}$	$b_{i,2}$	$b_{i,3}$
1	0.4303	0.5150	$-2.303*10^{-4}$	$0.9779*10^{-7}$	$-1.494*10^{-11}$
2	7.055	0.07749	$3.399*10^{-4}$	$-2.297*10^{-7}$	$3.770*10^{-11}$
3	178.1	0.1907	$-1.824*10^{-4}$	$0.5608*10^{-7}$	$-0.5122*10^{-11}$

Note: For the clear gas (i=0) the absorption coefficient is equal 0.

The effective thickness of the radiating layer can be calculated as follows:

$$L = 3.6\frac{V_{furn}}{A_{furn}},\ [m] \tag{I-27}$$

and the sum of partial pressures:

$$p = n_{m,\mathrm{CO_2}} + n_{m,\mathrm{H_2O}} \tag{I-28}$$

The total emissivity of the flue gas (for pulverised coal combustion) including the ash impact can be calculated as [110]:

$$\varepsilon_{total} = \varepsilon_{gas} + \varepsilon_{ash} - \varepsilon_{gas} \cdot \varepsilon_{ash} \tag{I-29}$$

where, the emissivity of the ash particles

$$\varepsilon_{ash} = 1 - \exp\left(-kpL\right)_{ash} \tag{I-30}$$

$$\left(kpL\right)_{ash} = \frac{4.1}{\sqrt[3]{d_{ash}{}^2 \cdot T^2}} \cdot \left[1 - \frac{0.6}{1 + 30 \cdot 10^3 \cdot \left(C^*_{ash} \cdot \rho_{gas} \cdot L\right)^{-2}}\right] \cdot C^*_{ash} \cdot \rho_{gas} \cdot L \tag{I-31}$$

I-3. Heat Transfer Formulas

After transformation of the general thermal energy balance equation (eq. 4.30) the following formulas for the outlet temperatures of the specific zones in the furnace can be obtained as follows:

a) Burner section zones

In the burner zones each burner row is considered as a separate zone. For the first zone the radiation towards the bottom part of the furnace is additionally considered. Heat release pattern is described by the burnout degree of the fuel fraction introduced in the given burner zones.

- First zone

$$t_{out,1} = \frac{\beta_1 \cdot \mathrm{LHV} + \dot{q}_{Air} + i_{\mathrm{B}}}{Vc_{p,t_{out}}} - \frac{\varepsilon_{furn}\sigma_0 T_{out}^4}{n_{\mathrm{B},1} \cdot \dot{M}_{\mathrm{B}} Vc_{p,t_{out}}} (\psi A_w)_1 \qquad \text{(I-32)}$$

$$(\psi A_w) = A_w \cdot \psi_w + A' \cdot \psi' + A'' \cdot \psi'' \approx A_w \cdot \psi_w + A' \cdot \psi_w + A'' \cdot \psi'' \qquad \text{(I-33)}$$

where ψ_w is the thermal effectiveness of the walls within the zone, A_w is the surface of the walls, ψ' and ψ'' are the thermal effectiveness of the imaginary windows towards the bottom of the furnace ($\psi' \approx \psi_w$) and higher located zone (assumed to be $\psi'' = 0.1$ according to [110]). A' and A'' are the corresponding surface areas of the zone windows.

- Next zones within the burner section

$$t_{out,i} = \frac{\left(n_{\mathrm{B},i} + \sum_1^{i-1} n_{\mathrm{B}} \Delta\beta_i\right) \cdot \mathrm{LHV} + n_{\mathrm{B},i}\dot{q}_{Air} + n_{\mathrm{B},i} i_{\mathrm{B}}}{\sum_1^{i} n_{\mathrm{B}} \left(Vc_{p,t_{out}}\right)} + \frac{\sum_1^{i-1} n_{\mathrm{B}} \left(Vc_{p,t_{in}}\right)}{\sum_1^{i} n_{\mathrm{B}} \left(Vc_{p,t_{out}}\right)} t_{in,i} -$$
$$- \frac{\varepsilon_{furn}\sigma_0}{2\sum_1^{i} n_{\mathrm{B}} \cdot \dot{M}_{\mathrm{B}} \left(Vc_{p,t_{out}}\right)} \left[\left(T_{in,i}^4 + T_{out,i}^4\right)\right](\psi A_w)_i \qquad \text{(I-34)}$$

$$(\psi A_w) \approx A_w \cdot \psi_w \qquad \text{(I-35)}$$

b) Upper zones above the burner section

$$t_{out,i} = \frac{\Delta\beta_i \cdot \mathrm{LHV}}{\left(Vc_{p,t_{out}}\right)} + \frac{\left(Vc_{p,t_{in}}\right)}{\left(Vc_{p,t_{out}}\right)} t_{in,i} - \frac{\varepsilon_{furn}\sigma_0}{2\dot{M}_{\mathrm{B}} \left(Vc_{p,t_{out}}\right)} \left[\left(T_{in,i}^4 + T_{out,i}^4\right)\right](\psi A_w)_i \qquad \text{(I-36)}$$

$$(\psi A_w) \approx A_w \cdot \psi_w + A'' \cdot \psi'' \approx A_w \cdot \psi_w + A'' \cdot \psi_w \cdot \chi \qquad \text{(I-37)}$$

For the furnace outlet conditions (without included platen superheater in the zone) ψ'' is the thermal effectiveness coefficient which characterises the heat transfer by radiation to the higher located zone and is assumed to be equal to ψ_w multiplied by the heat exchange efficiency factor χ (for solid fuels $\chi = 0.8$ at 1300°C [135]), A'' is the surface area of the zone window towards the higher located zone.

c) Zone at the furnace outlet (with a platen superheater case)

The thermal energy balance for the zone with a heat exchanger section placed at the furnace outlet is as follows:

$$\dot{Q}_{\mathrm{FG},in}+\dot{Q}_{\mathrm{EM},in}-\dot{Q}_{SH2}-\dot{Q}_{Rad}-\dot{Q}_{\mathrm{EM},out}-\dot{Q}_{\mathrm{FG},out}=0 \tag{I-38}$$

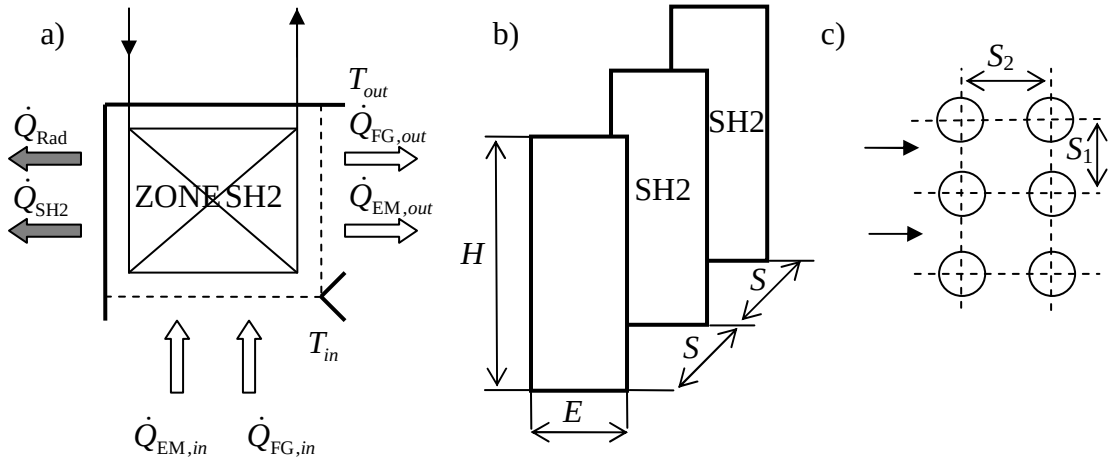

Figure I-2. a) Thermal balance of the furnace zone with a platen superheater, b) Dimensions of the platen superheater, c) Spacing between in-line tube bundle.

where $\dot{Q}_{FG}$ is the heat stream associated with the flue gas enthaphy for the inlet (*in*) and outlet (out) of the zone, $\dot{Q}_{EM}$ is the heat stream emitted to (*in)* or out of the current zone, $\dot{Q}_{\mathrm{SH2}}$ is the heat stream transferred into platen superheater and $\dot{Q}_{\mathrm{Rad}}$ is the heat steam transferred by the radiation into furnace walls within the analysed zone.

$$\dot{Q}_{\mathrm{FG},in}=\dot{M}_{\mathbf{B}}\left(Vc_{p,t_{in}}\right)t_{in} \tag{I-39}$$

$$\dot{Q}_{\mathrm{EM},in}=\varepsilon_{furn}\sigma_0\left(T_{in}\right)^4\left(\psi'A'\right)_{in} \tag{I-40}$$

$$\dot{Q}_{\mathrm{SH2}}=\left(\dot{M}_{\mathrm{Evap}}+\dot{M}_{\mathrm{Inject}}\right)\cdot\left(h_3\left(t_3,p_3\right)-h_2\left(t_2,p_2\right)\right)=k_{\mathrm{SH2}}A_{\mathrm{SH2}}\Delta T_{\log}+\dot{Q}_{\mathrm{RadFurn}} \tag{I-41}$$

$$\dot{Q}_{\mathrm{Rad}}=\varepsilon_{furn}\sigma_0\,0.5\left(T_{in}^4+T_{out}^4\right)\left(\psi_w A_w\right)_{Free} \tag{I-42}$$

$$\dot{Q}_{\mathrm{EM},out}=\varepsilon_{furn}\sigma_0\left(T_{out}\right)^4\left(\psi''A''\right)_{out} \tag{I-43}$$

$$\dot{Q}_{\mathrm{FG},out}=\dot{M}_{\mathbf{B}}\left(Vc_{p,t_{out}}\right)t_{out} \tag{I-44}$$

After transformation of thermal balance equation the following formula for the temperature at the outlet of the zone can be obtained:

$$\begin{aligned}t_{out}=&\frac{\Delta\beta_i\cdot\mathrm{LHV}}{\left(Vc_{p,t_{out}}\right)}+\frac{\left(Vc_{p,t_{in}}\right)}{\left(Vc_{p,t_{out}}\right)}t_{in,i}+\frac{\varepsilon_{furn}\sigma_0}{\dot{M}_{\mathrm{B}}\left(Vc_{p,t_{out}}\right)}T_{in}^4\left(\psi'A'\right)_{in}-\\&-\frac{\left(\dot{M}_{\mathrm{Evap}}+\dot{M}_{\mathrm{Inject}}\right)\cdot\left(h_3\left(t_3,p_3\right)-h_2\left(t_2,p_2\right)\right)}{\dot{M}_{\mathrm{B}}\left(Vc_{p,t_{out}}\right)}-\frac{\varepsilon_{furn}\sigma_0}{\dot{M}_{\mathrm{B}}\left(Vc_{p,t_{out}}\right)}0.5\left(T_{in}^4+T_{out}^4\right)\left(\psi_w A_w\right)_{Free}-\\&-\frac{\varepsilon_{furn}\sigma_0}{\dot{M}_{\mathrm{B}}\left(Vc_{p,t_{out}}\right)}T_{out}^4\left(\psi''A''\right)_{out}\end{aligned} \tag{I-45}$$

To determine the impact of the heat transfer conditions on the steam parameters of the platen superheater an additional thermal energy balance equation is required:

$$\left(\dot{M}_{\mathrm{Evap}}+\dot{M}_{\mathrm{Inject}}\right)\cdot\left(h_3\left(t_3,p_3\right)-h_2\left(t_2,p_2\right)\right)-k_{\mathrm{SH2}}A_{\mathrm{SH2}}\Delta T_{\log}-\dot{Q}_{\mathrm{RadFurn}}=0 \tag{I-46}$$

The radiant heat absorbed by the platen superheater surfaces is calculated as follows [135]:

$$\dot{Q}_{\mathrm{RadFurn}}=\dot{Q}_{\mathrm{Rad}jn}-\dot{Q}_{\mathrm{Rad}out} \tag{I-47}$$

where $\dot{Q}_{\mathrm{Rad}jn}$ and $\dot{Q}_{\mathrm{Rad},out}$ are the radiant heat flux at the inlet to the heating surface and the radiant flux at the outlet from the heating furnace onto subsequent heating surface, respectively:

$$\dot{Q}_{\mathrm{Rad},in}=\varepsilon_{furn}\sigma_0\left(T_{in}\right)^4\left(\psi'A'\right)_{in} \tag{I-48}$$

$$\dot{Q}_{\mathrm{Rad},out}=\frac{\dot{Q}_{\mathrm{Rad},in}\left(1-\varepsilon_{\mathrm{SH2}}\right)x_e}{\chi}+\varepsilon_{\mathrm{SH2}}\sigma_0\,0.5\left(T_{in}^4+T_{out}^4\right)\xi\psi_{\mathrm{SH2}}A_{\mathrm{SH2}} \tag{I-49}$$

A_{in} is the surface area of the furnace window in the zone towards the platen superheater, χ is the coeffcient which takes into account heat exchange efficiency between the furnace and platen superheater (for solid fuels $\chi=0.8$ at 1300^{o}C [135]) , and x_{e} is the angular coefficient of radiation from the inlet onto the outlet section of the calculated surfaces. For platen superheater it is determined by the formula:

$$x_{\mathrm{e}}=\left[\left(\frac{H}{S}\right)^2+1\right]^{0.5}-\frac{H}{S} \tag{I-50}$$

where S is the spacing between the platen surface [m], and H [m] is the height of the platens (in the direction of the flow), A_{SH2} is the surface area of the platen superheater outlet [m^2].

The third equation is needed to describe the thermal efficiency factor for the platen heat exchange surfaces:

$$\psi_{\mathrm{SH2}}=\frac{\varepsilon_d}{\varepsilon_{\mathrm{SH2}}}\left(\varepsilon_{\mathrm{SH2}}-\left(\frac{T_d}{0.5\left(T_{in}+T_{out}\right)}\right)^4\right) \tag{I-51}$$

where ε_d is the emmisivity of the deposit surface, T_d is the temperature of the deposit outer layer (K), ε_{SH2} is the emisivity of the flue gas in the zone with the platen superheater section, and $T_{in(out)}$ is the temperature (K) at the inlet and outlet, respectively.

The effective thickness of the radiating layer for the platen superheaters can be calculated as follows:

$$L = \frac{1.8}{\frac{1}{E}+\frac{1}{H}+\frac{1}{S}},\ [m] \tag{I-52}$$

where *E, H* and *S* are the depth, height and width of the space between platens, respectively (see Figure I-2).

The temperature of the outer layer of deposit can be calculated when the thermal resistance of the deposit is known:

$$T_d = T_s + R_{\mathrm{SH2}} \frac{\dot{Q}_{\mathrm{SH2}}}{A_{\mathrm{SH2}}},\ [K] \tag{I-53}$$

Calculation of the heat transfer coefficients:

The formula for the overall heat transfer coefficient is expressed by:

$$k = \frac{\alpha_1}{1+\left(R_d + \frac{1}{\alpha_2}\right)\cdot\alpha_1} \tag{I-54}$$

where the convective heat transfer coefficient from the flue gas side consists of the convective and radiant parts as follows:

$$\alpha_1 = \alpha_{con} + \alpha_{rad} \tag{I-55}$$

In case of the platen superheater it has the following form:

$$\alpha_1 = 0.85\left(\alpha_{con}\frac{\pi d}{2S_2\cdot x_e} + \alpha_{rad}\right) \tag{I-56}$$

where the angular coefficient x_e is dependent on the S_2/d ratio as follows:

Table I-6. Dependence of the angular coefficient on the superheater geometry.

S_2/d	5.0	3.0	2.0	1.0
x_e	0.28	0.44	0.6	1.0

The convective part of the convective heat transfer coefficient for the in-line tube bundle case is expressed by formula:

$$\alpha_{con} = 0.2 C_s C_n \frac{\lambda}{d}\mathrm{Re}^{0.65}\,\mathrm{Pr}^{0.33} \tag{I-57}$$

where:

$$C_s = \left[1 + \left(2\frac{S_1}{d} - 3\right)\left(1 - \frac{S_2}{d}\right)^3\right]^{-2} \tag{I-58}$$

$$\text{If } \frac{S_1}{d} \le 1.5 \text{ or } \frac{S_2}{d} \ge 2,\ C_s = 1.0 \tag{I-59}$$

when the numbers of rows,

$$n < 10 \qquad C_n = 0.91 + 0.0125 \cdot (n - 2) \tag{I-60}$$

$$n \ge 0 \qquad C_n = 1.0 \tag{I-61}$$

The radiant heat transfer coefficient is expressed by:

$$\alpha_{rad} = 5.698 \cdot 10^{-11} \frac{\varepsilon_d + 1}{2} \varepsilon_{gas} T_{gas}^3 \frac{1 - \left(\frac{T_d}{T_{gas}}\right)^4}{1 - \left(\frac{T_d}{T_{gas}}\right)} \tag{I-62}$$

The convective heat transfer coefficient corresponding to the steam side is as follows:

$$\alpha_2 = 0.023 \frac{\lambda_s}{d} \mathrm{Re}^{0.8}\ \mathrm{Pr}^{0.4} \tag{I-63}$$

In case of the calculation of the convective heat transfer for the air preheater case:

$$\alpha_{con} = 0.027 \frac{\lambda}{d} \mathrm{Re}^{0.8}\ \mathrm{Pr}^{0.4}\ C_t C_l \tag{I-64}$$

$C_t = 1.0,\ C_l = 1.1$

I-4. Phase Equilibrium Calculations

In this section the more detailed formulas are described which are used to calculate the inputs of the ash forming elements into to phase equilibrium model as well as the complete list of the compounds/solutions/phases used in calculations is listed.

Three phase equilibrium modules are defined as described in Chapter 4, section 5.2.2:

- EQ3 (calculated first) is used to determine the capture efficiency of the alkali metals captured by the alumina-silicate ash. As the input the reactive part of Al-Si based ash is used according to Nutalapati *et al.* [103] approach as well as the soluble part of sodium and potassium.
- EQ1 is used to determine the slag phase % and its viscosity at the high temperature range. Apart from the input of total amount of Al-Si based ash the captured alkali metals from EQ2 module are also introduced.
- EQ2 is used to assess the fate of alkali metals and other ash forming elements remaining in the gas phase able to condense at the lower temperature range and which were not captured by Al-Si based ash according to EQ2 module calculations.

The general formulas used to calculate the inputs of the ash forming elements (*El*) of the blended fuel (*c*) into specific phase equilibrium modules, including the corresponding mass fractions are defined as follows:

EQ3 input

$$El_{c,i}^{EQ3} = n_a^{mass} El_{a,i}^{tot} \cdot \left(n_{AlSi,a,i}^{Sol} + n_{REA}^{\mathrm{Rest}} \cdot n_{AlSi,a,i}^{\mathrm{Rest}} \right) + n_b^{mass} El_{b,i}^{tot} \cdot \left(n_{AlSi,b,i}^{Sol} + n_{REA}^{\mathrm{Rest}} \cdot n_{AlSi,b,i}^{\mathrm{Rest}} \right) \quad \text{(I-65)}$$

EQ1 input

$$\begin{aligned} El_{c,i}^{EQ1} = {} & n_a^{mass} El_{a,i}^{tot} \cdot \left(n_{AlSi,a,i}^{\mathrm{Rest}} + \left(1 - n_{Salt,a,i}^{Sol}\right) \cdot n_{AlSi,a,i}^{Sol} \right) + \\ & + n_b^{mass} El_{b,i}^{tot} \cdot \left(n_{AlSi,b,i}^{\mathrm{Rest}} + \left(1 - n_{Salt,b,i}^{Sol}\right) \cdot n_{AlSi,b,i}^{Sol} \right) \end{aligned} \quad \text{(I-66)}$$

EQ2 input

- Na and K elements

$$El_{c,i}^{EQ2} = n_a^{mass} \cdot El_{a,i}^{tot} \cdot \left(n_{Salt,a,i}^{Sol} \cdot n_{AlSi,a,i}^{Sol} \right) + n_b^{mass} \cdot El_{b,i}^{tot} \cdot \left(n_{Salt,b,i}^{Sol} \cdot n_{AlSi,b,i}^{Sol} \right) \quad \text{(I-67)}$$

- the rest of the ash forming elements

$$El_{c,i}^{EQ2} = n_a^{mass} \cdot El_{a,i}^{tot} \cdot \left(n_{Salt,a,i}^{Sol} \right) + n_b^{mass} \cdot El_{b,i}^{tot} \cdot \left(n_{Salt,b,i}^{Sol} \right) \quad \text{(I-68)}$$

where n_a^{mass} and n_b^{mass} are the mass shares of the parent and substitute fuels in the blend, denote here as *a* and *b*, respectively; n_{AlSi}^{Sol} is the fraction describing the reactive part of given element (soluble and organically bound) potentially able to interact with Al-Si based ash; n_{REA}^{Rest} is the mass fraction of Al-Si based ash particles defining their reactive layer towards capturing alkali metals according to Nutalapati *et al.* [103]; $n_{AlSi,a,i}^{Rest}$ is the fraction of the total amount of element which defines its association with Al-Si based ash; n_{Salt}^{Sol} is the fraction of the given element remaining the gas phase (for Na and K determined based on the EQ3 module calculations – corresponding capture efficiencies) able to form salts in the convective section of the boiler.

The assumed "reactivity" fractions for coals as well as the investigated biomass (straw) are summarised in Table I-7.

Table I-7. Fractions of the total ash forming elements introduced into phase equilibrium calculations.

i	*El*	COAL (*a*)			BIOMASS (*b*)		
		$n_{AlSi,a,i}^{Sol}$	$n_{Salt,a,i}^{Sol}$	$n_{AlSi,a,i}^{Rest}$	$n_{AlSi,b,i}^{Sol}$	$n_{Salt,b,i}^{Sol}$	$n_{AlSi,b,i}^{Rest}$
1	Si	0	0	1	0	0	1
2	Al	0	0	1	0	0	1
3	Fe	0	0	1	0	0	1
4	Ca	0	0	1	0	0.2	0.8
5	Mg	0	0	1	0	0.2	0.8
6	Na	0	0	1	1	$1-\eta_{Capt}^{Na}$	0
7	K	0	0	1	1	$1-\eta_{Capt}^{K}$	0

More specific inputs of the elements into phase equilibrium modules (EQ1, EQ2 and EQ3) for the sensitivity analysis cases investigated in Chapter 5, section 5.3.4, such as co-firing of the Colombian coal (CO1) with the wet sawdust (SD2wet) for different co-firing ratios (0th%, 10th% and 20th%), and fly ash layer reactivity % (5%, 10% and 20% REA) are summarised in Tables I-8 and I-9.

The complete list of the gas, solid species as well as solutions (liquid and solid phases) used in the phase equilibrium calculation is shown in Tables I-10..12.

Table I-8. Input of the elements into phase equilibrium modules for co-firing of Colombian coal (CO1) with wet sawdust (SD2) for 0th%, 10th% and 20th%, 5%REA.

	SA3	SA3DS2-10th%-5REA						SA3DS2-20th%-5REA					
g/kg wet fuel	EQ1	EQ1		EQ2		EQ3		EQ1		EQ2		EQ3	
C	667.4	624.6		624.6		624.6		587.4		587.4		587.4	
H	37.9	40.3		40.3		40.3		42.4		42.4		42.4	
O	80.4	124.0		124.0		124.0		161.9		161.9		161.9	
N	15.2	13.6		13.6		13.6		12.1		12.1		12.1	
S	3.8	3.4		3.4		3.4		3.0		3.0		3.0	
Cl	0.2	0.9		0.9		0.9		1.6		1.6		1.6	
H_2O	52.0	63.7		63.7		63.7		73.9		73.9		73.9	
Air O_2	2403	2235		2235		2235		2089		2089		2089	
Air N_2	8044	7482		7482		7482		6993		6993		6993	
AFM	SA3	SA3	DS2	SA3	DS2	SA3	DS2	SA3	DS2	SA3	DS2	SA3	DS2
Si	29.833	24.991	1.537	1.250	0.077	0.0	0.0	20.776	2.876	1.039	0.144	0.0	0.0
Al	25.902	21.698	0.048	1.085	0.002	0.0	0.0	18.038	0.090	0.902	0.005	0.0	0.0
Fe	4.404	3.689	0.044	0.184	0.002	0.0	0.0	3.067	0.082	0.153	0.004	0.0	0.0
Ca	9.614	8.053	0.404	0.403	0.020	0.0	0.101	6.695	0.755	0.335	0.038	0.0	0.189
Mg	0.949	0.795	0.093	0.040	0.005	0.0	0.023	0.661	0.175	0.033	0.009	0.0	0.044
Na	0.212	$0.178+\eta_{Capt}^{Na}0.061$		0.009	0.061	$\left(1-\eta_{Capt}^{Na}\right)0.061$		$0.148+\eta_{Capt}^{Na}0.114$		0.007	0.114	$\left(1-\eta_{Capt}^{Na}\right)0.114$	
K	0.713	$0.597+\eta_{Capt}^{K}2.393$		0.030	2.393	$\left(1-\eta_{Capt}^{K}\right)2.393$		$0.496+\eta_{Capt}^{K}4.476$		0.025	4.476	$\left(1-\eta_{Capt}^{K}\right)4.476$	

Table I-9. Input of the elements into phase equilibrium modules for co-firing of Colombian coal (CO1) with wet sawdust (SD2) for 20th%, 10% and 20%REA.

	SA3DS2-20th%-10REA						SA3DS2-20th%-20REA					
g/kg wet fuel	EQ1		EQ2		EQ3		EQ1		EQ2		EQ3	
C	587.4		587.4		587.4		587.4		587.4		587.4	
H	42.4		42.4		42.4		42.4		42.4		42.4	
O	161.9		161.9		161.9		161.9		161.9		161.9	
N	12.1		12.1		12.1		12.1		12.1		12.1	
S	3.0		3.0		3.0		3.0		3.0		3.0	
Cl	1.6		1.6		1.6		1.6		1.6		1.6	
H_2O	73.9		73.9		73.9		73.9		73.9		73.9	
Air O_2	2089		2089		2089		2089		2089		2089	
Air N_2	6993		6993		6993		6993		6993		6993	
AFM	SA3	DS2	SA3	DS2	SA3	DS2	SA3	DS2	SA3	DS2	SA3	DS2
Si	20.776	2.876	2.078	0.288	0.0	0.0	20.776	2.876	4.155	0.575	0.0	0.0
Al	18.038	0.090	1.804	0.009	0.0	0.0	18.038	0.090	3.608	0.018	0.0	0.0
Fe	3.067	0.082	0.307	0.008	0.0	0.0	3.067	0.082	0.613	0.016	0.0	0.0
Ca	6.695	0.755	0.670	0.076	0.0	0.189	6.695	0.755	1.339	0.151	0.0	0.189
Mg	0.661	0.175	0.066	0.017	0.0	0.044	0.661	0.175	0.132	0.035	0.0	0.044
Na	$0.148+\eta_{Capt}^{Na}0.114$		0.015	0.114	$\left(1-\eta_{Capt}^{Na}\right)0.114$		$0.148+\eta_{Capt}^{Na}0.114$		0.030	0.114	$\left(1-\eta_{Capt}^{Na}\right)0.114$	
K	$0.496+\eta_{Capt}^{K}4.476$		0.050	4.476	$\left(1-\eta_{Capt}^{K}\right)4.476$		$0.496+\eta_{Capt}^{K}4.476$		0.099	4.476	$\left(1-\eta_{Capt}^{K}\right)4.476$	

Table I-10. List of the gas species used in phase equilibrium calculations (FACT 53 database).

H(g)	Al(g)	Cl(g)
H2(g)	AlO(g)	Cl2(g)
C(g)	AlO2(g)	HCl(g)
CH4(g)	AlOH(g)-1_aluminum_h...	CCl4(g)
C2H6(g)	OAlOH(g)	ClCN(g)
N(g)	Si(g)	ClO(g)
N2(g)	SiH(g)	HOCl(g)
NH2(g)	SiH4(g)	COCl(g)
NH3(g)	SiC(g)	COCl2(g)
CN(g)	SiO(g)	ONCl(g)
HCN(g)	P(g)	NaCl(g)
O(g)	P2(g)	MgCl(g)
O2(g)	PH(g)	MgCl2(g)
OH(g)	PH2(g)	AlCl(g)
H2O(g)	PH3(g)	AlCl2(g)
HOO(g)	PN(g)	AlCl3(g)
HOOH(g)	PO(g)	OAlCl(g)
CO(g)	PO2(g)	SiCl4(g)
CO2(g)	(P2O3)2(g)	SCl(g)
H2CO(g)	(P2O5)2(g)	S2Cl(g)
C2H4O(g)	S(g)	SOCl2(g)
NO(g)	S2(g)	K(g)
N2O(g)	HS(g)	K2(g)
NO2(g)	H2S(g)	KH(g)
HONO(g)	CS(g)	KCN(g)-1_potassium_c...
HONO2(g)	CS2(g)	(KCN)2(g)
Na(g)	SO(g)	KO(g)
Na2(g)	SO2(g)	KOH(g)
NaH(g)	SO3(g)	(KOH)2(g)
NaCN(g)	O2S(OH)2(g)	K2SO4(g)
(NaCN)2(g)	COS(g)	KCl(g)
NaO(g)	Na2SO4(g)	(KCl)2(g)
NaOH(g)	MgS(g)	Ca(g)
(NaOH)2(g)	SiS(g)	CaO(g)
Mg(g)	PS(g)	CaOH(g)
MgO(g)		Ca(OH)2(g)
MgOH(g)		CaS(g)
Mg(OH)2(g)		CaCl(g)
		CaCl2(g)
		Fe(g)
		FeO(g)
		Fe(OH)2(g)
		FeS(g)
		FeCl2(g)
		FeCl3(g)

Table I-11. List of the solid species used in the phase equilibrium calculations (FACT 53, FToxid, FTsalt databases).

C(s)	FACT53 graphite	Na2O(s)	FToxid solid-a
Na(s)	FACT53 solid	MgO(s)	FToxid periclase
Mg(s)	FACT53 solid	Al2O3(s)	FToxid gamma
Mg(OH)2(s)	FACT53 brucite	NaAlO2(s)	FToxid solid
MgCO3(s)	FACT53 magnesite	SiO2(s)	FToxid quartz(l)
Al(s)	FACT53 solid	SiO2(s2)	FToxid quartz(h)
NaAl9O14(s)	FACT53 beta-alumina	SiO2(s3)	FToxid tridymite(l)
Na2Al12O19(s)	FACT53 beta2-alumina	SiO2(s4)	FToxid tridymite(h)
MgAl2O4(s)	FACT53 spinel	SiO2(s5)	FToxid cristobalite(l)
Si(s)	FACT53 solid	SiO2(s6)	FToxid cristobalite(h)
P(s)	FACT53 solid_(white)	SiO2(s7)	FToxid coesite
(P2O5)2(s)	FACT53 solid	SiO2(s8)	FToxid stishovite
Mg3P2O8(s)	FACT53 solid	Na2SiO3(s)	FToxid solid
AlPO4(s)	FACT53 solid-a	Na4SiO4(s)	FToxid solid
S(s)	FACT53 orthorhombic	Na2Si2O5(s)	FToxid solid
Na2S(s)	FACT53 solid	Na6Si2O7(s)	FToxid solid
MgS(s)	FACT53 solid	Na6Si8O19(s)	FToxid solid
K(s)	FACT53 solid	MgSiO3(s)	FToxid low-clinoenstatite
K2S(s)	FACT53 solid		
KAl(SO4)2(s)	FACT53 solid	MgSiO3(s2)	FToxid ortho-enstatite
Ca(s)	FACT53 solid_alpha	Mg2SiO4(s)	FToxid forsterite
CaOMgOSiO2(s)	FACT53 monticellite	NaAlSiO4(s)	FToxid nepheline-a
Ca3(PO4)2(s)	FACT53 whit..kite	NaAlSi2O6(s)	FToxid jadeite
Ca3(PO4)2(s2)	FACT53 solid-b	NaAlSi3O8(s)	FToxid low-albite
Ca5HO13P3(s)	FACT53 hydroxyapatite	NaAlSi3O8(s2)	FToxid high-albite
CaS(s)	FACT53 solid	Mg4Al10Si2O23(s)	FToxid sapphirine
CaCl2(s)	FACT53 hydrophilite	Mg3Al2Si3O12(s)	FToxid pyrope
Fe(s)	FACT53 bcc	Mg2Al4Si5O18(s)	FToxid cordierite
Fe3O4(s)	FACT53 magnetite	K2O(s)	FToxid solid
Fe(OH)2(s)	FACT53 solid	KAlO2(s)	FToxid solid
Fe(OH)3(s)	FACT53 solid	KAl9O14(s)	FToxid k-beta-alumina
(MgO)(Fe2O3)(s)	FACT53 solid	K2Al12O19(s)	FToxid k-beta2-alumina
FeSiO3(s)	FACT53 clino-ferrosilite(metast)	K2SiO3(s)	FToxid solid
FeS(s)	FACT53 solid	K2Si2O5(s)	FToxid solid
FeS2(s)	FACT53 pyrite	K2Si4O9(s)	FToxid solid
FeSO4(s)	FACT53 solid	KAlSiO4(s)	FToxid kaliophilite-hexagonal
Fe2(SO4)3(s)	FACT53 solid		
Ca2Fe2O5(s)	FACT53 solid	KAlSi2O6(s)	FToxid leucite(rhf)-a
---	---	KAlSi2O6(s2)	FToxid leucite(rhf)-b
NaOH(s)	FTsalt solid	KAlSi3O8(s)	FToxid microcline
Na2SO4(s)	FTsalt solid_a	KAlSi3O8(s2)	FToxid k-feldspar
Na2SO4(s2)	FTsalt solid_b	KAlSi3O8(s3)	FToxid sanidine
MgSO4(s)	FTsalt solid	CaAl2O4(s)	FToxid solid
NaCl(s)	FTsalt halite_(rock_salt_struct)	CaAl4O7(s)	FToxid solid
		CaAl12O19(s)	FToxid solid
MgCl2(s)	FTsalt chloromagnesite	Ca3Al2O6(s)	FToxid solid
KOH(s)	FTsalt solid	Ca3MgAl4O10(s)	FToxid solid
K2SO4(s)	FTsalt solid_alpha	CaSiO3(s)	FToxid wollastonite
K3Na(SO4)2(s)	FTsalt solid	CaSiO3(s2)	FToxid ps-wollastonite
KCl(s)	FTsalt sylvite_(nacl_rock)	Ca2SiO4(s)	FToxid

CaO(s)	FTsalt lime		gamma(olivine)
Ca(OH)2(s)	FTsalt portlandite	Ca2SiO4(s2)	FToxid alpha-prime
CaCO3(s)	FTsalt aragonite	Ca3SiO5(s)	FToxid hatrurite
CaSO4(s)	FTsalt anhydrite	Ca3Si2O7(s)	FToxid rankinite
K2Ca2(CO3)3(s)	FTsalt solid	Na2Ca2Si3O9(s)	FToxid solid
K2Ca2(SO4)3(s)	FTsalt solid	CaMgSi2O6(s)	FToxid diopside(cl-pyroxene)
		Ca2MgSi2O7(s)	FToxid akermanite(melilite)
		Ca3MgSi2O8(s)	FToxid merwinite
		CaAl2Si2O8(s2)	FToxid anorthite
		Ca2Al2SiO7(s)	FToxid gehlenite
		Ca3Al2Si3O12(s)	FToxid grossularite
		Fe2O3(s)	FToxid hematite
		Fe2SiO4(s)	FToxid fayalite
		Ca3Fe2Si3O12(s)	FToxid andradite(garnet

Table I-12. List of the solutions used in the phase equilibrium calculations.

Liquid solutions:
FToxid-slag-A: Al_2O_3-CaO-FeO-Fe_2O_3-MgO-SiO_2 + Na_2O+K_2O Salt melt (SALT-F): (K, Na)(SO_4, CO_3, Cl, OH)
Solid solutions:
(Na, K)2(SO4, CO3) (ss) (Na, K)(Cl) (ss) Complex silicates (wollastonite, olivine, mulite)

I-5. Slag Viscosity Formulas

The model used to determine viscosities is that of Kalmanovitch or the so-called ‘‘modified Urbain model” [148]. The model is based on the following calculations:

Step 1: Determination of the molar fractions of all components based on the chemical oxide composition. Fe_2O_3 is converted to equivalent FeO.

Step 2: Calculation of the *M* parameter:

$$M = \mathrm{CaO} + \mathrm{MgO} + \mathrm{Na_2O} + \mathrm{K_2O} + \mathrm{FeO} + 2\mathrm{TiO_2} \quad \text{(I-69)}$$

Step 3: Calculation of the α parameter:

$$\alpha = M/(M + \mathrm{Al_2O_3}) \quad \text{(I-70)}$$

Step 4: Calculation of the *B* parameter, where:

$$B = B0 + B1 \cdot SiO_2 + B2 \cdot (\mathrm{SiO_2})^2 + B3 \cdot (\mathrm{SiO_2})^3 \quad \text{(I-71)}$$

$$B0 = 13.8 + 39.9355\,\alpha - 44.049 \cdot (\alpha^2) \quad \text{(I-72)}$$

$$B1 = 30.481 - 117.1505 \cdot \alpha + 129.9978 \cdot (\alpha^2) \quad \text{(I-73)}$$

$$B2 = -40.9429 + 234.0486 \cdot \alpha - 300.04 \cdot (\alpha^2) \quad \text{(I-74)}$$

$$B3 = 60.7619 - 153.9276 \cdot \alpha + 211.1616 \cdot (\alpha^2) \quad \text{(I-75)}$$

Step 5:

$$\ln[A] = -(0.2812 \cdot B + 11.8279) \quad \text{(I-76)}$$

Step 6:

$$\ln \mu = \ln[A] + \ln[T] + (1000 \cdot B/T) \quad \text{(I-77)}$$

Step 7: Conversion of the natural logarithm $\ln\mu$ into $\log_{10}\mu$.

According to van Dyk *et al*. [148] the modified Urbain model can predict both viscosities of bulk coal ash melts as well as simple oxide glasses, with specific emphasis on CaO–MgO–Al_2O_3–SiO_2 systems.

I-6. Optimisation of Coal/Biomass Blends – Calculations

According to defined in Chapter 5 (sec. 5.2.3.2) slagging/HT fouling indices: three fuel related factors are of most importance in the assessment of slagging severity such as the average slag ratio, viscosity of the slag at the reference temperature and ash concentration in the flue gas. The average slag ratios for both specified regions are assessed by approximating the region under the slag ratio curve, calculating its area, and then divided by the temperature range considered, as follows (see Figure I-3):

$$\bar{f} = \frac{1}{b-a}\int_a^b f(x)dx \approx \frac{1}{b-a}\sum_{i=1}^{n} f(x_i)\Delta x_i \rightarrow \textit{for slagging}: \bar{\phi}_{SL} = \frac{1}{t_c - t_b}\sum_{i=1}^{n}\phi(t_i)\Delta t_i$$
$$\rightarrow \textit{for HT fouling}: \bar{\phi}_{HTF} = \frac{1}{t_b - t_a}\sum_{i=1}^{n}\phi(t_i)\Delta t_i \qquad \text{(I-78)}$$

The temperature range is divided into interval Δt_i of 25°C. Considering the shape of the slag distribution curve, the trapezoidal rule can be applied to obtain the best approximation of the area under the curve. This is calculated by the Delphi package integrated algorithm.

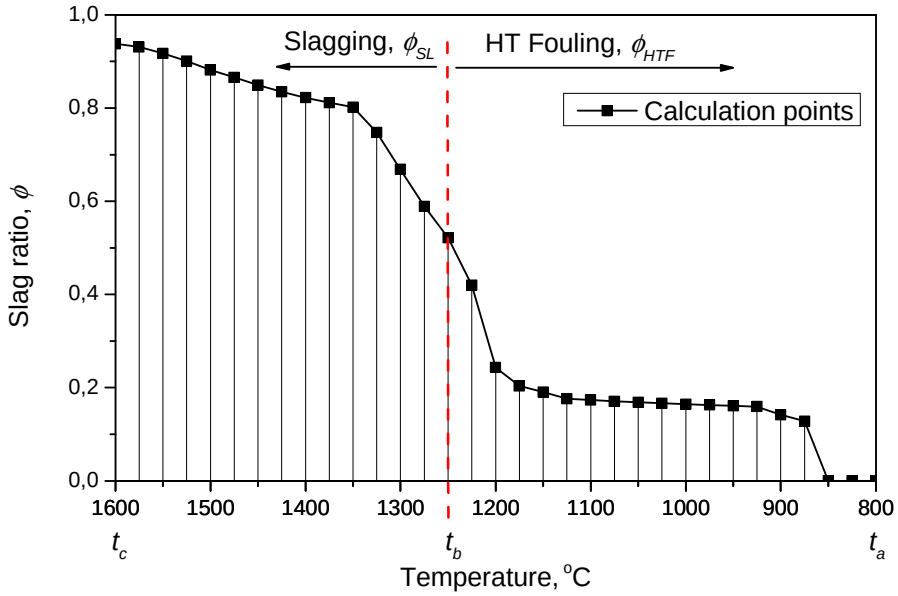

Figure I-3. Illustration of the slag ratios distribution for slagging and HT fouling regions with shown calculation points with the space interval of 25°C.

The calculated slagging/HT fouling key parameters used to optimise coal/biomass blends composed of the investigated pure coal blends (CO1, SA3 and AL1) and then co-fired with 20th% of straw (DS2) are summarised in tables I-13 and I-14. Additionally, the stickiness ratios are calculated ($\bar{\phi}_{SL(HTF)}/\log_{10}\mu_{Temp}$) which are then normalised according to the eq. 6.4 (Chapter 5, sec. 5.3.5.1) including both the assumed critical stickiness and its maximum

values obtained (see Table I-13, case: AL1-70, CO1-30, and Table I-14, CO1-80, DS2-20, respectively; both cases are marked in red colour).

Table I-13. Summary of the calculated slagging/HT fouling key parameters for the investigated coal blends.

FUEL MIX RATIOS, th%			Average Slag Ratio, Slag Viscosity, Ash Concentration				SLAGGING		HT FOULING	
CO1	SA3	AL1	$\bar{\phi}_{SL}$	$\bar{\phi}_{HTF}$	$Log_{10}\mu_{Temp}$	C_{ash}, g/kg gas	$\frac{\bar{\phi}_{SL}}{Log_{10}\mu_{Temp}}$	$\left(\frac{\bar{\phi}_{SL}}{Log_{10}\mu_{Temp}}\right)_{Norm}$	$\frac{\bar{\phi}_{HTF}}{Log_{10}\mu_{Temp}}$	$\left(\frac{\bar{\phi}_{HTF}}{Log_{10}\mu_{Temp}}\right)_{Norm}$
100	0	0	0.821	0.321	5.805	6.819	0.141	0.898	0.055	0.761
90	10	0	0.810	0.285	5.810	7.283	0.139	0.833	0.049	0.637
80	20	0	0.794	0.252	5.815	7.745	0.137	0.739	0.043	0.526
70	30	0	0.775	0.222	5.822	8.205	0.133	0.632	0.038	0.425
60	40	0	0.756	0.195	5.829	8.663	0.130	0.516	0.033	0.333
50	50	0	0.733	0.170	5.838	9.119	0.126	0.383	0.029	0.250
40	60	0	0.694	0.148	5.848	9.574	0.119	0.158	0.025	0.173
30	70	0	0.667	0.133	5.860	10.027	0.114	0.002	0.023	0.122
20	80	0	0.641	0.107	5.875	10.478	0.109	-0.157	0.018	0.037
10	90	0	0.613	0.090	5.894	10.928	0.104	-0.317	0.015	-0.024
0	100	0	0.587	0.076	5.917	11.375	0.099	-0.476	0.013	-0.070
90	0	10	0.781	0.255	5.803	8.654	0.135	0.676	0.044	0.540
80	0	20	0.750	0.218	5.800	10.427	0.129	0.503	0.038	0.413
70	0	30	0.723	0.181	5.797	12.140	0.125	0.357	0.031	0.289
60	0	40	0.703	0.152	5.794	13.797	0.121	0.244	0.026	0.193
50	0	50	0.686	0.130	5.791	15.401	0.118	0.149	0.022	0.117
40	0	60	0.671	0.111	5.787	16.953	0.116	0.069	0.019	0.053
30	0	70	0.658	0.095	5.782	18.456	0.114	0.000	0.016	0.000
20	0	80	0.647	0.082	5.777	19.913	0.112	-0.058	0.014	-0.045
10	0	90	0.638	0.070	5.771	21.325	0.111	-0.108	0.012	-0.083
0	0	100	0.629	0.060	5.763	22.695	0.109	-0.150	0.010	-0.116
0	10	90	0.633	0.061	5.776	21.562	0.110	-0.139	0.011	-0.114
0	20	80	0.636	0.062	5.789	20.428	0.110	-0.132	0.011	-0.110
0	30	70	0.638	0.063	5.803	19.295	0.110	-0.128	0.011	-0.108
0	40	60	0.640	0.064	5.818	18.162	0.110	-0.124	0.011	-0.104
0	50	50	0.642	0.066	5.833	17.030	0.110	-0.124	0.011	-0.100
0	60	40	0.619	0.067	5.848	15.898	0.106	-0.259	0.011	-0.096
0	70	30	0.617	0.069	5.864	14.767	0.105	-0.283	0.012	-0.091
0	80	20	0.611	0.071	5.881	13.636	0.104	-0.323	0.012	-0.085
0	90	10	0.602	0.073	5.899	12.505	0.102	-0.384	0.012	-0.078
80	10	10	0.770	0.228	5.808	9.018	0.133	0.610	0.039	0.445
70	10	20	0.739	0.194	5.805	10.753	0.127	0.440	0.034	0.334
60	10	30	0.715	0.155	5.803	12.443	0.123	0.305	0.027	0.201
50	10	40	0.695	0.136	5.800	14.084	0.120	0.195	0.023	0.138
40	10	50	0.679	0.115	5.796	15.674	0.117	0.105	0.020	0.068
30	10	60	0.664	0.098	5.792	17.215	0.115	0.028	0.017	0.010
20	10	70	0.652	0.084	5.788	18.709	0.113	-0.038	0.014	-0.038
10	10	80	0.642	0.072	5.782	20.157	0.111	-0.093	0.012	-0.078
70	20	10	0.756	0.202	5.814	9.439	0.130	0.527	0.035	0.359
60	20	20	0.726	0.166	5.811	11.135	0.125	0.365	0.028	0.236
50	20	30	0.703	0.144	5.809	12.796	0.121	0.237	0.025	0.163

40	20	40	0.685	0.121	5.806	14.413	0.118	0.134	0.021	0.085
30	20	50	0.670	0.102	5.803	15.985	0.115	0.051	0.018	0.022
20	20	60	0.657	0.086	5.799	17.511	0.113	-0.020	0.015	-0.030
10	20	70	0.645	0.073	5.795	18.991	0.111	-0.080	0.013	-0.073
60	30	10	0.740	0.187	5.820	9.874	0.127	0.435	0.032	0.306
50	30	20	0.713	0.153	5.818	11.538	0.123	0.283	0.026	0.193
40	30	30	0.692	0.127	5.816	13.173	0.119	0.166	0.022	0.106
30	30	40	0.675	0.106	5.814	14.768	0.116	0.072	0.018	0.036
20	30	50	0.660	0.089	5.811	16.320	0.114	-0.006	0.015	-0.021
10	30	60	0.648	0.075	5.807	17.829	0.112	-0.072	0.013	-0.067
50	40	10	0.724	0.157	5.828	10.312	0.124	0.342	0.027	0.207
40	40	20	0.700	0.129	5.827	11.952	0.120	0.204	0.022	0.111
30	40	30	0.680	0.111	5.825	13.562	0.117	0.096	0.019	0.052
20	40	40	0.665	0.092	5.823	15.136	0.114	0.010	0.016	-0.010
10	40	50	0.651	0.077	5.821	16.670	0.112	-0.063	0.013	-0.061
40	50	10	0.706	0.143	5.837	10.752	0.121	0.234	0.025	0.159
30	50	20	0.685	0.112	5.836	12.370	0.117	0.113	0.019	0.054
20	50	30	0.668	0.096	5.835	13.960	0.114	0.018	0.016	0.002
10	50	40	0.654	0.080	5.834	15.514	0.112	-0.058	0.014	-0.054
30	60	10	0.669	0.124	5.848	11.191	0.114	0.016	0.021	0.094
20	60	20	0.649	0.096	5.848	12.791	0.111	-0.095	0.016	0.001
10	60	30	0.633	0.082	5.848	14.362	0.108	-0.184	0.014	-0.046
20	70	10	0.646	0.106	5.861	11.631	0.110	-0.115	0.018	0.033
10	70	20	0.630	0.086	5.863	13.214	0.107	-0.208	0.015	-0.035
10	80	10	0.624	0.089	5.878	12.069	0.106	-0.249	0.015	-0.025

Table I-14. Summary of the calculated slagging/HT fouling key parameters for the investigated coal blends co-fired with 20th% straw (DS2).

FUEL MIX RATIOS, th%				Average Slag Ratio, Slag Viscosity, Ash Concentration				SLAGGING		HT FOULING	
CO1	SA3	AL1	DS2	$\bar{\phi}_{SL}$	$\bar{\phi}_{HTF}$	$\log_{10}\mu$	C_{ash}, g/kg gas	$\frac{\bar{\phi}_{SL}}{Log_{10}\mu_{Temp}}$	$\left(\frac{\bar{\phi}_{SL}}{Log_{10}\mu_{Temp}}\right)_{Norm}$	$\frac{\bar{\phi}_{HTF}}{Log_{10}\mu_{Temp}}$	$\left(\frac{\bar{\phi}_{HTF}}{Log_{10}\mu_{Temp}}\right)_{Norm}$
80	0	0	20	0.846	0.396	5.856	7.103	0.144	1.000	0.068	1.000
72	8	0	20	0.829	0.368	5.830	7.417	0.142	0.924	0.063	0.914
64	16	0	20	0.797	0.342	5.805	7.731	0.137	0.763	0.059	0.832
56	24	0	20	0.773	0.318	5.780	8.046	0.134	0.647	0.055	0.754
48	32	0	20	0.768	0.293	5.765	8.362	0.133	0.633	0.051	0.672
40	40	0	20	0.729	0.270	5.744	8.679	0.127	0.425	0.047	0.598
32	48	0	20	0.706	0.250	5.722	8.996	0.123	0.309	0.044	0.534
24	56	0	20	0.667	0.230	5.697	9.314	0.117	0.104	0.040	0.470
16	64	0	20	0.645	0.216	5.671	9.633	0.114	-0.006	0.038	0.423
8	72	0	20	0.622	0.193	5.654	9.952	0.110	-0.123	0.034	0.345
0	80	0	20	0.613	0.174	5.637	10.273	0.109	-0.163	0.031	0.284
72	0	8	20	0.803	0.352	5.913	8.197	0.136	0.713	0.059	0.842
64	0	16	20	0.771	0.304	6.027	9.304	0.128	0.457	0.050	0.665
56	0	24	20	0.751	0.268	6.037	10.424	0.124	0.342	0.044	0.546
48	0	32	20	0.726	0.238	6.046	11.556	0.120	0.205	0.039	0.448
40	0	40	20	0.706	0.214	6.056	12.701	0.117	0.088	0.035	0.371
32	0	48	20	0.687	0.196	6.065	13.857	0.113	-0.016	0.032	0.309

24	0	56	20	0.656	0.180	6.074	15.025	0.108	-0.192	0.030	0.257
16	0	64	20	0.655	0.166	6.082	16.204	0.108	-0.200	0.027	0.214
8	0	72	20	0.625	0.152	6.089	17.395	0.103	-0.365	0.025	0.166
0	0	80	20	0.612	0.142	6.097	18.595	0.100	-0.436	0.023	0.135
0	8	72	20	0.634	0.144	6.099	17.735	0.104	-0.320	0.024	0.140
0	16	64	20	0.622	0.150	6.100	16.881	0.102	-0.390	0.025	0.159
0	24	56	20	0.644	0.156	6.103	16.033	0.106	-0.270	0.026	0.179
0	32	48	20	0.632	0.160	6.105	15.190	0.104	-0.336	0.026	0.190
0	40	40	20	0.637	0.163	6.108	14.354	0.104	-0.311	0.027	0.201
0	48	32	20	0.640	0.169	6.110	13.524	0.105	-0.295	0.028	0.221
0	56	24	20	0.622	0.181	6.069	12.701	0.102	-0.372	0.030	0.262
0	64	16	20	0.618	0.182	5.917	11.885	0.104	-0.306	0.031	0.281
0	72	8	20	0.611	0.187	5.784	11.075	0.106	-0.265	0.032	0.312
64	8	8	20	0.783	0.326	5.911	8.514	0.133	0.609	0.055	0.758
56	8	16	20	0.751	0.285	6.026	9.624	0.125	0.354	0.047	0.605
48	8	24	20	0.724	0.251	6.047	10.747	0.120	0.194	0.042	0.492
40	8	32	20	0.701	0.225	6.057	11.882	0.116	0.061	0.037	0.405
32	8	40	20	0.680	0.205	6.066	13.030	0.112	-0.054	0.034	0.341
24	8	48	20	0.662	0.188	6.076	14.189	0.109	-0.158	0.031	0.285
16	8	56	20	0.645	0.170	6.084	15.360	0.106	-0.252	0.028	0.226
8	8	64	20	0.630	0.156	6.091	16.542	0.103	-0.338	0.026	0.180
56	16	8	20	0.761	0.304	5.901	8.831	0.129	0.495	0.052	0.688
48	16	16	20	0.733	0.268	6.019	9.945	0.122	0.257	0.045	0.551
40	16	24	20	0.708	0.238	6.058	11.071	0.117	0.101	0.039	0.449
32	16	32	20	0.687	0.213	6.068	12.209	0.113	-0.018	0.035	0.366
24	16	40	20	0.669	0.194	6.077	13.360	0.110	-0.123	0.032	0.304
16	16	48	20	0.652	0.178	6.085	14.522	0.107	-0.220	0.029	0.251
8	16	56	20	0.652	0.161	6.093	15.696	0.107	-0.220	0.026	0.196
48	24	8	20	0.741	0.284	5.889	9.150	0.126	0.391	0.048	0.622
40	24	16	20	0.715	0.252	6.011	10.266	0.119	0.169	0.042	0.500
32	24	24	20	0.694	0.226	6.069	11.395	0.114	0.015	0.037	0.407
24	24	32	20	0.658	0.191	6.087	13.691	0.108	-0.189	0.031	0.293
16	24	40	20	0.641	0.167	6.095	14.856	0.105	-0.280	0.027	0.214
8	24	48	20	0.640	0.150	6.105	0.000	0.105	-0.293	0.025	0.160
40	32	8	20	0.722	0.265	5.874	9.469	0.123	0.297	0.045	0.562
32	32	16	20	0.699	0.238	5.996	10.588	0.117	0.090	0.040	0.455
24	32	24	20	0.680	0.215	6.081	11.721	0.112	-0.065	0.035	0.371
16	32	32	20	0.663	0.194	6.090	12.865	0.109	-0.160	0.032	0.303
8	32	40	20	0.647	0.176	6.097	14.022	0.106	-0.252	0.029	0.242
32	40	8	20	0.704	0.246	5.852	9.788	0.120	0.212	0.042	0.502
24	40	16	20	0.684	0.223	5.976	10.911	0.114	0.020	0.037	0.407
16	40	24	20	0.667	0.207	6.085	12.047	0.110	-0.136	0.034	0.346
8	40	32	20	0.652	0.183	6.100	13.195	0.107	-0.227	0.030	0.266
24	48	8	20	0.668	0.230	5.824	10.109	0.115	0.029	0.039	0.451
16	48	16	20	0.650	0.213	5.952	11.235	0.109	-0.149	0.036	0.378
8	48	24	20	0.636	0.190	6.075	12.374	0.105	-0.300	0.031	0.290
8	56	16	20	0.634	0.200	5.927	11.559	0.107	-0.222	0.034	0.338
16	56	8	20	0.649	0.216	5.801	10.430	0.112	-0.062	0.037	0.408
8	64	8	20	0.631	0.196	5.792	10.752	0.109	-0.162	0.034	0.342

I-7. Langerlo Boiler Geometry

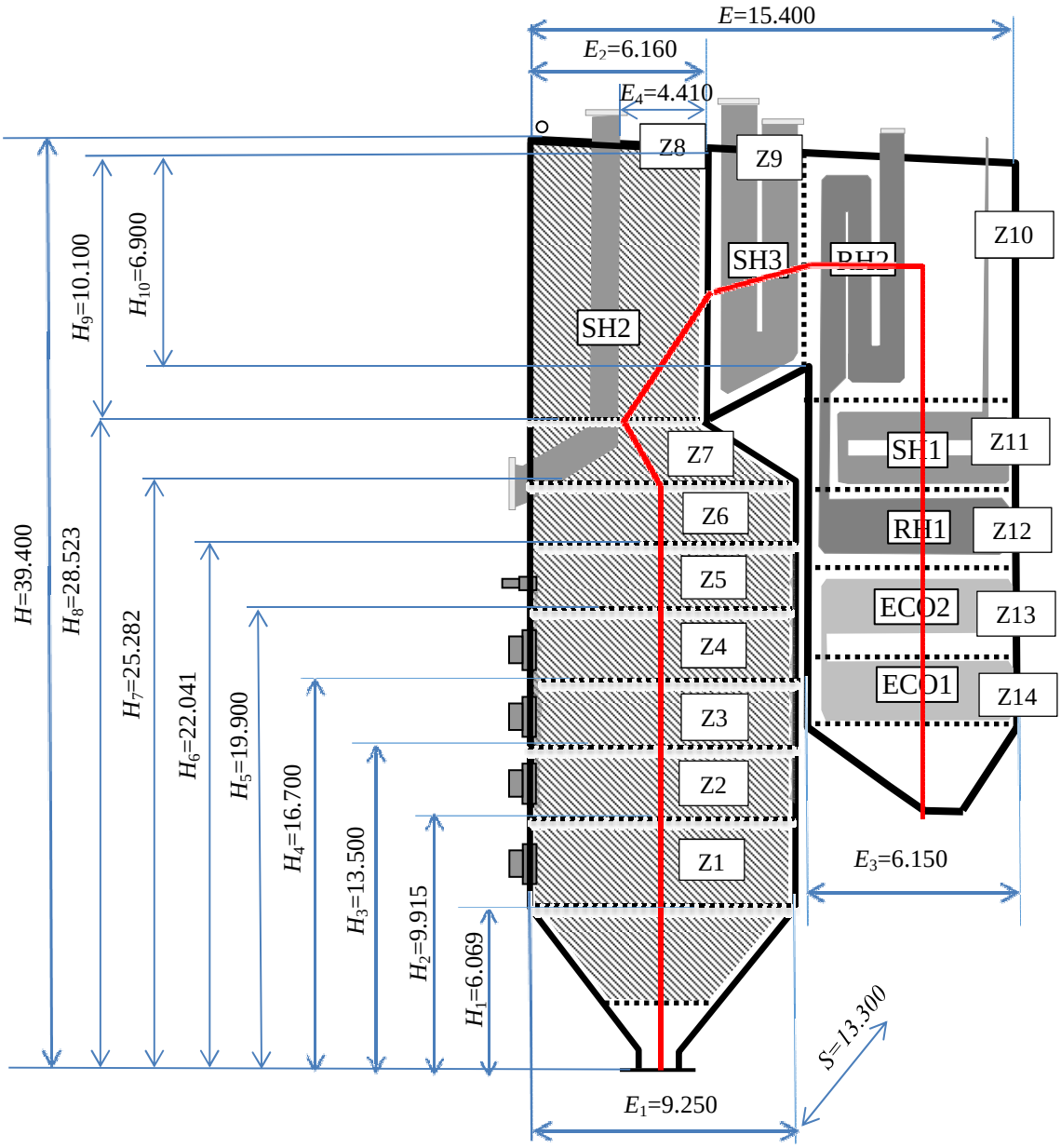

Figure I-4. Langerlo boiler geometry.

Table I-15. Dimensions of the zones – Langerlo boiler [54, 139**]**.

NO ZONE	Zone dimensions, m
Z1	$[E_1 \cdot (H_2 - H_1) \cdot 2 + S \cdot (H_2 - H_1) \cdot 2] \cdot \psi_{w,1} + [E_1 \cdot S] \cdot \psi'_1 + [E_1 \cdot S] \cdot \psi''_1 =$ $= 173.455 \cdot \psi_{w,1} + 123.025 \cdot \psi_{w,1} + 123.025 \cdot 0.1$
Z2	$[E_1 \cdot (H_3 - H_2) \cdot 2 + S \cdot (H_3 - H_2) \cdot 2] \cdot \psi_{w,2} = 161.684 \cdot \psi_{w,2}$
Z3	$[E_1 \cdot (H_4 - H_3) \cdot 2 + S \cdot (H_4 - H_3) \cdot 2] \cdot \psi_{w,3} = 144.32 \cdot \psi_{w,3}$
Z4	$[E_1 \cdot (H_5 - H_4) \cdot 2 + S \cdot (H_5 - H_4) \cdot 2] \cdot \psi_{w,4} = 144.32 \cdot \psi_{w,4}$
Z5	$[E_1 \cdot (H_6 - H_5) \cdot 2 + S \cdot (H_6 - H_5) \cdot 2] \cdot \psi_{w,5} = 96.559 \cdot \psi_{w,5}$
Z6	$[w1 \cdot (h7 - h6) \cdot 2 + d \cdot (h7 - h6) \cdot 2] \cdot \psi_{w,6} = 146.169 \cdot \psi_{w,6}$
Z7	$\left[(E_1 + E_2) \cdot (H_8 - H_7) \cdot 0.5 \cdot 2 + S \cdot (H_8 - H_7) + S \cdot \left[(H_8 - H_7)^2 + (E_1 - E_2)^2\right]^{0.5}\right] \cdot \psi_{w,7} +$ $+ [E_2 \cdot S] \cdot \psi''_7 = 152.606 \cdot \psi_{w,7} + 81.928 \cdot \psi''_7$
Z8	$A_{SH2} \approx 300.0\ m^2$, $A'_8 = E_2 \cdot S = 6.16 \cdot 13.3 = 81.93\ m^2$, $A''_8 = H_9 \cdot S = 10.1 \cdot 13.3 = 134.3\ m^2$, $A_{w,8} = E_4 \cdot H_9 \cdot 2 + E_4 \cdot S = 147.7\ m^2$
Z9	$A_{SH3} \approx 750.0\ m^2$, $A'_9 = A''_8$, $A''_9 = H_9 \cdot S = 6.9 \cdot 13.3 = 91.8\ m^2$,
Z10	$A_{RH2} \approx 1400.0\ m^2$, $A'_{10} = A''_9$
Z11	$A_{SH1} \approx 2100.0\ m^2$
Z12	$A_{RH1} \approx 4500.0\ m^2$
Z13	$A_{ECO2} \approx 3000.0\ m^2$
Z14	$A_{ECO1} \approx 3300.0\ m^2$
Z15	$A_{APR} \approx 20900.0\ m^2$

Appendix II – Slagging Predictor – Software Structure and Capabilities

II–1. Structure of the Developed Application

In general, the current structure of the *Slagging Predictor* consists of the four main modules, namely zone method (1) and thermo-chemical equilibrium (2) modules, fuel navigation and database module (3) and CAD/CFD module (4) used for a boiler geometry/mesh design and link with the CFD tools - future development. The set of functions, algorithms or sub-models included within the specific modules are listed in Figure II-1.

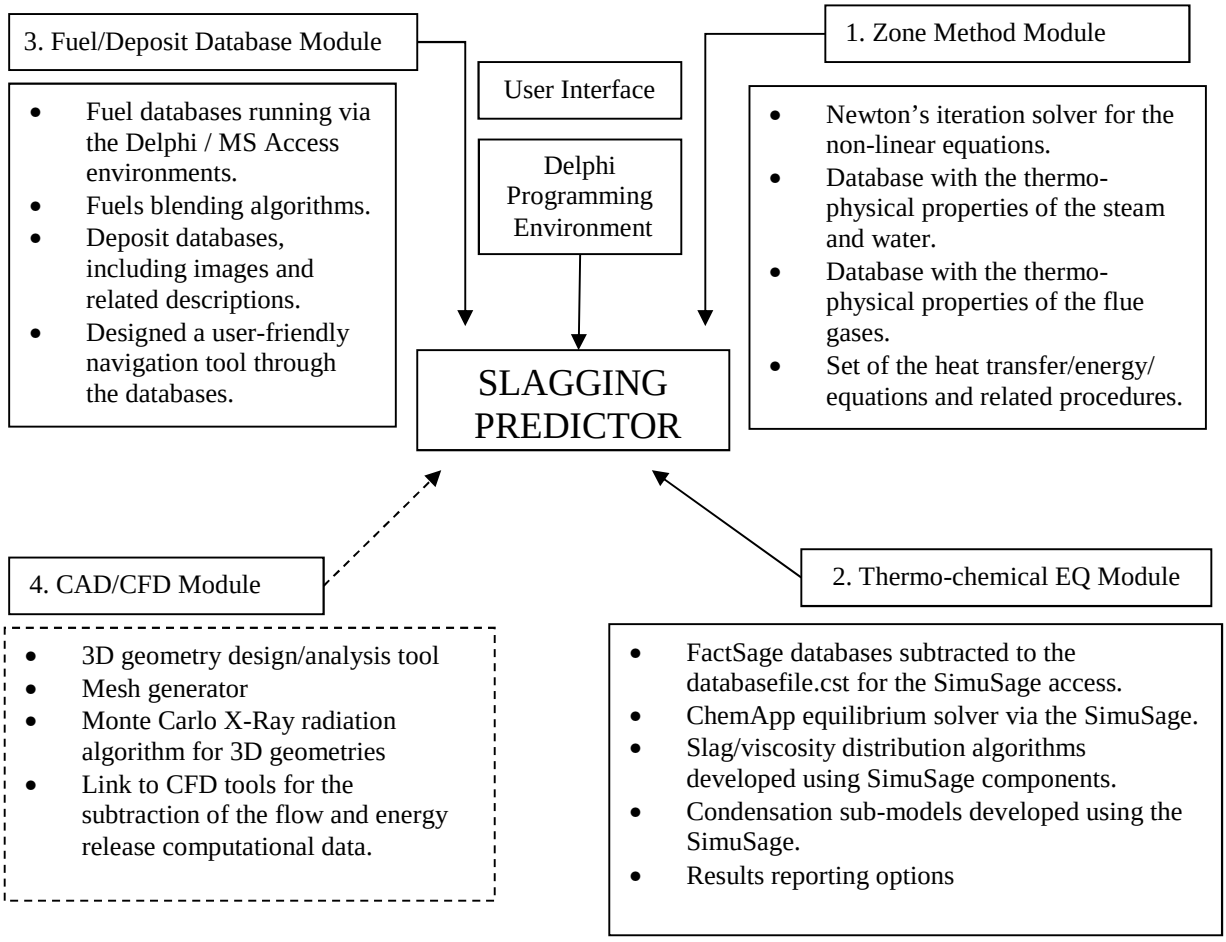

Figure II-1. Structure of the developed Slagging Predictor.

To enable easy navigation directly to all areas of the application there are seven sections designed within the menu of the *Slagging Predictor*. Functions and capabilities of these sections are summarised in Table II-1. Some of them are more advanced options and may be not available in a user friendly version.

Table II-1. Major sections of the menu of the developed application.

Section	Functions and capabilities
BLEND CALCULATOR	Input of fuel data into database. Fuels selection and blending (up to 5 individual fuels) with defined mass or thermal ratios. Assessment of the easily soluble (more reactive) REA-part of the ash-forming elements for a given biomass type (based on the chemical fractionation). Setting the interaction rate of silicates towards capturing the alkali metals released into the gas phase. Additionally, the ash deposits database is included. See Figures II-2..5.
BOILER	Setting boiler operational parameters, such as boiler load, fuel distribution, air excess. Defining boiler geometry and zones. The results obtained from zone model calculations are displayed in a numerical form, and include the temperatures of the flue gas and heating media as well as the heat transfer coefficients within the specific zones. See Figures II-6, 9..10.
1D TEMP PROFILE	Visualisation and comparison of the predicted results of the zone model in diagrams. See Figures II-7..8.
SLAGGING/FOULING	This section includes illustrative scheme of the developed high temperature slagging/fouling EQ model built with the aid of the SimuSage blocks. Visualisation and comparison of the predicted results (slag phase %, slag viscosity) of the slagging/fouling EQ module in diagrams. See Figures II-11..13.
SALTS DEPOSITION	This section includes illustrative scheme of the developed low temperature fouling EQ model built with the aid of the SimuSage blocks. Capable of predicting salts and aerosols formation. Apart from the graphical visualisation of the results, they can be also displayed in reporting form via the Report Editor of SimuSage. See Figures II-14..16.
HEAT TRANSFER	This section was designed to display graphically the impact of deposit accumulation on the heat transfer conditions change in analysed zone and its effect on the overall boiler performance.
INDICATORS	In this section, the predicted slagging/fouling indices are displayed and compared in diagrams.

II–2. Fuel Database and Blend Calculator

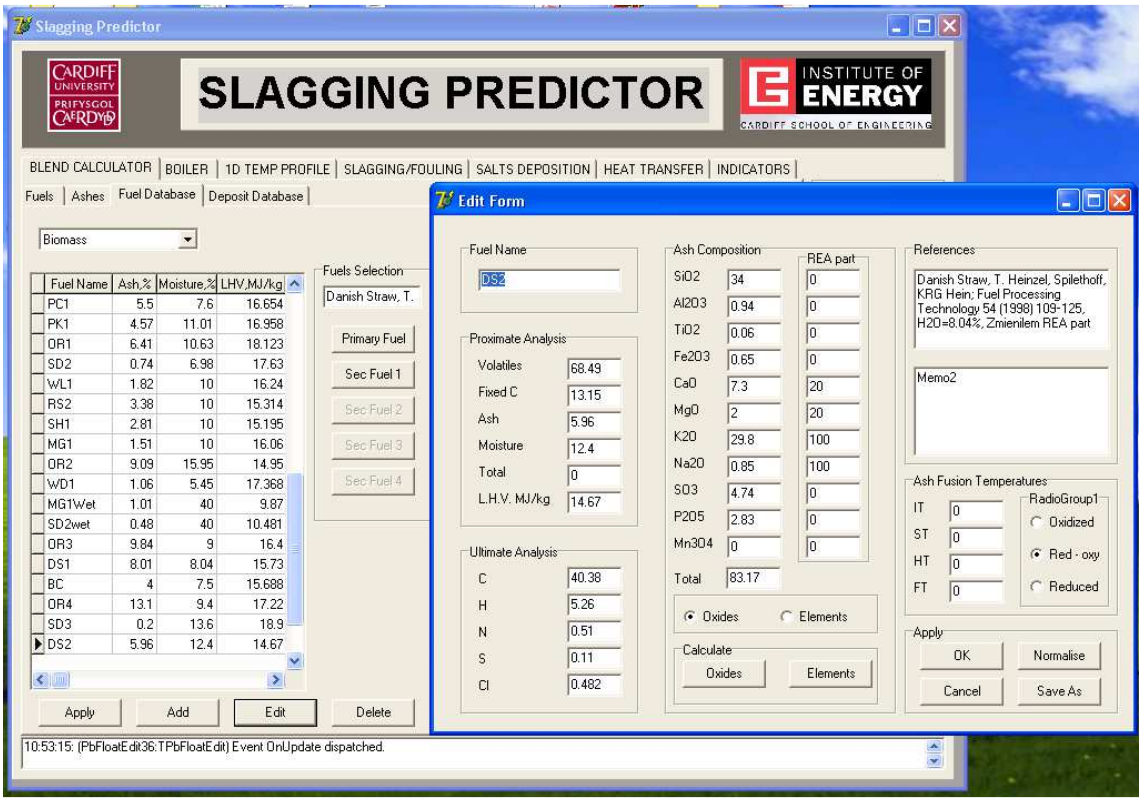

Figure II-2. Screenshot showing the fuel database and the input data algorithm.

The fuel database includes wide range of different quality coals and biomass fuels (currently > 20). Amongst biomass/waste group the following feedstocks can be found: energy crops (*miscanthus giganteus*, *sida hermafrodita*, willow), woody biomass (sawdust, wood pellets), agricultural residues (straw, olive residues, palm kernel etc.), animal residues (meat and bone meal) and sewage sludge.

Regarding the coal database, this includes various quality bituminous and lignite coals, namely South African, Colombian, Russian, Australian, Polish, US, Indonesian and others.

Fuel abbreviations on Figure II-2: PC – pine chips; PK – palm kernel; OR – olive residues; SD – sawdust; WL – willow; RS – rape straw; SH – *sida hermafrodita*; MG - *miscanthus giganteus*; WD – woody biomass; DS – Danish straw.

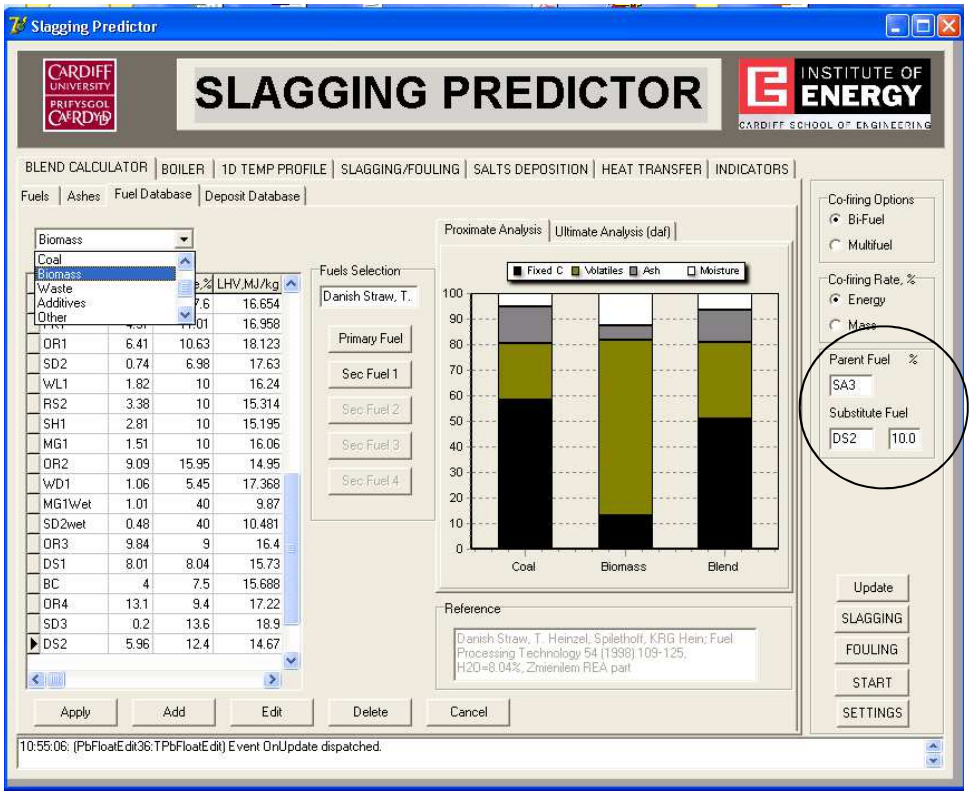

Figure II-3. Screenshot showing the fuel database and the fuel selection algorithm.

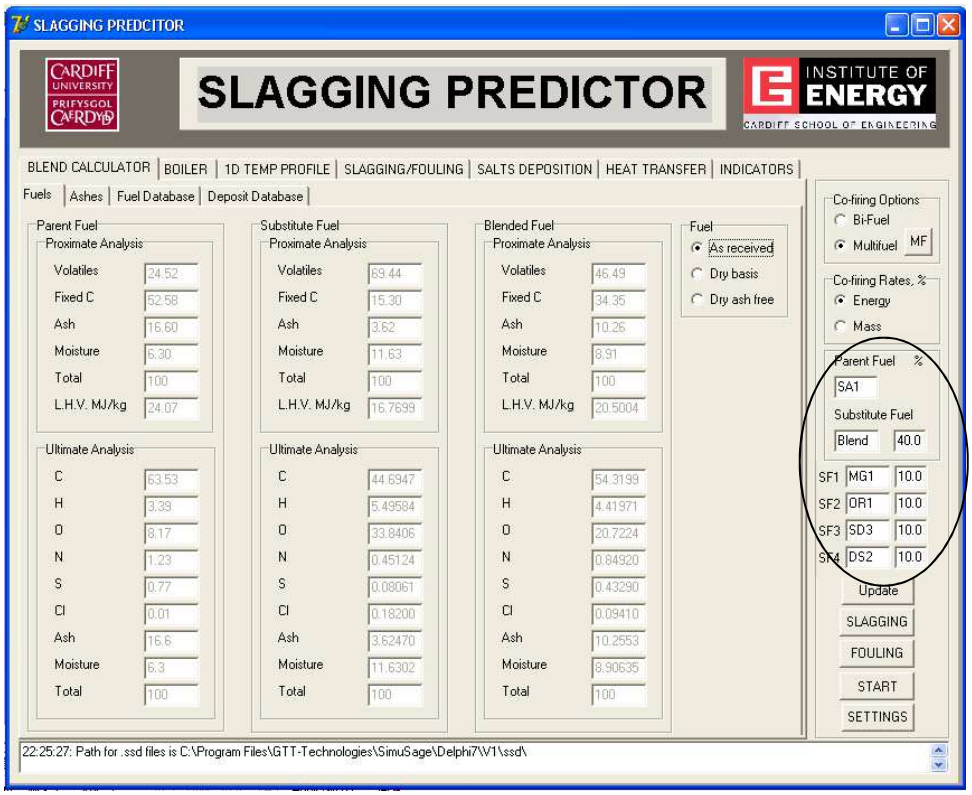

Figure II-4. Screenshot showing the user friendly interface of the developed Slagging Predictor.

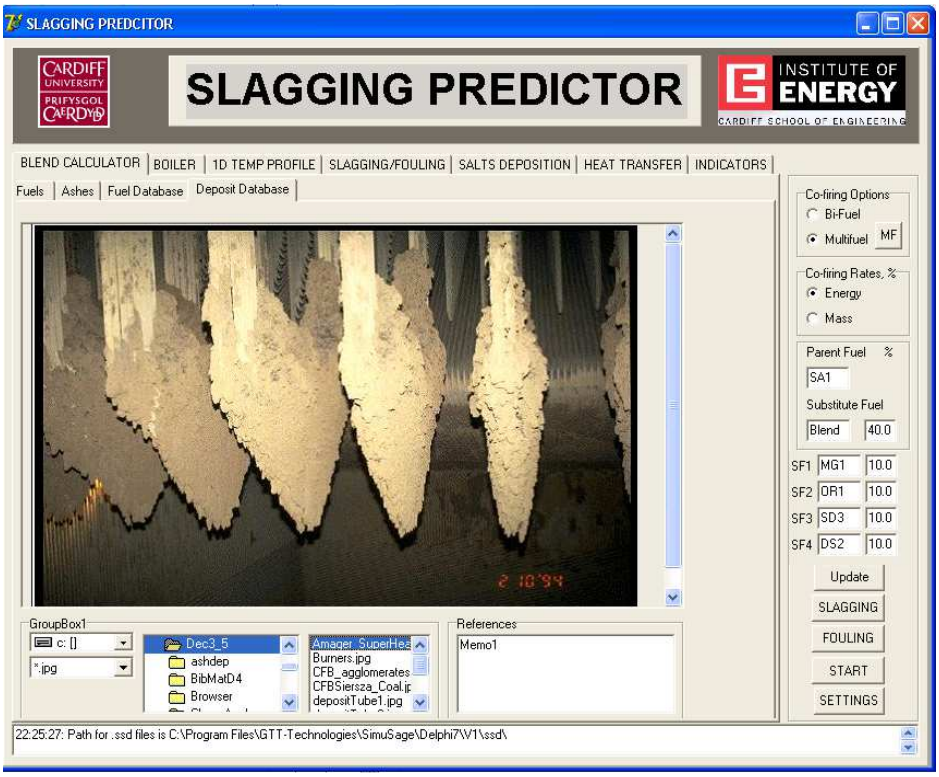

Figure II-5. Screenshot showing the concept of the ash deposit fuel databse

II–3. Boiler Input Data / Results Module

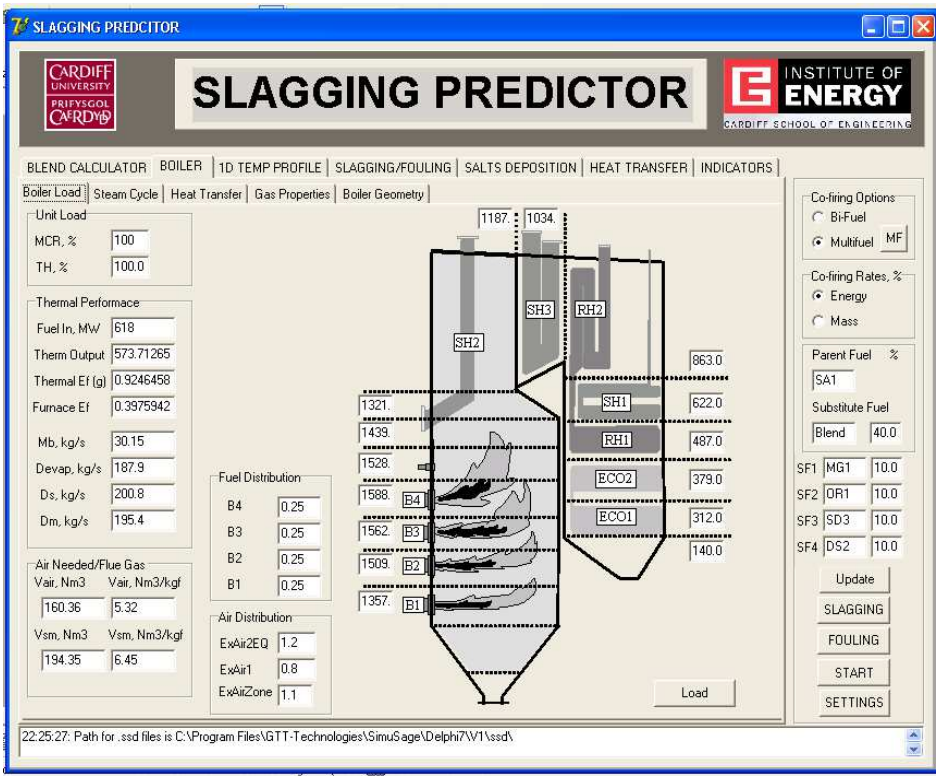

Figure II-6. Screenshot showing the boiler geometry, zones and main operational data of the investigated boiler.

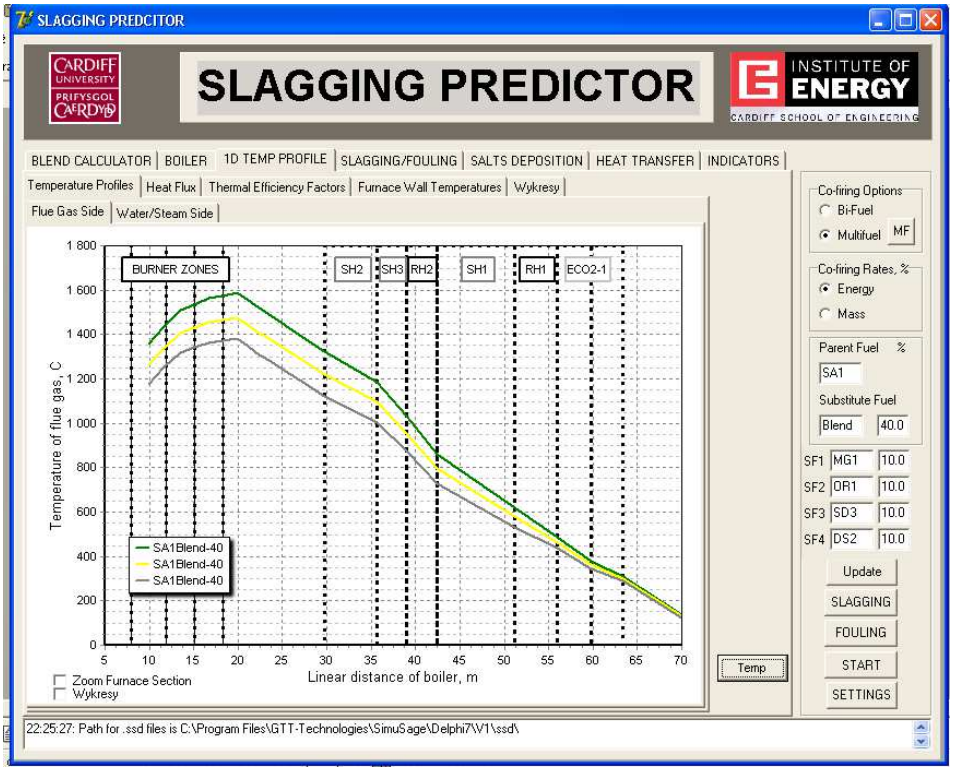

Figure II-7. Screenshot showing the predicted flue gas temperature profiles for various boiler's loads.

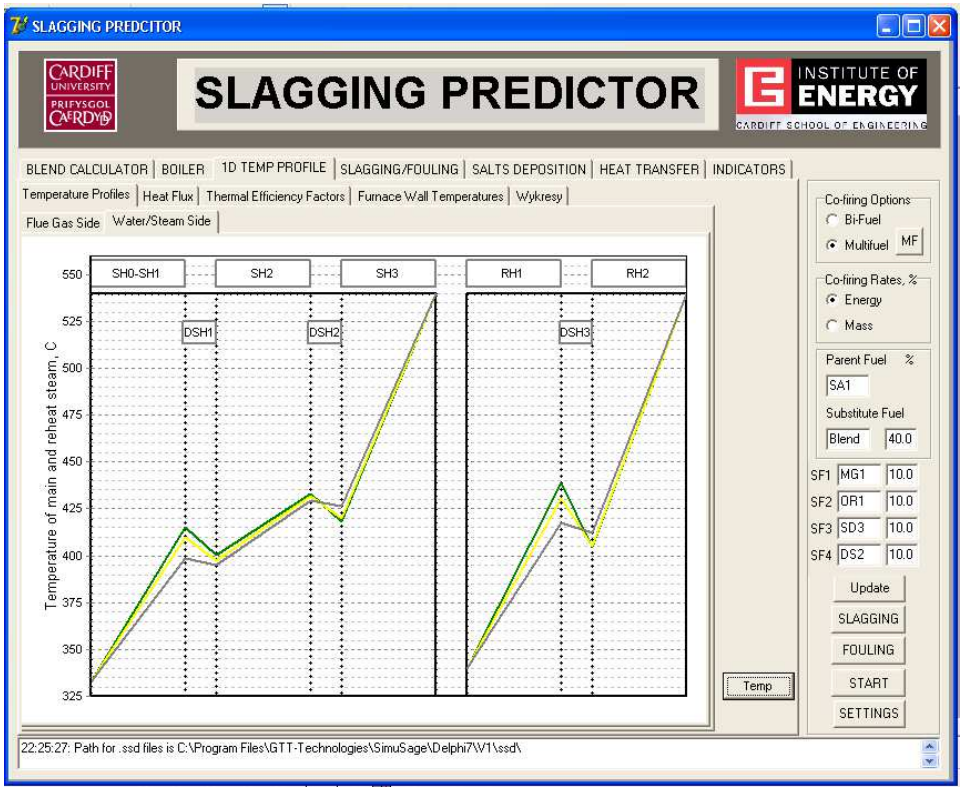

Figure II-8. Screenshot showing the predicted steam temperatures at the oulet of the subsequent steam heating sections (primary steam and reheated steam).

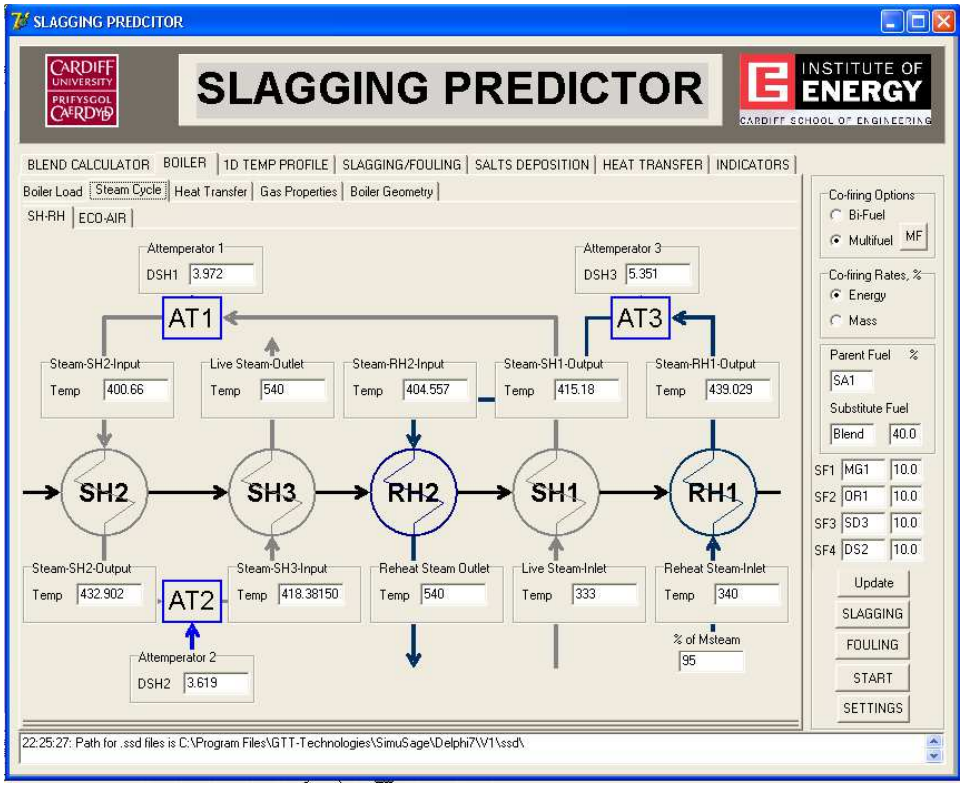

Figure II-9. Screenshot showing the thermal balance sheme for the heat transfer exchangers within the investigated boiler (for the primary and reheated steam sections).

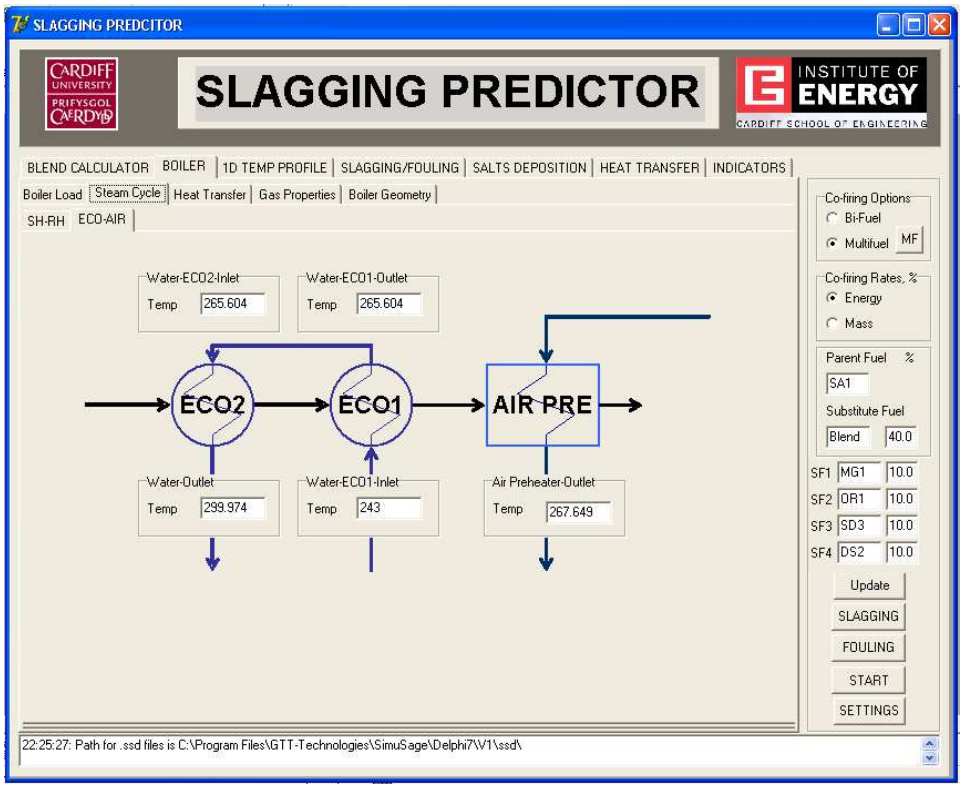

Figure II-10. Screenshot showing the thermal balance sheme for the economiser and air pre-heater sections.

II–4. SimuSage Flow-sheet Scheme for Slag and Viscosity Calculations – EQ1 Module

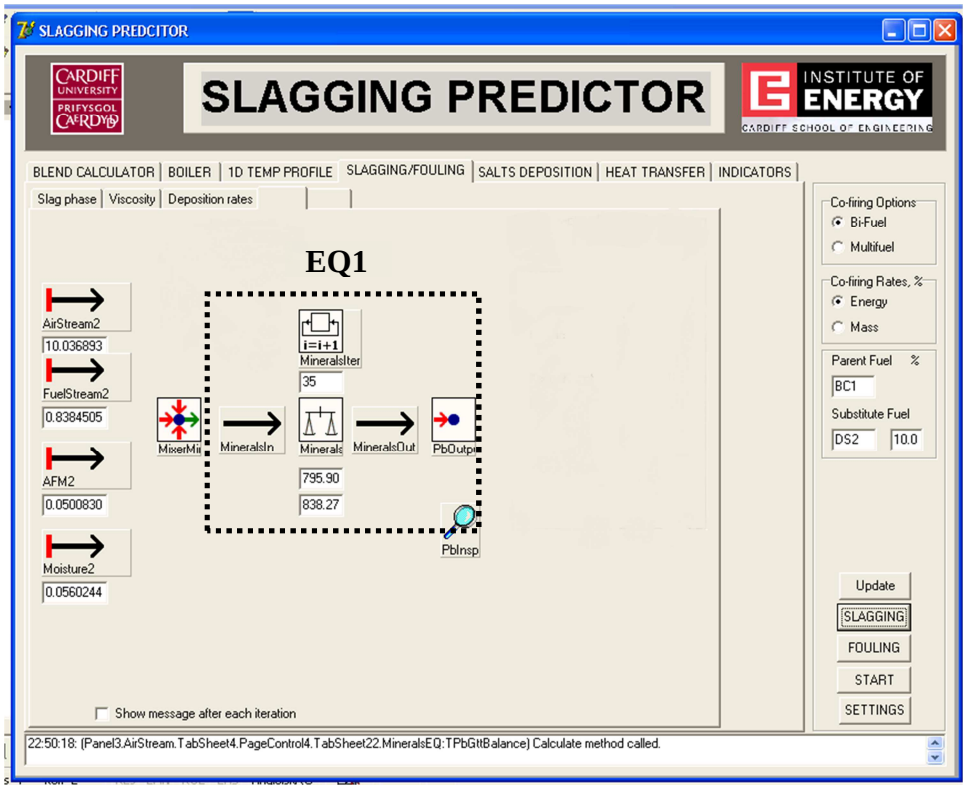

Figure II-11. Screenshot showing the implemented algorthm for the slag amount and viscosity calculations in EQ1 Module.

Where:

AirStream2 – mass stream (in kg) of the air required to burn 1 kg fuel, including excess air; FuelStream2 – mass stream (in kg) of combustible matter (including C, H, S and N) in 1 kg fuel; AFM2 – mass stream (in kg) of ash forming elemenmts (Si, Al, Fe, Ca, Mg, Na, K, Cl) in 1 kg fuel burnt; Moisture2 – mass stream (in kg) of moisture-H_2O in 1 kg fuel burnt; MixerMi – block enabling the mixing of the input streams. Minerals – the phase equilibrium calculations block; MineralsIn and MineralsOut – mass stream connectors between mixer (MixerMi) and phase equilibrium blocks, and phase equilibrium and PbOutput blocks, respectively; MineralsIter – iterative block used to define temperature intervals between phase equilibrium calculations.

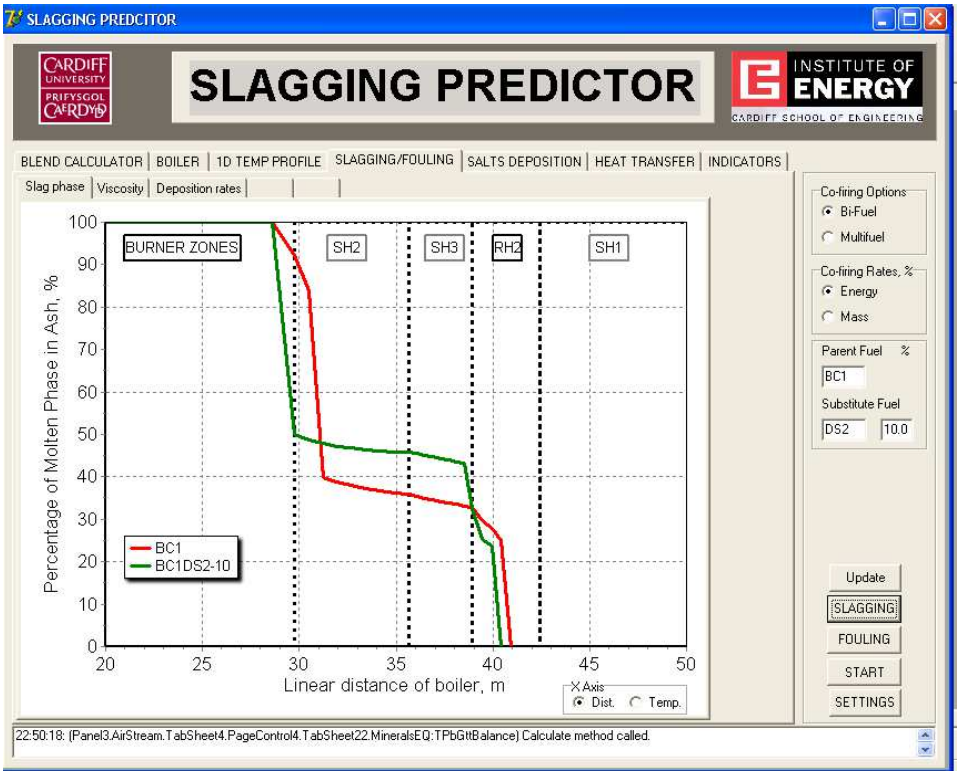

Figure II-12. Screenshots showing the ploted results of the slag amount and viscosity predictions obtained for a BC1 coal and with a blend of 10th% of straw (DS2).

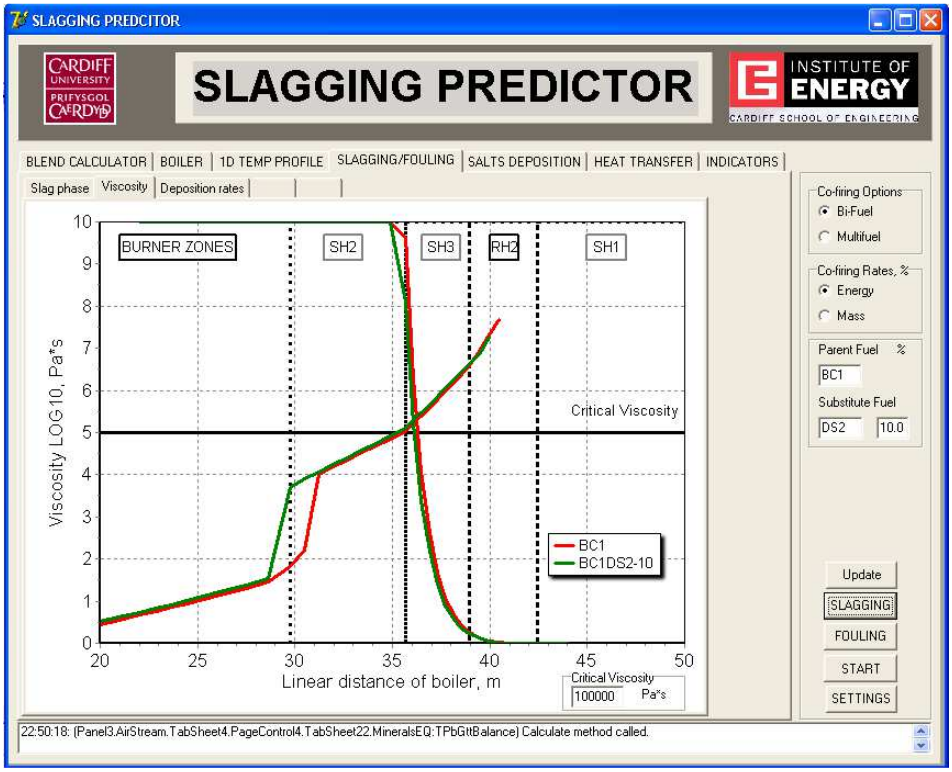

Figure II-13. Screenshots showing the ploted results of the slag amount and viscosity predictions obtained for the BC1 coal and for the 10th% blend with straw (DS2).

II–5. Development of a SimuSage Algorithm for Salts Condensation – EQ2 and EQ3 Modules

Figure II-14 shows the SimuSage flowsheet designed to assess the salts condensation downstream the furnace. There are three phase equilibrium stages implemented. The first one (EQ3) calculates the amount of interacted alkali metals at high temperature (1300^{o}C) with the reactive layer of the silicate-based ash. The captured mass of alkalis (in the SlagCond stream) is introduced to the EQ1 phase equilibrium module to assess its effect on the overall slag % and slag viscosity change (section II-4).

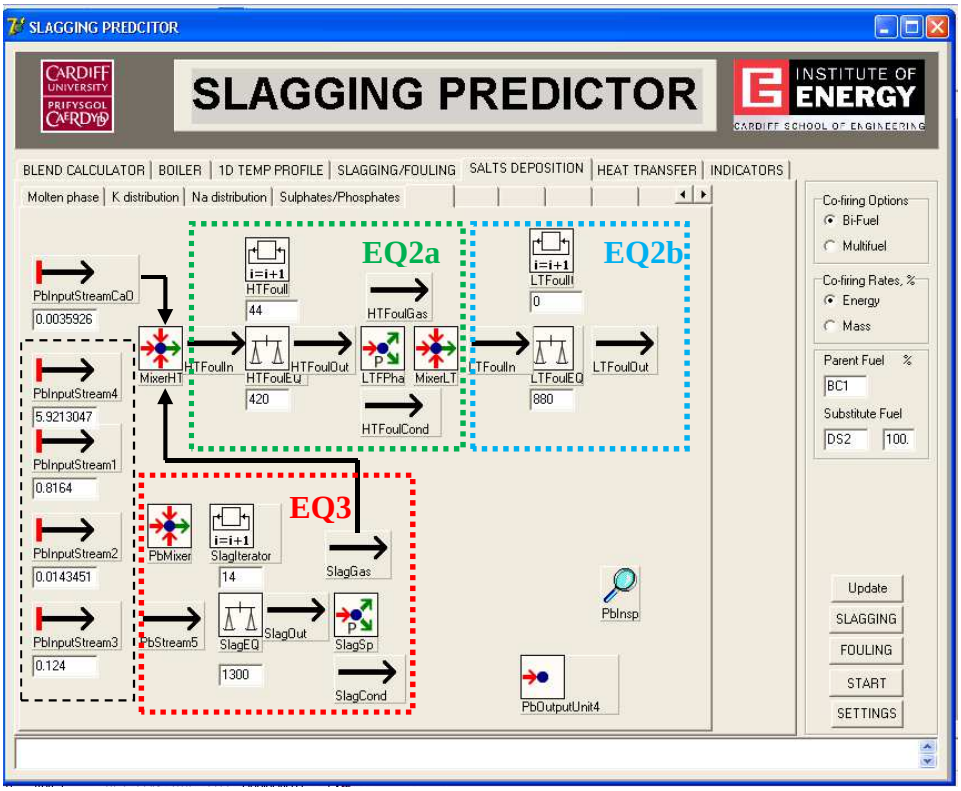

Figure II-14. Screenshot showing the designing stage of the implemented algorithm used for the assessment of the salts condensation downstream the furnace.

The remaining in the gas phase alkalis and other gasous species go through the second stage of phase equilibrium calculations (EQ2) in which the amount and speciation of the condensed phase is assesesed. The low temperature fouling module EQ2 can perform calculations for the whole temperature range or in two divided temperature ranges, e.g. 1300 ^{o}C-900^{o}C and 900 ^{o}C -500^{o}C between which the amount of condesed phase in these two steps (HTFoulCond and LTFoulOut streams respectively) is calculated. Apart form the gaseous species enetering the EQ2 module (via the SlagGas stream), additionally a part of unreacted with slicates/slag solid CaO particles can be introduced (via the PbInputStreamCaO stream. This may lead to $CaSO_4$

formation, and thus affecting sulphur availibility for the alkali sulphates formation incresing the risk of alkali chlorides presence.

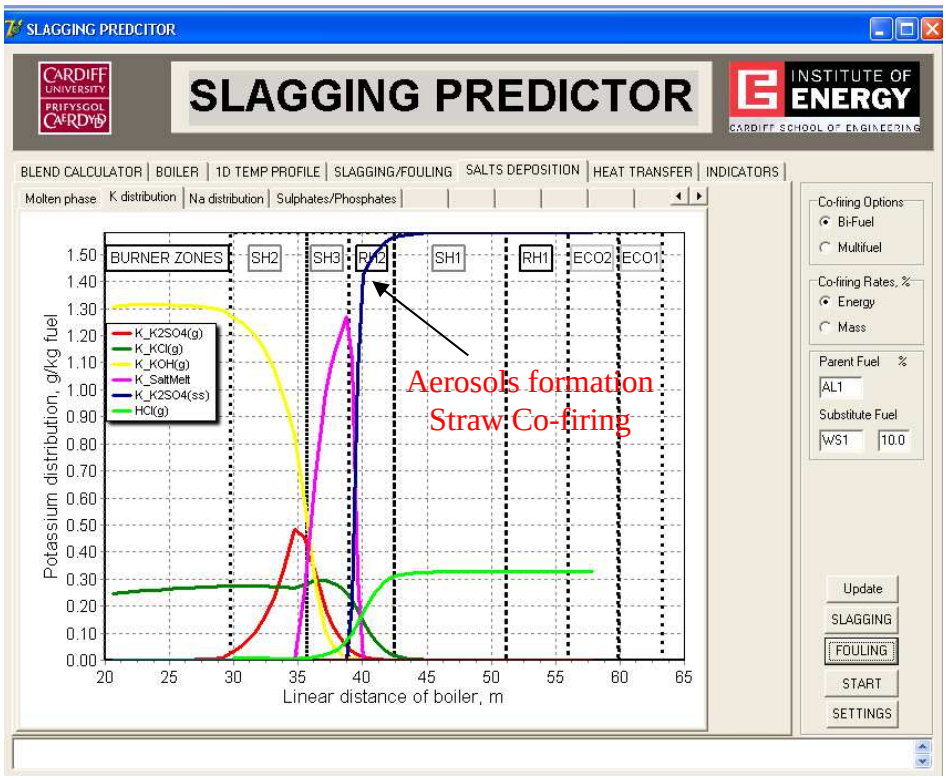

Figure II-15. Screenshot showing the predicted potassium distribution and aerosols formation throughtout the boiler when co-firing straw with coal for the 10th% coal substitution.

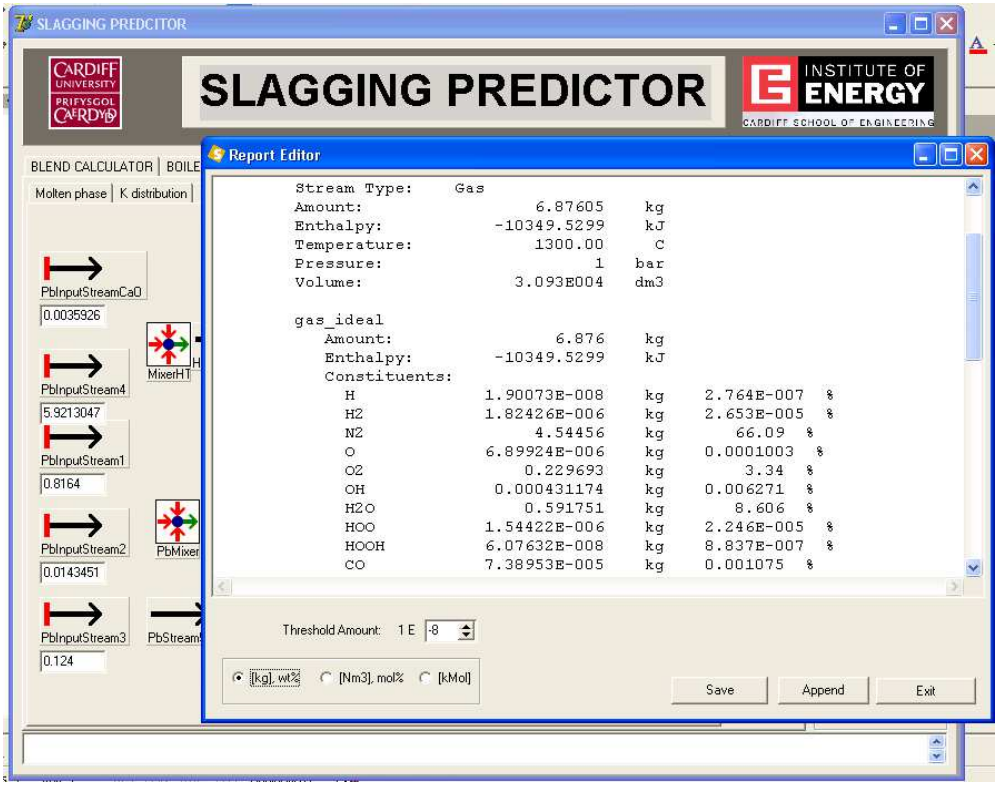

Figure II-16. Screenshot showing the predicted results displayed via the SimuSage Report Editor.

II–6. Development of a 3D Zone-Based Model – coupled with CFD tool

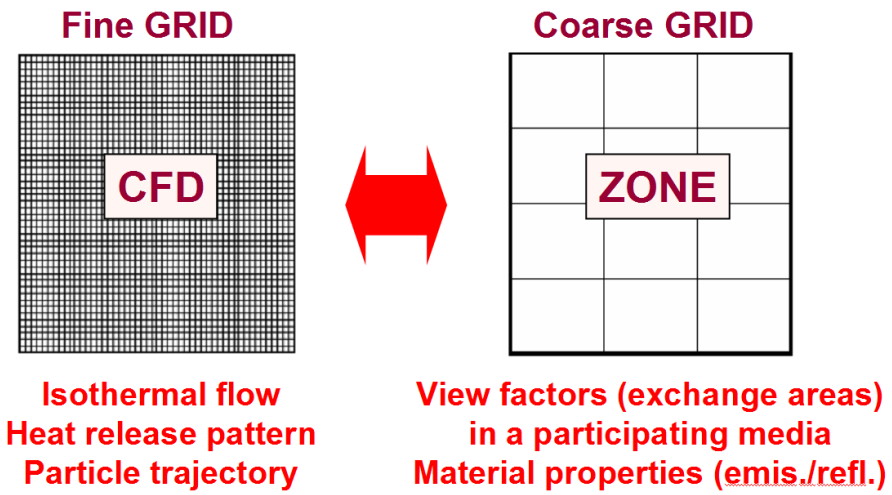

Figure II-17. Illustrative scheme of the inter-exchange data path between CFD and zone-based model.

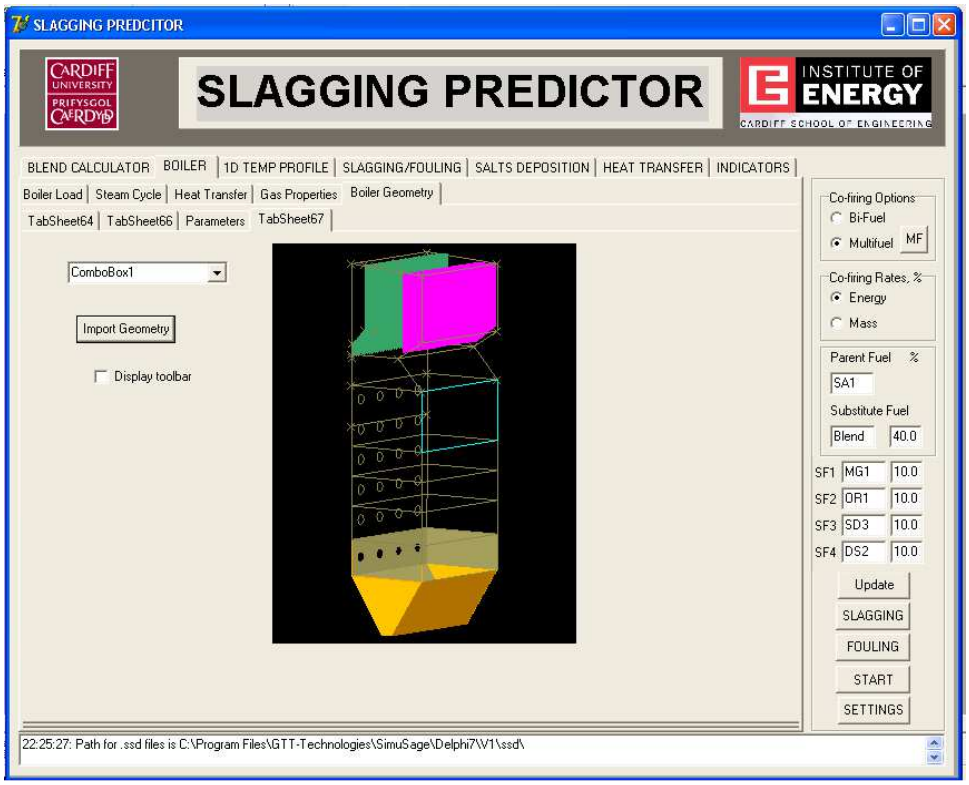

Figure II-18. Screenshot showing the 3-dimensional furnace geometry of the investigated Langerlo pf boiler drawn and numerically described with the aid of CAD algortims impemented into Slaggign Predictor.

Appendix III – Publications

Important International Paper Presentations:

1) Piotr Plaza, Optimisation of coal/biomass fuel blends to minimise slagging and fouling. SENERES Scientific Seminar, Power Engineering Institute, Warsaw, Poland, February 2013.
2) Piotr Plaza, Zone modeling approach for the assessment of the effects of biomass co-firing on pf boiler performance. Paper presented on *the 37th Clearwater Clean Coal Conference*, Florida, USA, June 2012.
3) Piotr Plaza, Ash deposition prediction tool for pf boilers fired with coal and biomass. Paper presented on *the 2nd IEA CCC Workshop on Co-firing Biomass with Coal*, Copenhagen, Denmark, March 2012.
4) Piotr Plaza, Slagging and fouling predictor for coal/biomass (co)-combustion in pf boilers. Paper presented on *the IOP Spring Meeting of the British Section of the Combustion Institute* - Combustion Modelling for Challenging Applications, Southampton, UK, May 2011.
5) Piotr Plaza, Predicting slagging/fouling propensities of solid fuels with the aid of experimental and modelling techniques. Paper presented on *the Energetyka 2010 International Conference*, Wroclaw, November 2010.
6) Piotr Plaza, Use of a predictive model for the impact of co-firing coal/biomass blends on slagging and fouling propensity. Paper presented on *the Energetyka 2010 International Conference*, Wroclaw, November 2010.
7) Piotr Plaza, Impact of co-firing of biomass/coal blends on slagging and fouling propensity, using a predictive model. *Impact of Fuel Quality on Power Production and the Environment*, Banf, Canada, October 2008.
8) Piotr Plaza, The development of a slagging and fouling prediction tool for coal/biomass fired boilers. Paper presented on *the 17th European Conference on Coal Research and its Application, ECCRIA*, Cardiff, UK, September 2008.

List of Publications and Reports:

1) Piotr Plaza and Wiebren de Jong, Direct impact of co-firing of biomass with coal on catalytic SCR DeNOx performance at the Maasvlakte Power Station – Energy from Biomass Project, Phase 1. *Report no. 2558, TU Delft*, November 2012.
2) Piotr Plaza, Anthony J. Griffiths, and Nick Syred, Slagging and fouling prediction tool for large pf utility co-fired boilers. *Archives of Energetics*, Vol. 40, no. 3, 2010.
3) Piotr Plaza, Wieslaw Ferens, Anthony J. Griffiths, Nick Syred, and Wieslaw Rybak: Predicting slagging/fouling propensities of solid fuels with the aid of experimental and modelling techniques. *Archivum Combustionis*, Vol. 30, no. 3, 2010.
4) Piotr Plaza, Anthony J. Griffiths, Nick Syred, and Tom Gralton, Use of a predictive model for the impact of co-firing coal/biomass blends on slagging and fouling propensity. *Energy and Fuels*, Journal of the American Chemical Society, 23 (7), p. 3437 – 3445, 2009.

5) Piotr Plaza, Jaroslaw Hercog, Grzegorz Hrycaj, Karol Krol, and Wieslaw Rybak, Predicting ash deposit formation during co-firig of coal with biomass. *W: Success and visions for bioenergy. Thermal processing of biomass for bioenergy, biofuels and bioproducts* [electronic document], Salzburg, Austria, [22-23] March 2007 / Ed. A. V. Bridgwater. [Newbury]: CPLpress, 2007.

6) Grzegorz Hrycaj, Karol Krol, Piotr Plaza, and Wieslaw Rybak, Thermal decomposition of sewage sludge and biomass-sludge blends. *W: Success and visions for bioenergy. Thermal processing of biomass for bioenergy, biofuels and bioproducts* [electronic document], Salzburg, Austria, [22-23] March 2007 / Ed. A. V. Bridgwater. [Newbury]: CPLpress, 2007.

7) Karol Krol, Grzegorz Hrycaj, Piotr Plaza, and Wieslaw Rybak, Ignition and co-ignition of coal and solid biofuels. *W: Success and visions for bioenergy. Thermal processing of biomass for bioenergy, biofuels and bioproducts* [electronic document], Salzburg, Austria, [22-23] March 2007 / Ed. A. V. Bridgwater. [Newbury]: CPLpress, 2007.